

NASA-CR-160,059

NASA-CR-160059

1981 000 3881

LIBRARY COPY

MAR 4 1981

LANGLEY RESEARCH CENTER
LIBRARY NASA
HAMPTON VIRGINIA



NF01604

A Service of:



The NASA STI Program ... in Profile

Since its founding, NASA has been dedicated to ensuring U.S. leadership in aeronautics and space science. The NASA Scientific and Technical Information (STI) Program plays an important part in helping NASA maintain its leadership role.

The NASA STI Program provides access to the NASA STI Database, the largest collection of aeronautical and space science STI in the world. The Program is also NASA's institutional mechanism for disseminating the results of its research and development activities.

A number of specialized services help round out the Program's diverse offerings, including creating custom thesauri, translating material to or from 34 foreign languages, building customized databases, organizing and publishing research results.

For more information about the NASA STI Program, you can:

- **Phone** the NASA Access Help Desk at (301) 621-0390
- **Fax** your question to NASA Access Help Desk at (301) 621-0134
- Send us your question via the **Internet** to help@sti.nasa.gov
- **Write to:**
NASA Access Help Desk
NASA Center for AeroSpace Information
800 Elkridge Landing Road
Linthicum Heights, MD 21090-2934

3 1176 01365 4653

NASA CR-160059

AVHRR/1 - FM
ADVANCED VERY HIGH RESOLUTION RADIOMETER
FINAL ENGINEERING REPORT

PREPARED BY

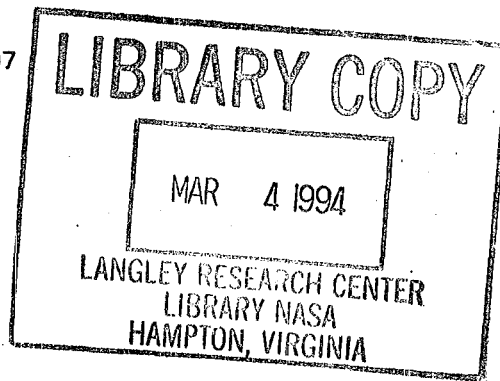
ITT AEROSPACE/OPTICAL DIVISION
FORT WAYNE, INDIANA

46803



FEBRUARY 1979

CONTRACT NO. NAS5-22497



PREPARED FOR

NATIONAL AERONAUTICS AND SPACE ADMINISTRATION
GODDARD SPACE FLIGHT CENTER
GREENBELT, MARYLAND

20771

(NASA-CR-160059) AVHRR/1-FM ADVANCED VERY
HIGH RESOLUTION RADIOMETER Final Report
(ITT Aerospace/Optical Div.) 311 p
HC A14/MF A01

CSSL 14B

N81-12392

Unclass

33/35 39900

N81-12392 #

TABLE OF CONTENTS

	<u>PAGE</u>
1.0 INTRODUCTION-----	1-1
1.1 General Instrument Description-----	1-2
1.1.1 The Scanner Module-----	1-2
1.1.2 Electronics Module-----	1-7
1.1.3 Radiant Cooler-----	1-8
1.1.4 Optical Subsystem-----	1-9
1.1.5 Baseplate Unit-----	1-10
2.0 SYSTEM SENSITIVITY-----	2-1
2.1 Solar Channels 1 and 2-----	2-1
2.1.1 Detector-----	2-1
2.1.2 Detector Responsivity-----	2-4
2.1.3 Solar Channels System Sensitivity-----	2-5
2.2 Channel 3 Detector and Sensitivity-----	2-12
2.2.1 Mercury-Cadmium-Telluride Detector-----	2-12
2.2.2 Channel 3 Sensitivity-----	2-16
2.3 Channel 4-----	2-21
2.3.1 Detector-----	2-21
2.3.2 Channel 4 Sensitivity-----	2-21
3.0 OPTICAL DESIGN-----	3-1
3.1 General Description-----	3-1
3.2 Scan Mirror-----	3-4
3.3 Telescope Design-----	3-4
3.4 Channels 1 and 2 Lens Design-----	3-9
3.5 Channel 3 and 4 Lens Design-----	3-13
3.6 AVHRR Tolerance Analysis-----	3-18
3.6.1 Summary of Mechanical Tolerances-----	3-18
3.6.2 Surface Quality for Filters, Beamsplitters-----	3-22
3.6.3 Mechanical Adjustment Data (Inches)-----	3-22
3.7 Dichroics, Beamsplitters and Cooler Windows-----	3-22
3.8 Spectral Definition-----	3-25
3.8.1 Spectral Definition of Solar Channels-----	3-25
3.8.2 Spectral Definition of Thermal Channels-----	3-35
3.9 Channel Registration-----	3-53
3.10 Polarization Sensitivity-----	3-54
3.11 Scattered Sunlight-----	3-57
3.11.1 Honeycomb Temperature Gradient-----	3-58
3.11.2 Sunlight Reflections from In-Flight Target-----	3-58
3.11.3 Signal Contamination-----	3-61
3.11.4 Sun Scatter Test Results-----	3-63
4.0 MECHANICAL DESCRIPTION-----	4-1
4.1 Overall Instrument Configuration-----	4-1
4.1.1 Structure-----	4-1
4.1.2 Materials in Structure-----	4-4
4.2 Scanner Subassembly-----	4-4
4.2.1 Scan Motor-----	4-4
4.2.2 Bearings-----	4-10

TABLE OF CONTENTS
(CONTINUED)

	<u>PAGE</u>
4.2.3 Bearing Fits-----	4-10
4.2.4 Lubrication-----	4-13
4.2.5 Jitter-----	4-13
4.2.6 Life Test-----	4-14
4.2.7 Angular Momentum-----	4-14
4.2.8 Venting of the Scanner Housing-----	4-15
4.3 Radiant Cooler Subassembly-----	4-15
4.3.1 Support Body-----	4-15
4.3.2 Detector Location-----	4-19
4.3.3 Deployable Earth Shield-----	4-19
4.3.4 Materials and Finishes in Cooler-----	4-21
4.4 Optics Subassembly-----	4-21
4.4.1 Optics Outline-----	4-21
4.4.2 Materials and Finishes Used in Optics-----	4-21
4.5 Electronics Package-----	4-21
4.5.1 Electronics Package Layout-----	4-21
4.5.2 Accessibility-----	4-21
4.5.3 Thermal Considerations-----	4-25
4.5.4 Radiation Considerations-----	4-25
4.5.5 Materials and Finishes in Electronics-----	4-25
4.6 Weight Breakdown-----	4-25
4.7 Materials-----	4-25
 5.0 ELECTRICAL SYSTEM-----	 5-1
5.1 Electronic Packaging-----	5-1
5.2 Electrical Design Considerations-----	5-4
5.3 Video Scan Timing-----	5-4
5.4 Power Subsystem-----	5-6
5.4.1 General-----	5-6
5.4.2 Turn on Transient-----	5-6
5.4.3 Electronics Switching Regulator-----	5-6
5.4.4 Power Converter-----	5-9
5.4.5 +5V Regulators-----	5-9
5.4.6 ±15V Regulators-----	5-9
5.4.7 Motor Power Supply Switching Regulator-----	5-10
5.5 Commands and Digital TM-----	5-11
5.6 Analog TM and Patch Control-----	5-17
5.6.1 Analog Telemetry-----	5-17
5.6.2 Patch Temperature Control-----	5-25
5.7 Motor Logics-----	5-29
5.8 Scan Count and Decode-----	5-30
5.9 Output Data Control-----	5-34
5.10 Ramp Calibration Generator-----	5-42
5.11 Auxiliary Scan Timing-----	5-46
5.12 Ch 3 Data Amplifier-----	5-50
5.13 Channel 4 Amplifier-----	5-55
5.14 Daylight Amplifiers-----	5-55
5.15 Multiplexer Board-----	5-59
5.16 Black Body Mux-----	5-60
5.17 Motor Power Supply-----	5-60
5.18 Power Profile-----	5-64
5.19 Interface Connectors-----	5-64
5.20 Electronics Drawings-----	5-64

TABLE OF CONTENTS
(CONTINUED)

		<u>PAGE</u>
6.0	RADIANT COOLER-----	6-1
6.1	Field of View-----	6-3
6.2	Shield-----	6-5
6.2.1	Cover Temperature-----	6-5
6.2.2	Shielding and View Factors-----	6-7
6.3	Radiator-----	6-10
6.4	Patch-----	6-14
6.5	Solar Exposure-----	6-16
6.6	Anti-Contamination Provisions-----	6-19
6.7	Optical Port Loading-----	6-20
6.7.1	Optical Loading on the Radiator-----	6-21
6.7.2	Optical Loading on the Patch-----	6-21
6.7.3	Absorptivity of the Instrument Patch Opening (Theoretical Model)-----	6-27
7.0	CALIBRATION-----	7-1
7.1	Thermal Channels Calibration-----	7-1
7.1.1	Calibration Accuracy-----	7-1
7.1.2	Chamber Calibration Targets-----	7-7
7.1.3	In-Flight Calibration Target-----	7-19
8.0	THERMAL DESIGN-----	8-1
9.0	TEST AND CALIBRATION DATA-----	9-1
10.0	LIST OF DESIGN INFORMATION REPORTS-----	10-1

1.0 INTRODUCTION

The Advanced Very High Resolution Radiometer (AVHRR) was developed under Contract NAS5-21900. This program covered the design, construction, and test of a Breadboard Model, Engineering Model, Protoflight Model, Mechanical/Structural Model, and a Life Test Model. Special bench test and calibration equipment was also developed for use on the program.

The Flight Model program objectives under Contract NAS5-22497 were to fabricate, assemble and test four of the Advanced Very High Resolution Radiometers along with a bench cooler and collimator. In addition, a group of parts known as "common parts" were procured and delivered.

Initially, the instrument was to operate from a 906 n.m. orbit and be thermally isolated from the spacecraft. The Breadboard Model and the Mechanical/Structural Model were designed and built to these requirements. During the Engineering Model assembly phase, the spacecraft altitude was changed to 450 n.m., IFOVs and spectral characteristics were modified, and spacecraft interfaces were changed. In addition, the final spacecraft design provided a temperature-controlled Instrument Mounting Platform (IMP) to carry the AVHRR and other instruments. The design of the AVHRR was modified to these new requirements and the modifications were incorporated in the Engineering Model. The Protoflight Model and the Flight Models conform to this design.

1.1 General Instrument Description

The AVHRR is a four channel scanning radiometer providing two channels in the visible-near IR region and two IR channels. The instrument utilizes an 8 inch diameter optical system. Cross-track scanning is accomplished by a continuously rotating mirror direct-driven by a hysteresis synchronous motor. The two IR detectors are cooled to 105K by a two-stage passive radiant cooler. The data from the four channels is simultaneously sampled at a 40 kHz rate and converted to 10-bit binary from within the instrument.

A summary of the AVHRR characteristics is given in Table 1-1. Figure 1-1 is a photograph of the Engineering Model instrument and Figure 1-2 shows the outline configuration of the instrument.

The AVHRR is comprised of five modules which are assembled together into a single unit instrument. These modules are:

- Scanner Module
- Electronics Module
- Radiant Cooler Module
- Optical Subsystem
- Baseplate Unit

These modules are shown in the exploded view of Figure 1-3.

1.1.1 The Scanner Module

This module includes the scan motor, the mirror and the scan motor housing. The scan motor design is based on the motor developed for the SCMR, an 80 pole hysteresis

Table 1-1 Summary of Characteristics

	<u>Ch 1</u>	<u>Ch 2</u>	<u>Ch 3</u>	<u>Ch 4</u>
Spectral Range (μM)	.58-.68	.725-1.0	10.5-11.5	3.55-3.93
Detector	Silicon	Silicon	HgCdTe	InSb
Resolution (N.M.)	.59	.59	.59	.59
IFOV (MR)	1.3 sq.	1.3 sq.	1.3 sq.	1.3 sq.
S/N @ .5% Albedo	>3:1	>3:1	-	-
NETD @ 300K	-	-	.12K	.12K
MTF (1 IFOV/Single Bar)	.30	.30	.30	.30
Optics	- 8 inch diameter afocal cassegrainian telescope			
Scanner	- 360 rpm hysteresis synchronous motor with beryllium scan mirror.			
Cooler	- Two-stage radiant cooler, IR detectors controlled at 105K			
Data Output	- 10 bit binary, simultaneous sampling at 40 KHz rate.			
Commands	- 28			
Telemetry	- 14 Digital, 20 Analog			

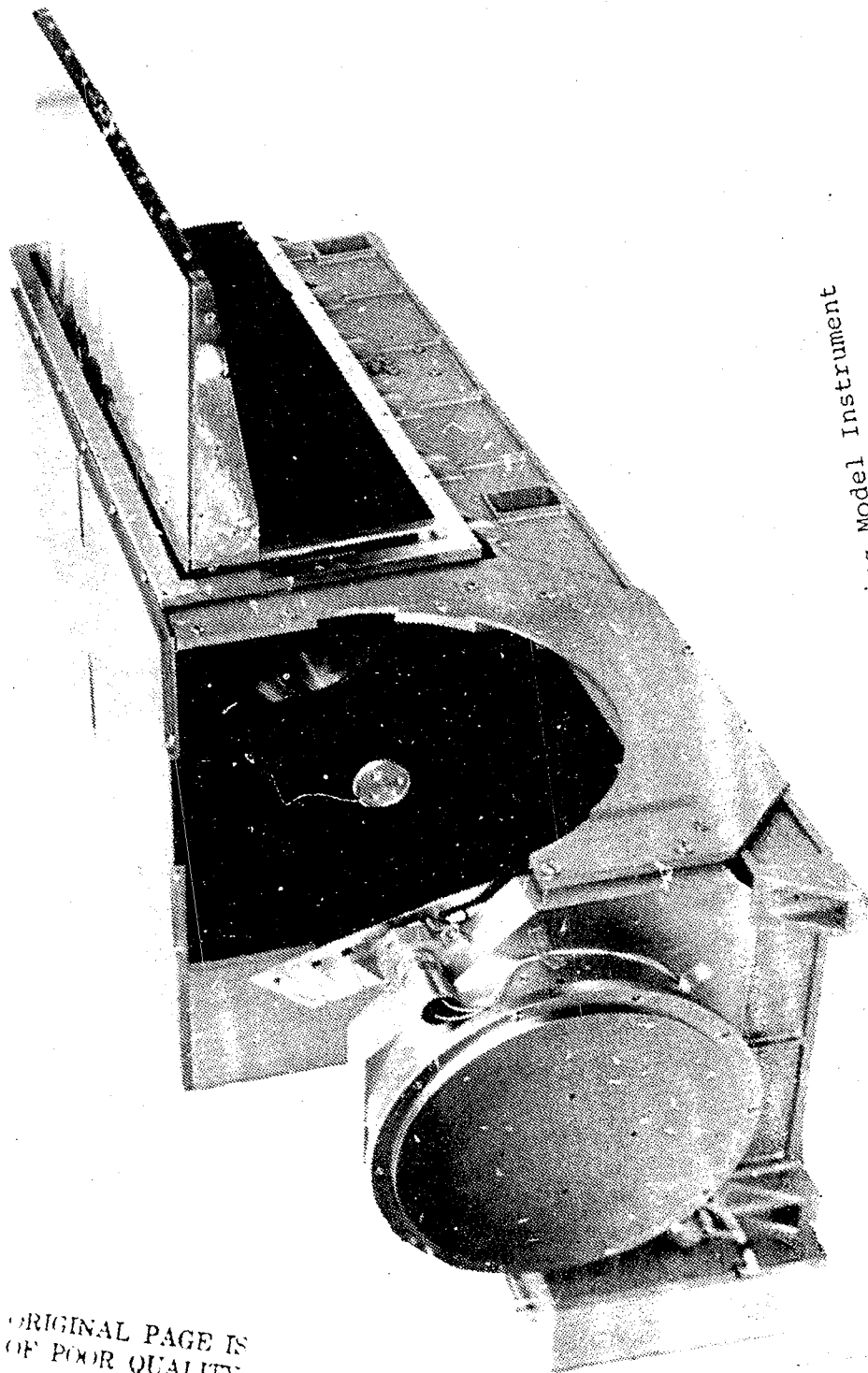
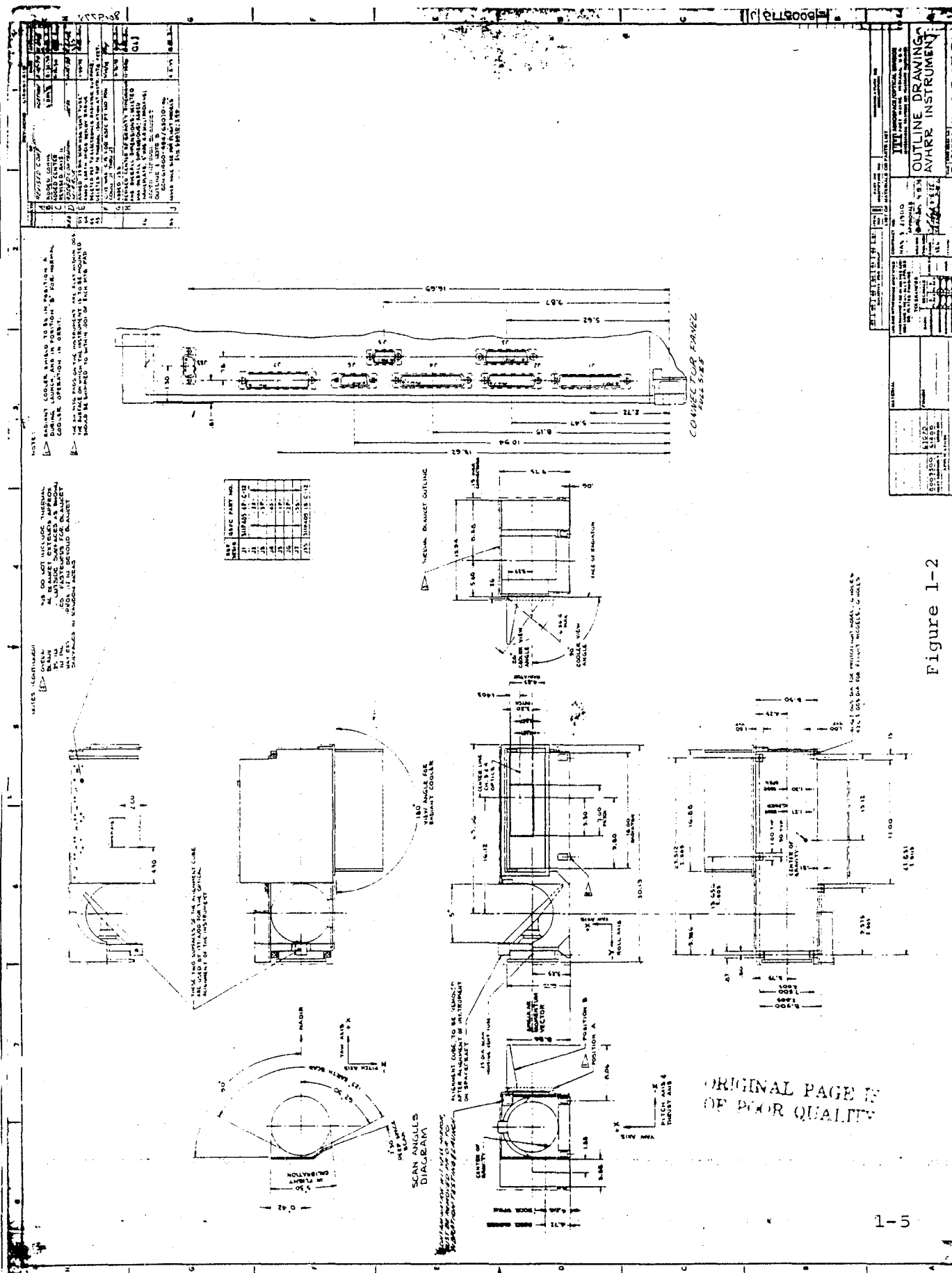


Figure 1-1 Engineering Model Instrument

ORIGINAL PAGE IS
OF POOR QUALITY



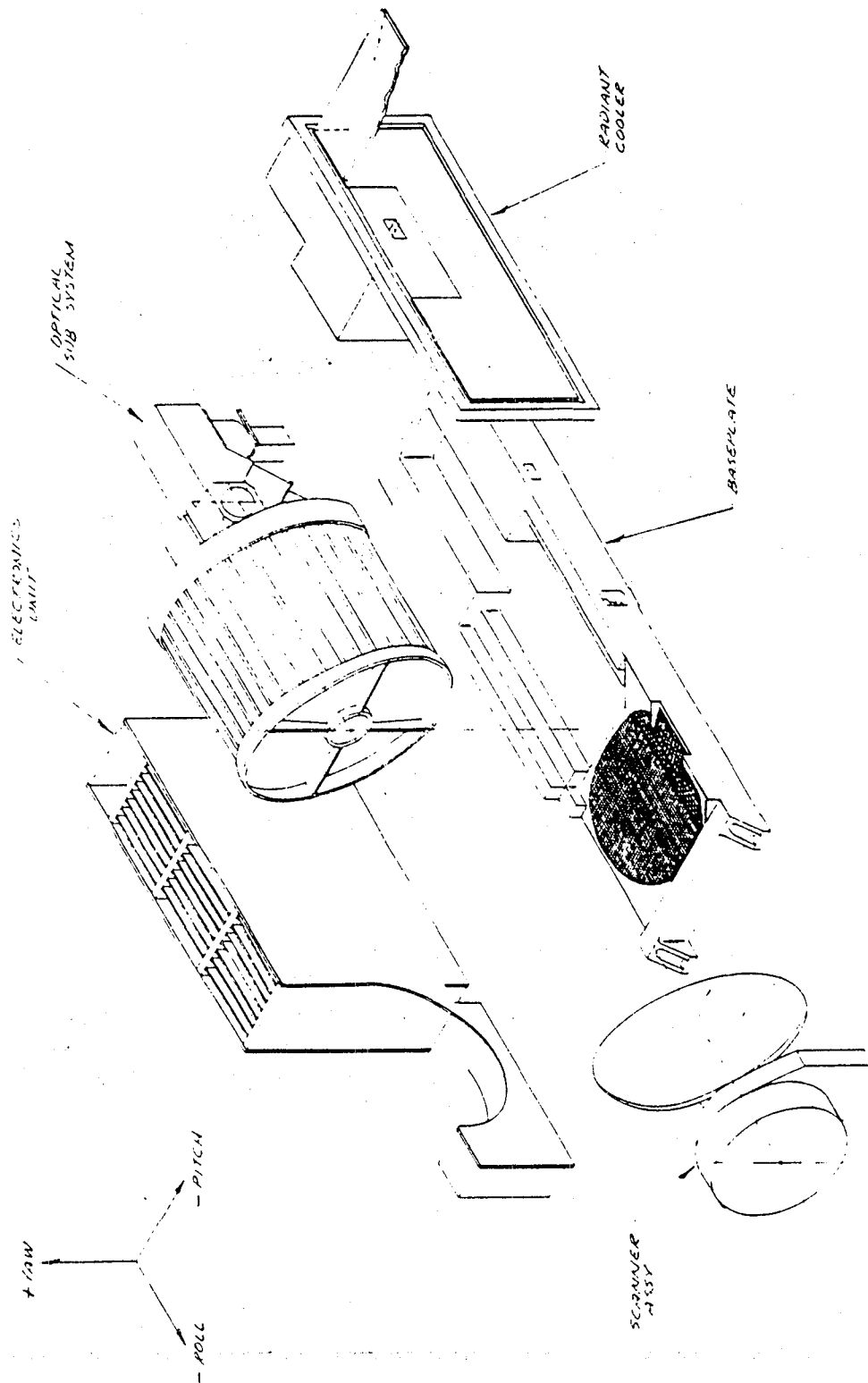


Figure 1-3 AVHRR Modules

synchronous motor. The motor has two power modes of operation. High power ($\approx 4-5$ watts) will be utilized for driving the scan mirror in air and low power (≈ 3.8 W) will be used for nominal in-orbit operation. The scanner housing is an integral part of the motor and is made of beryllium. The scan mirror is also made of beryllium and is ≈ 11.6 inches across the major axis and 8.25 inches across the minor axis. The scan motor rotates the mirror at the 360 RPM to produce a contiguous scan of the earth scene. The line-to-line jitter is less than 17 microseconds.

1.1.2 Electronics Module

The electronics module is in two sections both of which bolt on to the instruments inboard side panel. The curved box (Reference Figure 1-3) is the motor power supply. Twenty-five electronic modules are used to make up the electrical system of the AVHRR. Nineteen of these are located in the electronics box. The solar channel preamplifiers for the solar channels and IR channel 3 are located in the area of the secondary optics. The IR channel 4 preamplifier is located on the rear of the radiant cooler housing.

Except for Channels 1, 2 and 4 preamplifiers, all of the modules are accessible without the removal of the instrument from the spacecraft.

The following is a list of the electronics modules:

1. Power Converter and Switching Regulator
2. Logics Regulators
3. ± 15 V Regulators

4. Command Relay #1
5. Command Relay #2
6. Command Relay #3
7. Patch Temperature Control and T/M
8. T/M Board #2
9. Motor Logics
10. Scan Count and Decode
11. Interface Logics #1
12. Interface Logics #2
13. Ramp Calibration Generator
14. Auxiliary Scan Logics
15. IR Post Amplifier
16. Daylight Post Amplifier
17. Multiplexer
18. Black Body MUX logics
19. A to D Converter
20. IR Preamplifier
21. Channel 4 Preamplifier
22. Daylight Preamplifier (Ch. 2)
23. Daylight Preamplifier (Ch. 1)
24. Motor Power Supply
25. Switching Regulator

1.1.3 Radiant Cooler

The radiant cooler module is made up to four basic assemblies. These are (1) the cooler housing, (2) the first

stage radiator, (3) the patch or second stage radiator, and (4) the cooler cover. The first stage radiator is configured in such a manner as to shade most of its 55.2 inch² area from the earth by the cooler cover when the cover is deployed. A "single shot" solenoid actuated, spring driven deployment system is used to deploy the cover. Mounted on the patch are the two infrared detectors. The patch has a 22.4 in² radiating area. The cooler housing surrounds the cooler on all sides except for the radiation area. The housing is vacuum sealed so that when the bench cooler is clamped to the front of the housing a vacuum can be pulled on the entire cooler and the system permitted to cool as it would in space, i.e. radiation to a cold target located in the bench cooler (except that the cold target is at liquid nitrogen temperature).

Multilayer insulation thermally separates the first stage radiator from the housing and the first stage optical window is thermally isolated and heated several degrees warmer than the 171K radiator temperature. The patch is thermally isolated from the first stage by low emissivity surfaces (gold to gold) and runs at 95K with no control power. During nominal operation the patch temperature will be controlled at 105K.

1.1.4 Optical Subsystem

The optical subsystem was designed by Ferson Optics, a division of Bausch and Lomb, to ITT Specification. (Ferson

fabricated the BBM ETM and PTM optics; however, the Flight Model Optics are being fabricated by Perkin-Elmer, Costa Mesa, California.) The subsystem consists of an afocal 8.0 inch aperture telescope (two coaxial confocal paraboloidal mirrors) followed by secondary optics which split the radiant input into four discrete spectral bands and focus them onto their respective field stops. The spectral bands are:

Channel 1: 0.58 to 0.68 microns

Channel 2: 0.72 to 1.05 microns

Channel 3: 10.5 to 11.5 microns

Channel 4: 3.55 to 3.92 microns

The instantaneous field of view is 1.3 milliradians in all channels and is defined by an aperture plate in Channels 1 and 2 and by the detector active areas in Channels 3 and 4. In addition the optical subsystem has been designed to meet the total system MTF requirements with the detectors registered off axis by as much as 1.5 milliradians in Channels 1 and 2 and 1 milliradian in Channels 3 and 4.

Polarization effects have been minimized (<7% in Channels 1 and 2) by orienting the polarization sensitive elements in a predetermined way, thus having elements compensate for other elements.

1.1.5 Baseplate Unit

The baseplate unit is the common structure in which all other modules are secured. Dowel pins are used to establish and maintain alignment of the scanner and optics modules. Alignment of the cooler to the optics is established by shims.

2.0 SYSTEM SENSITIVITY

2.1 Solar Channels 1 and 2

2.1.1 Detector

Both solar channels use the same detectors with the same operating characteristics as before the modifications. The detectors used are Infrared Industries, Inc. silicon detectors which are operated at -15 volts bias. The device has an active area of 0.100 inch square and is packaged in a TO-5 can using a metallic hermetic seal. Some of the most pertinent characteristics of the device are given in Table 2-1.

The detector will be used as a current source for an op-amp preamplifier. In the current-to-voltage transducer operating mode, the combination gives excellent sensitivity and frequency response using a 4M ohm feedback resistor as the effective detector load.

The detectors are used as energy collection devices behind the 0.0238 inch square apertures which are the defining field stops for Channels 1 and 2. Optical analysis showed that using a 0.100 inch square detector active area at an effective optical distance of 0.146 inch behind the field stop, resulted in a well over 99% of the rays, which passed through the field stop, being collected by the detectors of both channels.

Table 2-1 Solar Channel Detector Characteristics

Type	Passivated, Planar Diffused Silicon Pin Photodiode
Manufacturer	Infrared Industries, Inc.
Active Area Size	0.100 Inch Square
Bias	-15 Volts
Spectral Peak	900 \pm 50 nmeters
Responsivity - Peak	0.62 Amp/Watt
Responsivity - Ch 1 Avg.	0.37 Amp/Watt
Responsivity - Ch 2 Avg.	0.54 Amp/Watt
Leakage Current at -15 V	17 Namp Maximum
Capacitance at -15 V	15 pf Maximum

Table 2-2 Responsivity Versus Temperature for Detector SN7

Wavelength (\AA)	Responsivity (Amps/Watt)		
	<u>-10°C</u>	<u>+22°C</u>	<u>+50°C</u>
4415	0.14	0.14	0.13
5013	0.28	0.27	0.27
5560	0.40	0.40	0.40
6000	0.41	0.43	0.42
6505	0.50	0.50	0.51
7010	0.59	0.57	0.59
7492	0.63	0.63	0.65
8011	0.72	0.74	0.76
8500	0.76	0.79	0.82
9000	0.73	0.78	0.81

Table 2-2 Responsivity Versus Temperature for Detector SN7
(Cont'd)

Wavelength (\AA)	Responsivity (Amps/Watt)		
	<u>-10°C</u>	<u>+22°C</u>	<u>+50°C</u>
9500	0.70	0.79	0.87
10148	0.43	0.58	0.74
10612	0.14	0.24	0.39
11014	0.06	0.10	0.18
11512	0.01	0.02	0.05

2.1.2 Detector Responsivity Versus Temperature

The question was raised early in the AVHRR program as to the effect of temperature upon the responsivity of the silicon detectors. Infrared Industries ran spectral response versus temperature data on one of the delivered units. The measured data is of historical interest only since the latest predictions indicate a maximum detector operating temperature of about 24°C. The data is shown in Table 2-2.

The AVHRR temperature is more controlled by the SPACECRAFT TCE and the maximum operating temperature is within a few degrees of the nominal detector test temperature of +24°C. The maximum overall temperature change under various operating conditions is about 10°C. The detector responsivity changes are insignificant over so small an excursion and so the AVHRR output will not sensibly change due to detector temperature variations.

2.1.3 Solar Channels System Sensitivity

For channels 1 & 2, the signal to noise ratio, S/N, is given by

$$S/N = \frac{\Phi_{\Delta\lambda}}{\alpha \text{ NEP}}$$

where $\Phi_{\Delta\lambda}$ = solar spectral flux incident on the detector

α = degradation factor due to electronic noise pickup, 1/f noise, etc.

NEP = effective detector Noise Equivalent Power

$\Phi_{\Delta\lambda}$ is given by

$$\Phi_{\Delta\lambda} = \frac{1}{\pi} I_{\Delta\lambda} \tau \rho_s A_o \theta^2 = \frac{1}{4} I_{\Delta\lambda} \tau \rho_s D_o^2 \theta^2$$

where $I_{\Delta\lambda}$ = solar spectral irradiance in the spectral band incident on the Earth's atmosphere

τ = transmission of optical system

ρ_s = scene spectral albedo

D_o = diameter of the collection aperture

θ = instantaneous field of view

The NEP is given by

$$\text{NEP} = \frac{\sqrt{i_s^2 + i_d^2 + i_l^2}}{R}$$

where i_s = shot noise current due to signal flux on the detector

i_d = photodiode leakage current noise.

i_l = load resistor Johnson noise current

R = detector responsivity in ampere/watt

Using Thekaekara's Tables we find that the total solar irradiance incident on the atmosphere in channels 1 and 2 (weighted by the relative response in each band) is:

$$I_{\Delta\lambda}^1 = 4.24 \times 10^{-2} \text{ W/cm}^2$$

$$I_{\Delta\lambda}^2 = 3.00 \times 10^{-2} \text{ W/cm}^2$$

This is the solar power in the 0.50 to 0.91 micron region (channel 1) and the 0.71 to 1.10 micron region of channel 2.

2.1.3.1 System Transmission

The elements affecting the system transmission can be divided into two broad categories, those that are spectrally variant and those that are not. The elements that are variant are the scan, telescope, and folding mirrors, and the gold dichroic beamsplitter. These elements are analysed in the section defining the spectral response. Also analyzed are the bandpass filters and detectors; however, for S/N purposes, it is assumed that the bandpass filters are invariant across the band and that the detector has an average responsivity in the spectral band of interest.

Table 2-3 gives the spectral efficiencies of the mirrors and gold dichroic used in these calculations. These are measured PTM values and represent expected flight model values. Combining the three mirror reflections and gold dichroic transmission for Channel 1 gives an average transmittance of 0.60 for this channel. Doing likewise for channel 2 (with one more mirror reflectance) gives 0.43. These are the transmissions through the spectrally variant elements only.

The elements which can be considered spectrally invariant are the inconel beamsplitter separating channel 1 and 2, the relay lenses in each channel, and each bandpass filter (the filter has a relatively flat response across each band). In addition the obscuration caused by the secondary mirror and its support must be considered. The values used in calculating the transmissions are also shown in Table 2-3. There are three relay lenses in each

Table 2-3 Optical Efficiency of AVHRR Elements
(PTM Measured)

SPECTRALLY INVARIANT ELEMENTS

Reflectivity of Inconel beamsplitter	= .225
Transmittance of Inconel beamsplitter	= .375
Transmittance of Chan. 1 filters	= 0.85
Transmittance of Chan. 2 Filter	= 0.90
Telescope Obscuration	= 0.94
Lens Transmittance	= 0.95

SPECTRALLY VARIANT ELEMENTS

<u>SPECTRAL POINT MICRON</u>	<u>SCAN MIRROR REFLECTIVITY</u>	<u>TELESCOPE MIRROR REFLECTIVITY</u>	<u>CH 2 FOLDING MIRROR REFLECTIVITY</u>	<u>GOLD DICHROIC TRANSMISSION</u>
0.50	.92	.88	-	.73
0.55	.93	.92	-	.772
0.60	.925	.93	-	.80
0.65	.92	.93	-	.81
0.70	.90	.93	.84	.81
0.75	.90	.93	.81	.79
0.80	.88	.92	.79	.765
0.85	.875	.915	.79	.73
0.90	.88	.93	.80	.69
0.95	.89	.935	.815	.642
1.00	.89	.93	.825	.59
1.05	.89	.93	.835	.56
1.10	.885	.925	.845	.54

channel so that the combined transmission for the invariant elements is 0.154 for channel 1 and 0.272 for channel 2. Combining these with the values for the variant elements gives:

$$\tau_1 = 0.092$$

$$\tau_2 = 0.117$$

for the expected total system transmission for each channel.

Allowing a degradation factor for dirt, dust, etc. on each element, will result in, perhaps, a more realistic overall system transmission. It is reasonable that lens surfaces sealed from ambient will not markedly degrade. For sensitivity calculations assume that each channel will suffer a 50% degradation overall thus

$$\tau_1 = .046$$

$$\tau_2 = .058$$

2.1.3.2 Detector NEP

The Solar Channel detector has a peak responsivity (ampere/watt) of at least 0.62. The average responsivity across the channel 1 spectral band is 0.37 ampere/watt while that in channel 2 is 0.54 ampere/watt.

Several factors contribute to the noise. The shot noise due to the detector dark current, the shot noise due to the detector scene generated current, and the Johnson noise in the preamplifier feedback resistor are the major noise sources. $1/f$ noise is negligible across the 14.5 KHz bandpass of the electronic filter. Contribution of pre-amplifier transistor noise is also very small compared to the above sources and so can be ignored.

Both channels use a 4 megohm feedback resistance in the pre-amplifier so that the Johnson noise at a 300K temperature over a 14.5 KHz bandwidth is 7.75×10^{-12} ampere. The detector dark current is 17 nanoamperes maximum in each channel giving a dark current noise of:

$$(i_d^1) = (i_d^2) = (2 \epsilon I_d \Delta f)^{1/2} = 8.88 \times 10^{-12} \text{ ampere}$$

The signal shot noise under minimum signal condition is based on the current flowing in the detector under that illumination. The minimum signal flux is calculated later to be 1.68×10^{-9} watt in channel 1 and 1.43×10^{-9} watt in channel 2. The minimum DC current out of the detectors then is 6.22×10^{-10} amp and 7.72×10^{-10} amp for channels 1 and 2. The shot noise then is

$$i_s^1 = 1.70 \times 10^{-12} \text{ amp rms}$$

$$i_s^2 = 1.89 \times 10^{-12} \text{ amp rms}$$

The total noise current in channel 1 is:

$$i_{T1} = ((7.75)^2 + (8.88)^2 + (1.70)^2)^{1/2} \times 10^{-12}$$

$$i_{T1} = 1.19 \times 10^{-11} \text{ amp}$$

similarly for channel 2

$$i_{T2} = 1.19 \times 10^{-11} \text{ amp}$$

The noise is essentially the same in both channels due to the predominance of i_ℓ and i_d .

A degradation factor α is included in the calculation. This accounts for stray noises as well as degradations in operation of the system. For this analysis a degradation factor of 1.6 based on the measured BBM and ETM values was used.

The detector NEP then is

$$NEP_1 = \frac{1.19 \times 10^{-11}}{0.37} = 3.22 \times 10^{-11} \text{ watt}$$

$$NEP_2 = \frac{1.19 \times 10^{-11}}{0.54} = 2.20 \times 10^{-11} \text{ watt}$$

2.1.3.3 Signal to Noise Ratio Calculation

Using the equation previously given and assuming a minimum scene as described in the AVHRR specification ($\rho_s = 0.5\%$), a collection aperture of 8.0 inches, and an IFOV of 1.31 milliradians, we have

$$\phi_{\Delta\lambda}^1 = 1.73 \times 10^{-9} \text{ watt}$$

$$\phi_{\Delta\lambda}^2 = 1.54 \times 10^{-9} \text{ watt}$$

and so

$$S/N = \frac{\phi_{\Delta\lambda}}{\alpha NEP}$$

$$S/N_1 = \frac{1.73 \times 10^{-9}}{1.6 \times 3.22 \times 10^{-11}} = 33:1$$

$$S/N_2 = \frac{1.54 \times 10^{-9}}{1.6 \times 2.20 \times 10^{-11}} = 44:1$$

Table 2-4 Solar Channel Sensitivity

	CH 1	CH 2
System Transmission (Degraded)	0.046	0.058
Detector Responsivity	0.37 A/W	0.54 A/W
Detector NEP (25°C)	3.22×10^{-11} W	2.20×10^{-11} W
S/N Ratio at Minimum Albedo (25°C)	33:1	44:1
Specified Minimum Signal to Noise Ratio	3:1	3:1

2.1.3.4 Sensitivity vs Temperature

The foregoing calculation is based on a detector dark current of 17 nanoamps. This is true at 25°C. At higher temperatures, the detector dark current (and the load Johnson noise to some extent) increases, thus increasing the noise and increasing the detector NEP. Based on data from the manufacturer and the results of the thermal math model which indicates very little variation in detector temperature, the signal to noise ratio for the solar channels will not perceptibly change in operation.

2.2 Channel 3 Detector and Sensitivity

2.2.1 Mercury-Cadmium-Telluride Detector

The mercury-cadmium-telluride detector is optimized for best sensitivity between 10.5 and 11.5 μm wavelengths when cooled to 105 Kelvin by the radiant cooler. The important characteristics of the detector are summarized in Table 2.2-1.

The Hg Cd Te element is mounted in a small metal enclosure shown in ITT-A/CD Figure 2.2-1. The aplanat lens is bonded directly to the metal enclosure and also serves as the window through which the optical beam passes. The alignment and spacing of the aplanat lens with respect to the sensing element is accurately maintained with this arrangement. The detector is tested by the manufacturer both before and after attachment of the lens to assure a qualified unit. The internal volume is filled with an inert gas and then sealed by the manufacturer. The detectors are inspected both before and after lens attachment by an ITT-A/OD Quality Control representative who also witnesses the important acceptance tests at the manufacturer's plant.

MERCURY-CADMIUM-TELLURIDE DETECTOR

<u>ITEM</u>	<u>CHANNEL 3</u>
Spectral Band	10.5-11.5 μ m
Width of Sq. Sensitive Area	0.0068 \pm 0.0004"
Operating & Spec. Temperature	105 Kelvin
Field of View, Min.	100 $^{\circ}$
Minimum Resistance	10 Ohms
Max. Bias Power	1.2 M.W.
Avg. D* In Spectral Band At 105K, 2KHz, 100 $^{\circ}$ FOV, 1.2 M.W., 1 HZ	$2.0 \times 10^{10} \frac{\text{CMHZ}^{1/2}}{\text{Watt}}$
Avg. Spectral Responsivity, Min.	5,500 $\frac{\text{Volts}}{\text{Watt}}$
Max. Change in Responsivity Per Kelvin at 105 Kelvin	5%
Long Wavelength Response	<1% at 18 μ m
Time Constant	<1 μ s
Spatial Responsivity Uniformity	<2 to 1
I/f Knee Frequency	<1 KHz

Table 2.2-1 HgCdTe Detector Characteristics

NOTE:

- 1 THE PLANE OF THE DETECTOR FACE IS TO COINCIDE WITH SURFACE -B- WITHIN .001. THE CENTER OF THE ACTIVE AREA OF THE DETECTOR SHALL BE LOCATED ON THE CENTER OF DIA -A- WITHIN .001 DIA. THE CENTER OF THE LENS SHALL BE CENTERED ON THE ACTIVE AREA OF THE DETECTOR WITHIN .001.
- 2 TOLERANCE FOR LOCATION OF .0637 DIA. HOLES: $\pm .0005$
TOLERANCE FOR LOCATION OF THREADED HOLES: $\pm .0030$
- 3 THE CENTER LINE OF THE .0637 DIA. HOLES SHALL COINCIDE WITH SURFACE -B- WITHIN .002 AND SHALL BE PARALLEL TO SURFACE -B- WITHIN .001.
- 4 THIS DIMENSION SHALL NOT EXCEED THE MEASURED LENS HEIGHT (.210 NOM.) PLUS THE MEASURED DIMENSION FROM SURFACE -B- TO THE INDICATED SURFACE (.180 NOM.).
- 5 THESE DIMENSIONS ARE TO BE MEASURED FROM THE CENTER LINE OF DIA. -A-.
- 6 APPLY PLUS (+) VOLTAGE MARKING AT PROPER PIN TO INDICATE OPTIMUM BIAS DIRECTION.
- 7 LENS TO BE SUPPLIED BY ITT A/OO.
- 8 ATTACH 3" MIN. LENGTH OF #32 AWG COPPER WIRE, POLYTHERMALEZE COATED, TO EACH ELECTRICAL LEAD PER NASA DOCUMENT NHB 9300.4 (3A); MIN. OF TWO TURNS OF WIRE AROUND PIN.
- 9 ONE SIDE OF SQUARE SENSITIVE AREA OF DETECTOR TO BE PARALLEL TO MOUNTING BASE WITHIN 10°.
- 10 BOND LENS TO HOUSING USING "TORR SEAL" EPOXY RESIN AND HARDENER. (VARIAN ASSOCIATES, VACUUM DIV.)

REVISIONS 61400-172		
ZONE/LTR	DESCRIPTION	DATE
A	ADDED THE LAST SENTENCE TO NOTE #1: "THE CENTER OF THE LENS, ETC." ECN 61400-178	8-15-74
B	ITEM 2 PT. NO. WAS 8008306-1 ECN 61400-181	9-12-74
C	IN NOTE 8 COINCIDENCE TOL. WAS .001 & ADDED PARALLELISM TOL. IN NOTE 6 ADDED "TO INDICATE, ETC."; ECN 8.0004 WAS .360 ± .002; .362 ± .005 WAS .361 ± .002 ECN 61400-286	1-18-75
D	ADDED ITEM 6 TO WL ECN 61400-393	4-20-75

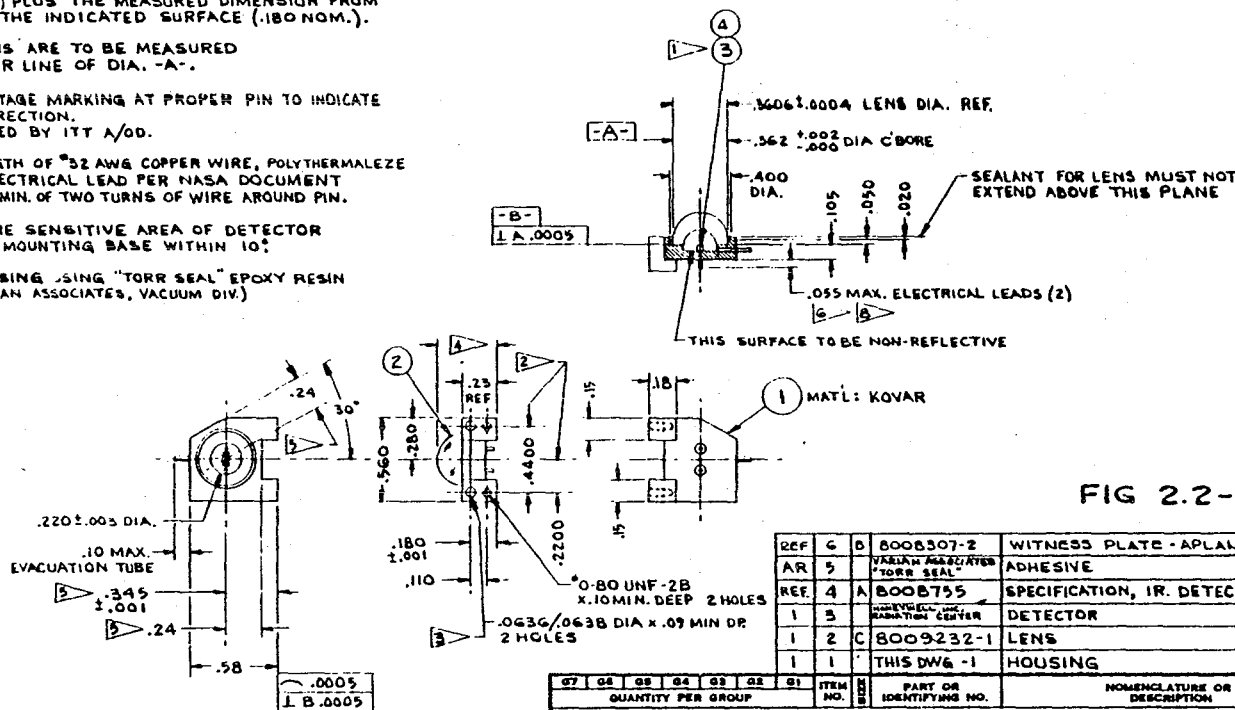


FIG 2.2-1

REF	Q	D	8008307-2	WITNESS PLATE - APLAWAT
AR	5		VARIAN ASSOCIATES "TORR SEAL"	ADHESIVE
REF	4	A	8008755	SPECIFICATION, IR. DETECTOR
1	3		HOUSING CENTER	DETECTOR
1	2	C	8009232-1	LENS
1	1		THIS DWG -1	HOUSING

QUANTITY PER GROUP		ITEM NO.	PART OR IDENTIFYING NO.	NOMENCLATURE OR DESCRIPTION
LIST OF MATERIALS OR PARTS LIST				
UNLESS OTHERWISE SPECIFIED		CONTRACT NO.		
DIMENSIONS ARE IN INCHES AND INCLUDE CHEMICALLY APPLIED OR PLATED FINISHES		HAS 5-21900		
TOLERANCES		APPROVALS		
BASIC	DECIMALS	DRAWN 7-12-74		
DIMENSION	PLACE PLACE	CHECKED 7-12-74		
UNDERS	± .02 ± .005	ENGR 7-12-74		
8-24 INCL	± .02 ± .010	ITTAO 7-12-74		
OVER 24	± .02 ± .030	OTHER		
DO NOT SCALE PRINT		C 31550 8008791		
COML. TOL. TO STOCK SIZES		SCALE 2/1		
SHOP PRACTICE, 28.101 APPLIES		SHEET		

MATERIAL		AS NOTED	
FINISH			
8008755	61400		
NEXT ASSEMBLY	USED ON		
APPLICATION			
EXCEPT AS MAY BE OTHERWISE PROVIDED BY CONTRACT, THESE DRAWINGS AND SPECIFICATIONS ARE THE PROPERTY OF ITT AEROSPACE/OPTICAL DIVISION AND ARE TO BE KEPT IN STRICT CONFIDENCE AND SHALL NOT BE REPRODUCED OR COPIED OR USED AS THE BASIS FOR THE MANUFACTURE OR SALE OF APPARATUS WITHOUT PERMISSION.			

ORIGINAL PAGE IS OF POOR QUALITY

The size of the sensitive area is determined by the effective focal length (EFL) of the optical system and the instantaneous field of view (IFOV), which is obtained from the specified resolution. They are related by the equation

$$w = \theta \times \text{E.F.L.}$$

where w = edge width of square sensitive area

θ = angular width of square IFOV

For Channel 3, EFL is 132.3 mm (= 5.209 inches) and θ = 1.31 milliradians which gives w equal to 0.0068 inch. A tolerance of ± 0.0004 inch has been established as being a reasonable amount consistent with detector fabrication capabilities and size of the IFOV. In the electrode-to-electrode direction, the length of the sensing element will be slightly greater (by 0.0005 inch) to compensate for electrode end effects where the detector normally has very little response.

A uniformity specification has been incorporated into the detector specification in order to minimize non-uniformity of response across the sensitive area. A total of nine equally spaced readings arranged in a 3 by 3 grid will be taken across the sensitive area and all readings must be equal to or greater than 50% of the largest reading. The diameter of the test spot is about 0.0015 inch and the readings are spaced by 0.002 inch; the measurements will be made on a standard "spot scan" test station by the manufacturer.

Acceptance tests are based on measurements made at the anticipated operating temperature of 105 Kelvin. Measurements are

made at 90, 95, 100, 110, 115 and 120 Kelvin in the event that the cooler must be operated at the backup temperature of 107 Kelvin or

a cooler malfunction occurs. Details of what measurements are made at the different temperatures are given in the procurement specification for the detector.

2.2.2 Channel 3 Sensitivity

System sensitivity in the infrared channels (numbers 3 and 4) is expressed in terms of the noise-equivalent-temperature difference, NEAT (NETD). The NETD is the difference in temperature between two targets (several times larger than the instantaneous field of view) which is required to produce a change in signal voltage equal to the rms noise of the radiometer. The equation used to calculate the NETD is given in Table 2.2-3, which also defines the various parameters used in the equation. The degradation factor, α , and the optical f-number have been made as small as feasible whereas factors in the denominator of the NETD equation have been maximized as much as possible. The detector detectivity is the highest available from any vendor for the spectral bands, operating temperature, field of view, etc. imposed by instrument requirements. The field of view, element dwell time (or electrical bandwidth) and change in scene radiance are all set by instrument performance specifications. We will discuss in this section only the degradation factor and the optical transmission since additional information on the other factors are given in the Optical Section (3.0) of this report.

The degradation factor, α , consists of two factors for the case under consideration, that due to $1/f$ noise from the infrared detector, and a second factor to account for some additional electronic noise. Diffraction effects are negligible

$$\text{NETD} = \frac{2 \sqrt{2} \alpha \text{fn}}{\pi D_o D_m^* \tau \theta \sqrt{t_d} \left(\frac{dN}{dT} \right)_T}$$

NETD = Noise Equivalent Temperature Difference

α = Degradation Factor Including 1/f Detector Noise

fn = Optical F-number

D_o = Diameter of Optical Entrance Aperture

D_m^* = Average detector detectivity in spectral band at the measuring frequency

τ = Transmission of optics including obscuration effects

θ = Angular width of square instantaneous field of view

t_d = Elemental dwell time (= $\frac{1}{2\Delta f}$ where Δf_o is the 3 db bandwidth of presampling filter)

$\left(\frac{dN}{dT} \right)_T$ = Change in scene radiance for small temperature change at temperature T

Table 2.2-3 Noise Equivalent Temperature Difference Equation
(Channel 3)

DEGRADATION FACTOR (α)

$$\alpha_{\text{total}} = \alpha_{1/f} \cdot \alpha_2$$

$$\alpha_{1/f} = \left[1 + \frac{f_c}{f_u - f_l} \cdot \ln \left(\frac{f_u}{f_l} \right) \right]^{1/2}$$

f_c = frequency where 1/f detector noise power equals G-R white noise

f_u = upper cutoff frequency of the system

f_l = lower cutoff frequency of the system

$$f_c \leq 1 \text{ KHz}$$

$$f_l \approx 1 \text{ Hz}$$

$$f_u = 14.5 \text{ KHz}$$

<u>ITEM</u>	<u>CHANNEL 3</u>
$\alpha_{1/f}$	1.29
α_2 (See text)	1.4
α_{total}	1.8

Table 2.2-4 Degradation Factor

AVHRR OPTICAL TRANSMISSION

<u>Item Description</u>	<u>Reflectance or Transmittance</u>	
	<u>Channel 3</u>	<u>Channel 4</u>
Scan Mirror	0.95	0.95
Telescope Mirrors (2 @ 0.97 Ea)	0.94	0.90
Transp. Gold B.S. (D1)	0.88	0.82
Folding Mirror (M3)	0.96	0.95
Ge Focus Lens (L1)	0.819	0.846
Ch 3 (2 @ .905)		
Ch 4 (2 @ .920)		
Irtran II Windows	Inner	0.95
	Outer	0.95
Infrared Dichroic (D2) (OCLI Guaranteed Minimum)	0.81 (T)	0.92 (R)
Ge Aplanat Lens (L2, L3)	0.94	0.94
Bandpass Filters (F4)		0.80
Telescope Obscuration	0.94	0.94
System Transmission (Product of Above)	0.333	0.331

Values Given Above Are Measured PTM Values.

Table 2.2-5 Optical Transmission For Channels 3 and 4

since we are considering scenes which are several times larger than an IFOV. The equation and parameters used to calculate the degradation factors are given in Table 2.2-4. The degradation factor for the electronic noise has been calculated by determining the noise voltage level from the infrared detector and from measurements on the BBM and ETM.

The apparent electronic pick up was somewhat higher on the ETM than expected. The apparent, α_2 , on the ETM was about 1.6 and the total degradation factor α_T was about 2.1. Several areas of potential pickup were redesigned on the PTM and a lower α_2 is expected. A value for α_2 of 1.4 and a total α of 1.8 seems reasonably conservative.

The optical transmission, τ , was determined from the measured transmittance or reflectance value for each optical component in the PTM optical system. The value for each component is listed in Table 2.2-5 for both Channels 3 and 4. Assuming some optical degradation as in the solar channels we assign a value of

$$\tau_3 = .20$$

$$\tau_4 = .20$$

for use in the sensitivity calculations.

Table 2.2-6 gives the parameters used and the calculated NE Δ T. As shown, the spec. value will be achieved.

2.3 Channel 4

2.3.1 Detector

The detector chosen for use in the channel 4 (3.55 to 3.93 microns) is a photovoltaic indium antimonide photodiode built by Cincinnati Electronics Corp. The detector has a 0.007 inch square active area and is used in a configuration identical to the silicon detectors of channels 1 and 2. That is, it is a current source to an amplifier used as a current to voltage amplifier with a 16.4 M ohm feedback resistance. The detector is mounted in a Kovar housing like the channel 3 detector with the aplanat forming a hermetic seal.

Photovoltaic InSb has better noise characteristics with a small amount of reverse bias; therefore, a bias on the order of -30 millivolts is used. The exact bias is determined by C.E.C. during acceptance testing of the photodiodes. The method used for bias generation and control is discussed in the section of the electronics describing the channel 4 preamplifier. Table 2.3-1 summarizes the channel 4 detector parameters.

2.3.2 Channel 4 Sensitivity

The sensitivity of the InSb photodiode is specified in terms of its quantum efficiency, η , and its noise output for a given thermal background irradiance. Since noise sources external to the detector-amplifier system are significant (i.e., background flux and signal shot noise), this concept is most applicable. The

use of D* implies a situation where system and detector noise are the limiting factors.

The following analysis determines the sensitivity of the system in terms of the detector output current for both the noise sources and the NEAT. The initial section determines the system noise. Following that are sections which define the detector output for the NEAT, effects of an albedo signal in this spectral region, and postamp gain and digitizer effects on the system sensitivity.

2.3.2.1 System Noise

For Channel 4 there are four noise sources. These are:

1. Background flux noise
2. Preamp noise
3. Signal shot noise
4. Stray pickup

These are discussed separately below. The stray pickup is handled as a degradation to the total noise.

In the nominal 3.55 to 3.93 micron band, a 300K background scene causes a signal current out of the detector given by:

$$I_{bs} = K A q n Q_B \quad \text{Eq. 1}$$

K = optical filtering factor

n = quantum efficiency (average in band)

q = 1.6×10^{-19}

A = detector area - $2.98 \times 10^{-4} \text{ cm}^2$

Q_B = background photon flux

This assumes that the filter is cold and mounted on the detector.

The optical filtering factor accounts for the fact that when the detector is mounted in the system on a cold patch, the incidence

Table 2.3-1 Channel 4 Detector Parameters

Spectral Band	3.55 to 3.93 Micron
Type of Detector Source	Indium Antimonide Cincinnati Electronics
Operating Temperature	105K
Operating Mode	Photovoltaic
Sensitive Area	0.007" Square
Quantum Efficiency in Spectral Band	0.75 Minimum
Background Noise Level	Maximum 10% over Theoretical Level
Bias Voltage	~ 30 mvolts
Preamplifier Gain	16×10^6

angle, θ , of the background is limited by the cooler windows and reduced by the transmissions of the inner window (τ_w), the band-pass filter (τ_F), and the aplanat (τ_a).

$$K = \tau_F \cdot \tau_w \cdot \tau_a \cdot \pi \sin^2 \theta \quad \text{Eq. 2}$$

For $\tau_w = \tau_F = \tau_a = .85$ and $\theta = 75^\circ$

$$K = 1.80 \text{ ster}$$

For a 300K scene, the photon flux, Q_B , in the nominal spectral band is 3.22×10^{14} photon cm^{-2} ster^{-1} sec^{-1} . Using $n = 0.75$, we have

$$I_{bs} = 2.07 \times 10^{-8} \text{ amp}$$

The noise in this background signal is given by:

$$i_b = \sqrt{2q I_{bs} \Delta f} \quad \text{Eq. 3}$$

The bandwidth, Δf , is 14.5 KHz and so

$$i_b = 9.80 \times 10^{-12} \text{ amp rms.}$$

The second noise source (the preamp) really consists of two sources. The input transistor contributes noise as does the feedback resistance which contributes Johnson noise. Noise data was measured by G.E. Sonnek on a preamp similar to that required for Channel 4. His measured data indicated that with a 16 Mohm feedback a total rms preamp noise of 4.42×10^{-12} amp is obtained in a 14.5 KHz bandwidth.

The third noise source, the signal shot noise, depends on signal level. Since the NEAT spec is at 300K, this is the scene level of interest. The maximum scene to be viewed is a 320K scene.

The detector output current due to the scene is given by:

$$I_s = N_s T R_\lambda \quad \text{Eq. 4}$$

where N_s = scene radiance

T = system thruput

R_λ = detector responsivity (amp/watt)

The system thruput T is given by:

$$T = A\Omega\tau \quad \text{Eq. 5}$$

where A = collecting area

Ω = solid angle of view

τ = system transmission

For AVHRR, A is 324 cm^2 , Ω is 1.72×10^{-6} ster, τ is about 0.33; therefore, T is $1.83 \times 10^{-4} \text{ cm}^2$ ster. Using the minimum specified quantum efficiency of 0.75 gives a R_λ of 2.26 amp/watt. The radiance of a 300K scene in the nominal spectral band is $1.70 \times 10^{-5} \text{ w/cm}^2$ ster. The detector output then, with no albedo contribution, using equation 4, is:

$$I_s = 7.03 \times 10^{-9} \text{ amp}$$

The rms noise, i_s , is

$$i_s = 5.71 \times 10^{-12} \text{ amp rms}$$

The last source, stray pickup is a source which is minimized by design, but never entirely eliminated. We will assume a 1.60 degradation in the TOTAL system noise performance since ETM and PTM noise degradation appeared to be less in this channel than in channel 3. This includes a 4% 1/f noise contribution. The total

noise current, i_n , under these conditions is:

$$i_n = 1.6 \left[(9.80)^2 = (4.42)^2 + (5.71)^2 \right]^{1/2} \times 10^{-12} \text{ amp Eq. 6}$$

$$i_n = 1.95 \times 10^{-11} \text{ amp rms.}$$

2.3.2.2 System Output for NEAT

The detector output caused by a 0.12K scene change at 300K is determined as follows. Using the Lowan & Blanch "Tables of Plancke Radiation and Photon Functions", we find that the photon flux of 301K scene in our band is 3.36×10^{14} photons cm^{-2} ster^{-1} sec^{-1} . For a 300K scene it is 3.22×10^{14} . The change in flux due to a 1.0K temperature change in the scene is then 1.37×10^{13} photon cm^{-2} ster^{-1} sec^{-1} K^{-1} . For a 0.12K NEAT, the Noise Equivalent Photon Flux is:

$$\text{NEF} = 1.64 \times 10^{12} \text{ photon cm}^{-2} \text{ ster}^{-1} \text{ sec}^{-1}$$

The noise equivalent flux on the detector is simply:

$$\text{NEF}_D = T \cdot \text{NEF}$$

$$\text{NEF}_D = 1.83 \times 10^8 \text{ photon sec}^{-1}$$

The detector output current change caused by the scene temperature change is:

$$I_{\text{NEF}} = n q (\text{NEF}_D)$$

$$I_{\text{NEF}} = 2.19 \times 10^{-11} \text{ amp}$$

By definition the NEAT of the system is the ΔT which causes a I_{NEF} equal to the total system rms noise i_n . This analysis then indicates that with the nominal spectral band, an NEAT of 0.12K is achievable with a S/N ratio of

$$(S/N)_4 = \frac{2.14 \times 10^{-11}}{1.95 \times 10^{-11}} = 1.12:1$$

The effective NEAT is expected to be .107K as shown in Table 2.3-2

Table 2.3-2 Channel 4 Sensitivity Parameters

Collection Optics	8.00" Diameter
System Transmission	0.20
I FOV	1.3 mrad
Bandwidth	14.5 KHz
Background Temp	300K
Degradation Factor	1.6
Quantum Efficiency	0.75
Specified NEAT	0.12K at 300K
Calculated NEAT	0.107K at 300K

2.3.2.3 Albedo Radiance

In this spectral channel, the sunlight reflected from the Earth Scene contributes to the total scene radiance. Using Thekaekara's table of solar irradiance we find that a 1.0 albedo scene at noon at the subsatellite point has a reflected radiance in the nominal spectral band of $1.06 \times 10^{-4} \text{ w/cm}^2 \text{ ster}$. According to NASA personnel, the maximum actual albedo of a scene in this band is about 0.10. Further, since the spacecraft is never over a noon nadir, this value of reflected radiance is reduced by $\sin 67^\circ$ (which is the maximum orbit normal to sun angle). These factors make the maximum reflected solar radiance $9.76 \times 10^{-6} \text{ w/cm}^2 \text{ ster}$. If we assume no atmospheric attenuation, this is the albedo contribution on the day side of the orbit.

The maximum scene temperature is specified as 320K. The spectral radiance of this scene is $3.76 \times 10^{-5} \text{ w/cm}^2 \text{ ster}$. The albedo radiance is then about 25% of the maximum thermal radiance, and the total scene radiance for a daylight 320K scene is $4.74 \times 10^{-5} \text{ w/cm}^2 \text{ ster}$, if the maximum albedo is 0.10 in this band.

2.3.2.4 Post Amp Gain and Digitizer Effects

The post amp gain is determined by the output voltage range and the maximum scene radiance level. As discussed previously, the maximum scene radiance for a 320K scene is $3.76 \times 10^{-5} \text{ w/cm}^2 \text{ ster}$. This causes a detector output of $2.04 \times 10^{-8} \text{ amp}$

(using equation 4). With a 16 Mohm feedback, the preamp output is a 0.326 volts. If 5.9 volts represents the output voltage swing for a full to zero radiance change, then the post-amp gain must be 181.

Since the A-D converter digitizes to 10 bits (1024 levels), each level corresponds to:

$$\frac{6.39375}{1823} = 6.25 \text{ m volts}$$

The detector current change caused by the NEAT is 2.19×10^{-11} amp. At the digitizer input this is:

$$2.19 \times 10^{-11} \times 16 \times 10^6 \times 18.7 = 6.5 \text{ m volts}$$

Thus each data bit will be about the same as the estimated noise level of this channel.

3.0 OPTICAL DESIGN

3.1 General Description

The optical configuration of the AVHRR is shown in Figure 3.1-1 (the rotating scan mirror is not illustrated for simplicity). The energy from the scene is collected by an 8.0 inch diameter clear aperture afocal telescope, the primary mirror being the entrance aperture. In the afocal design, the secondary mirror recollimates an incoming collimated beam with the angular spread of the exit beam being increased over that of the input beam by the ratio of diameters of the input to the exit beams.

Dichroic No. 1 transmits Channels 1 and 2 (solar channels) and reflects Channels 3 and 4 (infrared channels). The latter two channels are then partially focused by a germanium lens doublet (L1) which is axially adjustable for focusing. The beam passes through a window on the cooler housing and a window on the gold box (or low emissivity shield), the windows being used to provide a vacuum seal for bench testing the cooler and to prevent moisture from the multilayer getting onto a 105 Kelvin patch-detector assembly respectively. Channels 3 and 4 are separated by dichroic No. 2 which is mounted on the patch along with the detectors, bandpass filters and aplanat lenses (L2 and L3). Dichroic D2 is actually the Channel 3 bandpass filter designed for the 45° incident beam and is used also as the dichroic since it reflects the Channel 4 energy. The bandpass filters are multilayer interference type filters which provide the spectral response required by the AVHRR specification. Mounting of the two infrared detectors and dichroic No. 2 in a precision-machine mounting structure simplifies registration of these two channels to each other.

M1 MIRROR, TELESCOPE PRIMARY
 M2 MIRROR, TELESCOPE SECONDARY
 D1 DICHOIC, THIN GOLD ON GLASS
 M3, M4 FLAT FOLDING MIRRORS
 L1 INFRARED FOCUS LENS
 W1, W2 IRTAN II WINDOWS
 D2 INFRARED DICHOIC & CHANNEL 3 FILTER
 F1, F2 F3 BANDPASS FILTERS
 L2, L3 INFRARED APLANAT LENSES
 L4 FOCUS ACHROMAT LENS ASSY, CH. 1
 L5 FOCUS ACHROMAT LENS ASSY, CH. 2
 D3 BEAMSPLITTER, INCONEL

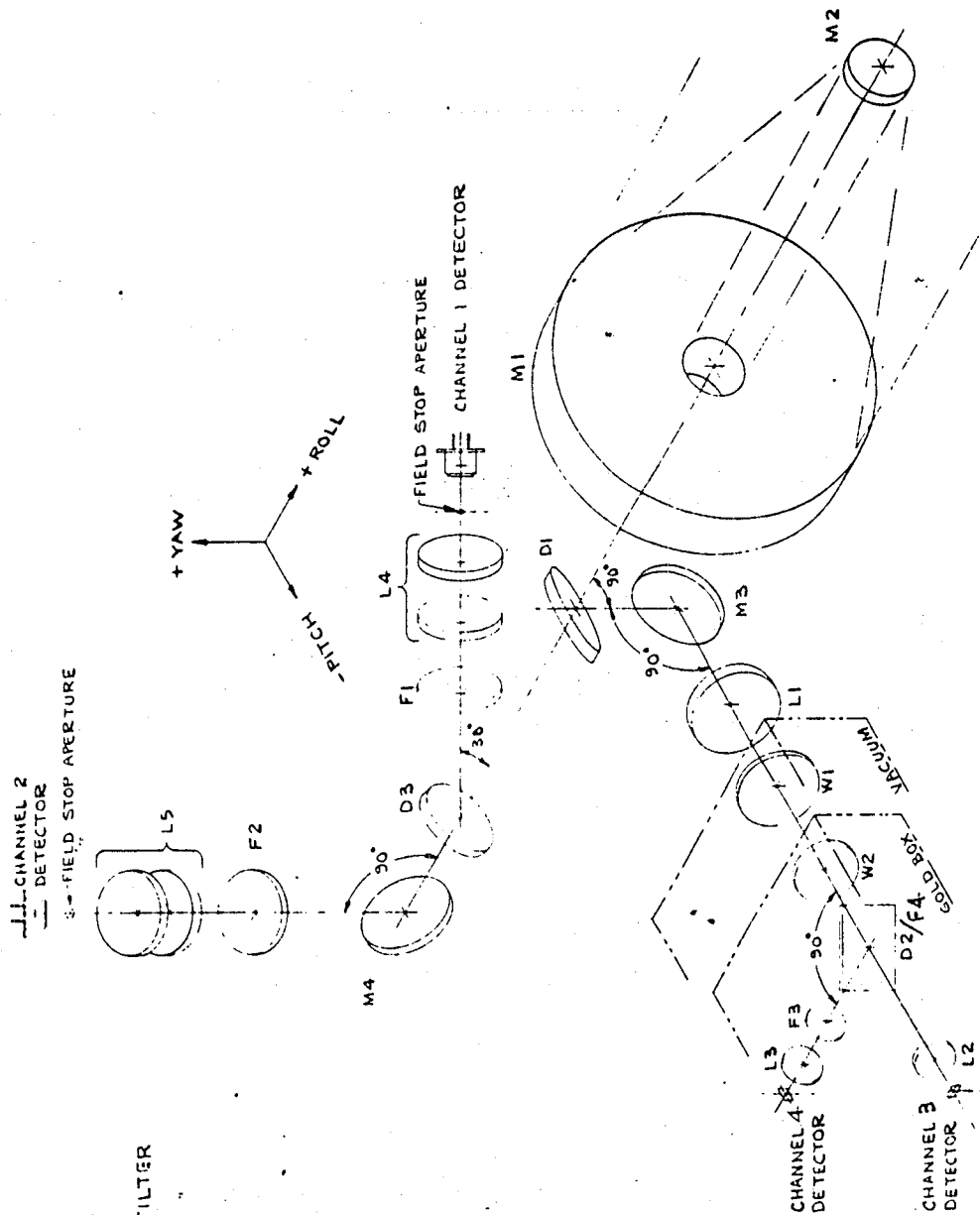


Figure 3.1-1 AVHRR OPTICAL LAYOUT

The beam which is transmitted by dichroic No. 1 is subsequently separated by beamsplitter D3 which reflects Channel 1 and transmits Channel 2. Mirror M4 and beamsplitter D3 are used to minimize polarization. Elements F1 and F2 are the spectral shaping filters for Channels 1 and 2 respectively; they both have flat faces on both sides and produce no focusing effect since they are in the collimated beam from the telescope. Lens assemblies L4 and L5 are re-focusing elements which form an image of the scene at the "field stop aperture" (i.e. an aperture plate located in the final focal plane of the system which contains an opening that determines the field of view for these two channels). The energy which passes through the aperture opening is then detected by silicon detectors are mounted in TO-5 housing with a flat glass window hermetically sealed to the housing).

The optical performance requirements are summarized in Table 3.1-1. In addition to the instantaneous field of view (IFOV) requirement, ITT imposed a larger, extended FOV on the optical subcontractor. That is, the optical system is designed so that the minimum MTF values given in Table 3.1-1 are obtained over a larger field of view than would be required by the IFOV. The reason for this is so that the detectors can be moved individually in their respective focal planes in order to register all channels simultaneously without losing MTF performance. In Channels 3 and 4, only the focus lens assembly L1 is designed for the EFOV since Channel 3 will be used as the reference channel (i.e. it will be located on the optical axis and the other detectors will be adjusted until aligned with it). Since the telescope operates over all four channels, it must cover the EFOV in all channels. The spatial frequencies listed in Table 3.1-1 correspond

to the subsatellite target sizes given in the AVHRR specification, i.e., 385 cycles/radian corresponds to a 0.59 nautical mile ground target, etc. A complete detailed description of the optical sub-assembly requirements is given to ITT-A/OD Spec. No. 8007907. A more detailed description of the optical system and components and the calculated performance is given in the following sections.

The initial design and fabrication of the development models of AVHRR (BBM, ETM, PTM) was performed by Ferson Optics Div. of Bausch and Lomb. The Flight Model optics are being obtained from Perkin Elmer, Costa Mesa, California.

3.2 Scan Mirror

The scan mirror configuration is shown in Figure 3.2-1 (ITT-A/OD Dwg. No. 8007928). It is made using a waffle or egg-crate construction to reduce weight while maintaining rigidity. The basic material is HP21 beryllium with a precision elastic limit of 4000 PSI minimum. After machining of the blank it is electroless nickel plated to provide a good polishing surface. After polishing to the specified flatness, the flat surface is aluminized and overcoated to give a high reflectance in all four spectral channels. The back surface is gold plated for thermal reasons. The scan mirror is mounted to the drive motor shaft and dynamically balanced as described in Section 4.0. The scan mirrors are being procured from Applied Optics Center, Burlington, Massachusetts.

3.3 Telescope Design

The telescope assembly is shown in Figure 3.3-1 (ITT Drawing #8009383). The telescope collects energy from an infinitely distant source (i.e., the earth) that subtends a solid angle of one IFOV which is located within the extended FOV. The diameter of the

OPTICAL PERFORMANCE REQUIREMENTS

	<u>CH 1</u>	<u>CH 2</u>	<u>CH 3</u>	<u>CH 4</u>
INSTANTANEOUS F.O.V. $\left(\begin{smallmatrix} \text{EDGE} \\ \text{OF SQ} \end{smallmatrix} \right)$	1.31 M.R.	1.31 M.R.	1.31 M.R.	1.31 M.R.
SPECTRAL BAND (μm)	0.58-0.68	0.725-1.1	10.5-11.5	3.55-3.93
EDGE WIDTH OF SQ. FIELD STOP	0.0238"	0.0238"	0.0068"	0.0068"
EXTENDED FOV (RADIUS)	1.1 M.R.	1.1 M.R.	2.2 M.R.*	2.2 M.R.*

TELESCOPE--AFOCAL CASSEGRAIN (TWO COAXIAL, CONFOCAL PARABOLOIDS)

TELESCOPE PRIMARY MIRROR--APERTURE STOP & ENTRANCE PUPIL

DIAMETER OF ENTRANCE PUPIL 8.00 \pm 0.01 INCHES

DIAMETER OF EXIT, AXIAL TELESCOPE BUNDLE 1.00 INCH

MAX. SECONDARY OBSCURATION (INC. BAFFLE) 2.00 INCHES

SPATIAL FREQUENCY (ALL CHANNELS)	<u>CYCLES</u> <u>RADIAN</u>		<u>MINIMUM SYSTEM M.T.F.</u>			
	<u>CH 1</u>	<u>CH 2</u>	<u>CH 3</u>	<u>CH 4</u>		
19	0.96	0.96	0.96	0.96		
257	0.91	0.93	0.90	0.91		
385	0.88**	0.90	0.86**	0.88**		

TELESCOPE MIRROR MATERIAL (OWENS-ILLINOIS) "CERVIT"

CHANNEL REGISTRATION SAME AS NASA/GSFC SPEC.

* APPLIES TO FOCUS LENS ONLY.

**DESIGN GOAL MTF IS 90%

Table 3, 1-1 - Summary of Optics Requirements

[illegible]

ORIGINAL PAGE 1
OF POOR QUALITY

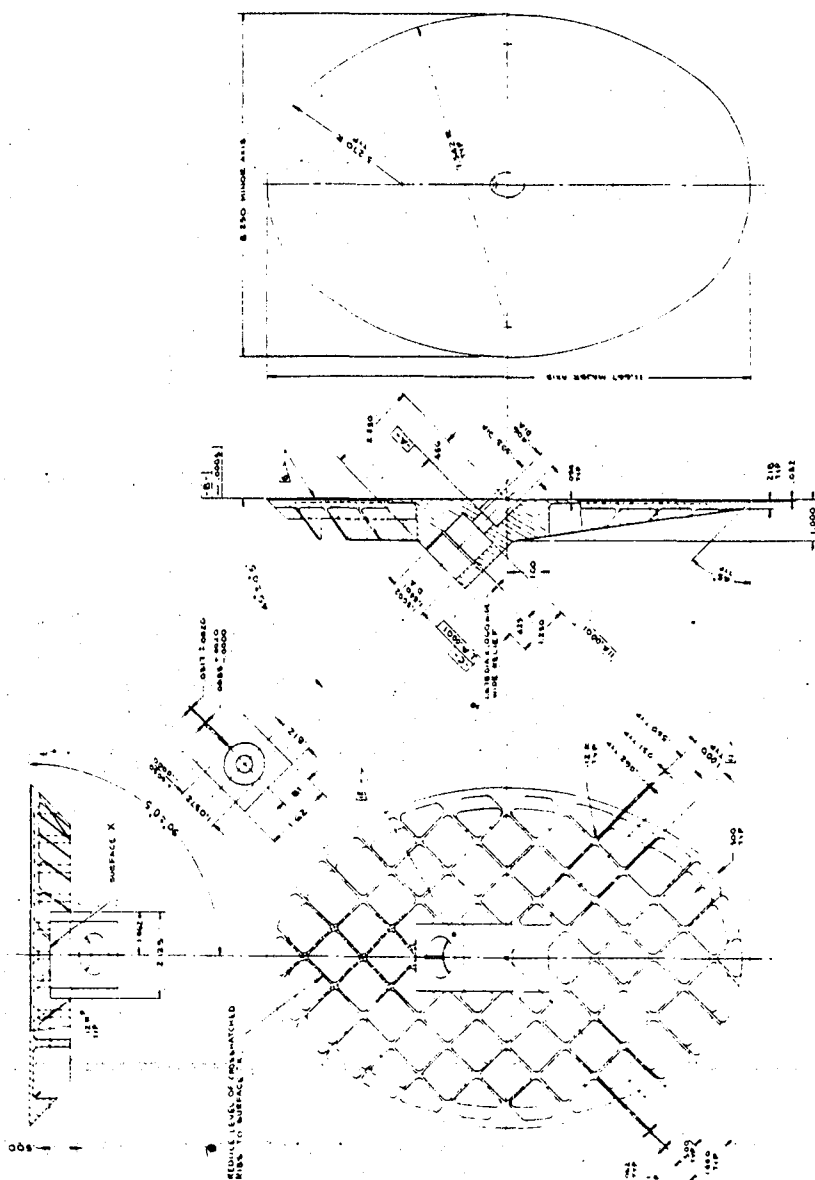


Figure 3.2-1

[illegible]

entrance beam into the telescope is 8.00 inches and the diameter of the exit beam, which leaves through the center hole of the primary mirror, is 1.0 inch. This reduction in beam diameter caused a corresponding increase in angular extent, i.e. the IFOV of 1.31 mr (milliradian) by 1.31 mr into the telescope leaves with 10.5 mr by 10.5 mr beam spread. The largest field angle over which the telescope must operate is the extended FOV which has a 4.4 mr diameter in object space (without the extended FOV, the telescope would have to cover a field of 1.85 mr).

The telescope consists of two confocal, coaxial paraboloidal mirrors which are called the primary (large) and secondary mirrors. The primary mirror clear aperture is both the aperture stop and entrance pupil of the optical system. It has an 8.00 inch diameter clear aperture and a focal length of 10 inches giving it an optical speed of 1.25. The intervertex distance (the axial separation of the primary and secondary mirrors) is 8.75 inches. This gives a 1.0 inch diameter beam reflected by the secondary for a collimated, axial beam into the telescope. Because of the extended field of view, the clear aperture of the secondary mirror must be a minimum of 1.040 inches. In order to re-collimate the beam, the secondary mirror must have the same optical speed of the primary mirror, i.e. 1.25. The focal length of the secondary mirror is therefore 1.25 inches.

A conical baffle is located around the secondary mirror to prevent radiation within the EFOV from getting past the secondary mirror and into the aft optics (i.e. the optical components behind the telescope). The telescope barrel is made of invar metal which has a very low coefficient of thermal expansion and therefore maintains

mirror alignment over the temperature range. The mirrors are made of Cervit (made by Owens-Illinois) and has a low coefficient of thermal expansion. After polishing, the mirrors are coated with a high reflectivity coating of aluminum which is protected by an overcoat layer of silicon monoxide; this coating is used because of its uniform spectral reflectance in all four channels. Other mechanical features of the telescope are described in Section 4.0.

A unique feature of the AVHRR telescope assembly is the absence of any coma or astigmatism. Thus the angular alignment of the reflective, reimaging optics following the telescope is not critical with respect to the telescope exit beam. A tolerance analysis of all optical elements was performed by Ferson Optics which showed that the only sensitive elements are the primary and secondary mirrors (i.e. the alignment with respect to each other). The optic subcontractor not only fabricates the mirrors (as well as all lens elements) but assembles and aligns the mirrors in the telescope housing assembly shown in Figure 3.3-1. The primary mirror is first potted in place and then the secondary mirror is adjusted by positioning the entire spider support in an annular ring at the front of the telescope). The performance of the completed telescope is checked as a subassembly after potting has cured.

3.4 Channels 1 and 2 Lens Design

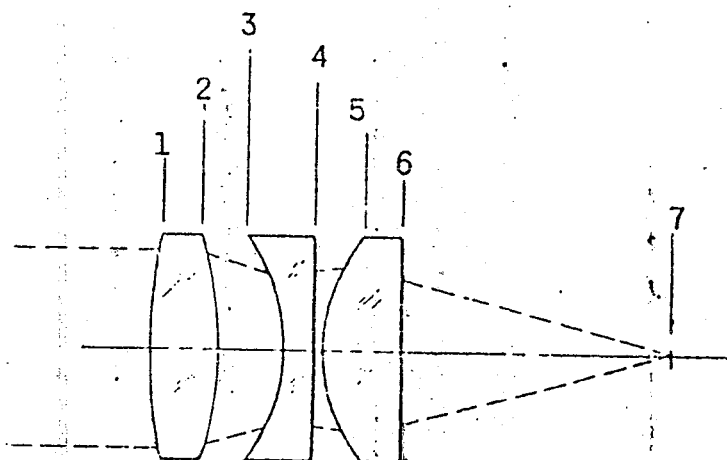
The reimaging optics for Channels 1 and 2 are AR coated lenses consisting of three elements. This triplet design is shown in Figure 3.4-1 which gives the radii of curvatures, axial thickness of each element, axial spacing, minimum half apertures for each lens surface

and the material. The lens materials were selected to control chromatic aberrations over the wide spectral bands, especially channel 1 (0.55 to 0.90 μm). The triplet design has more than adequate MTF performance over the extended FOV and has high transmission and low manufacturing sensitivity. It has been possible to achieve a single design which can be used for both channels 1 and 2 even at the relatively fast effective f/number.

The focal plane is located at position No. 7 in Figure 3.4-1. The field defining aperture (or "field stop") is located at this position; the size of the opening is 0.0238 inch by 0.238 inch and produces the 1.31 mr by 1.31 mr field of view in object space in Channels 1 and 2.

The optical performance data for Channels 1 and 2 is summarized in Table 3.4-1. The optical design was performed by Ferson Optics under subcontract to ITT-A/OD. Preliminary design was carried out using computers at Ferson's plant while the MTF data for the final design was obtained using the Grey Diffraction MTF Program on a CDC 6600 computer. Five wavelengths were used for evaluation for each channel and MTF data was determined for best alignment (on-axis) and worse alignment (at the edge of the extended FOV) for all channels. Note that the calculated MTF for 385 cycles per radian* at the edge of the EFOV is 97.4% for Channel 1 and 96.9% for Channel 2 and is much better on-axis. The required value at this optical

*385 cycles per radian corresponds to 0.831 line pairs per mm in the focal plane and to 0.5 nautical mile target on the earth's surface.



		(1)	(2)	
NO	RADIUS MM	THICK MM	HALF APT, MM	MATL.
1	80.24	10.00	17.00	PSK 53
2	-51.04	9.03	16.59	
3	-28.70	4.50	13.33	SF 18
4	420.65	1.00	13.57	
5	26.15	11.38	13.92	PSK 53
6	-1218.2	38.29	12.55	
7	IMAGE			

NOTE: 1) THICKNESS BETWEEN SURFACES ON AXIS
 2) HALF APT. SHOWN ARE FOR EFOV EDGE RAY.

DESIGN UNCHANGED BY MODS 6, 7 AND 8.

Figure 3.4-1 AVHRR Triplet Design CH 1 & 2

AVHRR OPTICAL SYSTEM MTF (PERCENT)

ON AXIS

	CH 1		CH 2		CH 3		CH 4	
CYCLES/RAD	SPEC	CALC	SPEC	CALC	SPEC	CALC	SPEC	CALC
19	96	>99	96	>99	96	>99	96	>99
257	93	98.7	91	>99	90	98	91	98.5
385	90	98.2	88	>99	86	97	88	97.7

FIELD EDGE

19	96	>99	96	>99	96	>99	96	>99
257	93	98.4	91	98.2	90	97	91	98
385	90	97.6	88	97.3	86	95	88	97

EFOV EDGE

19	96	>99	96	>99	96	>99	96	>99
257	93	98.2	91	97.9	90	96	91	96
385	90	97.4	88	96.9	86	94	88	94

Table 3.4-1 Calculated MTF Performance

frequency for Channel 2 is 90% and for Channel 1 it is 88% with a design goal of 90% for both channels (see Section 3.1). The high optical performance achieved in the design permits comparatively easy manufacturing tolerances for the lens elements and tolerable mechanical alignment tolerances (see Section 3.6 for tolerance analysis results).

3.5 Channel 3 and 4 Lens Design

The reimaging optics focus the energy coming out of the telescope onto as small a detector as possible. The optics consist of a focus lens assembly (doublet) made of germanium for Channels 3 and 4; the index of refraction of germanium does not change significantly between 4 and 12 μm . The slight difference in index is taken care of by locating each detector at the corresponding focal plane. The focus lenses are axially adjustable to obtain optimum focus by means of an adjustment external to the radiant cooler; this also permits use of a smaller opening in the cooler which lowers the thermal input thereto.

A third germanium lens, called an aplanat, is used just in front of each detector to do the final focusing of the beam (an aplanat introduces no additional coma or spherical aberration). The best signal-to-noise ratio is obtained by using the smallest possible detector area since detector noise depends somewhat on area in Channels 3 and 4. The detector area can be found from the Abbe sine law (see for example, R. C. Jones, Applied Optics, Vol. 1, p. 607, 1962 or D. Marcuse, Applied Optics, Vol. 10, p. 499, 1971).

$$A_o \theta^2 = A_d \pi \sin^2 \mu$$

where A_o = area of collecting optics = $\frac{\pi}{4} D_o^2$

θ = width of square IFOV

A_d = area of square detector = w_d^2

μ = maximum incidence angle of an axial ray at the detector.

This can be simplified to $D_o \theta = 2 w_d \sin \mu$. Using the sine definition of f-number, i.e., $f_n = \frac{1}{2 \sin \mu}$ this becomes $w_d = f_n$

$D_o \theta$. Since θ has been specified ($\theta = 1.31 \text{ m r}$) and we have chosen $D_o = 8.0$ inches, we can only minimize f_n (maximize μ).

About the maximum feasible value of μ is 50° ; this gives $f_n = 0.653$ and $w_d = 0.0068$ inch. The sensitive area of the infrared detector is the field defining "stop" in Channels 3 and 4; in both infrared channels the edge width of the square detector is nominally $0.0068 \text{ inch} \pm 0.0004 \text{ inch}$. If we note that $w_d/\theta = \text{EFL}$ (effective system focal length), then

$$f_n = \frac{\text{EFL}}{D_o}$$

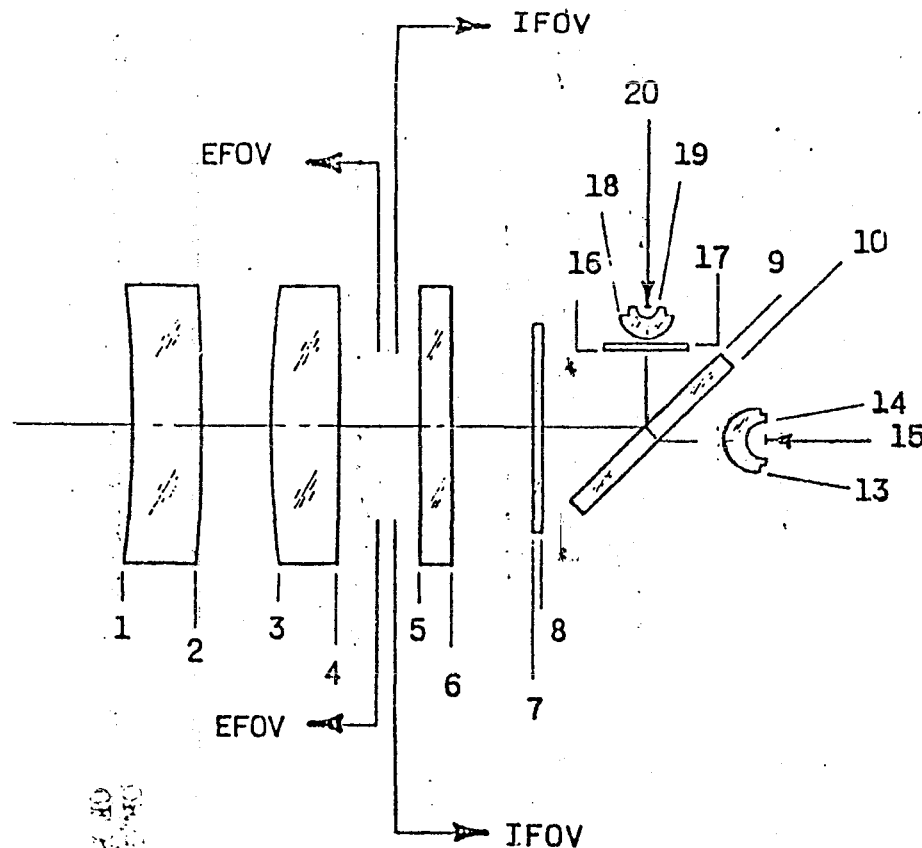
which is the common definition of f-number.

The aplanat has the effect of optically magnifying the size of the detector by the refractive index (about 4.0 for germanium at $12 \mu\text{m}$) so that the focus lens "sees" a detector image 0.0272 inch on an edge. Since the focus lens sees an angular field spread of 10.48×10^{-3} radians from the telescope (Channel 3), it has a focal length of about 2.6 inches. The speed of the focus lens is also about 2.6 since the beam is 1.0 inch in diameter (neglecting field spread); the actual clear aperture diameter of the focus lens is large enough to accept the beam spread plus some allowance for mechanical tolerance.

The detail design information for the Channel 3 and 4 re-imaging optics is given in Figure 3.5-1. An enlarged scale drawing of the optical elements mounted inside the radiant cooler is shown in Figure 3.5-2. The sensitive area of the Channel 3 infrared detector is located at position 15 and that of the Channel 4 detector at position 20. The position of the aplanat lens is held very accurately with respect to the detector sensitive area by mounting the aplanat directly to the detector housing. This is shown in Figure 2.2-2 (ITT-A/OD Drawing 8008791), the housing for the Channel 3 infrared detector. The aplanat lens also serves as the window for the housing since it is hermetically bonded in place. The same type of construction has been successfully used by the same detector vendor on the infrared detectors for other programs.

The MTF performance of the infrared bands for both on-axis and edge of the EFOV is given in Table 3.1-1. The MTF data given in the table includes the effects of diffraction. Since Channel 3 is used as the reference channel for registration, the detector-aplanat assembly for this channel is positioned on-axis. Achievement of the 86% MTF requirement for this channel is therefore not expected to present a problem. The calculated MTF values for both infrared channels is appreciably higher than the required values imposed on the optical vendor by ITT-A/OD. Tolerance analysis studies indicate that the required performance is achievable without undue difficulty. The axial astigmatism in Channel 3 which is caused by the tilted dichroic (D2) was analyzed and was found to be masked by diffraction effects at these long wavelengths.

NO.	RADIUS M M	THICK MM ON AXIS	HALF APT MM	MAI L
1	-185.15	10.00	19.66	G E
2	-294.56	10.00	20.54	
3	166.29	10.00	22.15	G E
4	-3238.3	4.32	21.53	
5	--	4.78	15.87	IRTRAN
6	--	17.40	15.35	2
7	--	1.57	11.10	IRTRAN
8	--	15.77	10.93	2
9	--	2.54	--	G E
10	--	7.60	--	
11				FILTER
12				DELETED
13	4.58	3.00	4.43	G E
14	2.80	2.48	2.42	
15	IMAGE PLANE CH 3			
9	--	11.5	--	
16	--	1.01	4.18	G E
17	--	0.25	4.12	
18	3.90	3.00	3.52	G E
19	1.93	1.57	1.51	
20	IMAGE PLANE CH 4			



AVHRR CH 3 & 4
ELEMENT PRESCRIPTION

Figure 3.5-1 Infrared Reimaging Optics Data

3.6 AVHRR Tolerance Analysis

A tolerance analysis was run on the AVHRR Optical Design using a Ferson Optics computer program. The program provides information of changes in the OPD* (in Raleigh units) due to perturbation of optical design parameters about their nominal values. From the OPD variations due to perturbations, the mechanical tolerances for manufacture can be determined. The data presented here is for individual elements as well as groups of elements which are mounted on subassemblies. Figures 3.6-1 and 3.6-2 show concentricity and parallelism for group data in schematic presentation. Mirrors and dichroics are not shown but must be considered when distributing the parallelism and concentricity tolerances. A summary of the recommended tolerances follows.

3.6.1 Summary of Mechanical Tolerances**

Channel 1 and 2 - Focus Lens

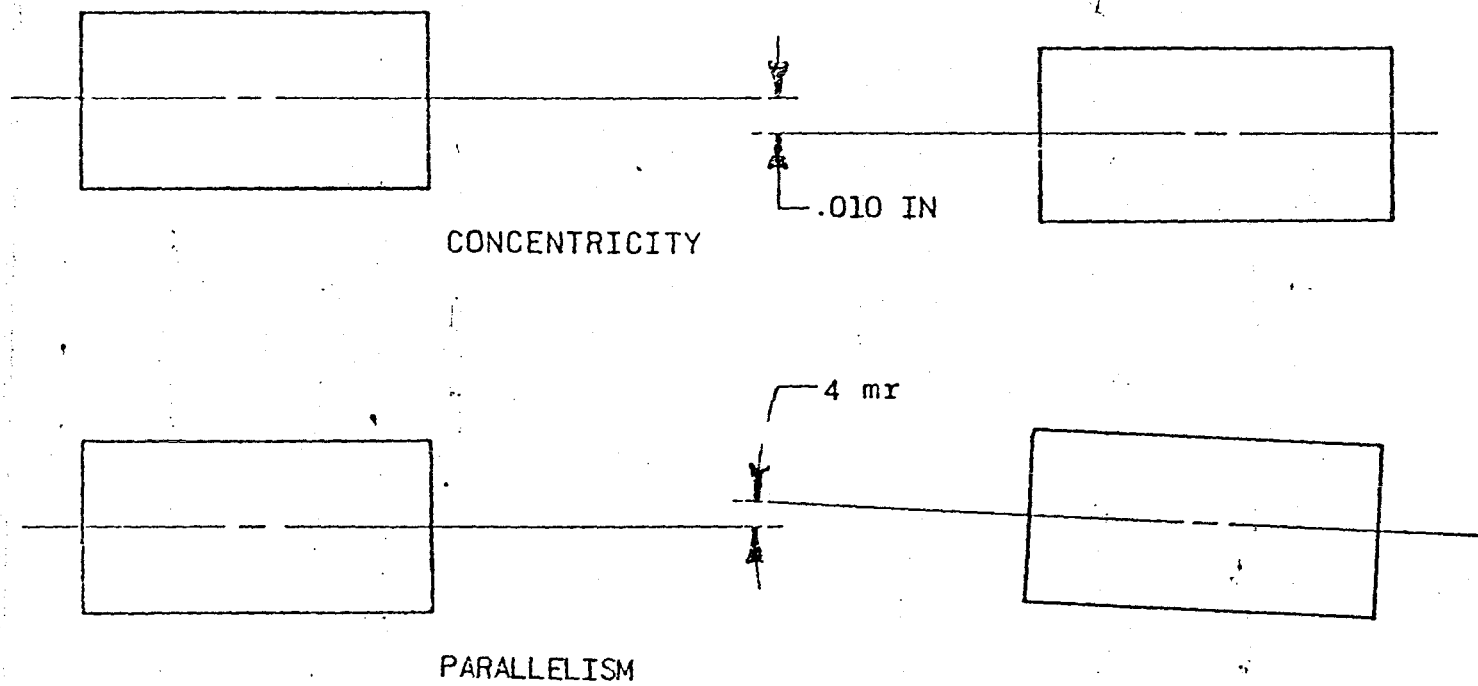
- a. Focus Lens Diameter - OD + 0.000 -0.002
- b. Focus Lens Cell - ID +0.002 -0.000
- c. Minimum Clearance for Thermal Expansion - 0.001
- d. Triplet concentricity relative to telescope optical axis - 0.010
- e. Triplet parallelism relative to telescope optical axis - 4 mr

* OPD = Optical path difference.

** Linear dimensions in inches, angles in milliradians (mr).

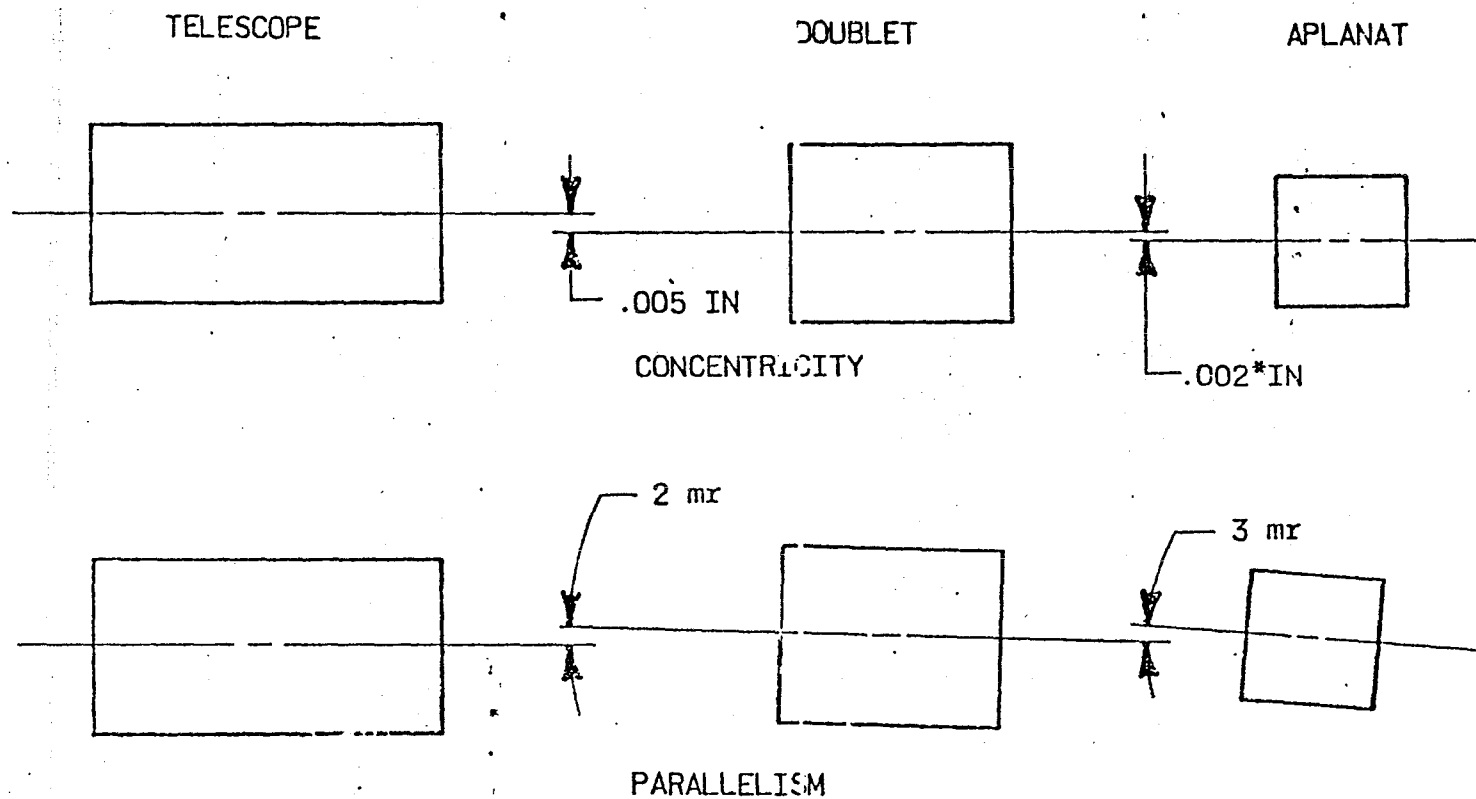
TELESCOPE

TRIPLET



CHANNEL 1 & 2 TOLERANCE DATA
FOR ELEMENT GROUPS

FIGURE 3.6-1



*0.002 INCH IS TOL. OF APLANAT WITH RESPECT
TO DETECTOR CENTER; TOLERANCE INDICATED
SHOULD BE 0.015 INCH.

CHANNEL 3 & 4 TOLERANCE DATA
FOR ELEMENT GROUPS

FIGURE 3.6-2

f. Spacer Data

Lenses	16-17*	17-18*
Length	± 0.002	± 0.003
ID	± 0.001	± 0.001
OD	$+0.000 -0.002$	$+0.000 -0.002$

*See Figure 3.4-1.

Channels 3 and 4 - Focus Lens

- a. Focus Lens Dia. - OD $+0.000 -0.002$
- b. Focus Lens Cell - ID $+0.002 -0.000$
- c. Minimum clearance for thermal expansion - 0.001
- d. Doublet concentricity relative to telescope optical axis - 0.005
- e. Spacer Data
 - Length - ± 0.003
 - ID - ± 0.002
 - OD - $+0.000 -0.002$

Channels 3 and 4 - Aplanat

- a. Outsider Diameter Aplanat - $+0.000 -0.002$
- b. Diameter aplanat cell - $+0.002 -0.000$
- c. Concentricity of cell diameter relative to detector axis - 0.002
- d. Mounting Surface deviation relative to detector surface - ± 0.001

3.6.2 Surface Quality for Filters, Beamsplitters

	Ch. 1 and 2	Ch. 3 and 4
a. Scratch	60	80
b. Dig	40	50
c. Flatness	10 fr	2 fr
d. Irregularity	1 fr	2 fr
e. Wedge	1 mr	1 mr

3.6.3 Mechanical Adjustment Data (Inches)

	Back Focus	Focus Adjust	X-Y Adjust
Channel 1	1.512	± 0.050	± 0.040
Channel 2	1.515	± 0.050	± 0.040
Channel 3	0.0976 ± 0.002	$\pm 0.050^*$	± 0.040
Channel 4	0.062 ± 0.002	$\pm 0.050^*$	± 0.040

*An additional adjustment of 0.0606 for Channel 3 and 0.0343 for Channel 4 toward the focus lens is required for room temperature testing.

Position of Channel 4 aplanat relative to Channel 3 aplanat - ± 0.002 .

3.7 Dichroics, Beamsplitters and Cooler Windows

Dichroics D1 and D2, Beamsplitter D3, the Irtran cooler windows and the Channel 3 filter are being obtained from OCLI (Optical Coating Labs, Inc., Santa Rosa, Calif.). The function of the two dichroics and the beamsplitter is to separate the optical beam exiting the telescope into four separate beams before final focussing in each of the four channels. Dichroic D1 consists of a thin "Transparent" coating of gold evaporated onto a flat glass substrate. This type dichroic reflects

radiation in Channels 3 and 4 with approximately 82% efficiency and transmits Channels 1 and 2 with approximately 75% and 70% efficiency, respectively. It does polarize the energy in Channels 1 and 2 and is the reason why an additional folding mirror (M3) is used. More complete details of this dichroic are given in ITT-A/OD Spec. No. 8009262.

Dichroic D2 reflects Channel 4 radiation and transmits Channel 3. This dichroic is the bandpass filter for Channel 3 which is designed for a 45° incidence angle and the focused optical beam when cooled to 105 Kelvin. The "filter-dichroic" reflects energy in the 3.5 to 4.0 μm spectral band. The reflectance for Channel 4 radiation is 90% minimum and the transmittance for Channel 3 radiation is 75% minimum. The substrate material for the dichroic is optical grade germanium; the thickness was made as large as feasible to minimize bending when it is cooled to operating temperature. More complete details of this dichroic are given in ITT-A/OD Spec. No. 8008792.

A detail layout drawing showing the extreme optical rays at Dichroic D1, Beamsplitter D3 and folding mirrors M3 and M4 is shown in Figure 3.7-1. The angle of beamsplitter D3 with respect to the optical axis was minimized in order to reduce polarization effects. Since the spectral bands of Channels 1 and 2 overlap each other, D3 cannot be a dichroic beamsplitter but must be a neutral density separator. The neutral density beamsplitter consists of a thin evaporated coating of inconel on an optically-polished, flat glass substrate. The minimum average reflectance is 22% for Channel 1 energy and the minimum average transmittance is 34% for Channel 2. Complete details for beamsplitter D3 are given in ITT-A/OD Spec. No. 8007932.

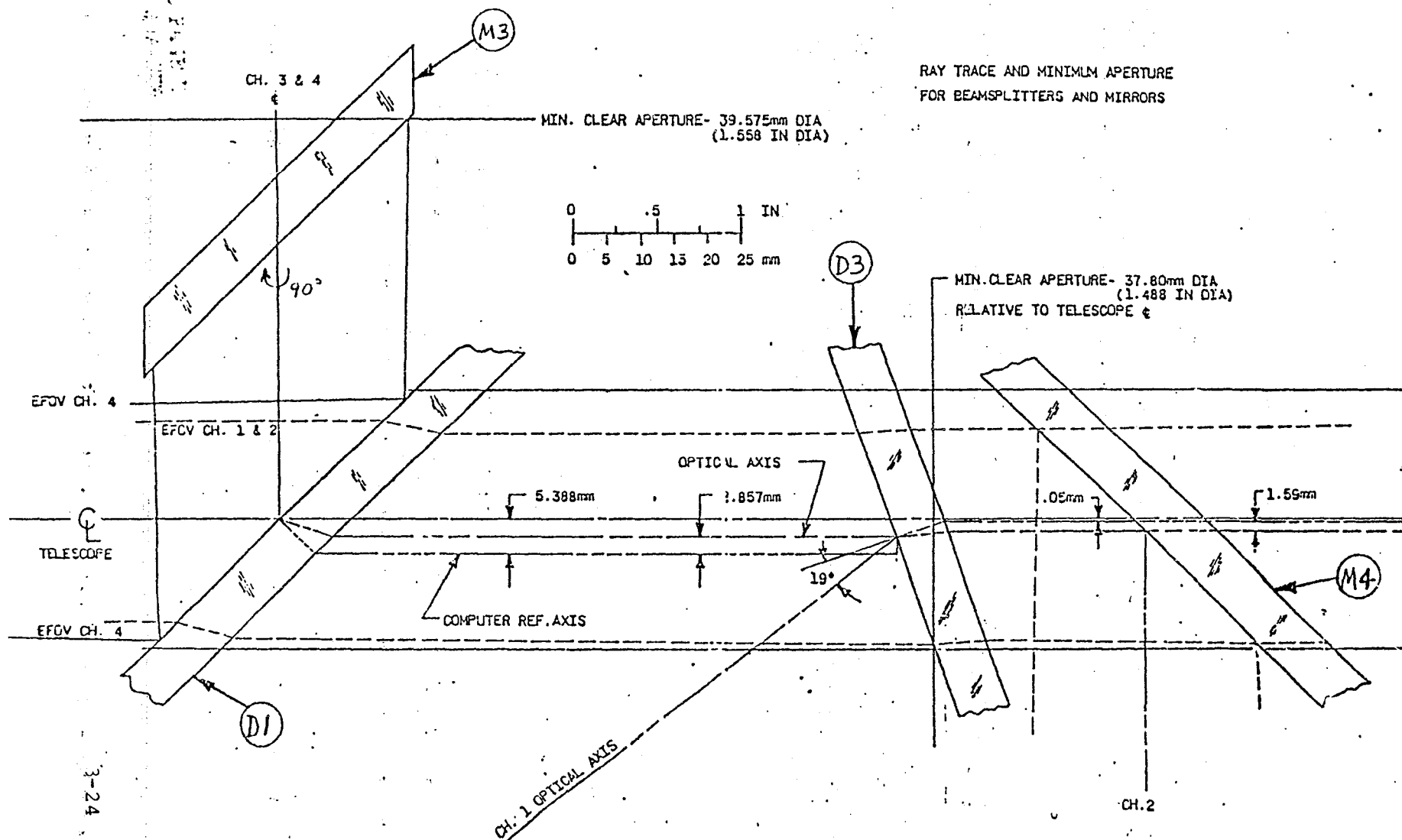


FIGURE 2-7-1 RAY TRACE AND MINIMUM APERTURE FOR BEAMSPLITTERS AND MIRRORS

The cooler windows are optically-polished, flat circular discs of Irtran 2 material (Eastman Kodak trade name). They are antireflection coated by OCLI to give a minimum transmission of 85% in both Channels 3 and 4. The coated windows meet standard military specifications for adherence, hardness and humidity. The outer cooler window (W1) is comparatively thick since it must withstand atmospheric pressure when the cooler is evacuated for bench cooling tests.

The Channel 4 bandpass filter is a conventional multilayer coating on a polished germanium substrate. The bandpass characteristics such as cuton and cutoff slopes, tolerances on location of the 50% transmission wavelength, etc., are given in Section 3.8.2.

3.8 Spectral Definition

3.8.1 Spectral Definition of Solar Channels

In order to determine the AVHRR system spectral response in Channels 1 and 2, it is necessary to determine the effects of those elements having a varying spectral characteristic. These elements are:

- a. Mirror Coatings
- b. Gold Beamsplitter
- c. Lens AR Coatings
- d. Silicon Detectors
- e. Spectral Bandpass Filters

Since the relative spectral response of the above elements affects the system spectral response in the given bands, and since their absolute response affects the signal to noise ratio, both requirements (spectral and sensitivity) must be considered together. The spectral

characteristics of the above five groups will be discussed individually below, followed by their combined effects.

3.8.1.1 Mirror Coatings

A complete study of the various potential mirror coatings was done in the preliminary design of the AVHRR. It was decided that to achieve maximum sensitivity in Channel 2 (where overcoated aluminum mirrors have a dip in their reflectivity) silver mirrors would be used for the telescope mirrors. For polarization compensation, however, the scan mirror and the folding mirror behind the solar channel beam-splitter were aluminized. The silver coating chosen was the Muffelto Optics "low pit" coating which was supposed to survive the required humidity and temperature extremes.

In the process of building the Breadboard and Engineering Model telescopes, no silver coating was found (at reasonable cost) which passed the humidity test. In all cases the mirrors degraded extensively when placed in the humidity test. Therefore, the decision was made to use aluminum mirrors which have a reflectivity equal to or greater than that shown in Figures 3.8-1 and 3.8-2. The coating after which the reflectivity curves were fashioned is the Evaporated Metal Films Corp. "enhanced aluminum" coating.

3.8.1.2 Gold Beamsplitter

The dichroic to split Channels 1 and 2 from Channels 3 and 4 is the thin gold film type at 45° to the incident beam with the near IR and visible energy being transmitted. Figure 3.8-3 shows the measured solar channel reflectivity of the gold dichroic used in the PTM.

REV C

DRAWING NUMBER
800878

"EXCEPT AS MAY BE OTHERWISE PROVIDED BY CONTRACT, THESE DRAWINGS AND SPECIFICATIONS ARE THE PROPERTY OF ITT AEROSPACE/OPTICAL DIVISION, ARE LOANED TO YOU IN STRICT CONFIDENCE, AND SHALL NOT BE REPRODUCED, OR COPIED, OR USED AS THE BASIS FOR THE MANUFACTURE OR SALE OF APPARATUS WITHOUT PERMISSION."

ITT
ROSPACE/OPTICAL DIVISION
JRT WAYNE, INDIANA, U.S.A.
INTERNATIONAL TELEPHONE AND TELEGRAPH CORPORATION

ORIGINAL PAGE IS
OF POOR QUALITY

NOTE: 90% MINIMUM @ 525 n.m.

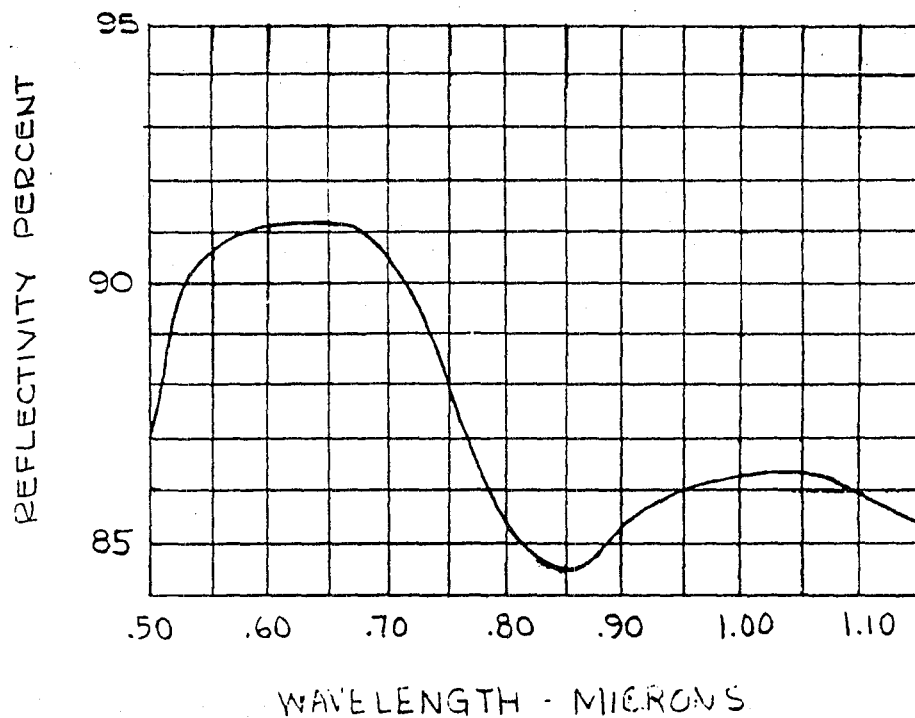


FIG 3.8-1 ABSOLUTE SPECTRAL
REFLECTIVITY REQUIREMENT
(ALL MIRRORS EXCEPT CHAN 2 FOLDING)

DWG CODE IDENT NO.

A

SIZE

31550

8008787

SCALE

SHEET 3-27

ITT
INTERNATIONALAEROSPACE/OPTICAL DIVISION
MARTIN LUTHER KING, JR. WAYNE, INDIANA, U.S.A.
TELEPHONE AND TELEGRAPH CORPORATION

"EXCEPT AS MAY BE OTHERWISE PROVIDED BY CONTRACT, THESE DRAWINGS AND SPECIFICATIONS ARE THE PROPERTY OF ITT AEROSPACE/OPTICAL DIVISION, ARE LOANED TO YOU IN STRICT CONFIDENCE, AND SHALL NOT BE REPRODUCED OR COPIED IN ANY MANNER OR USED AS THE BASIS FOR THE MANUFACTURE OR SALE OF APPARATUS WITHOUT PERMISSION."

DRAWING NUMBER

800878

REV

B

REFLECTIVITY PERCENT

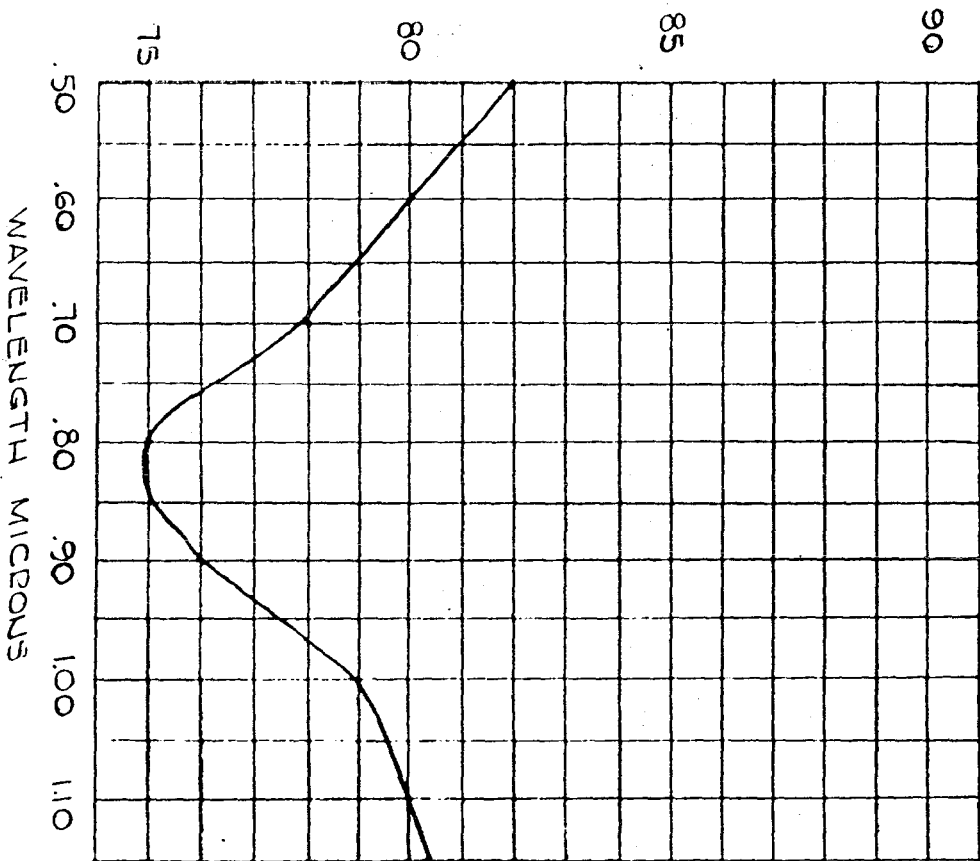


FIG 3.8-2 ABSOLUTE SPECTRAL
REFLECTIVITY REQUIREMENT
(CHAN 2 FOLDING MIRROR)

DWG CODE IDENT NO.

A

31550

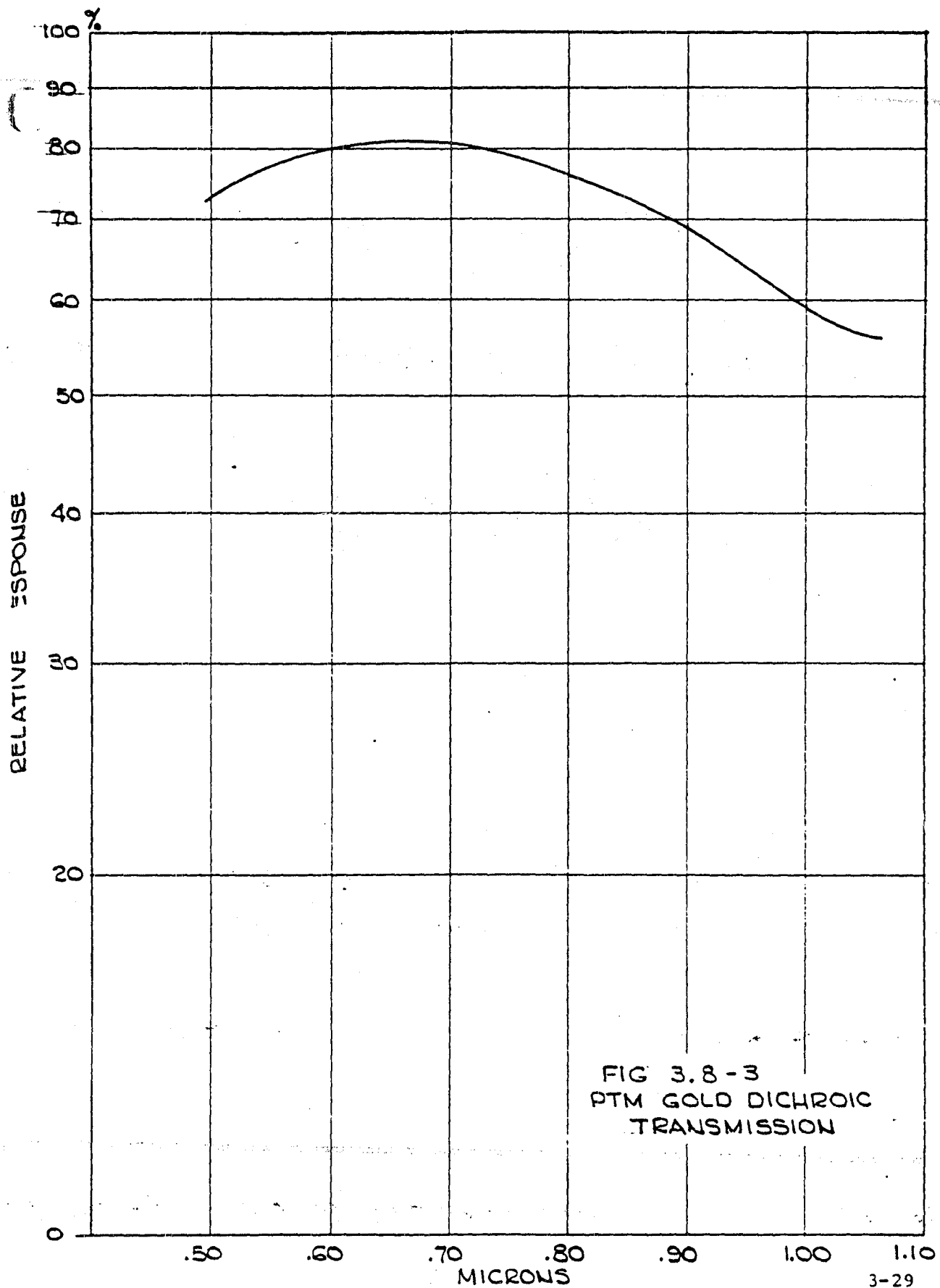
8008787

SIZE

SCALE

SHEET

3-28



3.8.1.3 Lens AR Coatings

The anti-reflection coatings on the three relay optic lenses used in each channel do not materially affect the relative spectral response of the solar channels. A MgF_2 type single layer coating is used and the total lens transmission will change from about 97% near the band center to 95% near the edges. Even for three lenses, the effect is insignificant.

3.8.1.4 Silicon Detectors

Because of the wide spectral bands covered by Channels 1 and 2, the detector in each is an important factor in defining the band edges. Quotes were solicited from six different companies, and all were requested to define the spectral characteristics of their proposed device. Selection of the vendor was based on both the relative spectral response and the absolute sensitivity. The definition of the Channel 1 spectral band edges is complicated by the fact that the silicon detector relative response is down to about 30% at 0.50 micron. This means that above some relative transmission value (about 40%) the spectral bandpass filter does not define the system response. The response is basically defined by the detectors and the other spectrally variant elements. This effect could have been reduced by cutting the detector peak spectral response and lowering the system signal-to-noise ratio; however, it was decided that the slow cuton of the system spectral response is more acceptable than a reduced signal-to-noise ratio.

As stated previously, one detector design is used for both solar channels. This approach provides excellent sensitivity in both channels and simplifies (and so reduces the cost of) the detector. The measured spectral response of one of the detectors, shown in figure 3.8-4, is typical of that measured on all detectors.

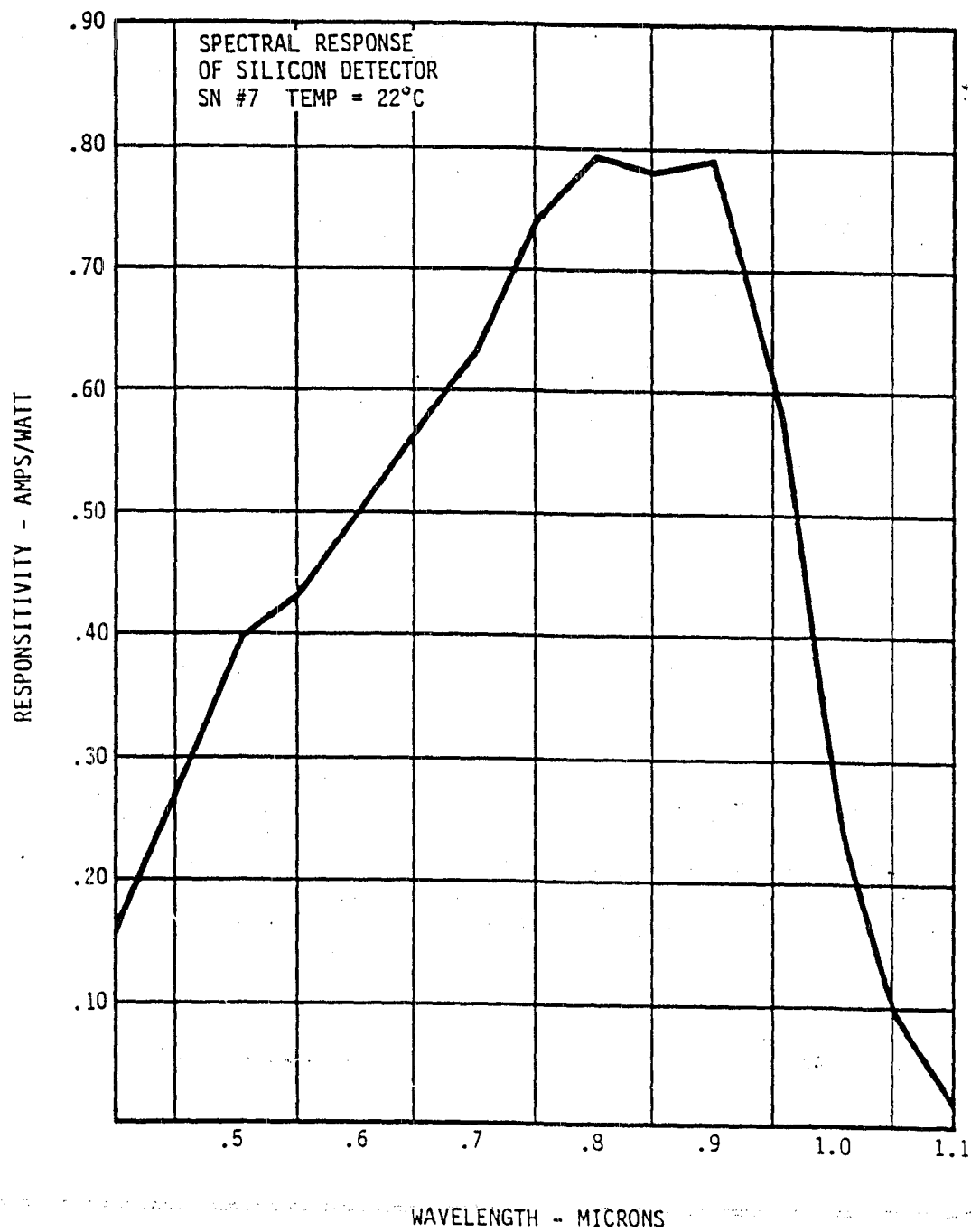


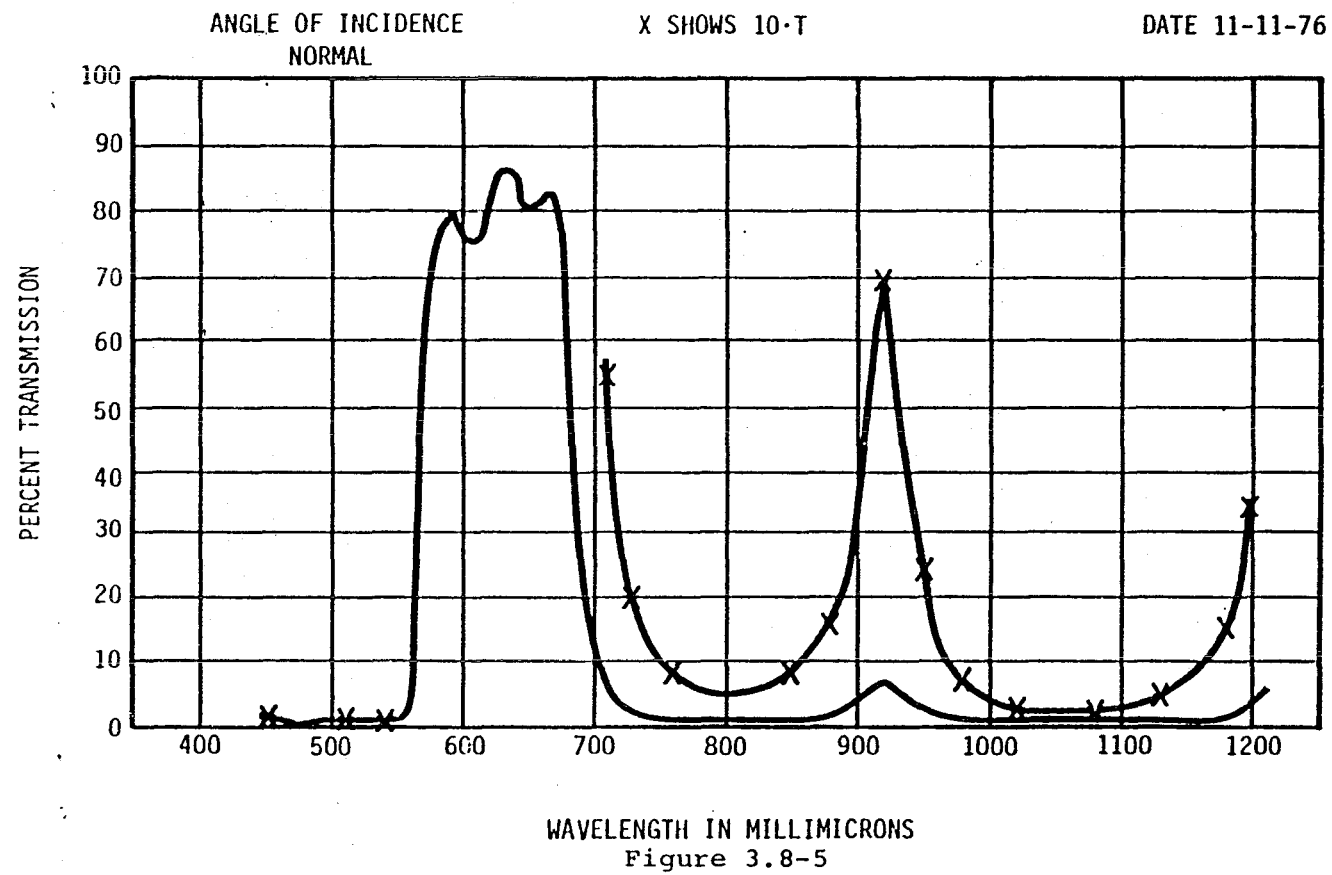
Figure 3.8-4

3.8.1.5 Spectral Bandpass Filters

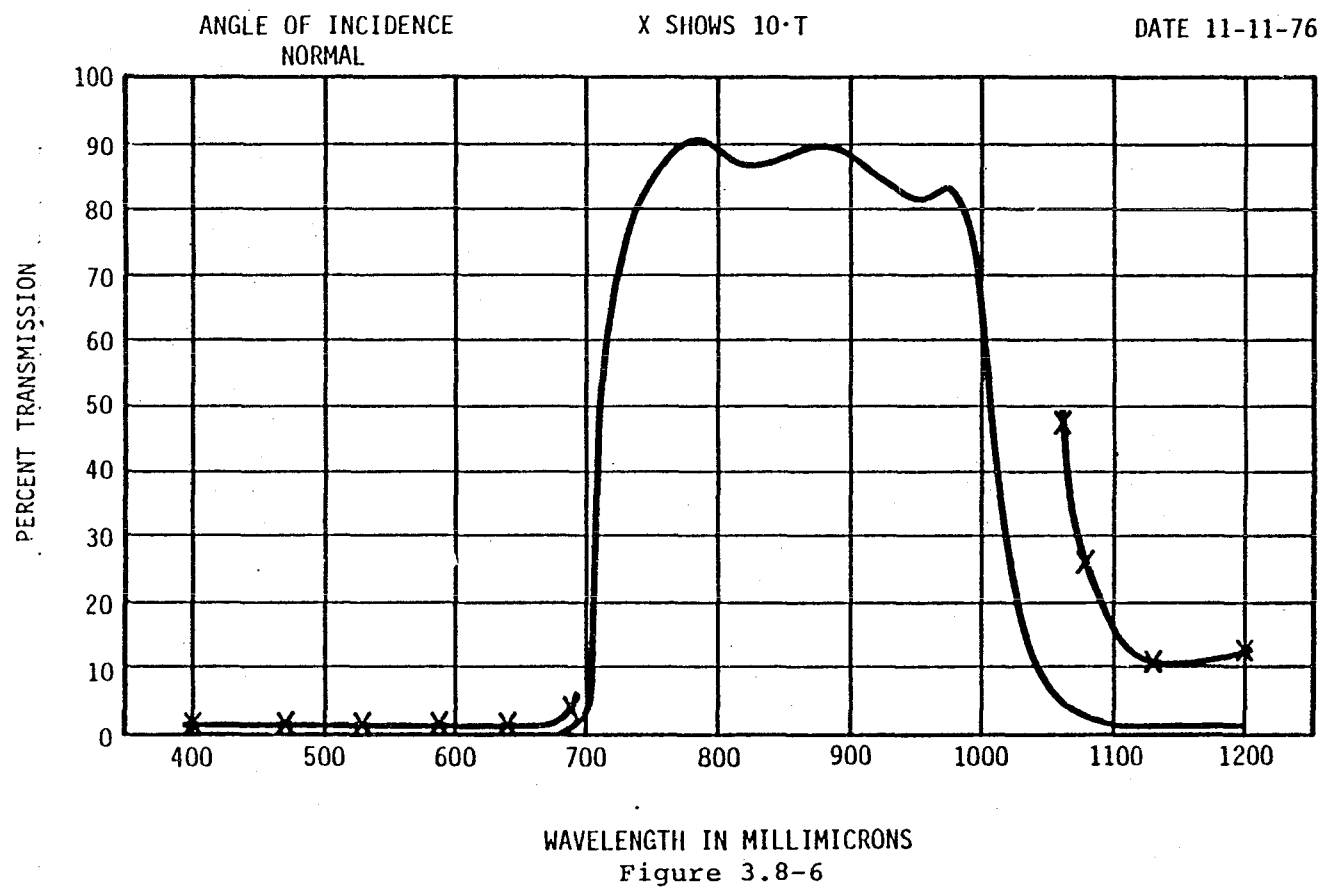
The spectral filters were purchased from Fish-Schurman Corporation and have the responses shown in Figures 3.8-5 and 3.8-6. The filters consist of a two piece laminated sandwich with one piece being a 3 mm thick Schott glass filter and the other being a 2 mm thick clear substrate upon which a multilayer coating is applied. The multilayer is placed inside the sandwich and is sealed by the epoxy sealant from ambient conditions. The problem of spectral variations as a function of absorbed water is eliminated. This approach was used in the ATS-F VHRR solar channel filter. The epoxy sealant is Summers Laboratory C-59 which meets MIL-3920 and has measured outgassing characteristics of 2.94% weight loss and 0.108% condensable materials. (This information was supplied to ITT by NASA/GSFC). This is the same sealant used to seal and focus lenses in each solar channel of the AVHRR.

The filter generates its spectral bandpass using a Schott glass filter for the short wave cut-on and a multilayer coating for the long wave cut-off. The slopes of the filters are all about 6% between the 5% and 80% response points. Short wave out-of-band blocking is defined by the Schott glass and is complete. Long wave out of band blocking is defined by the multilayer and, while not as good as the Schott glass, results in an out of band signal well below that specified as discussed later (the detector has cut off by the time the filter transmission comes back up).

CHANNEL 1 FILTER
SERIAL 202



CHANNEL 2 FILTER
SERIAL 202



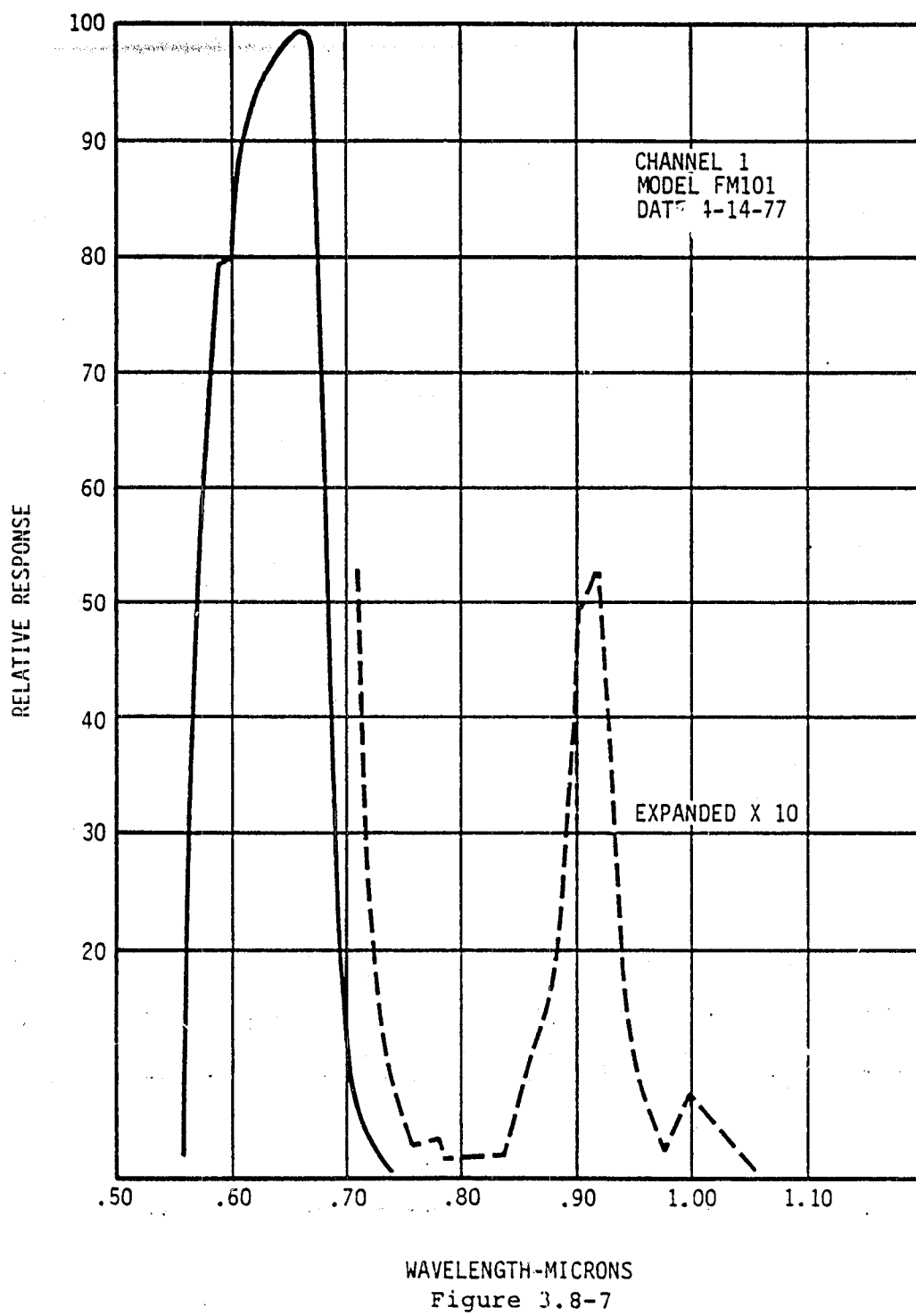
3.8.1.6 System Spectral Response

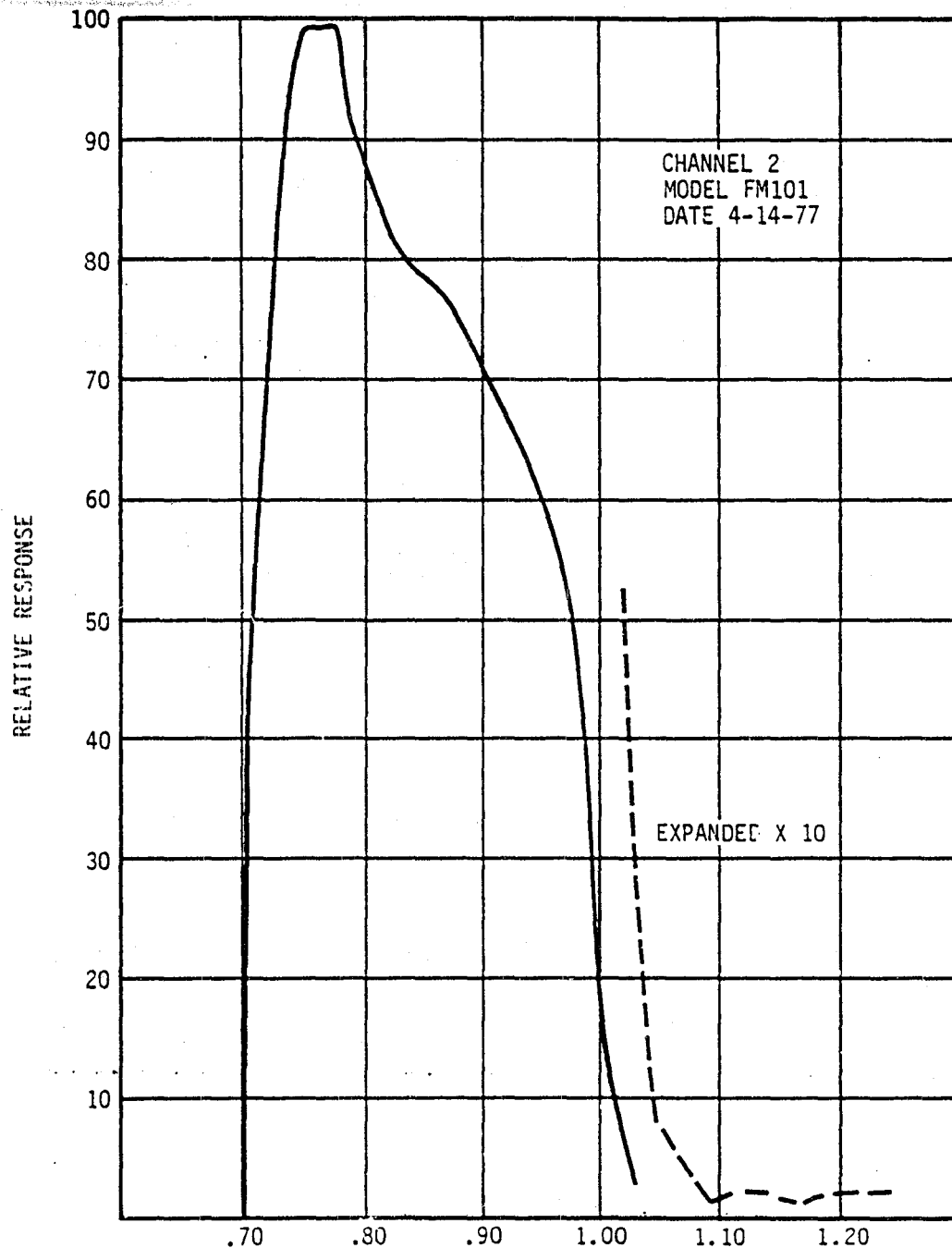
Figures 3.8-7 through 3.8-14 show the measured channel 1 and channel 2 spectral response curves for the AVHRR/1 flight model instruments.

3.8.2 Spectral Definition of Thermal Channels

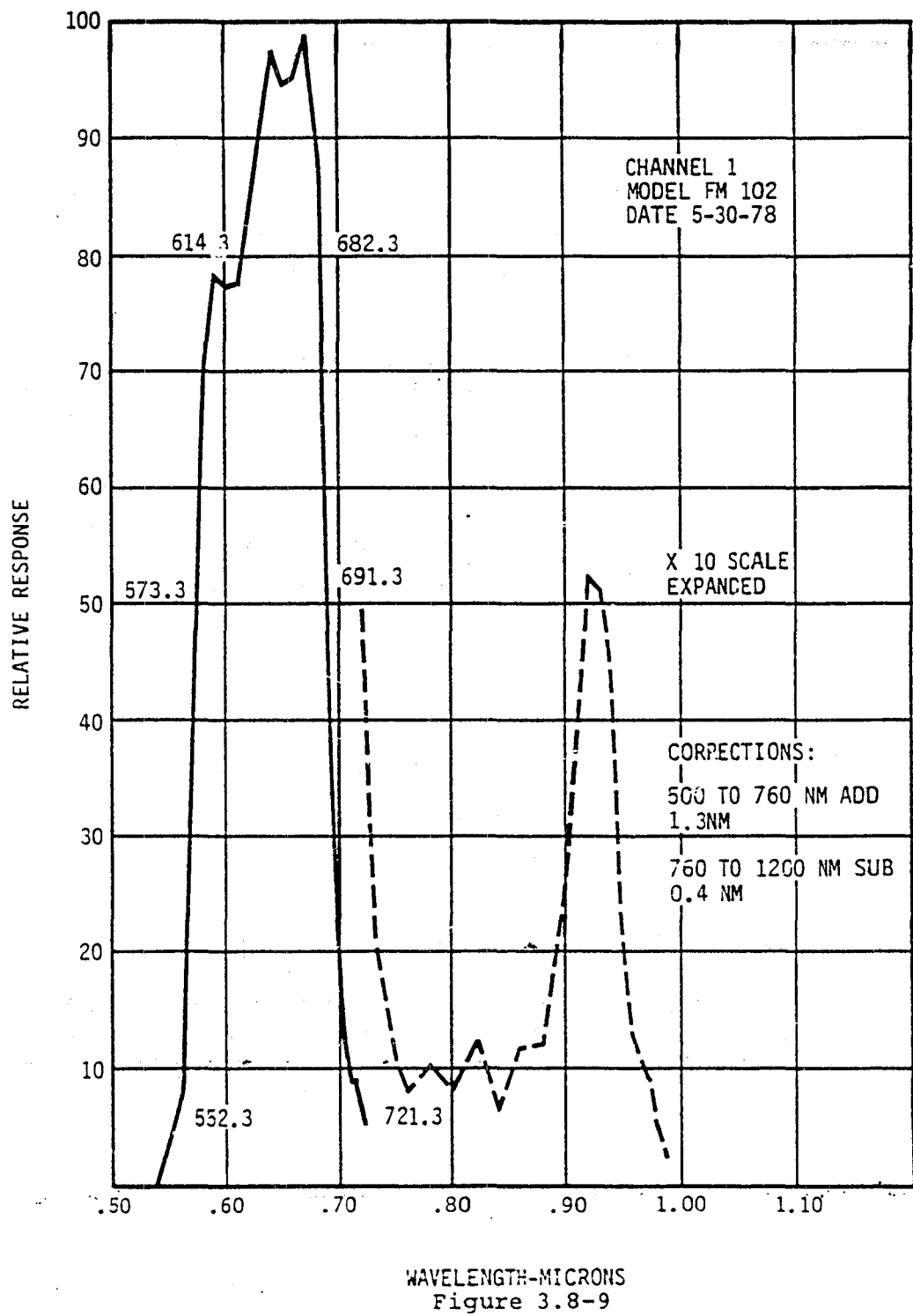
The spectral characteristics of typical bandpass filters for Channels 3 and 4 are summarized in Table 3.8-3. The filters are the dominant element in defining the spectral response of the AVHRR instrument. The response of the indium antimonide detector varies smoothly from 3.5 to 4.0 μm , being about 5% less at the shorter wavelength side of the band. The Hg Dc Te detector procurement specification contains a requirement that the response at any wavelength between 10.5 and 11.5 μm be no less than 80% of the maximum in-band response. Therefore, the detectors should not appreciably affect the system response. The complete procurement specifications for the bandpass filters are contained in ITT-A/OD Specifications 8008790 (Channel 4) and 8008792 (Channel 3).

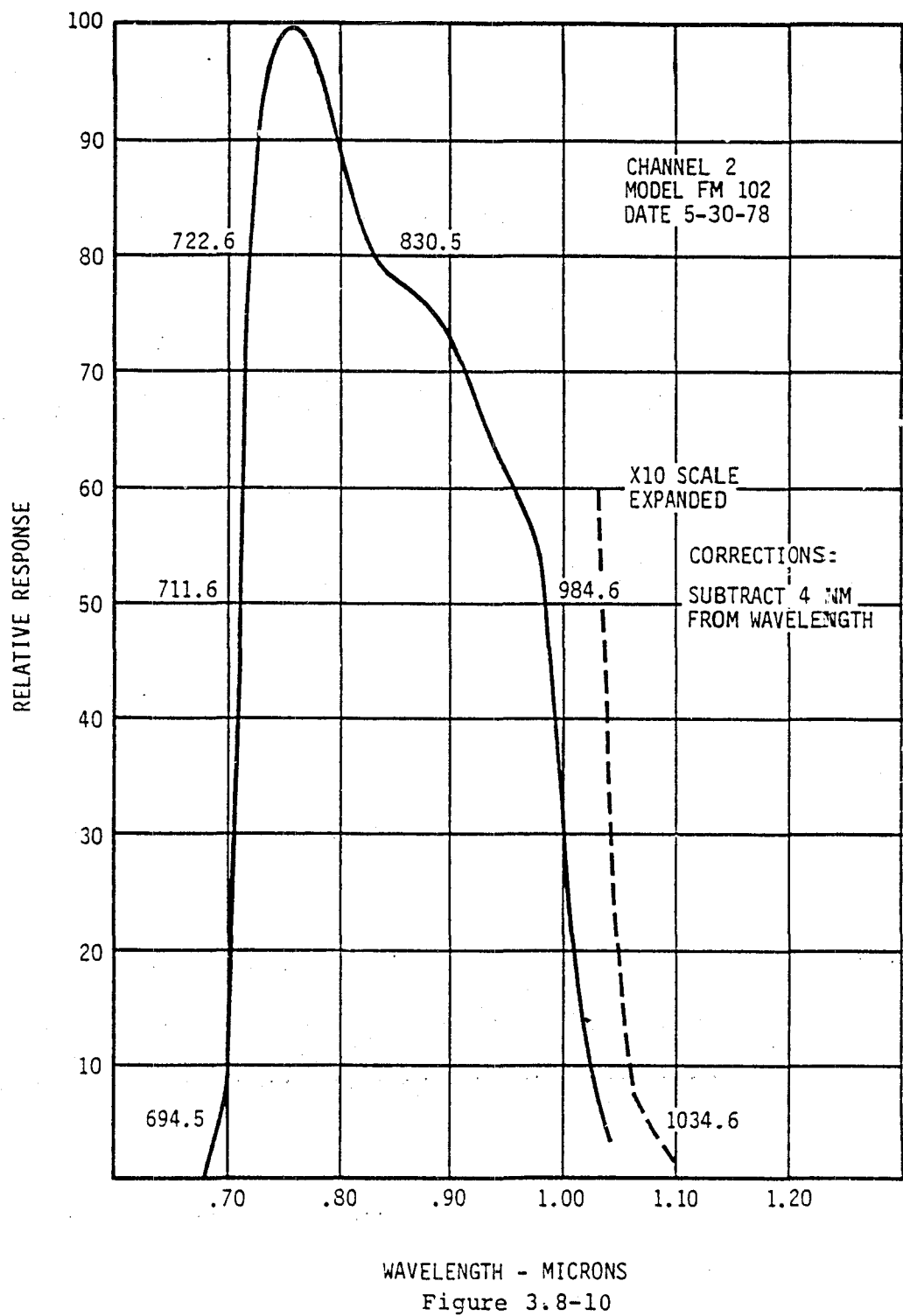
The germanium lenses have some effect on the response of Channel 3 due to their increased absorption toward longer wavelengths. This effect causes the Channel 3 response to be somewhat skewed to shorter wavelengths in the band. Figures 3.8-15 through 3.8-22 show the measured channels 3 and 4 spectral response for the AVHRR/1 flight models.

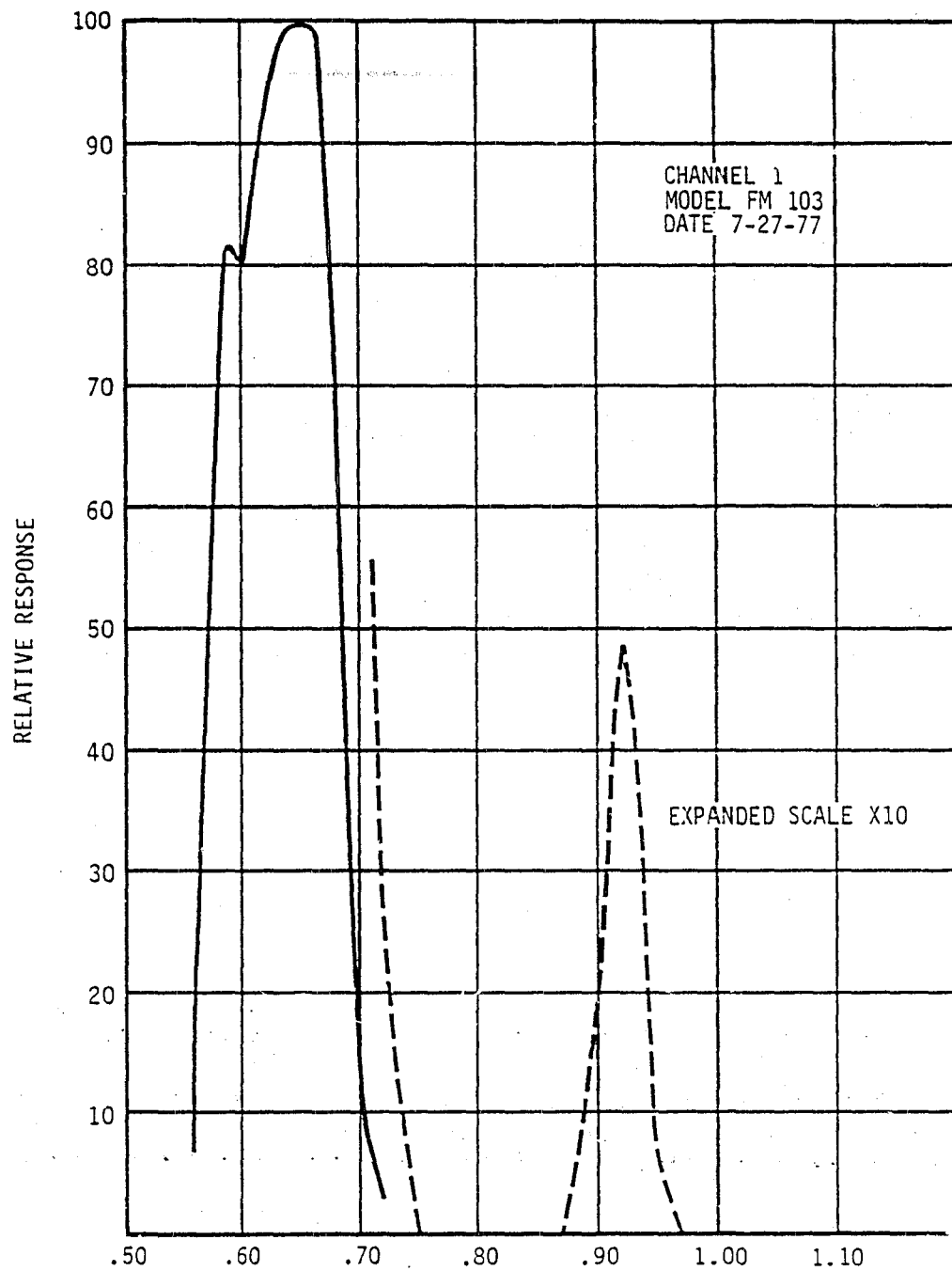




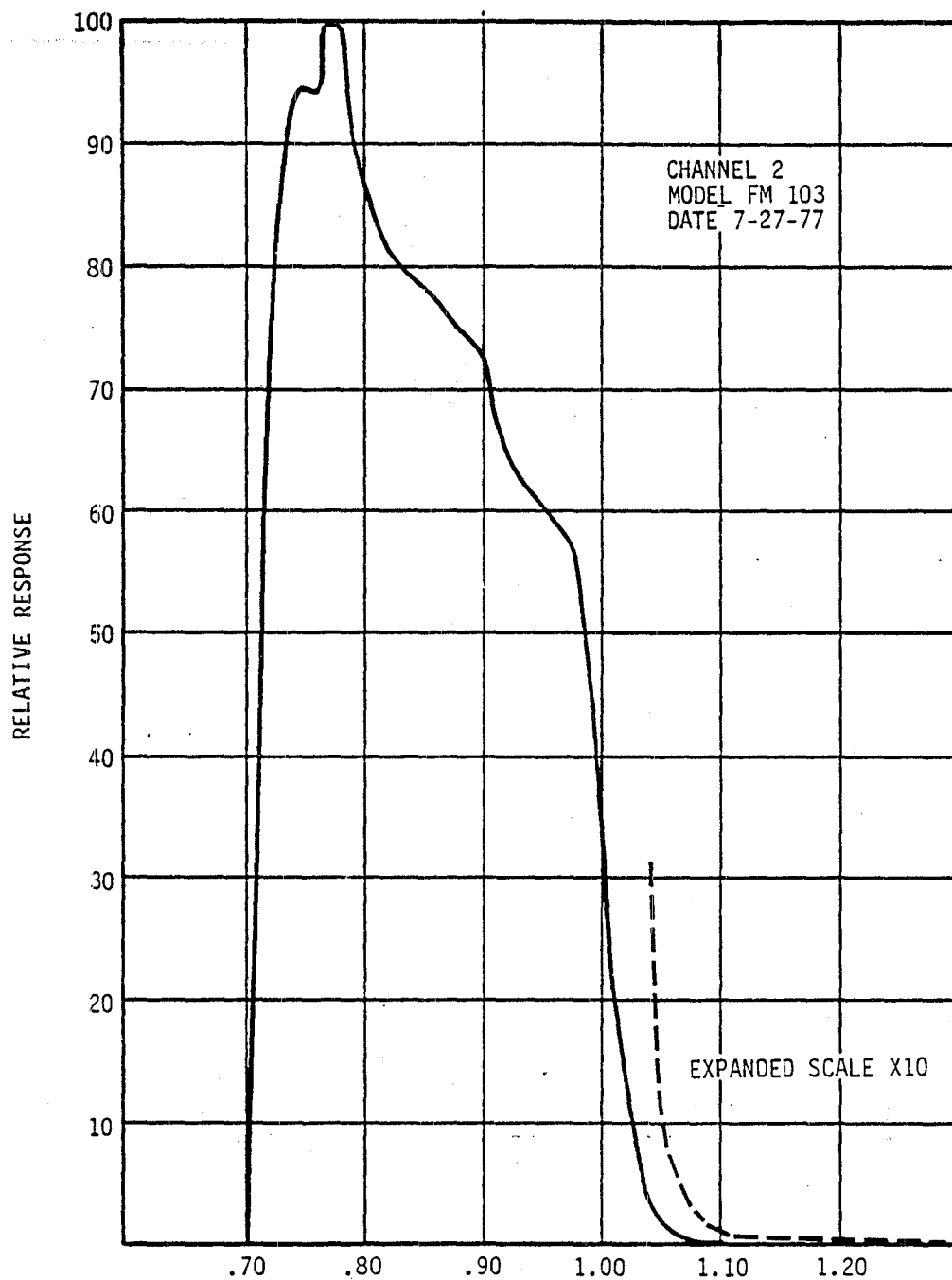
WAVELENGTH-MICRONS
Figure 3.8-8



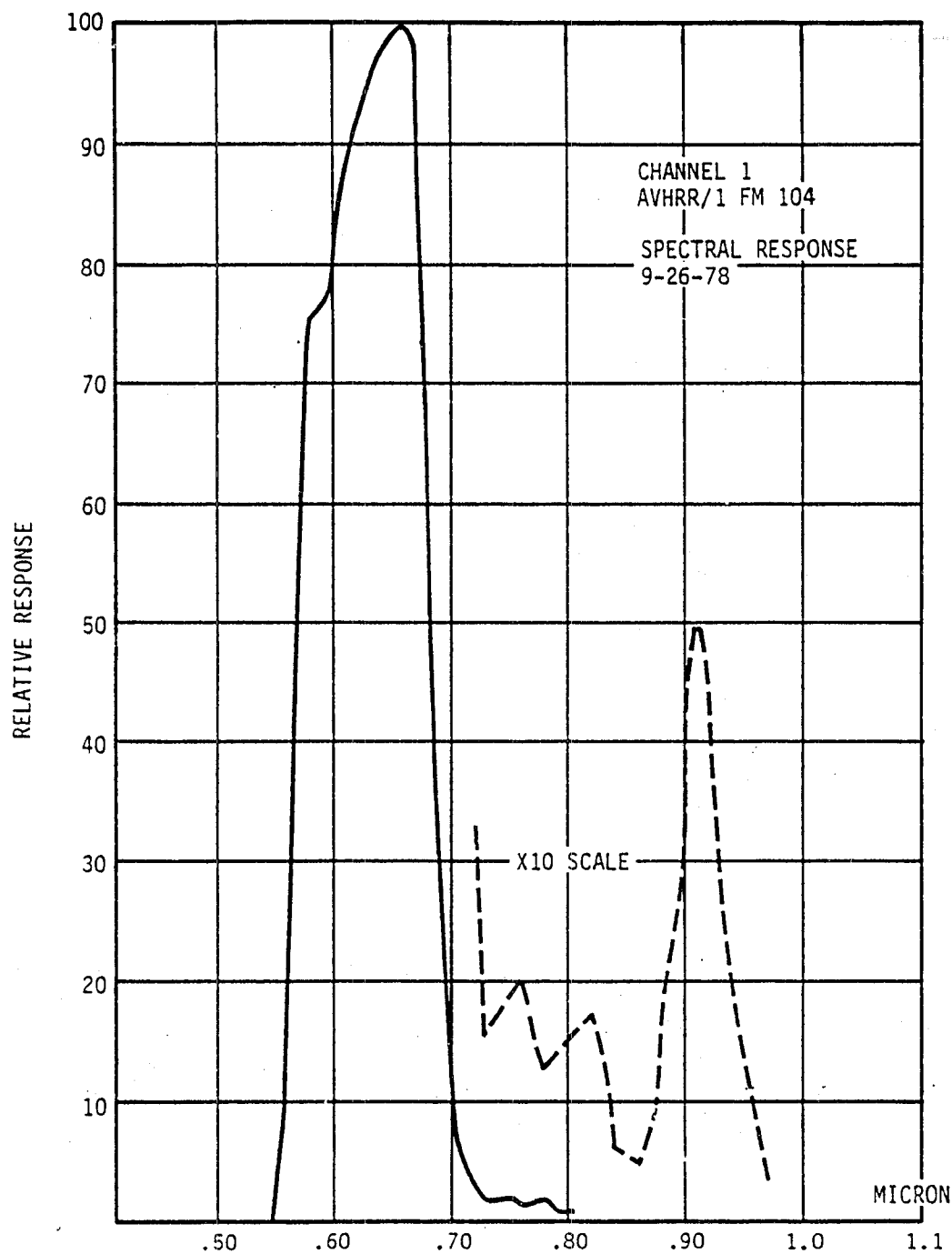




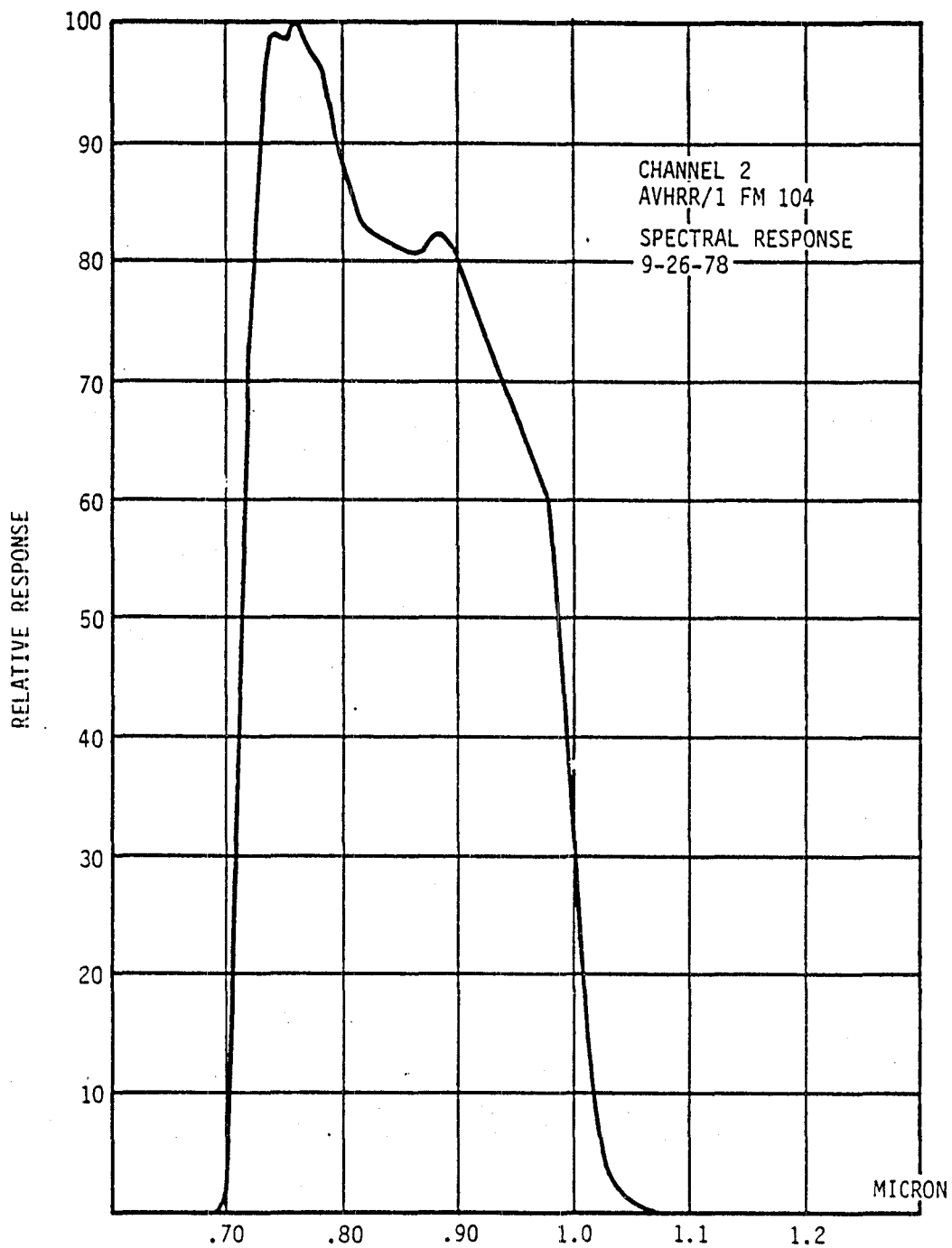
WAVELENGTH - MICRONS
Figure 3.8-11



WAVELENGTH - MICRONS
Figure 3.8-12



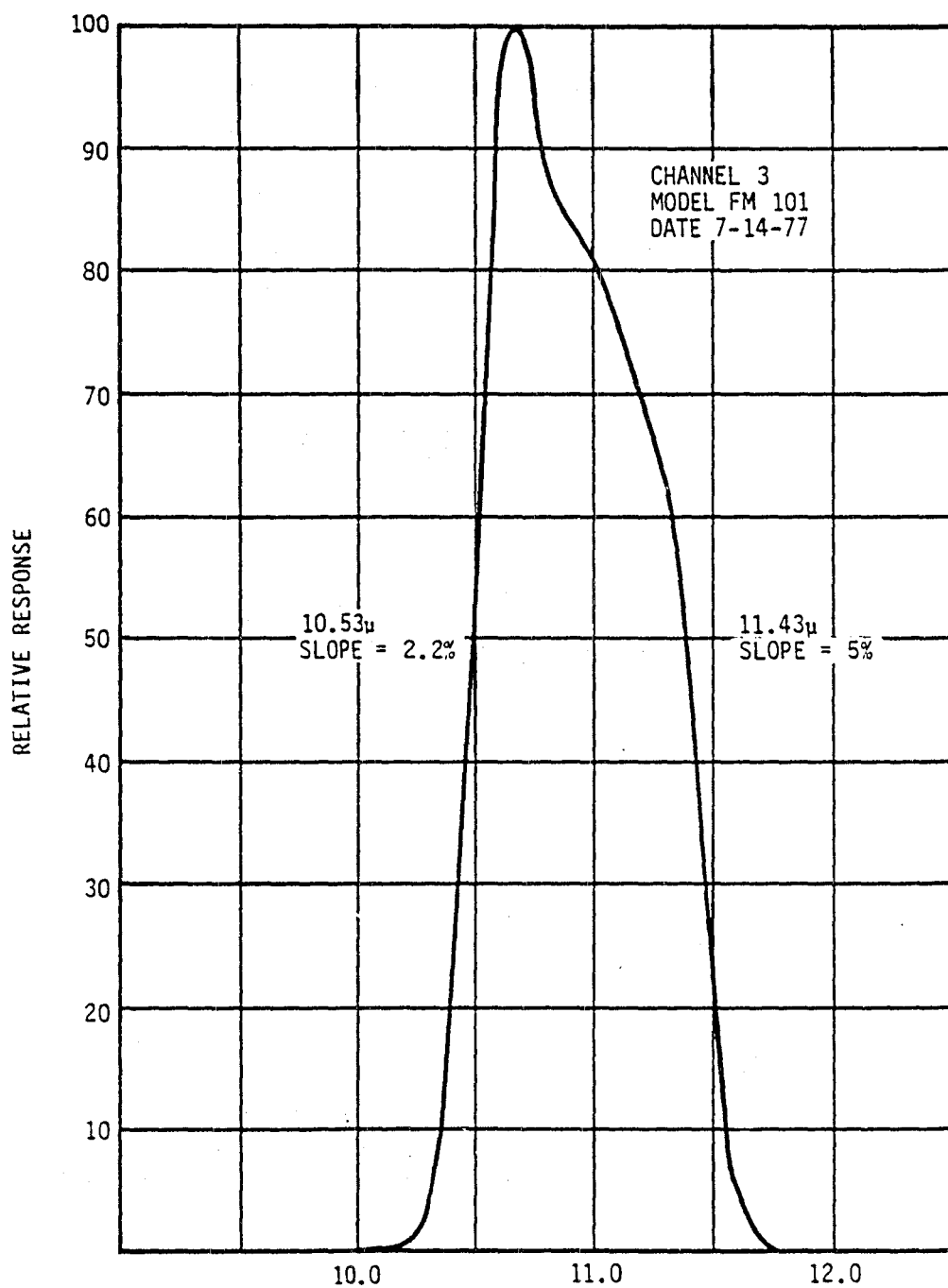
WAVELENGTH - MICRONS
Figure 3.8-13



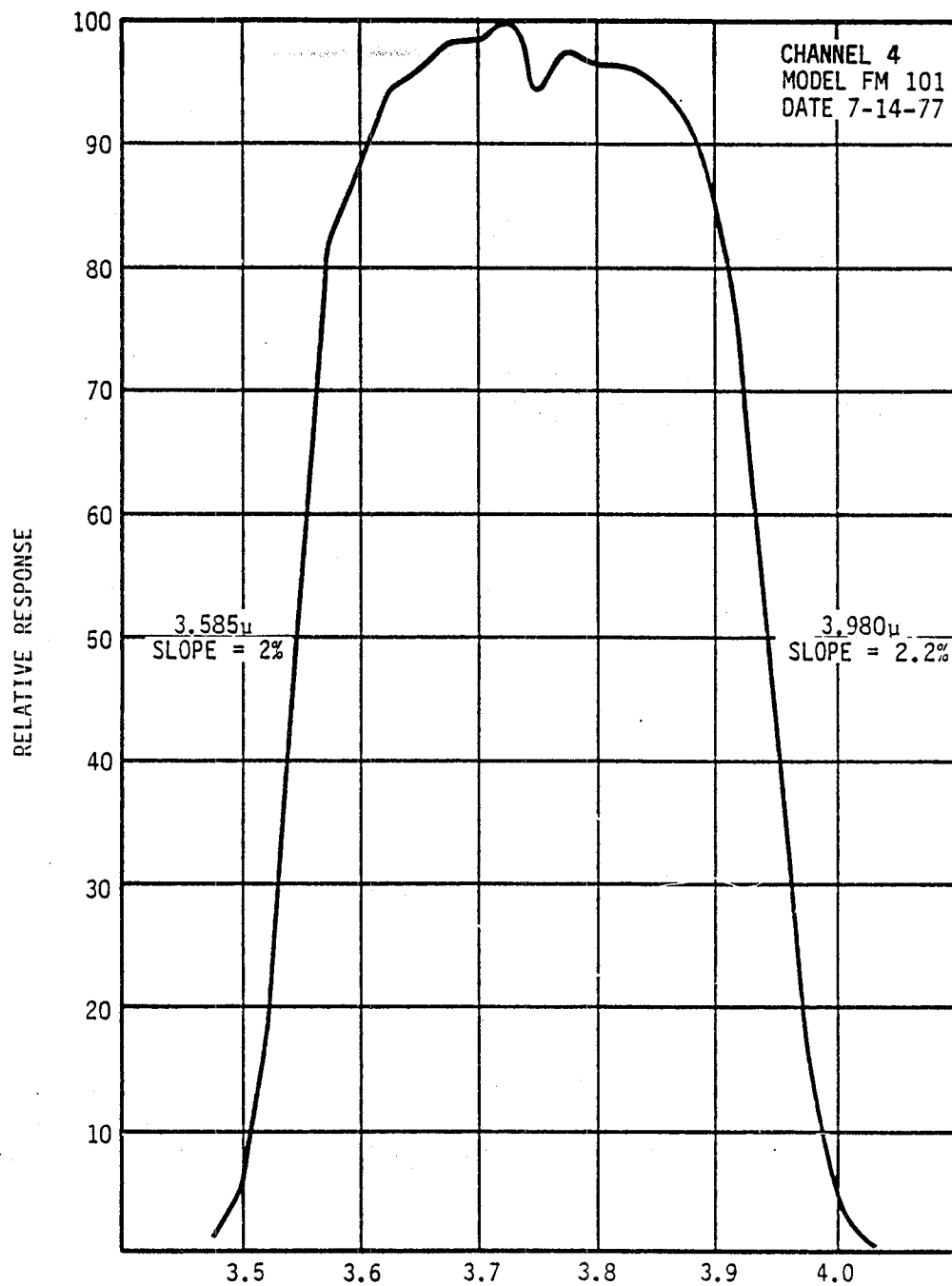
WAVELENGTH - MICRONS
Figure 3.8-14

TABLE 3.8-3
FILTER CHARACTERISTICS

<u>CHARACTERISTIC</u>	<u>CHANNEL 3</u>	<u>CHANNEL 4</u>
50%-of-Peak Cuton Wavelength	10.5±0.09μm	3.55±.06μm
50%-of-Peak Cutoff Wavelength	11.5±0.09μm	3.93±.06μm
Cuton and Cutoff Slopes	≤ 3%	≤ 3%
Response at 10.0 and 12.0μm	≤ 1%	N.A.
Response at 3.40 and 4.12μm	N.A.	≤ 1%
Transmission less than 0.1%	From 1.8 to 9.8μm and from 12.2 to 18.0μm	From 1.8 to 3.2μm and from 4.3 to 7.0μm
In-Band Transmission	≥ 75% Avg.	≥ 75% Avg.

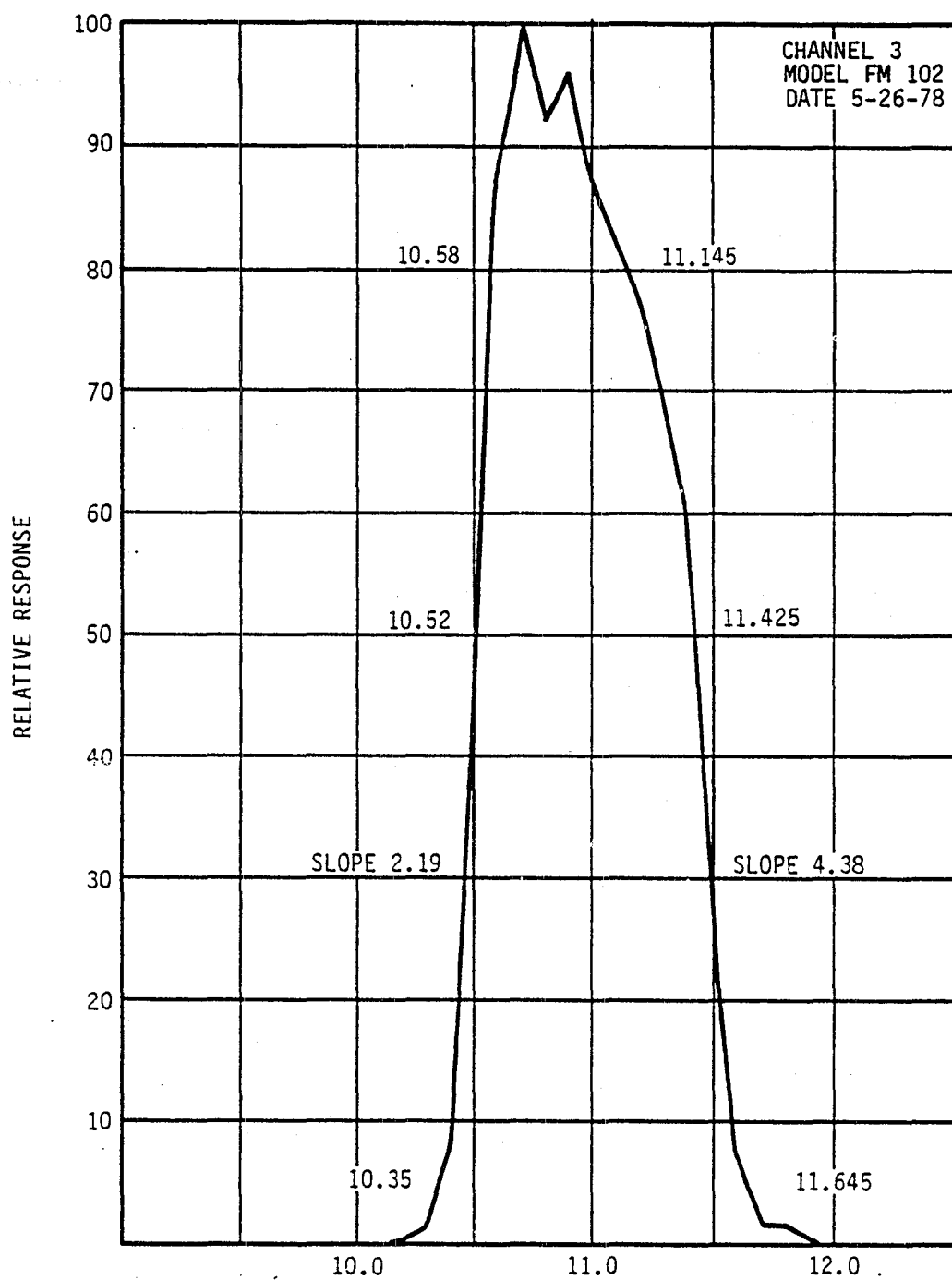


WAVELENGTH - MICRONS
Figure 3.8-15

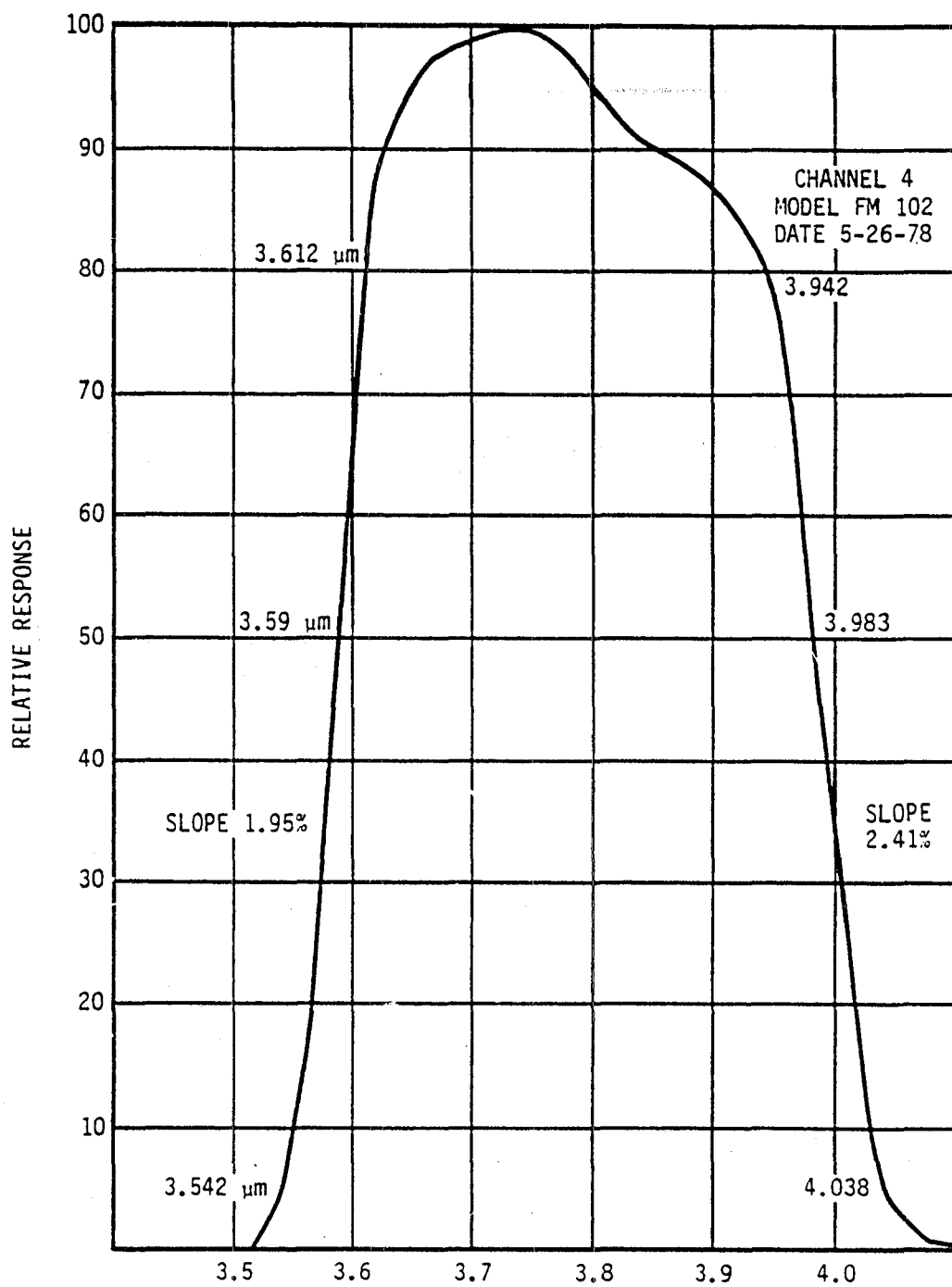


WAVELENGTH - MICRONS
Figure 3.8-16

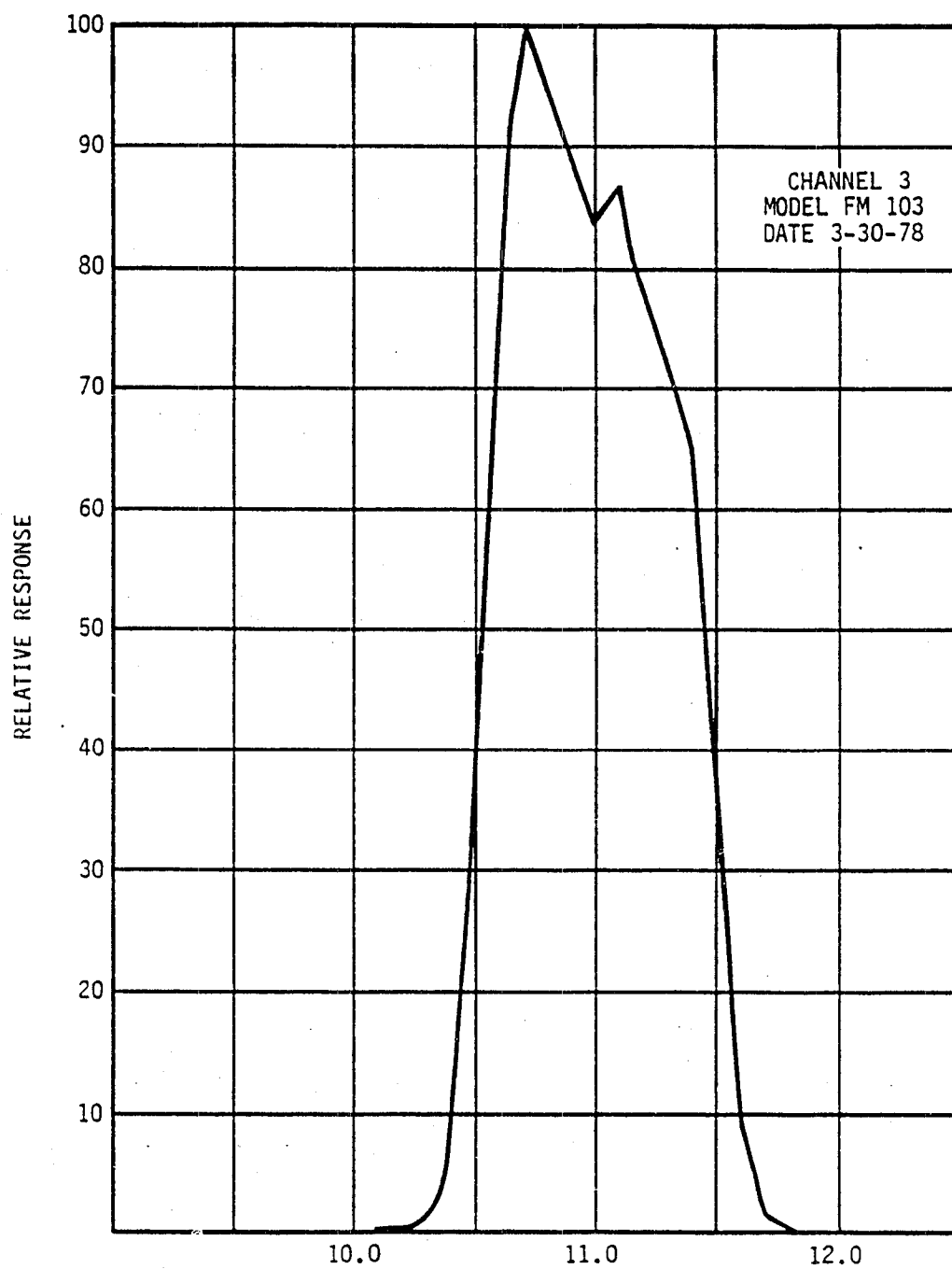
ORIGINAL PAGE IS
OF POOR QUALITY



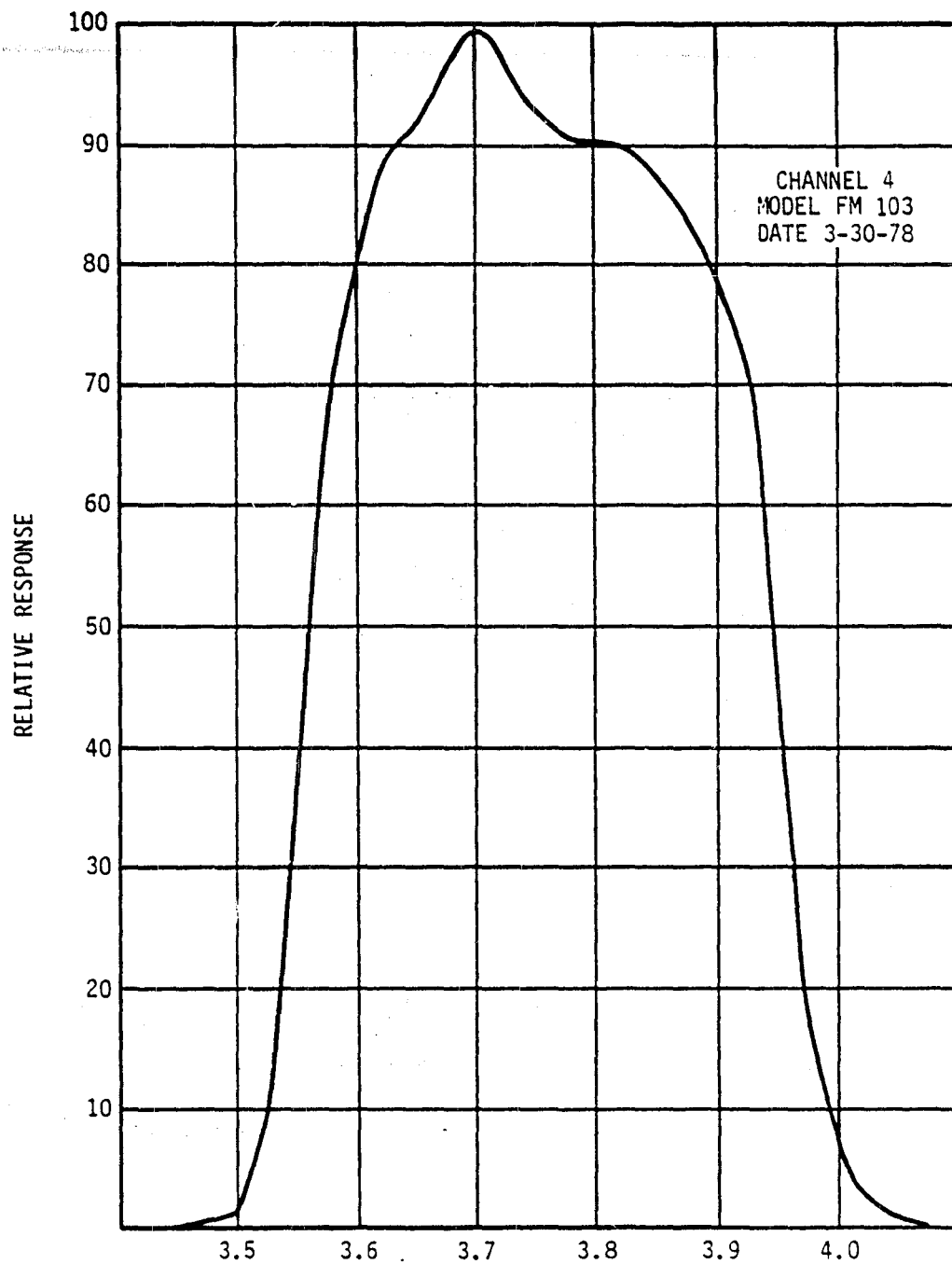
WAVELENGTH - MICRONS
Figure 3.8-17



WAVELENGTH - MICRONS
Figure 3.8-18



WAVELENGTH - MICRONS
Figure 3.8-19



WAVELENGTH - MICRONS
Figure 3.8-20

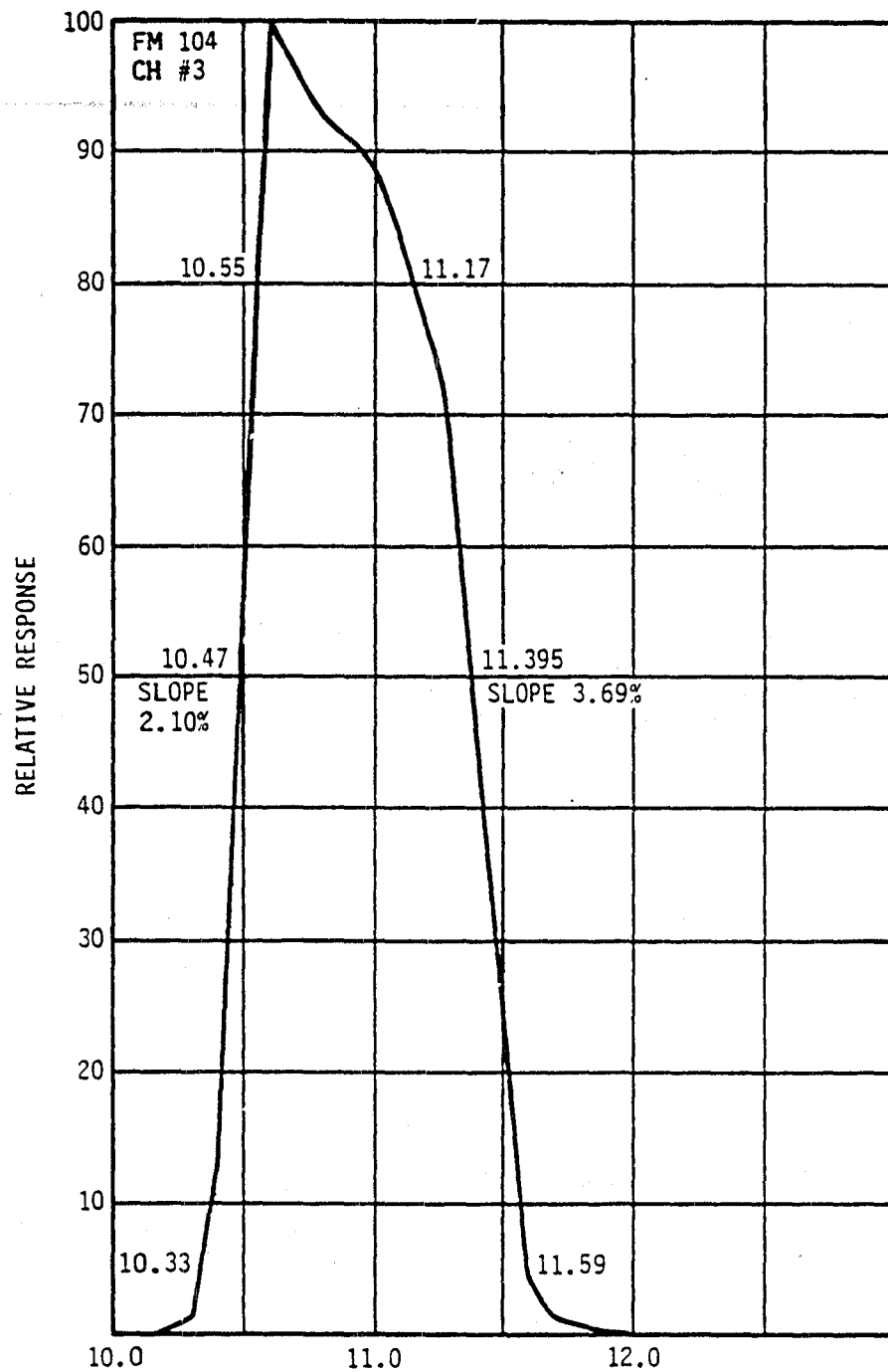


Figure 3.8-21

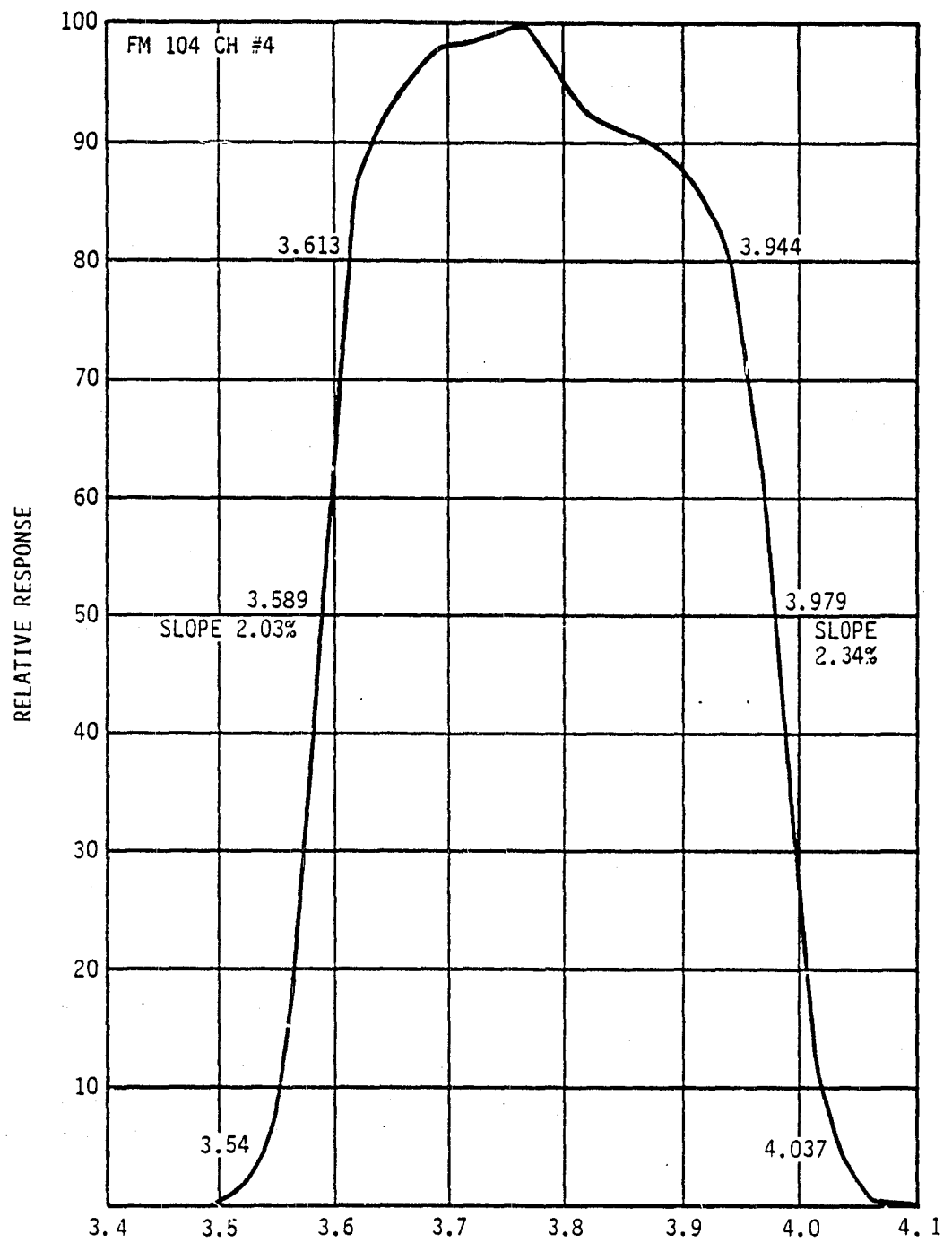


Figure 3.8-22

3.9 Channel Resigtration

The approach used to register the AVHRR channels consists of first registering the two thermal channels at a subassembly level. The patch, with both detectors mounted, is placed in a test vacuum dewar and illuminated through the relay optics, by a collimated beam. The collimator is a germanium lens which has a slit target and chopped radiation source. The slit is moved while the outputs of the two channels are recorded. The difference between the 50% response points is the misregistration. This is repeated with a slit rotated 90° so that the distance that each detector must move is measured. The patch is then removed from the dewar, the adjustment made, and the patch retested to verify alignment.

The following procurement is used for channel registration.

- a. Determine the physical location of the focal points for Channels 3 and 4 with reference to the optics subassembly during optics acceptance tests.
- b. Place the subassembly into the AVHRR and mount the cooler to place the detectors in their proper position.

- c. With the solar channels centered in their EFOV, determine the misregistration between all the channels. If the error is more than can be corrected by moving the solar channels, reposition the cooler to place the IR detectors in the correct location.
- d. Remeasure the misregistration and move the solar channel detectors to complete the registration procedure.

Step c. essentially eliminates the tolerance buildup problem in the instrument by actually measuring the positions and correcting accordingly. If the initial placement of the cooler is sufficiently close to place the IR detectors within the solar channel EFOV, then no cooler repositioning will be required.

The procedure has been used to register both the ETM and PTM instruments well within the specified value.

3.10 Polarization Sensitivity

An analysis was made of the polarization sensitivity of Channels 1 and 2 with the object of meeting the requirements of the GSFC Specification.

$$P = \frac{T_1 - T_2}{T_1 + T_2} \leq .053$$

This equation holds at nadir (or at 90° from nadir) as a result of the orientation of the optical elements that contribute to the polarization. (On the Flight Model instruments, the maximum allowed polarization sensitivity is .07.) The transmittances obtained for the parallel and perpendicular polarizations are the extremes for any linearly polarized wave that travels through the optical train.

The theoretical and measured polarizations of the elements are given in the tables contained in the DIR's. The channel transmittances were calculated by giving a weight of 1/2 to the spectral end points (i.e., originally 0.5 and 0.9 μm in Channel 1 and 0.75 and 1.00 μm in Channel 2; revised to 0.55 to 0.9 μm in Channel 1 and 0.725 and 1.1 μm (silicon detector cutoff) in Channel 2).

The analysis performed during the design phase of the AVHRR program considered several options including the angular position of the dichroics and beamsplitters, the addition of reflecting surfaces for compensation, and the types of coatings on reflective surfaces. The complete analysis is detailed in AVHRR D.I.R. #6 and 7.

Several changes have been made to the original polarization sensitivity design of the AVHRR. In particular, the gold dichroic has been made by OCLI so that the percent polarization of that element is considerably less than originally thought. The scan mirror coating is the major compensating element for the polarization of the gold dichroic. The high reflectivity coating used on the PTM and Flight Models also has less polarization (because the reflectivity dip around 0.86 micron is minimal). The combination results in a measured PTM polarization sensitivity as listed in Table 3.10-1. The Polarization sensitivity as a function of scan mirror position was measured on the PTM as a matter of interest. As can be seen the instrument performs quite well and it can be expected that the Flight Model units will be well within the 0.07 allowed.

C-2

TABLE 3.10-1

MEASURED PTM AVHRR POLARIZATION
SENSITIVITY

<u>SCAN MIRROR</u> <u>POSITION</u>	<u>CHANNEL 1</u> <u>P.S.</u>	<u>CHANNEL 2</u> <u>P.S.</u>
50° (Sunside)	.032	.047
25° (Sunside	.039	.049
Nadir	.037	.053
25° (Antisunside)	.038	.047
50° (Antisunside)	.030	.049

3.11 Scattered Sunlight

We have studied the following effects of direct sunlight:

- a. The temperature gradient it produces across the honeycomb of the in-flight target.
- b. Its reflection from the in-flight target and the resultant calibration errors.
- c. Scattering and the resultant signal contamination.

Because the above occurs only during the nighttime portion of the orbit, we need to consider only Channel 3 (10.5 to 11.5 μm) and Channel 4 (3.55 to 3.93 μm).

From our studies to date, we conclude that:

- a. The honeycomb gradient is not sensibly changed from its value in the 906 n mi orbit.
- b. Under the worst conditions, reflection of sunlight from the in-flight target introduces a significant error (0.65K) in Channel 4. As a result, it may be desirable to restrict the Channel 4 calibration period, e.g., to the portions of the orbit when the target is shaded by the earth, spacecraft, instruments or sunshields (if added). The corresponding error in Channel 3 is negligible (0.002K).

The temperature errors quoted in b are for the preliminary TIROS-N instrument/spacecraft layout shown in NASA/GSFC Drawing GDSK-4799. Two separate instrument orientations are of interest, for scattering from the telescope and from the scan mirror.

3.11.1 Honeycomb Temperature Gradient

This problem was analyzed in DIR #18 (Worst Case Honeycomb Temperature Gradient in the In-Flight Thermal Calibration Target, May 9, 1974; included in Section 7.1). The analysis was revised for the new altitude of 450 n mi and the new range of sun angle β (memo of May 2, 1974). The results are:

For $\beta \leq 27.83^\circ$, min. $\theta = 62.17^\circ$ at $\beta = 27.83^\circ$

For $\beta \geq 27.83^\circ$, min. $\theta = 62.17^\circ$

$$(T_o - T_\ell)_1 = 2.513^\circ$$

$$(T_o - T_\ell)_2 = 0.639^\circ\text{C}$$

Effective cell gradient = $(T_o - T_\ell) = 0.95^\circ\text{C}$

Effective calibration gradient = $0.079 (T_o - T_\ell) = 0.075^\circ\text{C}$.

The effective calibration gradient is not sensibly changed from its previous value of 0.077°C .

3.11.2 Sunlight Reflections from In-Flight Target

Sunlight reflected from the in-flight target introduces a calibration error in addition to those errors we have previously considered. The error is negligible in Channel 3, but can be significant in Channel 4.

The solar exitance reflected from the target is given by

$$M_s = E_s \rho \frac{A_s}{A_T}$$

- where E_s = direct solar incidence (irradiance) in the wavelength band and perpendicular to the sun's rays.
- ρ = diffuse hemispherical reflectivity of the in-flight target
- A_s = exposed target area projected perpendicular to the sun's rays
- A_T = effective target area viewed by radiometer
= $\pi (8)^2 / 4 \text{ in}^2$.

The values of solar incidence were calculated from the table given by Thekaekara (Optical Spectra, March 1972, p. 32); the results are

$$\text{Channel 3 (10.5 - 11.5 } \mu\text{m)}, E_s = 1.71 \times 10^{-5} \text{ Wcm}^{-2}$$

$$\text{Channel 4 (3.55 - 3.93 } \mu\text{m)}, E_s = 2.52 \times 10^{-4} \text{ Wcm}^{-2}$$

The reflectivity ρ can be calculated from the limiting formula of Treuenfels (J. Opt. Soc. Am. 53, 1162, 1963) or by interpolation from the graph of Sparrow and Cess (Radiation Heat Transfer, Brooks/Cole, 1966 p. 165). In either case, an assumed paint emissivity of 0.92 (3M 401 black) results in a hemispherical cavity emissivity of 0.980 and a reflectivity of 0.020. As shown in the graph of Sparrow and Cess, the limiting emissivity of a cylindrical cavity is reached at a length to radius ratio of about 2:1 when the paint emissivity exceeds 0.7. The length to radius ratio of a honeycomb cavity is 8:1. The ratio of flat to total target area is 0.045, so that the hemispherical reflectivity is 0.0227. It would be desirable to have spectral emissivity (or reflectivity) data on the 3M 401 in the bands of interest. However, data could only be found for 3M 101 and; therefore, an average 401 value of approximately 0.92 was used.

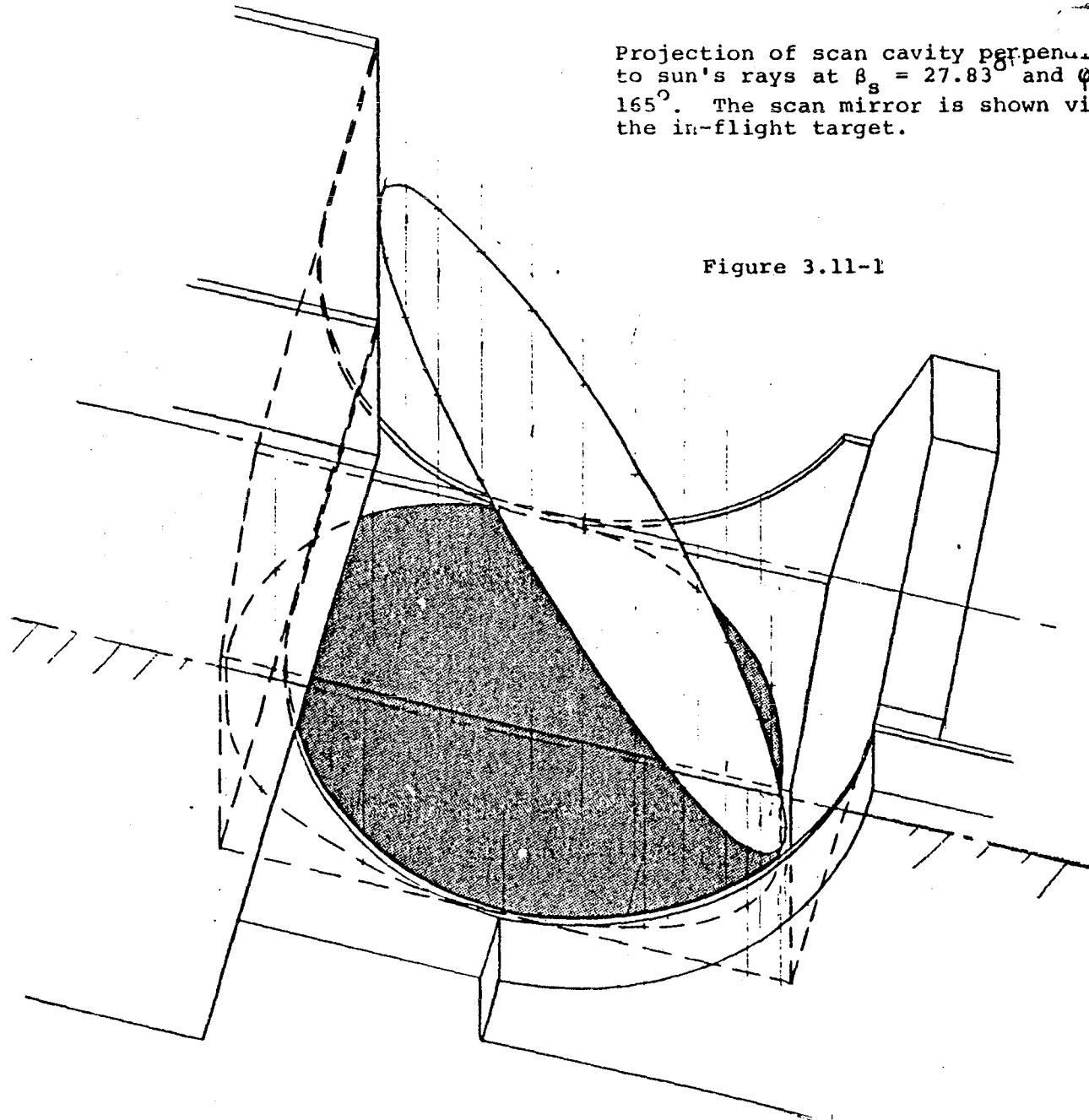
The exposed area A_s normal to the sun's rays was determined from scan cavity projections supplied by J. D. Crawford. The worst case situation is shown in Figure 3.11-1. It occurs at a δ angle of 27.83° , when the spacecraft leaves the earth's shadow, and an orbital position 15° north of the plane of the ecliptic in the night-time part of the orbit. The value of A is 10.9 square inches when shading from the anticipated spacecraft is included. We then have (in the absence of any sun shield)

$$M_s (\text{Ch. 3}) = 8.43 \times 10^{-8} \text{ Wcm}^{-2}$$

$$M_s (\text{Ch. 4}) = 1.24 \times 10^{-6} \text{ Wcm}^{-2}$$

Projection of scan cavity perpendicular
to sun's rays at $\beta_s = 27.83^\circ$ and $\phi_s =$
 165° . The scan mirror is shown viewing
the in-flight target.

Figure 3.11-1



ORIGINAL PAGE IS
OF POOR QUALITY

The comparative effect of the reflected sunlight is shown in Figure 3.11-2. In Channel 3, the sunlight produces an exitance level that is more than 4 orders of magnitude below that of the 295K self-emission. On the other hand, the reflected sunlight in Channel 4 is only about an order of magnitude below the self-emission.

The calibration error introduced by reflected sunlight may be expressed as an effective temperature increase; it is given by

$$\delta T_s = \frac{M_s}{dM/dT}$$

where dM/dT is the rate of change of in-band blackbody exitance at the nominal target temperature of 295K (22°C). For the bands of interest, we have

$$\frac{dM}{dT} \text{ (Ch. 3)} = 4.263 \times 10^{-5} \text{ Wcm}^{-2} \text{ K}^{-1} \text{ at } T = 295\text{K}$$

$$\frac{dM}{dT} \text{ (Ch. 4)} = 1.905 \times 10^{-6} \text{ Wcm}^{-2} \text{ K}^{-1} \text{ at } T = 295\text{K}$$

The calibration errors for the worst case are then

$$\delta T_s \text{ (Ch. 3)} = 0.002^\circ\text{C}$$

$$\delta T_s \text{ (Ch. 4)} = 0.65^\circ\text{C}$$

3.11.3 Signal Contamination

With the AVHRR mounted as shown in Figure 2 of GSFC Specification S-731-P-118 (Rev. C), there is a large effective sunshield (i.e., the spacecraft itself) that limits direct solar exposure of the instrument to the night-time portion of the orbit. During this time, of course, Channels 1 and 2 are not used. As a result, we need to consider the effect of scattered sunlight only in Channels 3 and 4. In common with the reflections from the in-flight target, the larger effect is in Channel 4.

We may define the required attenuation coefficient for scattered sunlight as the normal solar incidence (irradiance) outside the earth's atmosphere divided by one-third of the minimum radiant signal,

$$a = \frac{E_s}{(1/3)(\text{NER})A\Omega}$$

where NER = noise equivalent radiance = 1.6×10^{-6}

$\text{Wcm}^{-2} \text{ ster}^{-1}$ (Ch. 3), 8.0×10^{-8}

$\text{Wcm}^{-2} \text{ ster}^{-1}$ (Ch. 4)

$A\Omega$ = throughput of optics = $5.43 \times 10^{-4} \text{ cm}^2 \text{ ster}$.

The NER values were supplied by R. J. Koczor for the nominal spectral bands and a 0.12K NETD. We therefore require

$$a(\text{Ch. 3}) = 5.87 \times 10^4 \text{ cm}^{-2} = 3.79 \times 10^5 \text{ in}^{-2}$$

$$a(\text{Ch. 4}) = 1.74 \times 10^7 \text{ cm}^{-2} = 1.12 \times 10^8 \text{ in}^{-2}$$

Attenuation coefficients for scattered sunlight were measured as part of an earlier study on the HRIR (Final Technical Report, Solar Sun Shield Study for the HRIR on TIROS-M Satellite, Feb. 6, 1967, ITT-A/OD Report No. 14-16400). The HRIR had a 3.7 μm band channel and was to operate in a 750 to 900 n mi sun-synchronous orbit over a sun angle range from 37.5° to 50° . The instrument had a modest external shield and simple internal baffles with a Cassegrain telescope and a reflective secondary optic. With the scan mirror looking 45° from nadir on the sun side, attenuation coefficients of $0.6 \times 10^8 \text{ in}^{-2}$ and higher were measured, the value depending on the sun angle and orbital position.

3.11.4 Sun Scatter Test Results

The BBM AVHRR was tested to determine the level of scattered light getting into Channels 1, 2 and 4. The tests for Channels 1 and 2 were run together while that for Channel 4 required a modified set up.

3.11.4.1 Channel 1 & 2 Test Setup

The BBM was placed on a 2-axis rotary table which rotated the instrument about its pitch and yaw axes. A 9 inch aperture Astrola telescope was used to illuminate the scan cavity. A 24 Hz chopper and a tungsten iodide lamp (with a Lucalox diffuser) were used as the radiation source at the Astrola focal plane.

Signals were taken out of the Channels 1 and 2 preamplifiers (to reduce system noise) and fed to an electrical bandpass filter (20 to 31 Hz) then to a Ballantine True RMS voltmeter. The BBM was operated from the P.T.E.

3.11.4.2 Test Procedure

As discussed in Section 3.11.3 the procedure is to calculate an attenuation factor for the scattered light at various angles of irradiance. The detectors in the BBM were used for the test. They were removed from the unit (mechanically not electrically) and illuminated directly by the chopped collimator signal, thru the appropriate spectral filter. They were then placed back in the unit in their proper location to measure any scattered signal.

The collimator is used to irradiate the scan cavity at sun angles θ of 0° to 67° and orbit angles μ_s of 280° to 230° . Initial readings were taken with the scan mirror positioned at nadir and $\pm 45^\circ$ from nadir; however, no change was observed and so further testing was done with a nadir-looking scan mirror only.

3.11.4.3 Test Results Channel 1 & 2

The data obtained in this phase of the test is given in Table 3.11-1. The data is given as a function of sun angle then orbit angle. The irradiance level signal measured at the scan cavity was 6.40 volts in Channel 2 and 4.00 volts in Channel 1. As can be

Measured Irradiance Onto Scan Cavity

		Channel 1 4.0 volts		Channel 2 6.4 volts			
SUN GLE	ORBIT ANGLE	CHANNEL 1 SIGNAL			CHANNEL 2 SIGNAL		
		.58 mv	NADIR	-45°	+45°	NADIR	-45°
67°	280°	.58 mv	.58 mv	.60 mv	.53 mv	.55 mv	.53 mv
	270	.56	.58	.61	.52	.53	.54
	260	.62	.63	.62	.51	.53	.53
	250	.60	.60	.63	.52	.53	.55
	240	.63	.60	.62	.54	.52	.57
	230	.66	.63	.66	.56	.57	.58
58°	280	.65	.60	.60	.55	.50	.52
	270	.65	.65	.65	.50	.50	.50
	260	.58	.60	.60	.53	.46	.53
	250	.56	.57	.57	.45	.48	.52
	240	.58	.62	.57	.51	.50	.50
	230	.57	.57	.58	.55	.53	.53
50°	280	.62	.56	.60	.52	.54	.62
	270	.60	.61	.59	.54	.53	.52
	260	.60	.60	.58	.52	.51	.51
	250	.65	.63	.62	.54	.50	.53
	240	.65	.62	.64	.55	.54	.54
	230	.64	.67	.65	.63	.62	.64
41°	280		.62			.55	
	270		.58			.52	
	260		.58			.52	
	250		.60			.56	
	240		.62			.60	
	230		.63			.60	
29°	280°		.55 mv			.58 mv	
	270		.56			.59	
	260		.62			.58	
	250		.65			.58	
	240		.63			.61	
	230		.63			.60	
18°	280		.58			.55	
	270		.60			.57	
	260		.63			.57	
	250		.60			.60	
	240		.60			.60	
	230		.56			.56	
9°	280		.63			.56	
	270		.61			.57	
	260		.61			.59	
	250		.62			.61	
	240		.60			.60	
	230		.61			.62	

TABLE 3.11-1
CHANNELS 1 & 2 SCATTERED SIGNAL AND NOISE LEVEL

seen in Table 3.11-1, the measured signal and noise level Channel 1 was on the order of 0.65 m volts. This is a ratio of

$$\frac{4000}{.65} = 6150:1$$

Similarly in Channel 2 the ratio is

$$\frac{6400}{.58} = 11000:1$$

There was no evidence of a measurable scattered light signal in either channel at any of the measurement points. This was verified by blocking off the source. The numbers given in the Table are only the noise in the test setup.

Using the formula given earlier, we have

$$a = \frac{E_s}{E_s/\pi \times .005 \times 1/3 \times \Omega A}$$

In the above case the coefficient gives the attenuation required for the scatter to be equal to the specified noise equivalent albedo ($1/3$ of $1/2$). Using the coefficient we can calculate the required ratio of S_1 (collimator irradiance) to S_2 (scatter signal measured in system) as

$$S_1/S_2 = A_d \times A$$

Where A_d is the test detector area. In our case AVHRR thruput is $5.43 \times 10^{-4} \text{ cm}^2 \text{ ster}$ (including secondary obscuration) so that

$$a = 2.24 \times 10^7 \text{ in}^{-2}$$

The test detector has a 0.010" square aperture so that the ratio that would be measured in the test set up if the scattered signal were equivalent to the specified Noise Equivalent Albedo is

$$S_1/S_2 = (.01)^2 \times 2.24 \times 10^7 = 2240:1$$

In both channels our test ratio was at least 3x better than this. Therefore, we conclude that if there is any scattered signal in the orbits and at the angles measured (which are the computer-projected "worst cases"), they are at least three times less than the Noise Equivalent Albedo specified.

3.11.4.4 Channel 4 Test Set Up

The BBM AVHRR was in place on the two axis table with the collimator in position as for Ch 1 and 2. However, an .027" square active area InSb detector was placed at the focus of the IR Relay lenses. A Channel 4 filter is set in place in front of the detector so that only the spectral band of interest is viewed. This detector-filter combination is placed at the scan cavity for incidence measurement as above. The radiance source is a 900°C blackbody source chopped as before at 24 Hz.

The scan mirror was checked at several angles on various sun positions, but no measurable effect was observed. All recorded data is for the scan mirror at nadir.

The procedure was basically identical to that previously described; however, since Channel 4 can be used at night, the orbital angles which were checked were extended to a range of 230° to 310°. Table 3.11-2 gives the measured results.

3.11.4.5 Test Results Channel 4

The maximum measured scattered signal plus noise was 85 microvolts. With an incidence signal of .636 volts, we have a ratio of

$$\frac{636000}{85} = 7480:1$$

ORBIT
ANGLE
S

SUN ANGLE β_s

	<u>7°</u>	<u>18°</u>	<u>29°</u>	<u>38°</u>	<u>48°</u>	<u>54°</u>	<u>67°</u>
230°	20	20	15	15	20	15	25
240	20	20	15	15	25	20	30
250	20	15	15	15	15	30	25
260	15	25	20	20	25	20	30
270	25	30	20	25	45	50	85
280	15	25	25	20	25	35	30
290	20	20	30	15	20	20	15
300	20	15	15	15	30	25	25
310	25	15	15	30	20	25	20

Readings are in microvolts

MEASURED IRRADIANCE ONTO SCAN CAVITY IS .636 volt rms

1 NER = 24 microvolts

TABLE 3.11-2

CHANNEL 4 SCATTERED SIGNAL PLUS NOISE LEVELS

The required attenuation coefficient for Channel 4 has been calculated to be $1.12 \times 10^8 \text{ in}^{-2}$ for a scattered signal equal to 1/3 NER. The ratio S_1/S_2 for this channel is

$$S_1/S_2 = (1.12 \times 10^8) (.027 \text{ in})^2 = 81650$$

where .027" is the InSb detector width. This means that the maximum scattered signal found is equivalent to

$$\frac{81650}{3 \times 7480} = 3.6 \text{ NER}$$

SUMMARY

Measurements in the solar channels indicate that no measurable scattering exists in these channels at solar incidence angles which computer projections indicate are worst case conditions. In Channel 4, the measured scattered signal is less than two NER's for orbits with sun angles below about 48° and at all orbit angles except 270° . The maximum measured anywhere is 3.6 NER's.

It is apparent that no sun shield is required for the solar channels. Further because of the low level and limited extent of the scattered signal in Channel 4, it is probable that no sun shield is required in that channel. Further, assuming a reasonably sized shield attached to the AVHRR, it is not possible to eliminate the scattered signal completely since the irradiance is reaching the telescope through the shield area which would be cut out to allow an earth view at the maximum scan angle.

4.0 MECHANICAL DESCRIPTION

4.1 Overall Instrument Configuration

The AVHRR instrument design provides for a basically modular configuration. An exploded view of the instrument which depicts the various modules is shown in Figure 4.1-1. The basic modules are:

1. Base plate with related cover plates
2. Scanner
3. Optics
4. Radiant Cooler
5. Electronics

An outline drawing of the assembled instrument is shown in ITT Drawing No. 8008778 which is reproduced in Figure 4.1-2.

4.1.1 Structure

The baseplate can be seen in Figure 4.1-1. Provision is made for locating the scanner and optics on the base plate by means of dowel pins. The radiant cooler is positioned by means of shims in order to align the Channel 3 and 4 detectors to the optical axis. The electronics package attaches to the side of the instrument by means of machine screws and dowel pins for rigidity.

The structural integrity of the instrument was proven during the extensive vibration testing given both the Mechanical Structural Model and the Engineering Model. The Engineering Model successfully passed vibration tests per ITT Procedure No. 8120266 and acceleration tests per ITT No. 8120267 with the exception of

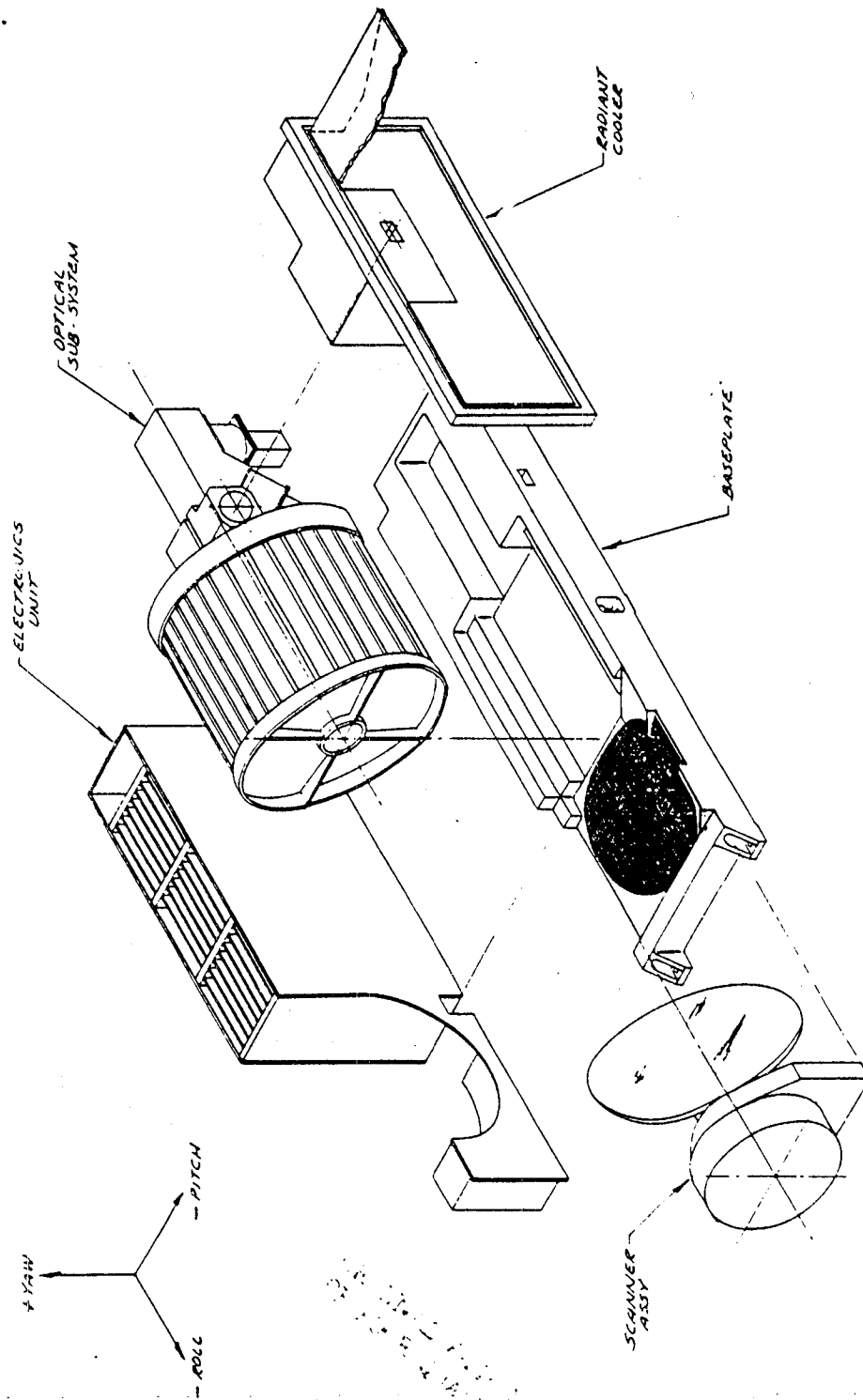
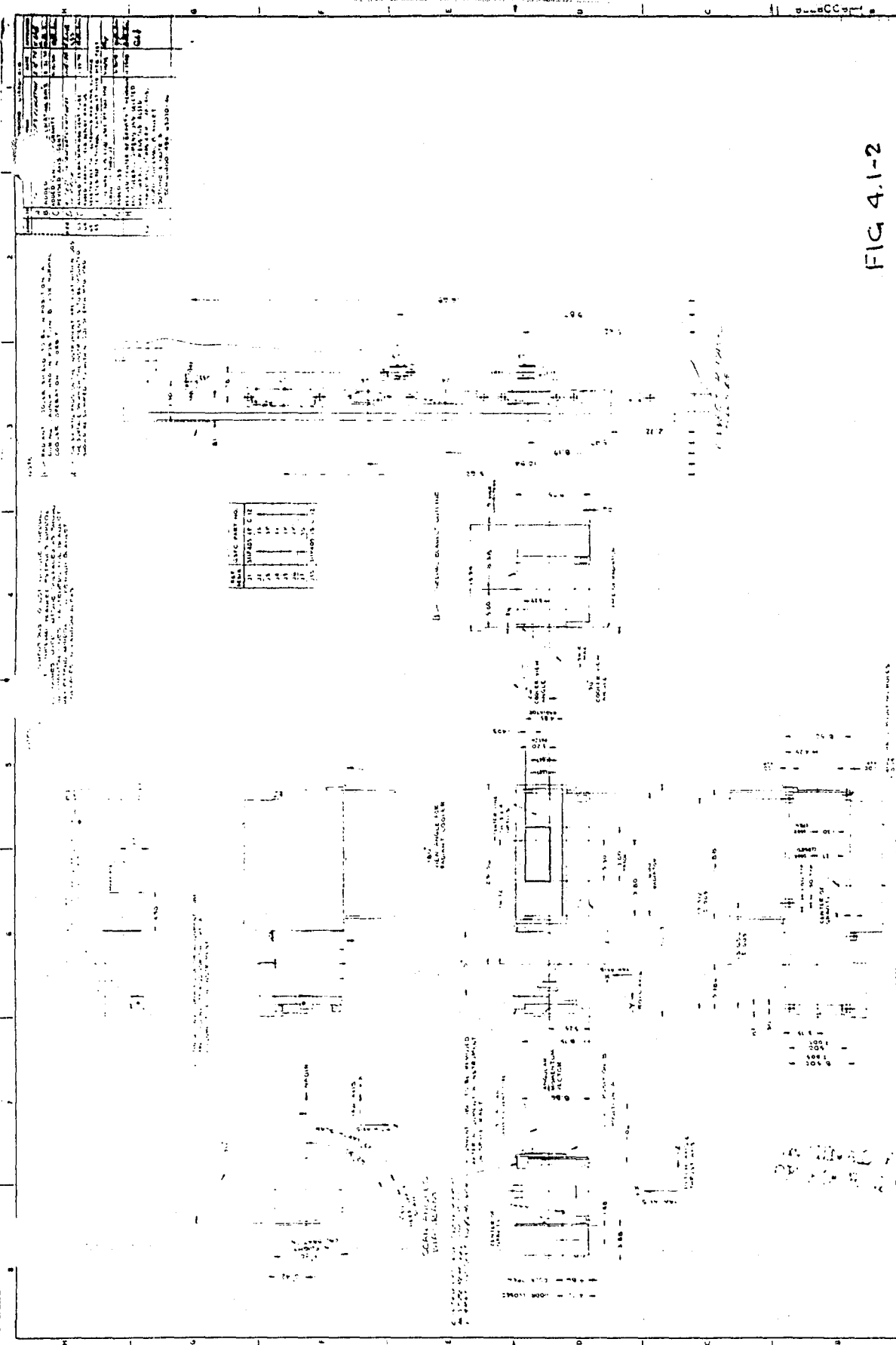


Figure 4.1-1 AVHRR Modules



NO.	REVISION	DATE	BY	CHKD.	APP'D.
1	ISSUED FOR CONSTRUCTION	10/1/54	J. J. JONES	J. J. JONES	J. J. JONES
2	REVISION	10/1/54	J. J. JONES	J. J. JONES	J. J. JONES
3	REVISION	10/1/54	J. J. JONES	J. J. JONES	J. J. JONES
4	REVISION	10/1/54	J. J. JONES	J. J. JONES	J. J. JONES
5	REVISION	10/1/54	J. J. JONES	J. J. JONES	J. J. JONES
6	REVISION	10/1/54	J. J. JONES	J. J. JONES	J. J. JONES
7	REVISION	10/1/54	J. J. JONES	J. J. JONES	J. J. JONES
8	REVISION	10/1/54	J. J. JONES	J. J. JONES	J. J. JONES
9	REVISION	10/1/54	J. J. JONES	J. J. JONES	J. J. JONES
10	REVISION	10/1/54	J. J. JONES	J. J. JONES	J. J. JONES

NO.	REVISION	DATE	BY	CHKD.	APP'D.
1	ISSUED FOR CONSTRUCTION	10/1/54	J. J. JONES	J. J. JONES	J. J. JONES
2	REVISION	10/1/54	J. J. JONES	J. J. JONES	J. J. JONES
3	REVISION	10/1/54	J. J. JONES	J. J. JONES	J. J. JONES
4	REVISION	10/1/54	J. J. JONES	J. J. JONES	J. J. JONES
5	REVISION	10/1/54	J. J. JONES	J. J. JONES	J. J. JONES
6	REVISION	10/1/54	J. J. JONES	J. J. JONES	J. J. JONES
7	REVISION	10/1/54	J. J. JONES	J. J. JONES	J. J. JONES
8	REVISION	10/1/54	J. J. JONES	J. J. JONES	J. J. JONES
9	REVISION	10/1/54	J. J. JONES	J. J. JONES	J. J. JONES
10	REVISION	10/1/54	J. J. JONES	J. J. JONES	J. J. JONES

TITLE OUTLINE DRAWING INSTRUMENT	
PROJECT NO. 3150-800877B	
DRAWN BY J. J. JONES	
CHECKED BY J. J. JONES	
APPROVED BY J. J. JONES	
DATE 10/1/54	
SCALE 1/4" = 1'-0"	
SHEET NO. 1 OF 1	

channel registration. The required registration stability was achieved on the PFM after improved methods of securing certain optical elements were incorporated into the design and pinning and staking procedures were improved.

In order to prove the structural integrity of the radiant cooler prior to vibration, a computer analysis of the configuration was conducted by Computer Sciences Corp. and Butler Analyses, Inc., under NASA Contract NAS 5-24012 Mod. 10. Copies of the Final Report of this analysis were reviewed and are on file.

4.1.2 Materials in Structure

The primary structural material is 6061-T6 Aluminum tooling plate (Alcoa Type 200). The scanner housing is fabricated from HP-20 grade Beryllium or equivalent. In some low stress areas structural parts are fabricated from AZ31B magnesium.

The magnesium surfaces are finished with DOW-7, and the aluminum is finished with Alodine 600. Where thermal control is required, the surfaces are painted.

Beryllium is electroless nickel plated.

4.2 Scanner Subassembly

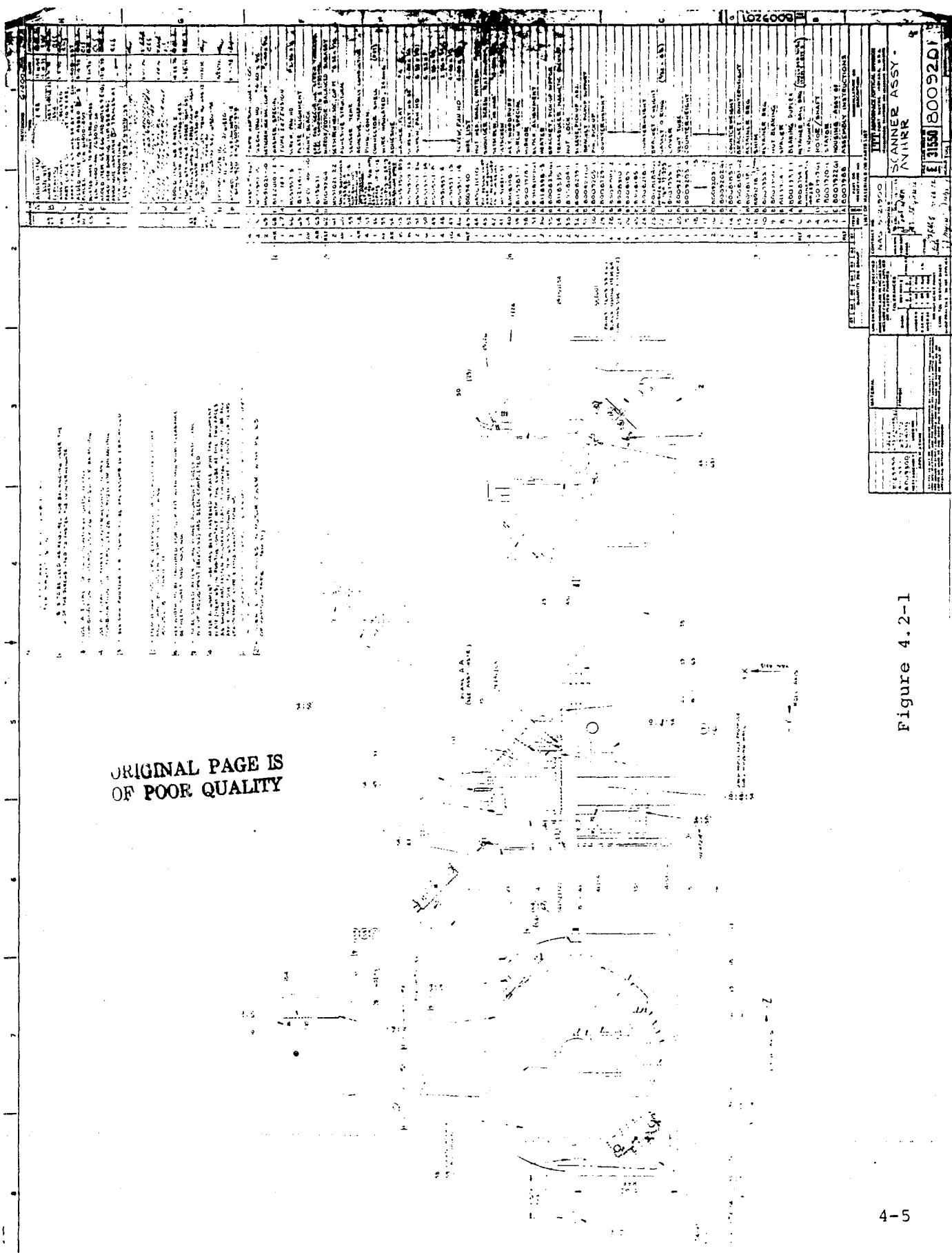
An assembly drawing of the scanner is shown in ITT Drawing No. 8009201 which is reproduced in Figure 4.2-1.

4.2.1 Scan Motor

The 80 pole hysteresis synchronous scan motor was procured from Schaeffer Magnetics, Inc., Chatsworth, California. The motor is described in ITT Specification No. 8007929. Typical performance test curves for the scanner motors are shown in Figures 4.2-2 through 4.2-5.

ORIGINAL PAGE IS
OF POOR QUALITY

Figure 4.2-1



LTM MOTOR 5/NO04
 KRYTOX LUBE
 2-6-74

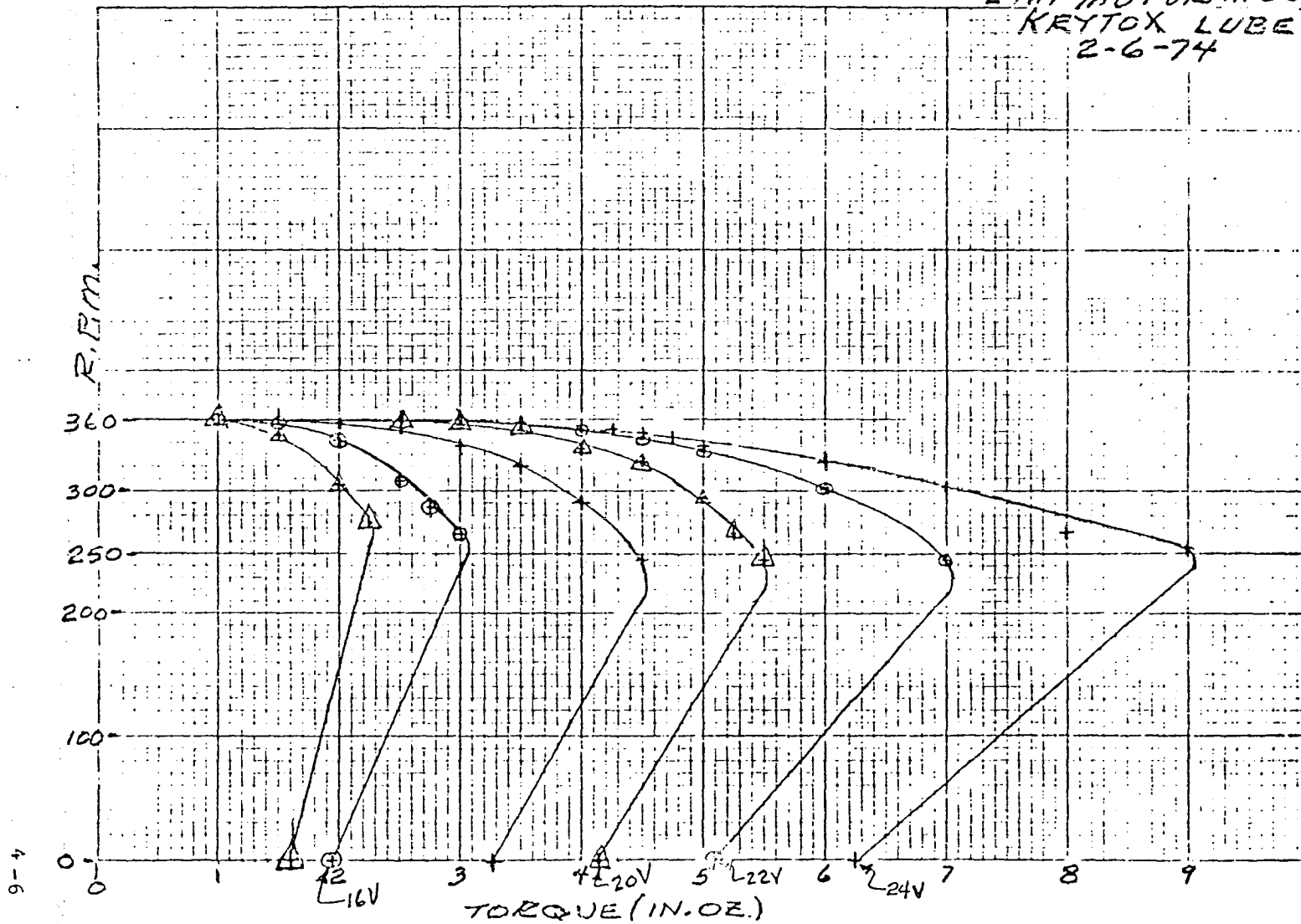


Figure 4.2-2

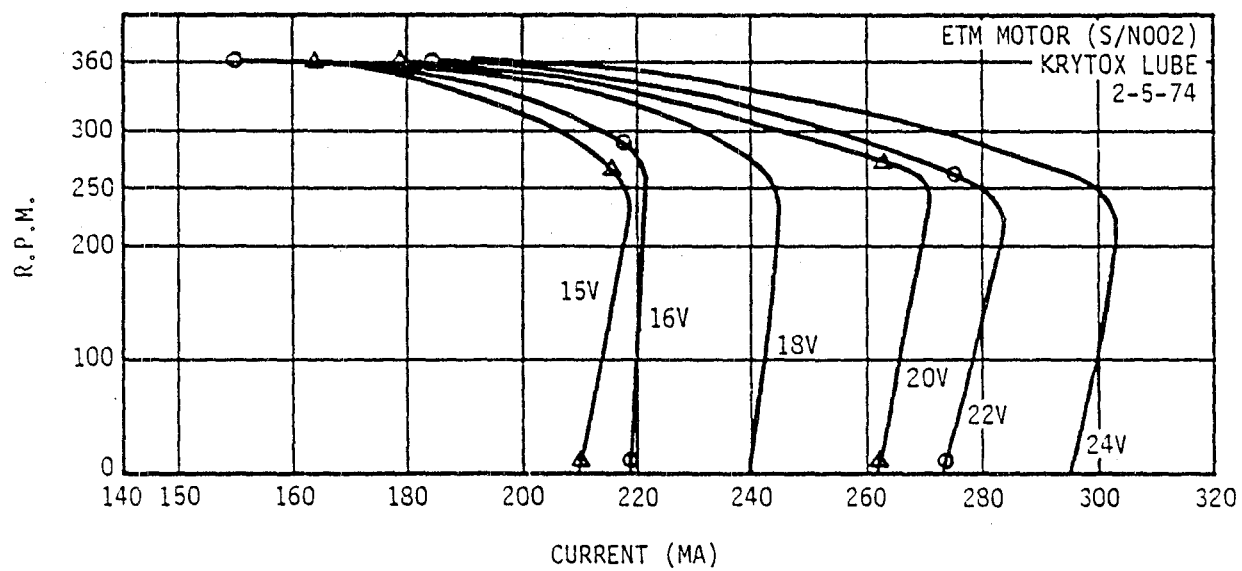


Figure 4.2-3

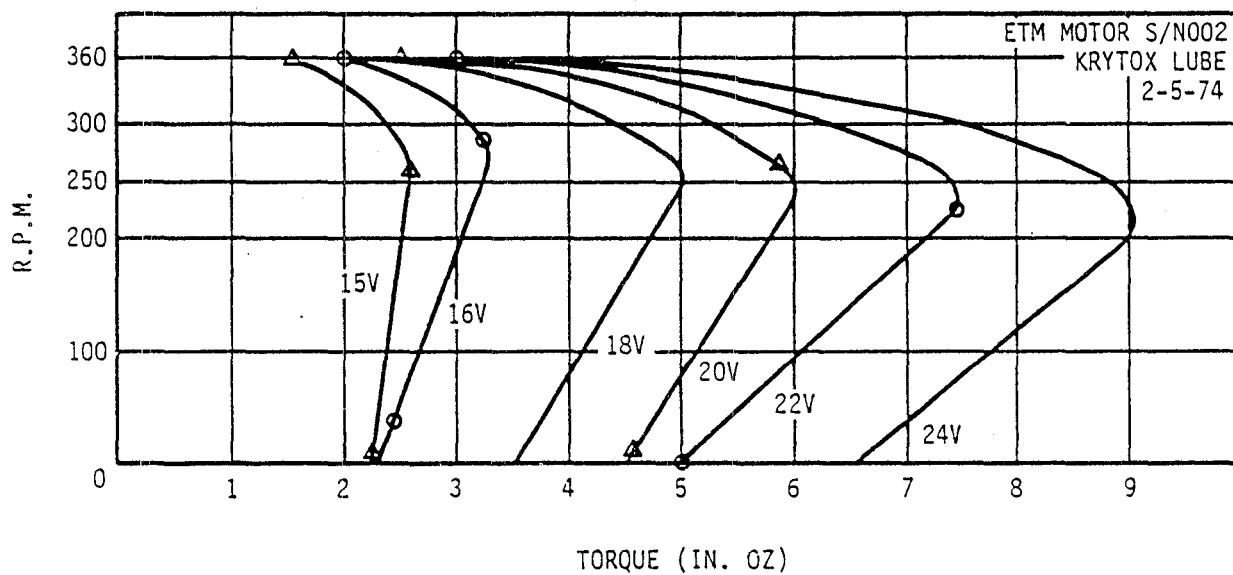


Figure 4.2-4

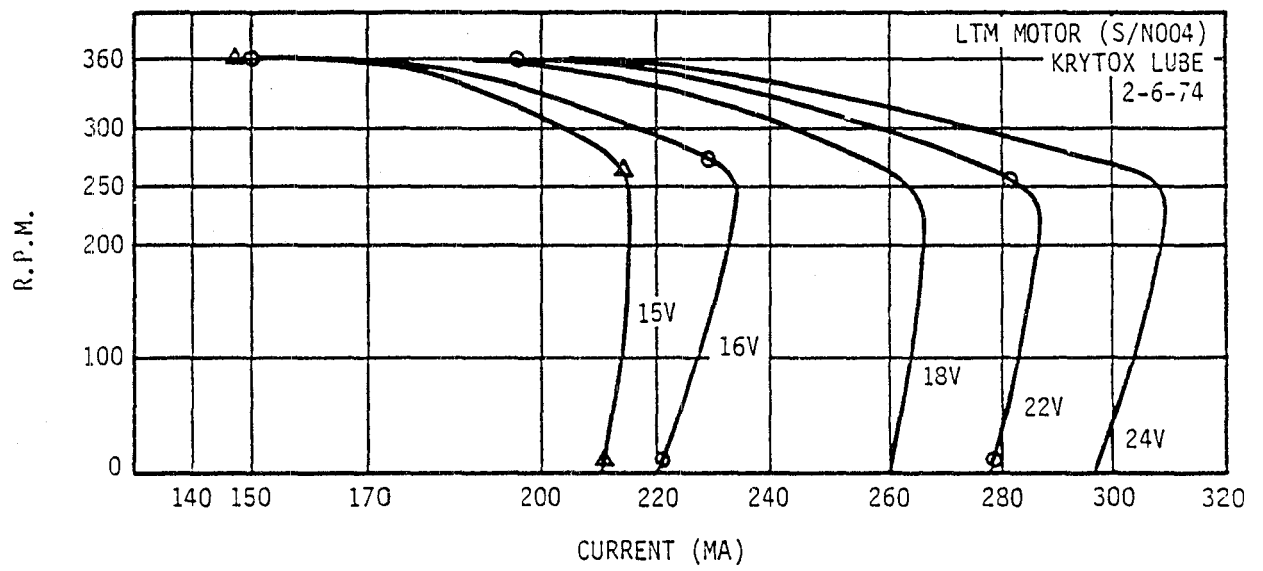


Figure 4.2-5

4.2.2 Bearings

The motor shaft bearings are a set of DB duplex bearings separated by 2 inch spacers. The bearings are specified in ITT Drawing #8007937. Each bearing has a static radial non-brinell load capacity of 602 lb. and a dynamic radial load capacity of 125 lb. for 17,500 hours of operation at 360 rpm.

An unusual feature of this bearing is the square ball pockets in the retainer. It was determined during the SCMR program that the shape of retainer ball pocket is a major factor influencing jitter. Square ball pocket bearings exhibited less jitter than round pockets. Based upon that, the AVHRR bearings were procured with square ball pockets.

Tests have shown that bearings with improved surface finish on the races (achieved both by diamond honing by the manufacturer and running in at ITT) can perform within specification when lubricated with the proper amount of lubricant. Tests have also shown that performance is appreciably degraded when too much lubricant is used.

4.2.3 Bearing Fits

Table 4.2-1 shows the shaft and housing fits for the AVHRR.

4.2.3.1 Thermal Consideration of Bearing Fit

Bearing, shaft and housing materials and coefficients of thermal expansion are noted in Table 4.2-2. The deviation from nominal bearing fit over the temperature range, 0 to +40°C, is considered negligible.

TABLE 4.2-1

SHAFT, BEARING, AND HOUSING DIMENSIONS

ID		OD	
Bearing	Shaft	Bearing	Housing
$\frac{1.0623}{1.0625}$	$\frac{1.0622}{1.0620}$	$\frac{1.5000}{1.4998}$	$\frac{1.5000}{1.5002}$

SHAFT, BEARING AND HOUSING FITS

ID		OD	
Loose	Loose	Tight	Loose
0.0001	0.0005	0.0000	0.0004

TABLE 4.2-2
THERMAL EXPANSION CHARACTERISTICS
OF BEARINGS

<u>Item</u>	<u>Material</u>	<u>Coefficient of Thermal Expansion</u>
Bearing	440 C SS	$5.6(10)^{-6}$ /°F
Shaft	Inconel X750	$6.96(10)^{-6}$ /°F
Housing	Beryllium	$6.4(10)^{-6}$ /°F

With all parts measuring nominal dimensions at 20°C, the total changes in fit at ±20°C from nominal will be:

Change in Bearing to Housing Fit	$-4.32(10)^{-5}$ IN	$+4.32(10)^{-5}$ IN
Change in Bearing to Shaft Fit	$-6.13(10)^{-5}$ IN	$+6.13(10)^{-5}$ IN

4.2.4 Lubrication

The bearings of the scanner are lubricated with Krytox 143AB. This lubricant was selected after evaluating a number of lubricants and upon the recommendation of GSFC.

A summary of the pertinent characteristics of KRYTOX 143AB is shown in the following:

Weight loss % - 30 days at 50°C & 10 ⁻⁶ mm Hg	.023%
Lubricity - cycles - Al51550 Block 150 lb. @ 100 RPM	10 ⁶ + cycles
Viscosity 32F	140 CS
Viscosity 77F	49 CS
Viscosity 100F	36 CS
Radiation Resistance - min. safe dosage	10 ⁸ rads

The amount of lubricant in each bearing is critical for achieving proper scanner performance. Nominally, 7 +1 mg of KRYTOX
-0

143AB is used in each bearing. To achieve this level, ITT Procedure No. 8008007 is followed for cleaning and lubricating each bearing.

4.2.5 Jitter

The current jitter spec calls for:

"scan line to scan line jitter as measured on the leading edge of the synchronization pulse shall be less than 1/2 of an IFOV for 98% of the data points when data is taken every scan line for a 20 minute period.

"The jitter of the synchronization pulse between any two scan lines within a 20 minute period shall be within an IFOV (34 microseconds)."

Jitter characteristics of the flight model instruments were all within the required specification. Details of the tests can be found in the individual instrument test reports.

4.2.6 Life Test

A nominal one year life test was run at ITT on the Life Test Model Scanner. The motor survived the life test as indicated by its end-of-test performance characteristics.

LTM performance characteristics are noted below.

	<u>Start-of-Test</u>	<u>End-of-Test</u>
Coast Down	1.21 min.	2.25 min.
Jitter-Line/Line	78.7% (within 8 μ sec)	99.9% (within 8 & 16 μ sec)
Torque	3.3 in oz at Drop Out	4.0 in oz at Drop Out

4.2.7 Angular Momentum

Angular momentum of the ETM scanner is calculated to be 35.8 in. oz sec based upon a measured moment of inertia of .9502 in. oz sec². Momentum vector direction is along y axis.

Moment of inertia was measured with a Model XR50 moment of inertia tester manufactured by Space Electronics, Inc.

4.2.8 Venting of the Scanner Housing

Because of the limited torque margin of the scanner motor, shaft seals are not used. A close clearance labyrinth cap does cover the shaft clearance through the housing for the purpose of limiting the outgassing toward the scan mirror and optics. Details of the cap are shown in Figure 4.2-8.

A vent hole is included in the motor housing to allow an escape path for air during decompression to preclude large volumes of air from rushing through the bearings and causing contamination. Some concern has been expressed because open vent holes could allow lubricant vapor to escape after the instrument is in orbit. While this does not appear to be a problem when Krytox is used provision has been made for a fitting to be attached to the vent hole as requested by NASA/GSFC.

4.3 Radiant Cooler Subassembly

An exploded view of the radiant cooler is shown in Figure 4.3-1.

4.3.1 Support Body

The radiator is supported by nine support rods fabricated of glass epoxy composite tubing (G10 Synthane) and stainless steel inserts, or end caps:

2 pcs .25" O.D. x .19" I.D. x 1.31" total length or .98" thermal length
2 pcs .25" O.D. x .19" I.D. x 0.82" total length or .52" thermal length
5 pcs .38" O.D. x .28" I.D. x 3.40" total length or 3.15" thermal length

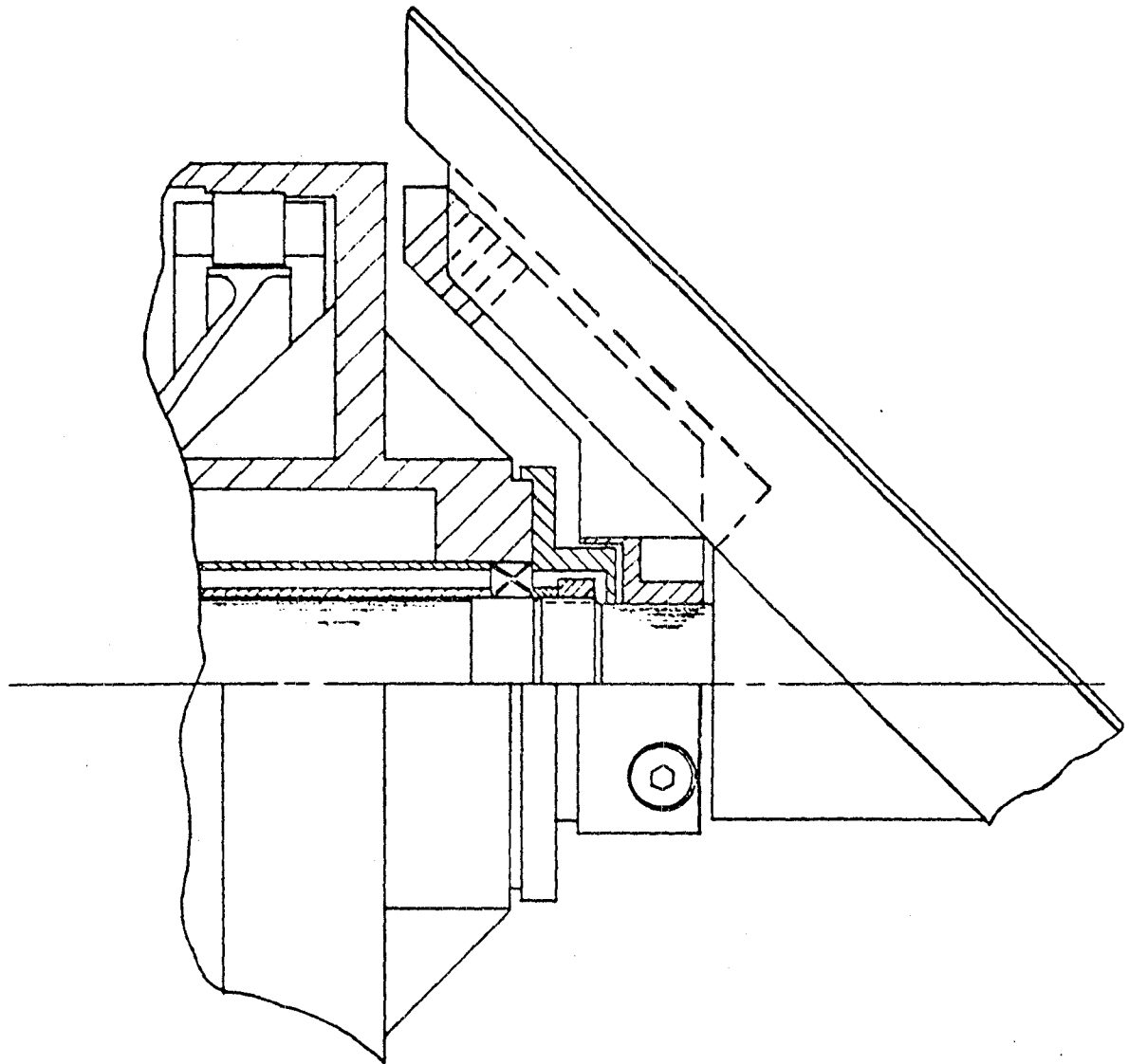
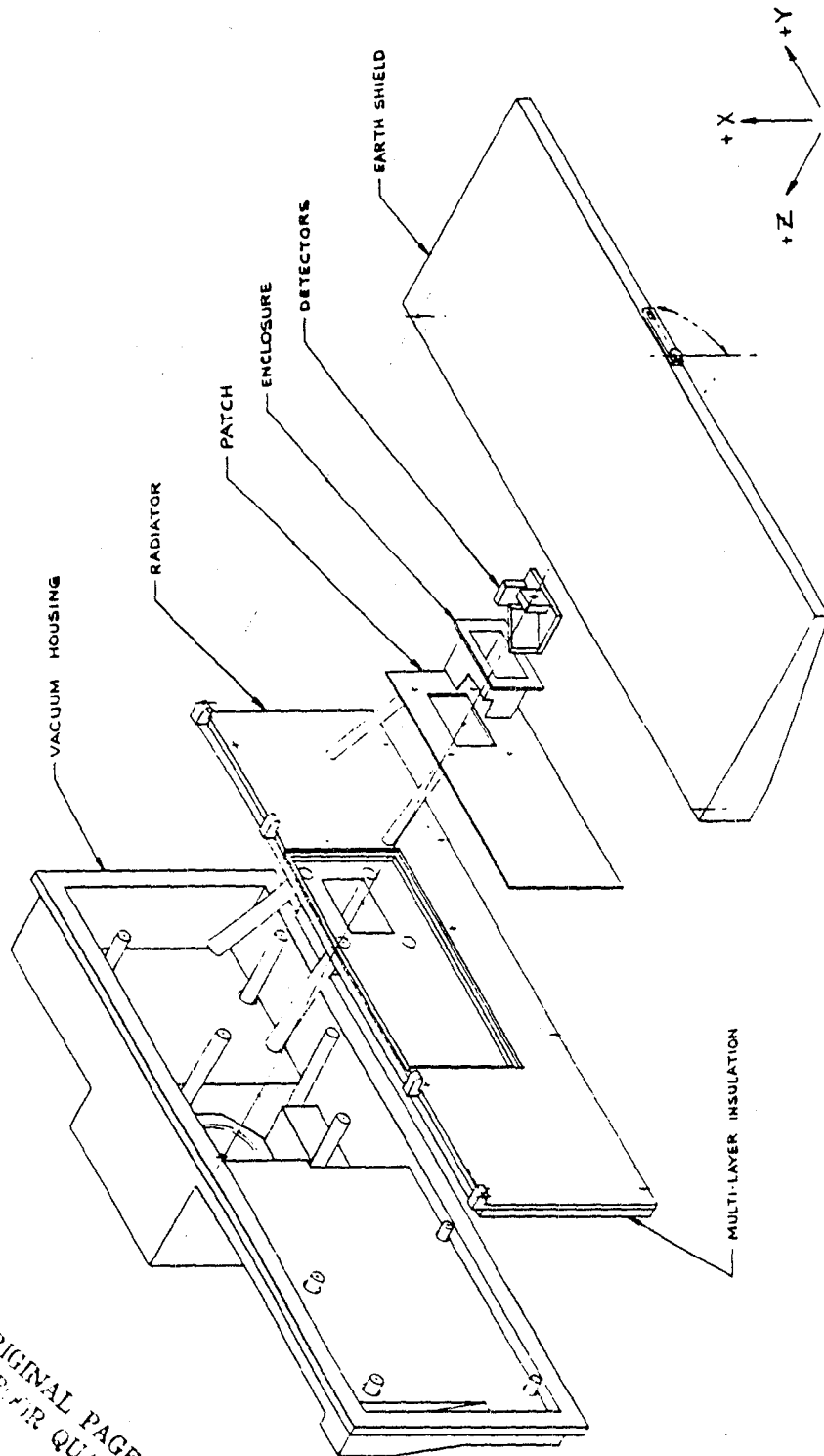


Figure 4.2-8 Shaft Clearance Cap

ORIGINAL PAGE IS
OF BETTER QUALITY



Exploded View Radiant Cooler

FIG 4.3-1

The patch is supported by four rods of the same materials as above:

.19" O.D. x .16" I.D. x 3.06" total length or 2.70" thermal length

4.3.2 Detector Location

The detectors for Channels 3 and 4 are located on the patch. A layout of the detectors on the patch is shown in Figure 4.3-2.

4.3.3 Deployable Earth Shield

The radiant cooler Earth shield is a "one-shot" device which will be deployed by torsion springs located at the hinge pins. A mechanical latch holds the shield in the closed (undeployed) position. Two rotary solenoids are utilized to release the latch. Each is independent of the other and each capable of unlatching the shield.

Switches located at both the open and closed positions will indicate shield position.

A positive mechanical stop which is an integral part of the radiator will stop the shield in the open position.

Hinges consist of music wire torsion springs rotating in polyimide bushings. No lubricant is required.

The shield can be manually closed without the aid of special tools.

In order to deploy the shield in a 1g gravity field for test, the torsion springs develop 162 in. oz of torque of which 40 in. oz are required to lift the weight of the shield and 2 in. oz are required to overcome friction in the bearings. With torsion springs designed to produce 162 in. oz torque, the torque margin in orbit is greater than 80:1.

An analysis of the earth shield door motion was made and reported in DIR #36.

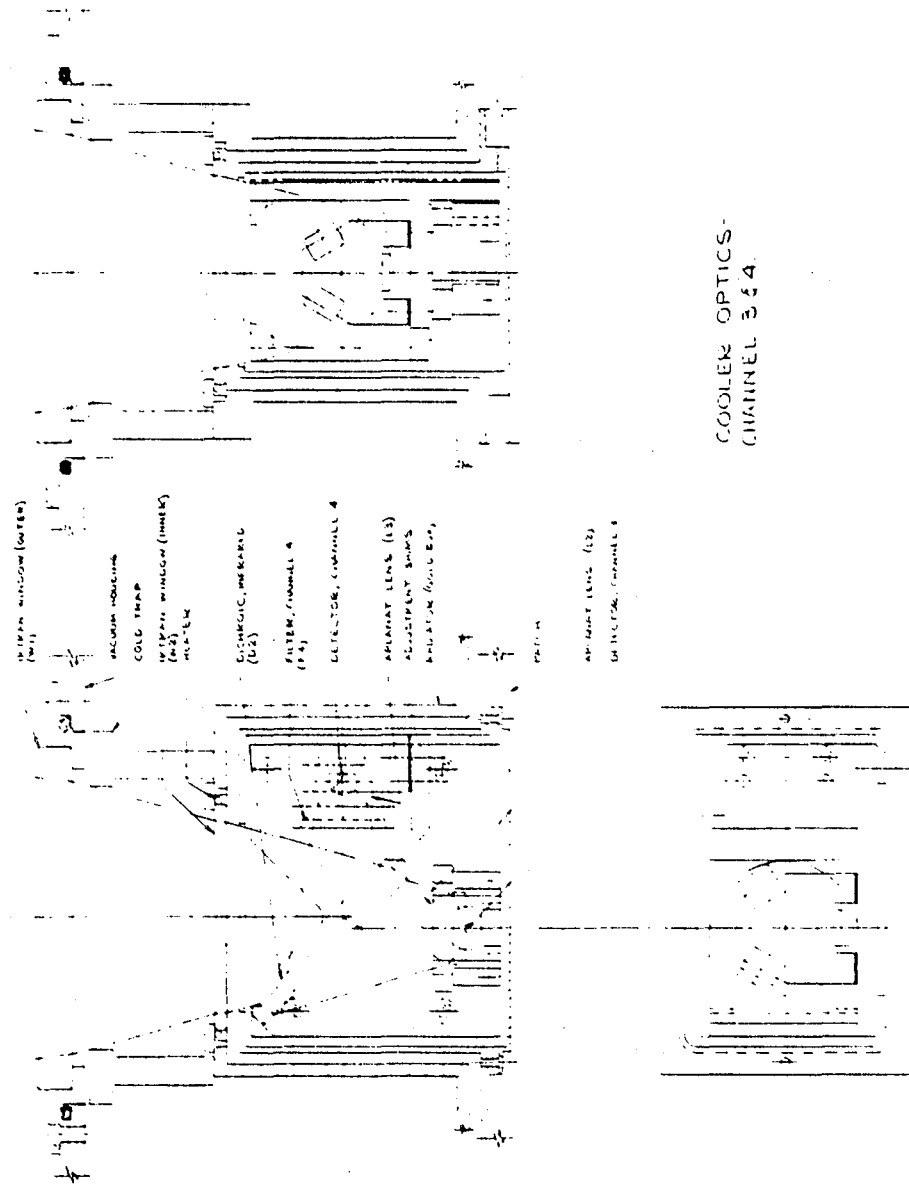


Figure 4.3-2

ORIGINAL PAGE IS
UNCLASSIFIED

4.3.4 Materials and Finishes in Cooler

Generally, the major cooler components are fabricated from 6061 T6 aluminum. Radiator surfaces are electroplated gold and painted black with 3M401. The back of the patch and the surfaces of the gold box are electroplated gold. The earth shield is electroless nickle plated and polished optically. Then it is coated with evaporated aluminum. Aluminized polyester film multi-layer insulation is used inside the cooler with polyester mesh separators.

4.4 Optics Subassembly

4.4.1 Optics Outline

The optics assembly is shown in ITT Drawing No. 8008030 - Figure 4.4-1.

4.4.2 Materials and Finishes Used in Optics

Generally, 6061 Aluminum is used as the main structural material. The corrugated tube in the telescope is invar. Graphite filled polyimide is used as the separator material for lens elements.

4.5 Electronics Package

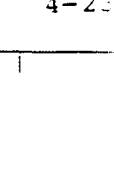
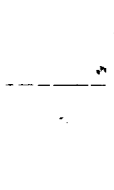
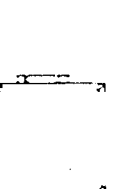
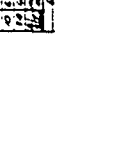
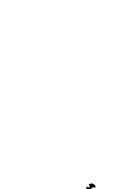
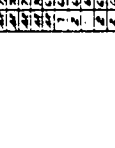
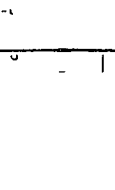
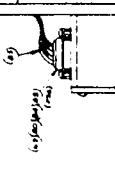
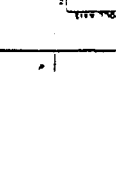
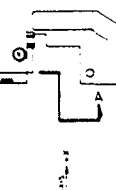
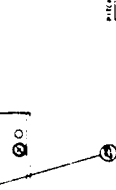
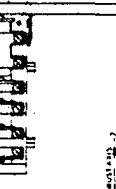
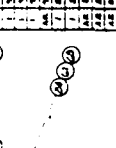
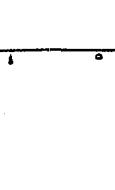
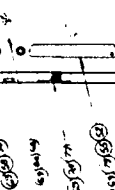
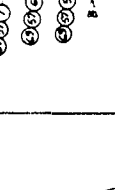
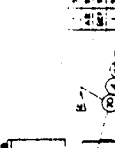
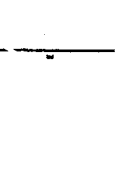
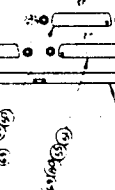
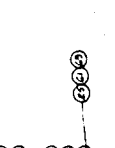
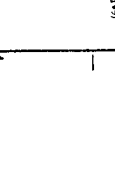
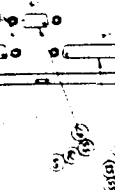
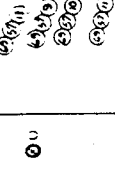
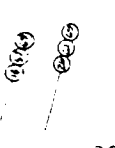
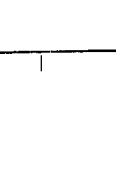
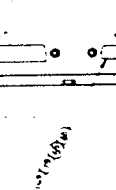
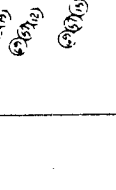
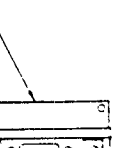
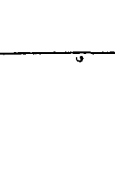
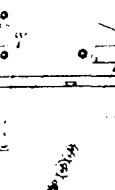
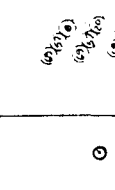
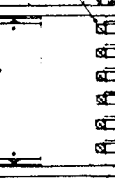
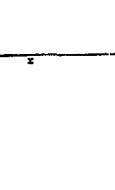
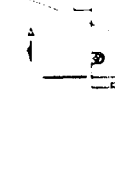
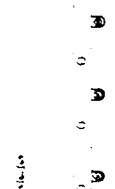
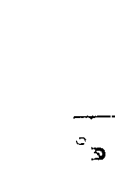
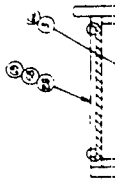
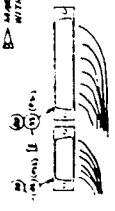
4.5.1 Electronics Package Layout

The Assembly Drawing No. 8009235 of the electronics package is shown in Figure 4.5-1.

4.5.2 Accessibility

All electronics modules are accessible from the Earth side of the instrument when it is mounted on the spacecraft with the exception of Channels 1 and 2 preamps.

NOTES:
 1. ASSEMBLE PER BOOTSTRAP ASSY INSTRUCTIONS.
 2. MARK REPAIRS AND REWORKS IN THE MARGINS SHOWN WITH PENCILS. MARKS MUST BE ON REAR (OPP) SIDE.
 3. SEE NEXT ASSY DWG FOR LOCATION OF PSI EPS.
 4. APPLY ADHESIVE TO SCREW HEADS AND/OR NUTS ONLY - NOT TO "SHREDS".
 5. FOR THE ELIMINATION OF THE PART NO FOR THE A TO U COMPUTER IS SUGGESTED.
 6. SEE INSTRUCTIONS FOR THE PART NO. WHERE THE END OF THE PART NO. IS SHOWN. THE PART NO. IS SHOWN IN THE MARGINS.

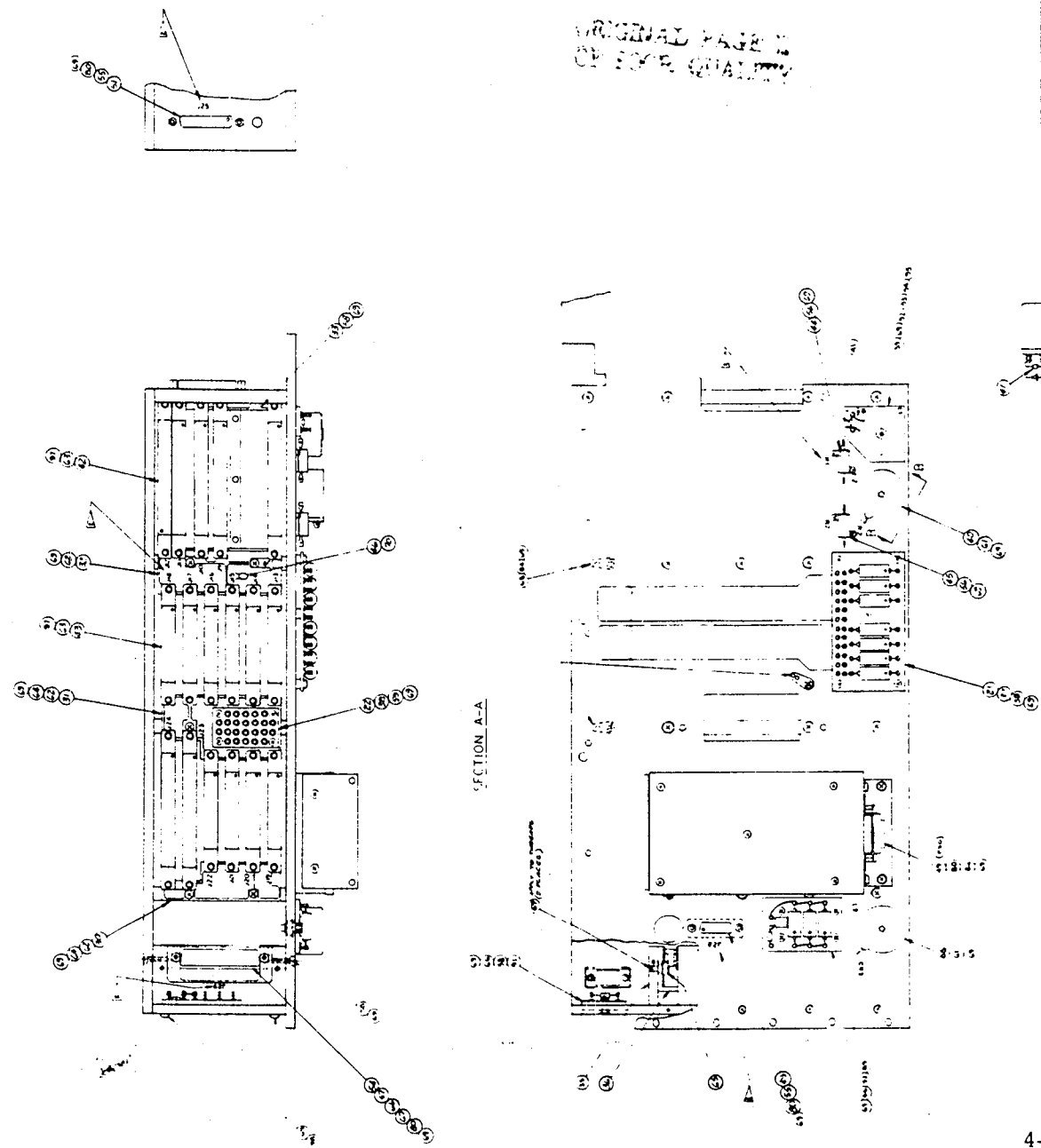


ITEM	QTY	DESCRIPTION	REMARKS
1	1	SCREW	
2	1	NUT	
3	1	WASHER	
4	1	SPACER	
5	1	PLATE	
6	1	BRACKET	
7	1	SCREW	
8	1	NUT	
9	1	WASHER	
10	1	SPACER	
11	1	PLATE	
12	1	BRACKET	
13	1	SCREW	
14	1	NUT	
15	1	WASHER	
16	1	SPACER	
17	1	PLATE	
18	1	BRACKET	
19	1	SCREW	
20	1	NUT	
21	1	WASHER	
22	1	SPACER	
23	1	PLATE	
24	1	BRACKET	
25	1	SCREW	
26	1	NUT	
27	1	WASHER	
28	1	SPACER	
29	1	PLATE	
30	1	BRACKET	
31	1	SCREW	
32	1	NUT	
33	1	WASHER	
34	1	SPACER	
35	1	PLATE	
36	1	BRACKET	
37	1	SCREW	
38	1	NUT	
39	1	WASHER	
40	1	SPACER	
41	1	PLATE	
42	1	BRACKET	
43	1	SCREW	
44	1	NUT	
45	1	WASHER	
46	1	SPACER	
47	1	PLATE	
48	1	BRACKET	
49	1	SCREW	
50	1	NUT	
51	1	WASHER	
52	1	SPACER	
53	1	PLATE	
54	1	BRACKET	
55	1	SCREW	
56	1	NUT	
57	1	WASHER	
58	1	SPACER	
59	1	PLATE	
60	1	BRACKET	
61	1	SCREW	
62	1	NUT	
63	1	WASHER	
64	1	SPACER	
65	1	PLATE	
66	1	BRACKET	
67	1	SCREW	
68	1	NUT	
69	1	WASHER	
70	1	SPACER	
71	1	PLATE	
72	1	BRACKET	
73	1	SCREW	
74	1	NUT	
75	1	WASHER	
76	1	SPACER	
77	1	PLATE	
78	1	BRACKET	
79	1	SCREW	
80	1	NUT	
81	1	WASHER	
82	1	SPACER	
83	1	PLATE	
84	1	BRACKET	
85	1	SCREW	
86	1	NUT	
87	1	WASHER	
88	1	SPACER	
89	1	PLATE	
90	1	BRACKET	
91	1	SCREW	
92	1	NUT	
93	1	WASHER	
94	1	SPACER	
95	1	PLATE	
96	1	BRACKET	
97	1	SCREW	
98	1	NUT	
99	1	WASHER	
100	1	SPACER	

[illegible]

Figure 4.5-1 (Cont'd)

ORIGINAL PAGE IS
OF POOR QUALITY



4.5.3 Thermal Considerations

Louvers on the spacecraft platform are used for thermal control. Heat sinks on each PC board conducts the heat into the structure of the electronics package.

4.5.4 Radiation Considerations

Nominally 1/8 inch thick magnesium plates are used for all external walls of the electronics package. This thickness will provide adequate radiation shielding.

4.5.5 Materials and Finishes in Electronics

The entire electronics package is fabricated from AZ31B magnesium with Dow 7 finish.

4.6 Weight Breakdown

A weight breakdown is shown in Table 4.6-1.

4.7 Materials

The Materials List has been issued as ITT Drawing No. 8009466.

MASS PROFILE

ITEM	WEIGHT
STRUCTURE	6,200 GMS
SCANNER	4,370 GMS
OPTICS	4,200 GMS
COOLER	2,575 GMS
ELECTRONICS	9,433 GMS
THERMAL BLANKET	425 GMS
	<hr/>
TOTAL IN GRAMS (GMS)	27,198
EQUIVALENT IN PDS (LBS)	59.96

TABLE 4.6-1.

5.0 ELECTRICAL SYSTEM

The basic function of the AVHRR electronics is to provide outputs of four data channels in digital form and supporting telemetry signals. Given inputs of power, a reference clock, and commands, the AVHRR electronics provides the command storage, power conversion and regulation, timing and control signal generation, a signal amplification, and analog-to-digital conversion necessary to perform its function.

A simplified block diagram of the AVHRR electronics is shown in Figure 5-1. This diagram shows the basic functions and interconnections of the electronics.

5.1 Electronic Packaging

The majority of the AVHRR electronics are mounted on printed circuit boards. The following is a list of the AVHRR boards:

1. Power Converter Assembly in a metal can
consisting of:
 - a. Power Converter and Switching Regulator
 - b. Logic Regulators
2. ± 15 Volt Regulators
3. Command Relay No. 1
4. Command Relay No. 2
5. Command Relay No. 3
6. Scan Count and Decode Logics
7. Motor Logics
8. Auxiliary Scan
9. Patch Temperature Control and Telemetry
10. Telemetry Board No. 2
11. Interface Logics No. 1
12. Interface Logics No. 2

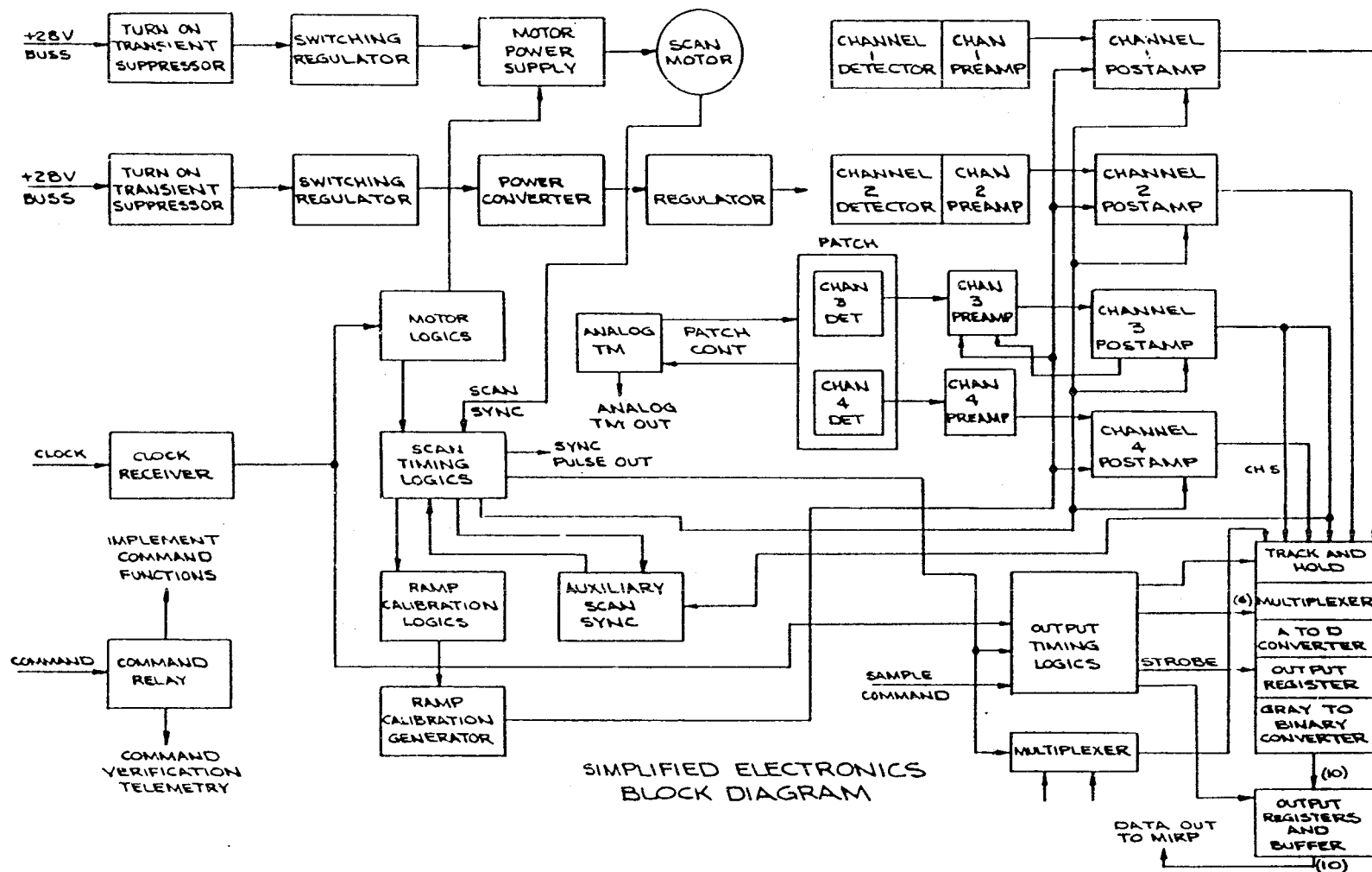


Figure 5-1

13. IR Post Amplifier
14. Daylight Post Amplifier
15. Multiplexer
16. Ramp Calibration
17. Blackbody Mux
18. Motor Power Supply
19. Switching Regulator
20. Ch 3 IR Preamplifier
21. Ch 4 IR Preamplifier
22. Daylight Preamplifier

The first 17 cards listed are mounted as plug-in units in the electronics assembly.

Items 18 and 19 are mounted in a metal can which is located between the electronics assembly and the scan motor. These two cards are hard-wired inside the can. The entire can assembly is a plug-in unit with two connectors, one to the electronics assembly, the second to the scan motor.

The Ch 3 IR Preamplifier (Item 20) is mounted in a metal can. The assembly is mounted outboard of the electronics package.

The Ch 4 IR Preamplifier (Item 21) is located on the cooler vacuum housing in the proximity of the cooler interface headers. The preamplifier board is mounted in a metal can.

Two daylight preamplifiers (Item 22) are located within the optics package with the silicon detectors connected directly to the PC board. The board is hard-wired within the optics module and is provided with copper shielding.

Break connectors are provided between the electronics package and the wiring required in the remainder of the instrument making the electronics package in its entirety a plug-in unit.

The final major assembly of the AVHRR electronics is the analog-to-digital converter. This unit is located in the electronics package with short connections to the post amplifiers and output connectors.

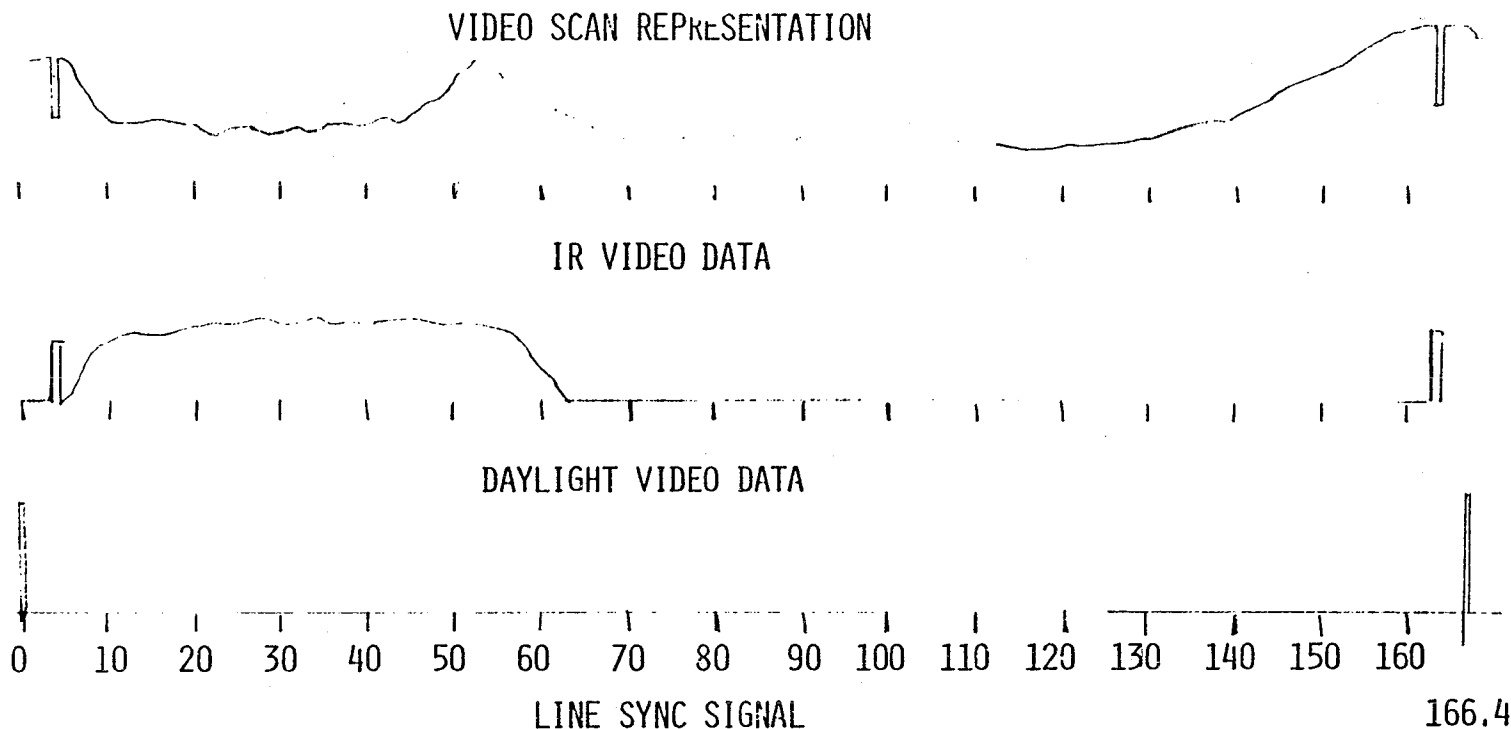
5.2 Electrical Design Considerations

The electrical design is to the extent possible based upon existing designs used on space qualified instruments. Parts selection criteria include the use of parts on the NASA/GSFC Preferred Parts List where possible and the use of previously approved parts where the PPL parts are not suitable. Derating of parts is in accordance with the requirements of the PPL and consideration of the special environment of the AVHRR.

5.3 Video Scan Timing

Figure 5-2 shows the timing relationship of the scene as viewed by the scan mirror and the sync pulse which is the time reference point. Time intervals of 1 millisecond before and after the sync pulse have been provided by insertion by the MIRP of coded pre-cursor signals. The tolerance of the viewing times due to spacecraft attitude control tolerance are indicated.

The times indicated on this drawing and times and frequencies listed on all other timing diagrams and schematics are based on a normal 1 MHz clock. To obtain actual times the numbers must be multiplied by 1.0016. To obtain actual frequencies multiply numbers of 0.9984.



0-0.1	LINE SYNC	34.2	NADIR NOMINAL
0.5-1.5	MIRP PRE-CURSOR TIME	62.6	SPACE START WORST CASE - EARLY S/C ATTITUDE
1.8	RADIOMETER SPACE VIEW START	63.1	SPACE START NOMINAL
1.9-3.5	RADIOMETER SPACE SAMPLE	63.6	SPACE START WORST CASE - LATE
3.5-4.0	RAMP CALIBRATION	65.6-65.8	IR TARGET TEMPERATURE
4.13	SPACE END WORST CASE - EARLY	65.8-66.0	PATCH TEMPERATURE
		117.1	IR TARGET FULL VIEW START
5.3	SPACE END NOMINAL	117.6-118.4	IR TARGET SAMPLE
5.8	SPACE END WORST CASE - LATE	119.0	IR TARGET FULL VIEW END
	S/C ATTITUDE	165.0-166.0	MIRP PRECURSOR TIME

5.4 Power Subsystem

5.4.1 General

The +28V DC input from the spacecraft is regulated to obtain isolation from spacecraft voltage variations, converted to develop a system ground, and re-regulated to obtain noise rejection and precision.

The schematic for the Power Converter and Switching Regulator Board is shown in Figure 5-3. The schematic for the Logic Regulator is shown in Figure 5-4. Both boards are assembled in a conetic can with LC EMI filters on all inputs and outputs with the exception of the clock signals.

5.4.2 Turn on Transient

Turn on transients are suppressed by limiting the base voltage rise time of the input pass transistor Q4 of the PC & SR. The changing path is through T2 and R17. This circuit limits the surge current into the input filtering. The input switching regulators have long time constants on the reference inputs which slows the build-up of all the circuits beyond that point.

5.4.3 Electronics Switching Regulator

Two input switching regulators are provided using Harris HA2620 amplifiers as comparators: The circuits are self starting and driven by a 62.4 Kh signal for synchronization with the spacecraft clock. A +34V boost voltage derived from the Power Converter provides the drive voltage for the pass transistor to provide good saturation for minimum dissipation.

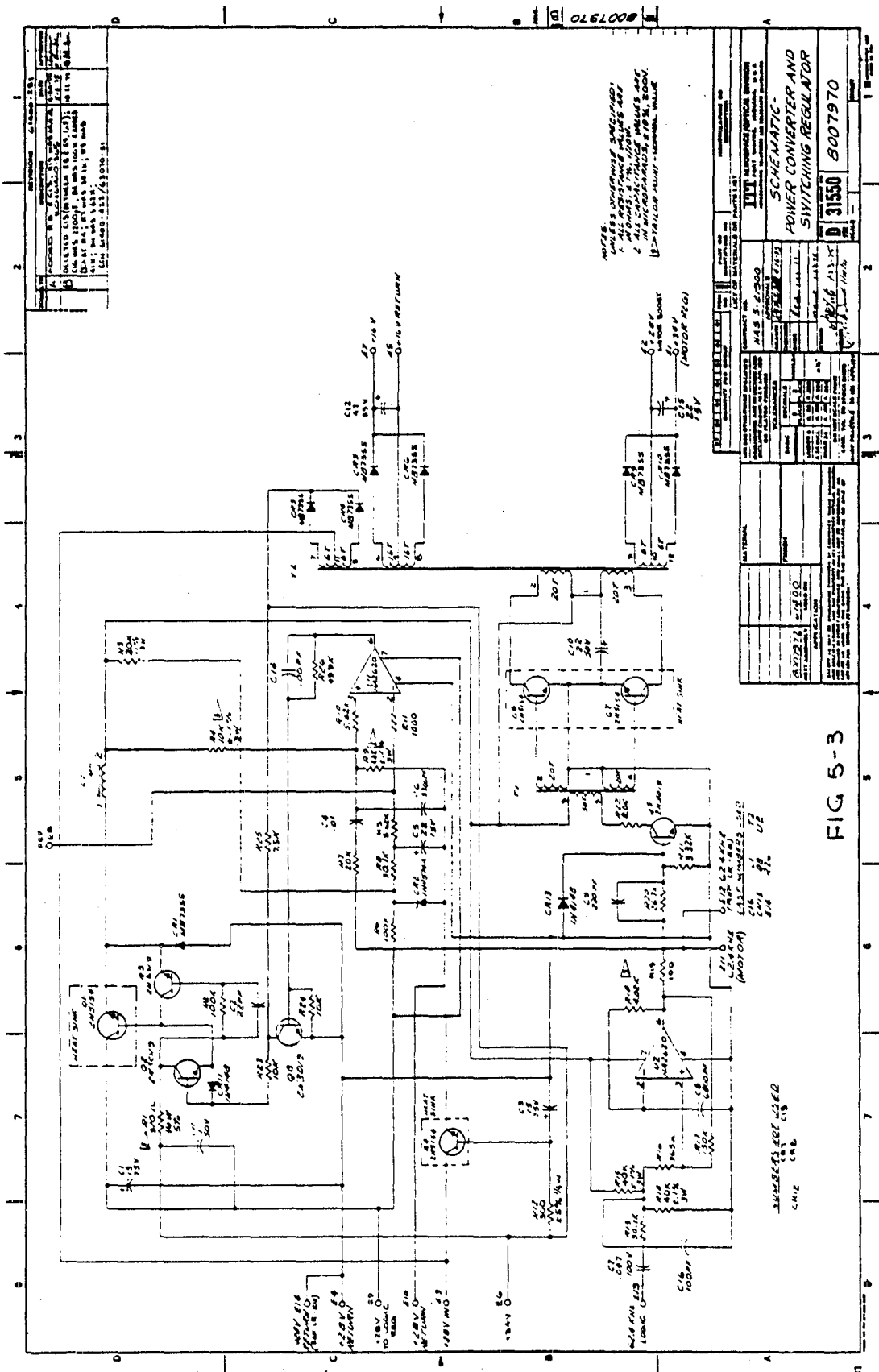


FIG 5-3

SCHEMATIC
 POWER CONVERTER AND
 SWITCHING REGULATOR

D 31550 8007970

REVISIONS	
NO.	DESCRIPTION
1	INITIAL DESIGN
2	REVISION 1
3	REVISION 2
4	REVISION 3
5	REVISION 4
6	REVISION 5
7	REVISION 6
8	REVISION 7
9	REVISION 8
10	REVISION 9
11	REVISION 10
12	REVISION 11
13	REVISION 12
14	REVISION 13
15	REVISION 14
16	REVISION 15
17	REVISION 16
18	REVISION 17
19	REVISION 18
20	REVISION 19
21	REVISION 20
22	REVISION 21
23	REVISION 22
24	REVISION 23
25	REVISION 24
26	REVISION 25
27	REVISION 26
28	REVISION 27
29	REVISION 28
30	REVISION 29
31	REVISION 30
32	REVISION 31
33	REVISION 32
34	REVISION 33
35	REVISION 34
36	REVISION 35
37	REVISION 36
38	REVISION 37
39	REVISION 38
40	REVISION 39
41	REVISION 40
42	REVISION 41
43	REVISION 42
44	REVISION 43
45	REVISION 44
46	REVISION 45
47	REVISION 46
48	REVISION 47
49	REVISION 48
50	REVISION 49
51	REVISION 50
52	REVISION 51
53	REVISION 52
54	REVISION 53
55	REVISION 54
56	REVISION 55
57	REVISION 56
58	REVISION 57
59	REVISION 58
60	REVISION 59
61	REVISION 60
62	REVISION 61
63	REVISION 62
64	REVISION 63
65	REVISION 64
66	REVISION 65
67	REVISION 66
68	REVISION 67
69	REVISION 68
70	REVISION 69
71	REVISION 70
72	REVISION 71
73	REVISION 72
74	REVISION 73
75	REVISION 74
76	REVISION 75
77	REVISION 76
78	REVISION 77
79	REVISION 78
80	REVISION 79
81	REVISION 80
82	REVISION 81
83	REVISION 82
84	REVISION 83
85	REVISION 84
86	REVISION 85
87	REVISION 86
88	REVISION 87
89	REVISION 88
90	REVISION 89
91	REVISION 90
92	REVISION 91
93	REVISION 92
94	REVISION 93
95	REVISION 94
96	REVISION 95
97	REVISION 96
98	REVISION 97
99	REVISION 98
100	REVISION 99
101	REVISION 100

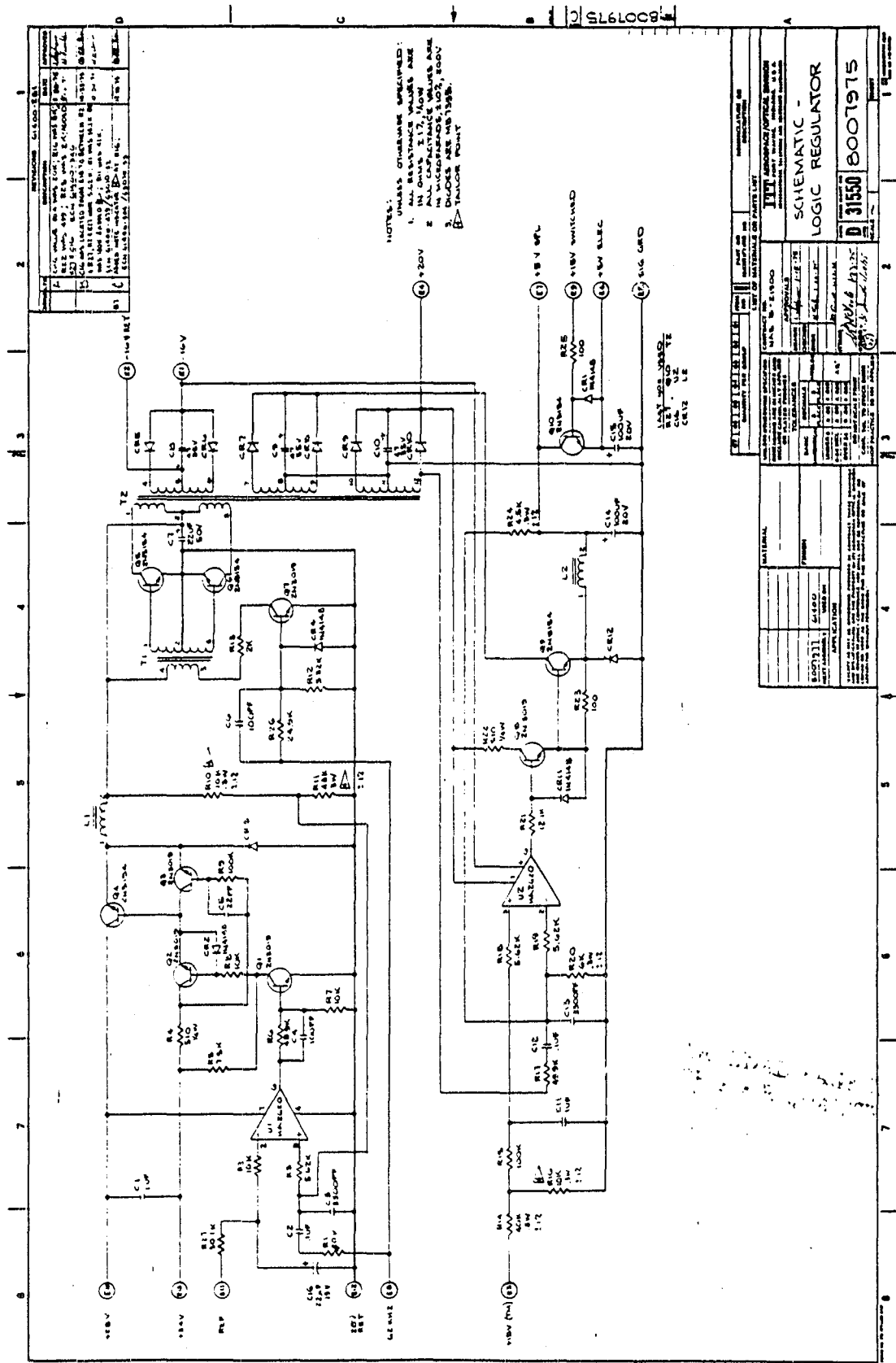


Figure 5-4

5.4.4 Power Converter

Two DC/DC Converters are provided, one powered from each Switching Regulator. These circuits establish signal ground for the AVHRR and provide the proper voltage inputs to the electronics regulators. They are driven converters being synchronized with the same 62.4 Kh clock signal as the switching regulators. The converters operate from switching regulator outputs and therefore the maximum VCE on the converter transistors is limited to 44V.

5.4.5 +5V Regulators

A switching regulator is used to provide +5 volts for logic circuits. The output of the switching regulator directly feeds the logic circuits required for motor frequency countdown and the input clock circuits. The major portion of the logics is powered through a switching transistor from the regulator output. This transistor is turned on with the Electronics ON command.

5.4.6 ± 15V Regulators

The 15 volt regulators are linear circuits utilizing the Harris HA2620 I.C. as the voltage comparator. The schematic for the ± 15V Regulators is shown in Figure 5-5.

Also on this board are the pass transistors for the channel enable/disable commands and Electronics ON command.

The +15 volt regulator uses a +20 volt "boost" voltage from the power converter to enable a low input/output differential and minimize the pass transistor power loss. The circuit will regulate under full load with an input/output differential equal to the collector/emitter saturation voltage of the pass transistor which is typically 0.2 volt.

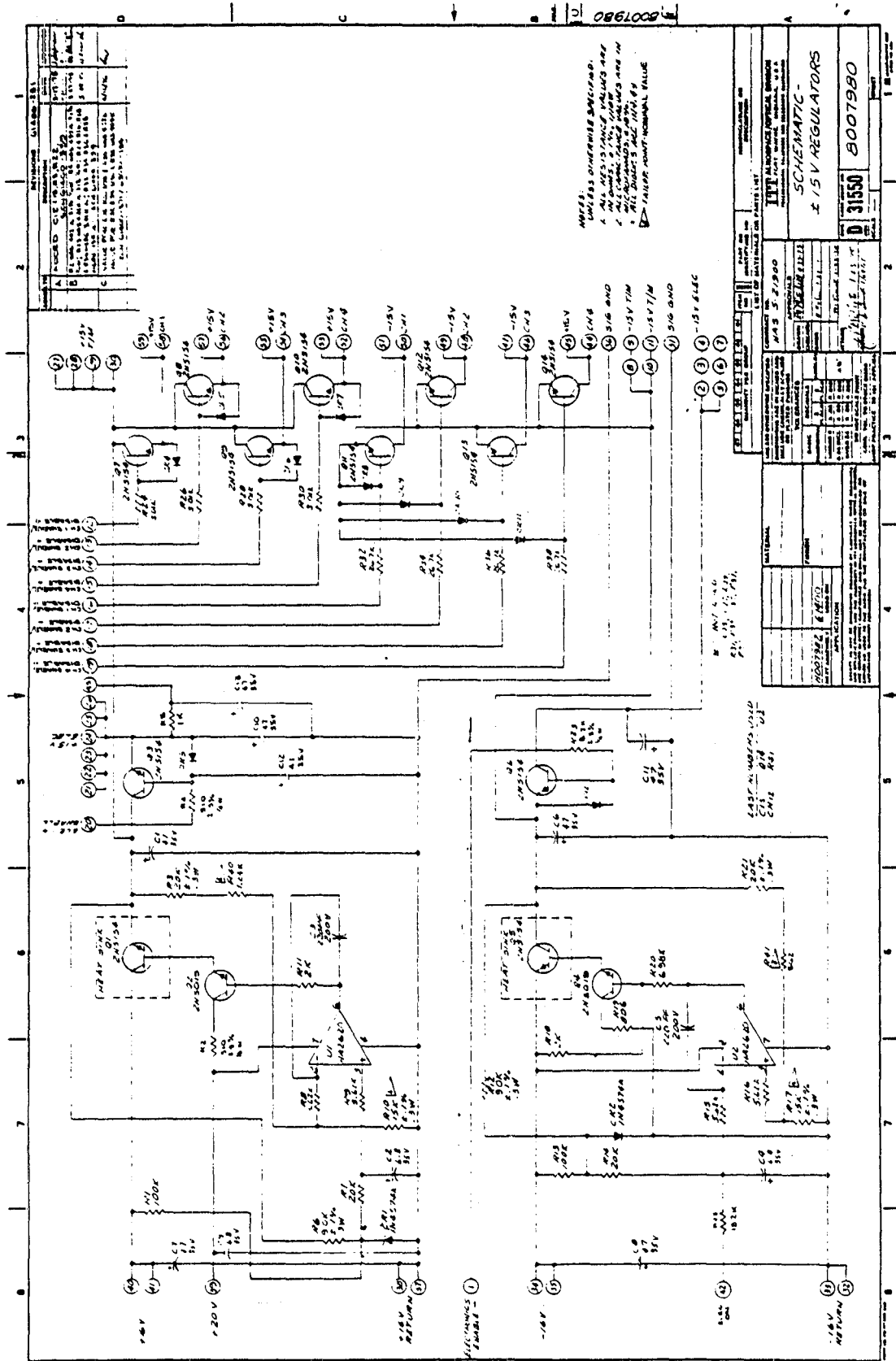


Figure 5-5

5.4.7 Motor Power Supply Switching Regulator

The schematic for the motor power supply switching regulator is shown in Figure 5-6.

The circuitry is similar to the electronics switching regulator, the exception being that the motor switching regulator will regulate at one of two voltage levels selected upon command.

5.5 Commands and Digital TM

The following is a list of the presently planned commands for the AVHRR:

1. Scan Motor/Telemetry ON
2. Scan Motor/Telemetry OFF
3. Electronics/Telemetry ON
4. Electronics/Telemetry OFF
5. Ch 1 Enable
6. Ch 1 Disable
7. Ch 2 Enable
8. Ch 2 Disable
9. Ch 3 Enable
10. Ch 3 Disable
11. Ch 4 Enable
12. Ch 4 Disable
13. Voltage Calibrate ON
14. Voltage Calibrate OFF
15. Patch Control High Mode
16. Patch Control Low Mode



Figure 5-6

17. Cooler Heat ON
18. Cooler Heat OFF
19. Scan Motor High Mode
20. Scan Motor Low Mode
21. Telemetry Locked ON
22. Telemetry Unlocked
23. Earth Shield Deploy
24. Earth Shield Disable
25. Patch Control ON
26. Patch Control OFF

The following is a list of the functions performed by executing the listed commands.

<u>Command No.</u>	<u>Function</u>
1. Scan Motor/Telemetry ON	Applies Power to: <ol style="list-style-type: none"> 1. Electronics sw. regulator 2. Motor sw. regulator 3. Power converter 4. $\pm 15V$ regulators 5. +5V logic reg. 6. Clock receiver 7. Motor logic 8. Analog telemetry circuits 9. Patch temp. control
2. Electronics/Telemetry	Applies Power to: <ol style="list-style-type: none"> 1. Electronics sw. regulator 2. Power converter 3. $\pm 15V$ regulators

2. Electronics/Telemetry - Continued

4. +5V logic regulator
 5. +5V electronics circuits
 6. Analog telemetry circuits
 7. A/D Converter
 8. Scan timing logic
 9. Clock receiver
 10. Motor logic
 11. Patch temp. control
5. Ch 1 Enable
- If "Electronics ON" has been executed - Applies Power to:
1. Ch 1 preamplifier
 2. Ch 1 Post Amplifier
7. Ch 2 Enable
- If "Electronics ON" has been executed - Applies Power to:
1. Ch 2 Preamplifier
 2. Ch 2 Post Amplifier
9. Ch 3 Enable
- If "Electronics ON" has been executed - Applies Power to:
1. Ch 3 Preamplifier
 2. Ch 3 Post Amplifier
11. Ch 4 Enable
- If "Electronics ON" has been executed - Applies Power to:
1. Ch 4 Preamplifier
 2. Ch 4 Post Amplifier
13. Voltage Calibrate
- If "Electronics ON" has been executed -
1. Deactivate IR & Daylight detectors.

13. Voltage Calibrate (Cont'd)

2. Provides simulated earth scene and backscan video.

15. Patch Control High Mode

If "Telemetry ON" has been executed

1. Sets patch temp control point to 107°K

16. Patch Control Low Mode

If "Telemetry ON" has been executed

1. Sets patch temp control point to 105°K

17. Cooler Heat ON

If "Electronics ON", "Motor ON" or "Telemetry ON" has been executed - Applied Power to:

1. Radiator Decontamination Heater
2. Patch Decontamination Heater

19. Scan Motor High Mode

If "Motor ON" has been executed -

1. Sets motor sw. regulator voltage to HIGH LEVEL

20. Scan Motor Low Mode

If "Motor ON" has been executed -

1. Sets motor sw. regulator voltage to LOW LEVEL

21. Telemetry Locked ON

Applies Power to:

1. Electronics sw. regulator
2. Power converter
3. ±15V regulators
4. +5V logic regulator
5. Clock Receiver
6. Motor Logic

21. Telemetry Locked ON (Cont'd)

7. Analog Telemetry Circuits

8. Patch control circuitry

Applies Power to:

1. Earth Shield Circuitry

Removes Power from:

1. Earth Shield Circuitry

23. Earth Shield Deploy

24. Earth Shield Disable

25. Patch Control ON

If "Telemetry ON" has been executed -

1. Applies Controlled Heat to Patch

Digital T/M

The following is a list of the Digital T/M functions:

1. Scan Motor Status	"1"	ON
	"0"	OFF
2. Electronics Status	"1"	ON
	"0"	OFF
3. Ch 1 Status	"1"	ON
	"0"	OFF
4. Ch 2 Status	"1"	ON
	"0"	OFF
5. Ch 3 Status	"1"	ON
	"0"	OFF
6. Ch 4 Status	"1"	ON
	"0"	OFF
7. Voltage Calibrate Status	"1"	ON
	"0"	OFF
8. Patch Control Mode	"1"	107°K
	"0"	105°K
9. Cooler Heat Status	"1"	ON
	"0"	OFF
10. Scan Motor Mode	"1"	
	"0"	LOW POWER

11. Telemetry Status	"1"	ON
	"0"	OFF
12. Earth Shield Status	"1"	DEPLOY
	"0"	DISABLE
13. Patch Control	"1"	ON
	"0"	OFF

The schematics for Command Relay #1, 2 and 3 are shown in Figures 5-7, 5-8 and 5-9. Command Relay's are P&B HL11D 12VDC Latching Type. For Commands and Digital T/M "1" true or 0.0V Level "0" = False or +5.0V Level.

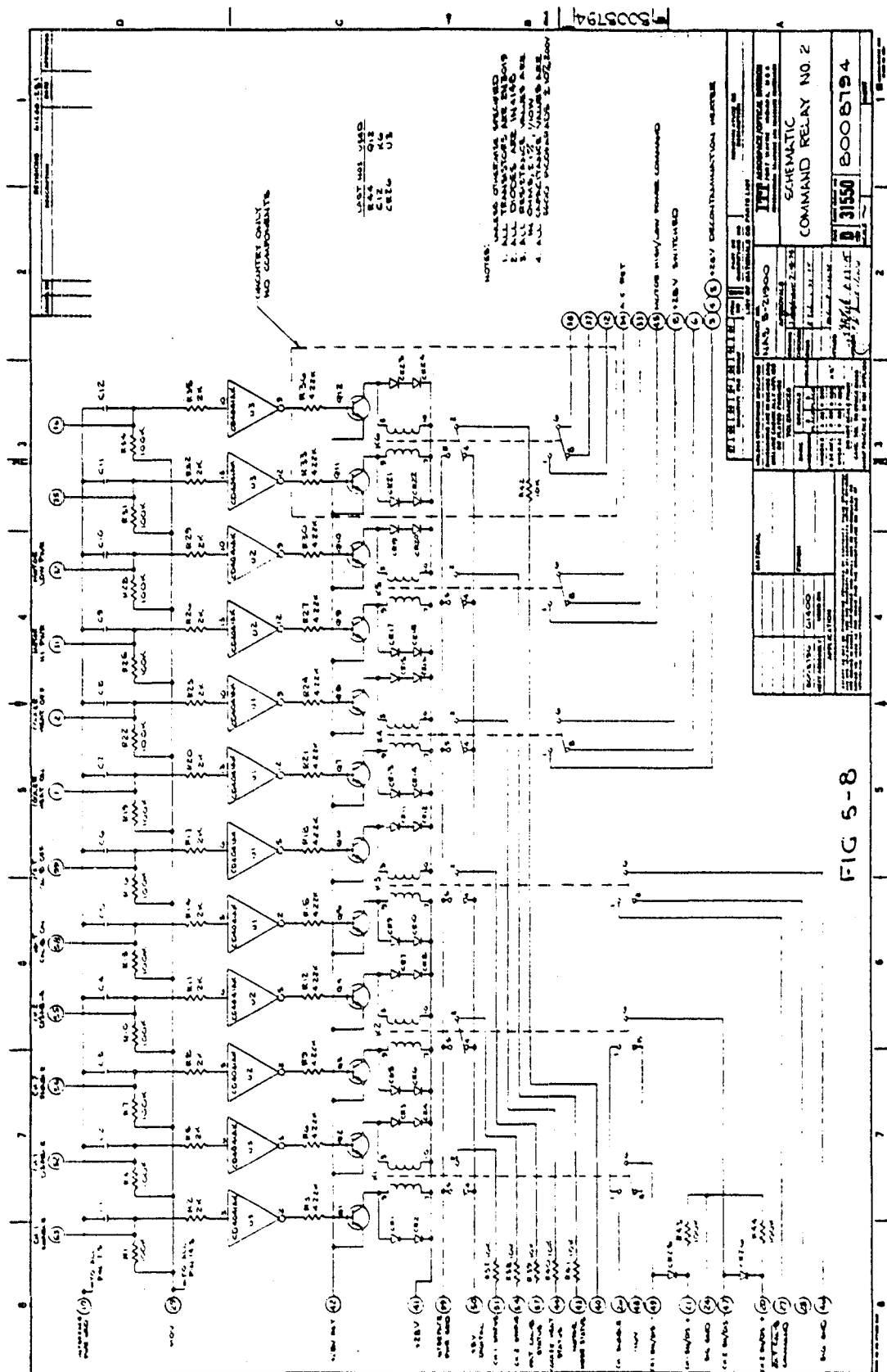
5.6 Analog TM and Patch Control

5.6.1 Analog Telemetry

The following is a list of the presently planned analog telemetry points.

1. Patch Temperature
2. Patch Temperature Extended
3. Patch Power
4. Radiator Temperature
5. Blackbody No. 1 Temperature
6. Blackbody No. 2 Temperature
7. Blackbody No. 3 Temperature
8. Blackbody No. 4 Temperature
9. Electronics Current
10. Motor Current
11. Earth Shield Position
12. Electronics Temperature
13. Cooler Housing Temperature
14. Baseplate Temperature

[illegible]



15. Motor Housing Temperature
16. A/D Converter Temperature
17. Detector No. 3 Bias Voltage
18. Blackbody Temperature IR Ch 3
19. Blackbody Temperature IR Ch 4
20. Reference Voltage

The circuitry for telemetry points 1-16 is located on the Patch Temperature Control and Telemetry Board shown schematically in Figure 5-10 and the Telemetry #2 Board shown schematically in Figure 5-11.

The following is a list of the range and resolution of the analog telemetry points.

	<u>Range</u>	<u>Resolution</u>
1. Patch Temperature	+0.2V = 90.7 ^o K +5.0V = 115.5 ^o K	0.1935V/Degree
2. Patch Temperature Extended	+0.2V = 99.4 ^o K +5.0V = 316.0 ^o K	0.02216V/Degree
3. Patch Power	+0.2V = 0.08 MW +5.0V = 50.0 MW	0.067V/mm at 32 mw out.
4. Radiator Temperature	+0.2V = 148.7 ^o K +5.0V = 317.3 ^o K	0.0285V/Degree
5, 6, 7, 8. Blackbody Temp 1, 2, 3 & 4	+0.2V = 5.086 ^o C +5.0V = 44.974 ^o C	0.1203V/Degree
9. Electronics Current	+0.2V = 39.3 MA +5.0V = 982.5 MA	5.088MV/Milliamp.
10. Motor Current	+0.2V = 12 MA +5.0V = 300 MA	16.6 MV/Milliamp
11. Earth Shield Position	3 Levels	+5.0V Open +3.0V In Between +1.0V Closed
12. Electronics Temperature	+0.2V = 38.73 ^o C +5.0V = 10.8 ^o C	0.171735V/ ^o C
13, 14, 15. Cooler Housing Temperature Baseplate Temperature Motor Housing Temperature	+0.2V = 33.24 ^o C +5.0V = 3.95 ^o C	0.129V/ ^o C

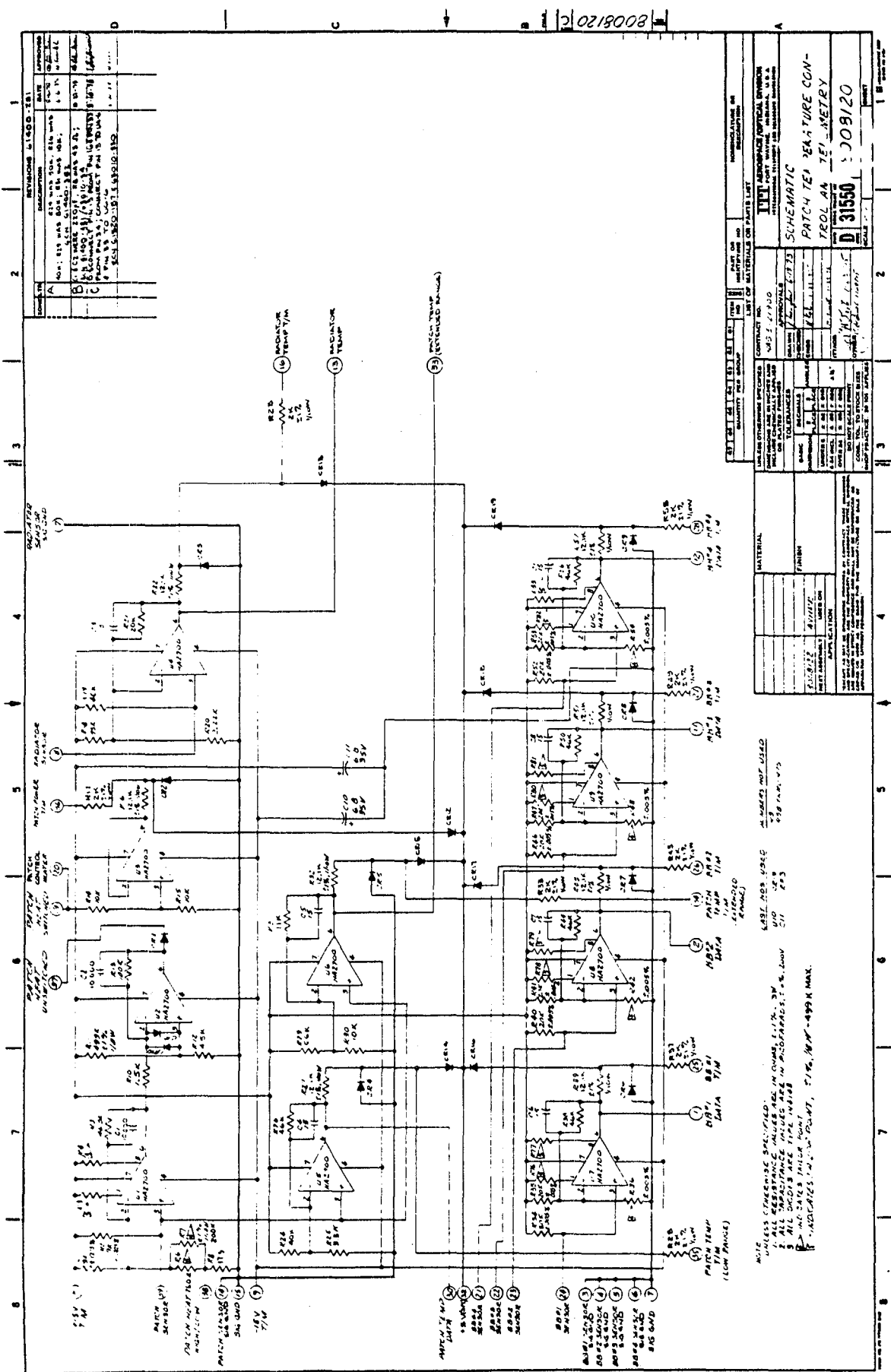
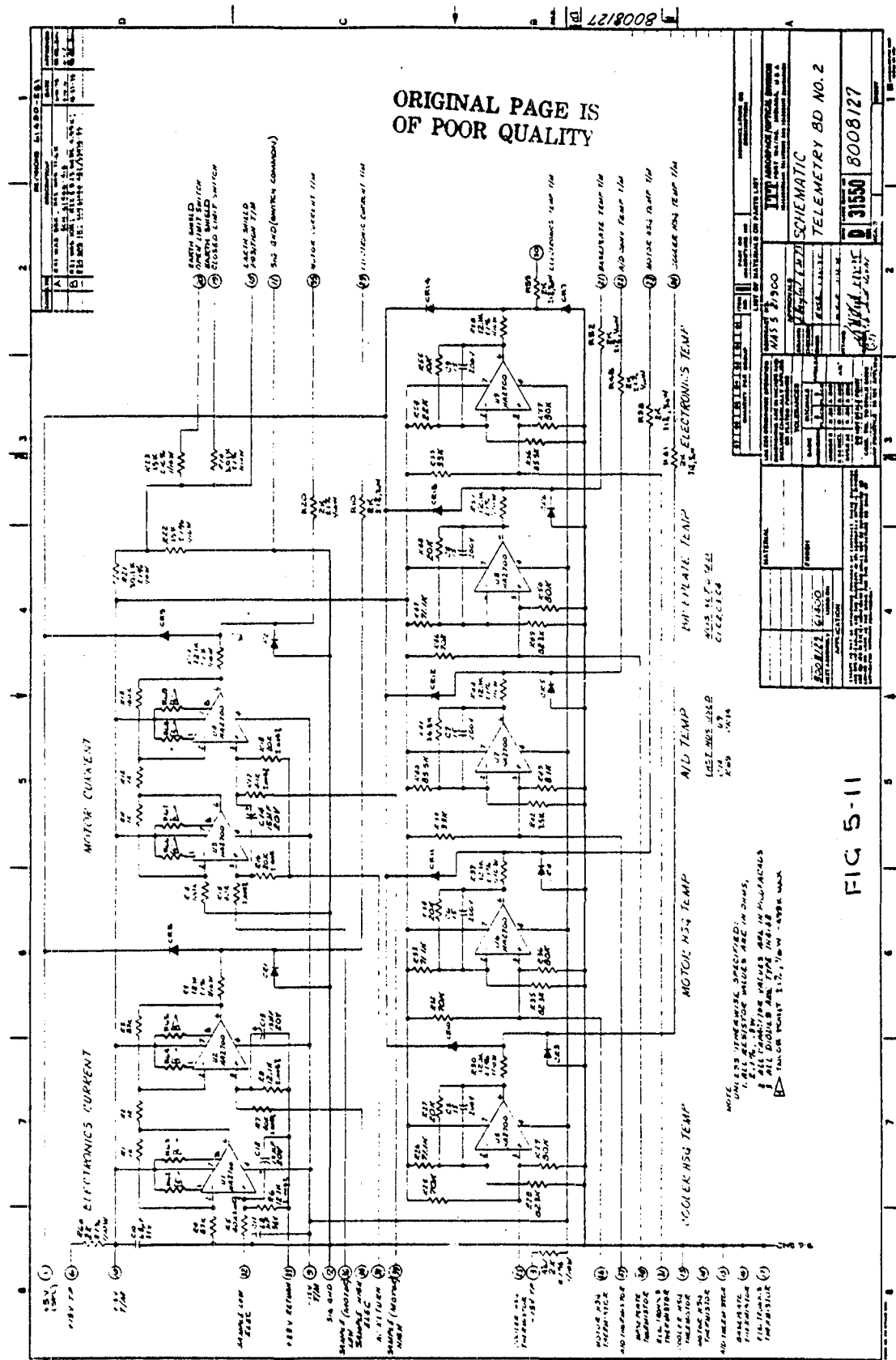


Figure 5-10



16.	A/D Converter Temperature	+0.2V = 84.49°C +5.0V = 44.51°C	0.12V/°C
17.	Detector #3 Bias Volt.	1.923 = -13V 2.384 = -11V	0.23/V/V
18.	Blackbody Temp. IR Ch 3	To be Calibrated*	
19.	Blackbody Temp. IR Ch 4	To be Calibrated*	
20.	Reference Voltage	+0.2V = 0.266V +5.0V = 6.657V	0.750V/V

*Range and value of calibration dependent on individual instrument calibration. Equations derived from EM matched to Calibration from 0°C to 40°C are

$$\text{Ch 3} - ^\circ\text{C} = 1.1\text{V}^2 - 13.2 \text{ V} + 330.2$$

$$\text{Ch 4} - ^\circ\text{C} = -3\text{V}^2 + 11\text{V} + 302.3$$

2000 Ohm ice Point Platinum sensors are used for the following telemetry.

1. Patch Temperature
2. Radiator Temperature
3. BB No. 1
4. BB No. 2
5. BB No. 3
6. BB No. 4

30K ohm Y.S.I. Thermistors, 0.1°C interchangeability, are used for the following telemetry.

1. Baseplate Temperature
2. A/D Converter Temperature
3. Electronics Temperature
4. Cooler Hsg. Temperature
5. Motor Hsg. Temperature.

Diodes have been provided on all operational amplifier outputs to limit analog telemetry points voltage range to -0.7V to +6.0.

5.6.2 Patch Temperature Control

The circuitry for temp. control is shown on the Patch Temp Control and Telemetry schematic, Figure 5-10.

It is a proportional control with a DC output (steady state) to eliminate transients.

The temperature sensor is a platinum resistance unit, Rosemount Model. No. 146MA with an ice point resistance of 2000 ohms. This will provide the input amplifier with a low impedance, stable, and linear source with a resistance change of approximately 8.6 ohms/degree.

The heating unit on the patch is a high rel. RNR55 2000 ohm resistor.

The operational amplifiers are Harris devices, HA-2700. They were selected for the low offset voltage, typically 0.5 mv and offset voltage as a function of temperature typ. 0.25 mv from 0 to 50°C.

5.6.2.1 Theory and Operation

The R3, R4 resistors are used to zero the 1st stage amplifier offset voltage at +25°C.

The R6, R7, R8, combination is tailored to match the platinum sensor resistance at 105 and 107 Kelvin. R-2 limits the sensor dissipation to the values in the following table and establishes the input voltage change to the 1st stage amplifier at 12.5 mv/degree.

<u>Sensor Power Dissipation</u>	<u>Sensor Dissipation/mw</u>
95°	1.31
100°	1.41
105°	1.50
110°	1.59
323°	3.15

R-5 is selected for a first stage gain of approximately 70 and the amplifier output is 0.0 volts at the selected control point.

With the 0.0 volt inverting input on the second stage and 0.134 volt established by R11, R12 on the non-inverting input, the second stage amplifier output = $(0.34 \times 67.6) = 9.07$ VDC. With a 0.6 volt drop across CRL the patch control output is 8.4 volts at the selected temp. control point. With the 2.0K heating unit on the patch, the patch control circuitry provides 35 milliwatts at 105.0 or 107.0 degree Kelvin.

Figure 5-12 indicates the deviation in temperature of the control point with variations in control heat requirements (35 mw nominal).

5.6.2.2 Circuit Stability

The resistor types used in the patch control are Vishay S202 high rel units with shelf life and load life data available. Calculations from these data indicate that the resistor stability is a negligible factor.

The operational amplifier stability can be related to a millivolt/degree factor at the first amplifier input. The typical initial offset voltage for the HA2700 is 0.5 millivolts which is compensated for at board test. With the loop gain indicated on the schematic, a long term offset voltage change of 1.25 millivolts would be required to result in an error in temperature control of 0.1 degree.

The relative location of the detectors, temperature sensor and heater is shown on ITT Dwg. #8008799 Detector/Frame Assembly, Channel 3 and 4 Figure 5-13.

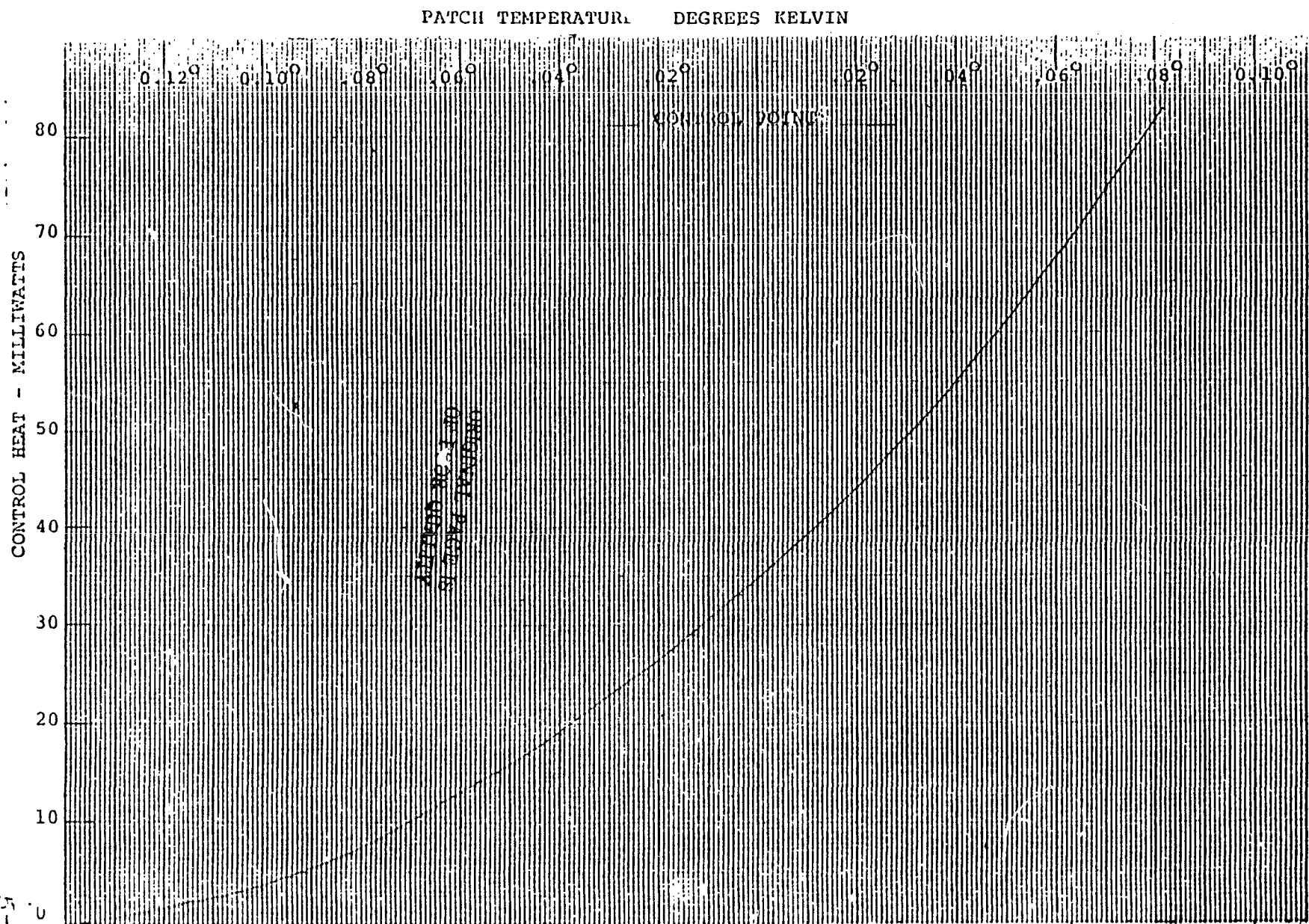


Figure 5-12

NOTE:

1. ASSEMBLE PER 8007987 ASSY INSTRUCTIONS.

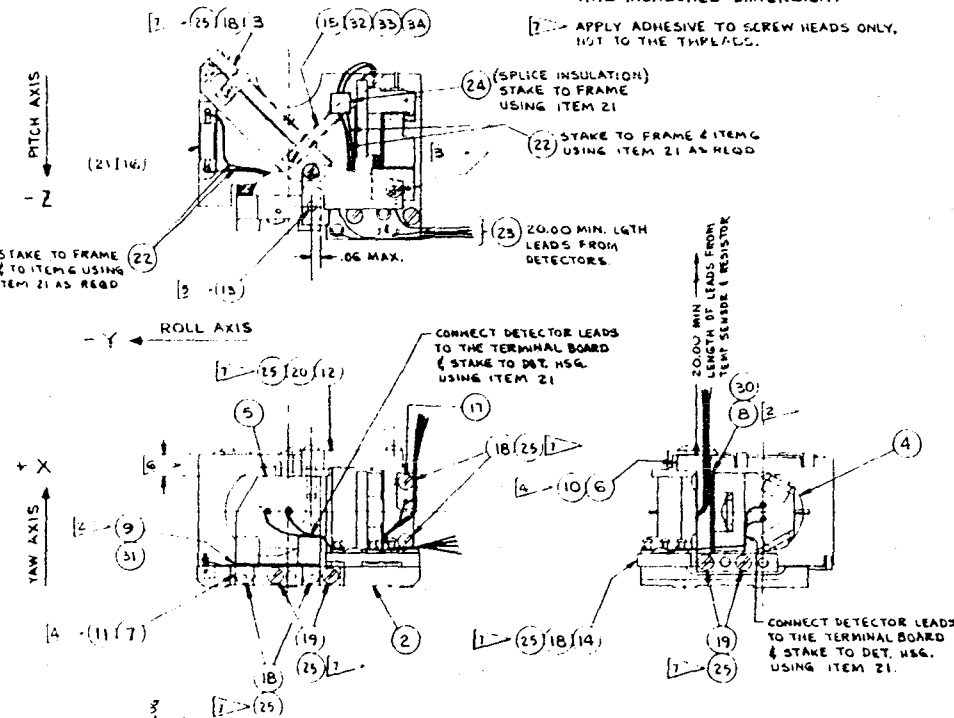
2. QTY & PT NO. OF ITEMS 8 & 9 TO BE DETERMINED BY OPTICS ALIGNMENT REQUIREMENTS. ITEM 8 TO BE CHOSEN FROM 8008798-1, 31-5, AND ITEM 9 FROM 8008798-2, 4-6. TO LOCATE THE DETECTORS AT THE NOMINAL POSITION, .015 THICKNESS IS REQUIRED FOR EACH CHANNEL. AFTER OPTICS ALIGNMENT, REPLACE ITEM 8 WITH ITEM 30 AND REPLACE ITEM 9 WITH ITEM 31 PER ASSY INSTRUCTIONS. AFTER OPTICS ALIGNMENT, TAP .00-80 THRU ITEM 6 LOCATED FROM EXISTING HOLE IN ITEM 12.

4. QTY & PART NO. OF ITEMS 10 & 11 TO BE DETERMINED BY OPTICS ALIGNMENT REQUIREMENTS. ITEM 10 TO BE CHOSEN FROM 8008745-1 THRU -4 AND ITEM 11 FROM 8008744-1 THRU -6. SPACERS MAY BE MACHINED TO REQUIRED THICKNESS. 8008745-2 (.07 THK) AND 8008744-3 (.08 THK) ARE REQUIRED TO LOCATE DETECTORS AT THEIR NOMINAL POSITION.

5. AFTER OPTICS ALIGNMENT, MACHINE A PILOT HOLE THRU ITEM 12 AND .14 MAX. DEEP INTO ITEM 5. REAM TO .0620/.0625 DIA THRU ITEM 12 AND .09 MIN DEEP INTO ITEM 5.

6. AFTER OPTICS ALIGNMENT, MACHINE ITEM 12 TO THIS MEASURED DIMENSION.

7. APPLY ADHESIVE TO SCREW HEADS ONLY, NOT TO THE THREADS.



REVISIONS 61400-321			
ZONE	DATE	DESCRIPTION	APPROVED
A	8-21-75	ADDED ITEMS 17, 27, 28, 29; ITEM 14 WAS 800869941; REVISED ITEM 14 PICTORALLY; ADDED ITEM 17 PICTORALLY; ADDED WIRING DIAGRAMS. ECM 61400-325	CL5
B	7-22-76	ITEM 15 PT NO WAS 8118331-1; ITEM 16 PT NO WAS 815502001F; ECM 61400-327	CL5
C	8-11-76	ADDED -5 TO PT NO ITEM 8, -6 TO ITEM 9; ITEM 11 WAS -1 THRU -5; REVISED NOTES 2 & 4 PER ABOVE. ECM 61400-327 / 63070-176	CL5
D	9-2-76	ADDED ITEM 30 & 31; ITEM 8 & 9 WERE "A" SIZE; ADDED LAST SENTENCE TO NOTE 2. ECM 61400-328 / 63070-186	CL5
DA	9-15-77	FL WAS ON THIS DWG; DELETED PT CIRCLE 21 AT SENSOR (ITEM 18) AND ADDED 32, 33, 34. ECM 63070-281	CL5

Figure 5-13

SEE SEPARATE PARTS LIST

5-28

WIRING DIAGRAM

07	08	09	04	03	02	01	ITEM NO.	PART OR IDENTIFYING NO.	NOMENCLATURE OR DESCRIPTION
QUANTITY PER GROUP							LIST OF MATERIALS OR PARTS LIST		
UNLESS OTHERWISE SPECIFIED							CONTRACT NO. NAS 5-21900		
DIMENSIONS ARE IN INCHES AND INCLUDE CHEMICALLY APPLIED OR PLATED FINISHES							APPROVALS		
TOLERANCES							DRAWN 61400-327 7-24-74		
BASIC							CHECKED 61400-327 8-2-75		
DECIMALS							ENGR 61400-327 8-2-75		
DIMENSION							ITTAOD 61400-327 8-2-75		
FRACTION							OTHER 61400-327 8-2-75		
UNDER 8							SCALE 2/1		
8-24 INCL							SHEET		
OVER 24							8008799		
DO NOT SCALE PRINT							8008799		
COML. TOL. TO STOCK SIZES							8008799		
SHOP PRACTICE, 38.101 APPLIES							8008799		

8008799

The sensor and heater is located as close as possible to the detectors to minimize sensor/detector/heater gradients and provide the input circuitry with feedback which is a monitor of detector temperature as opposed to the patch temperature.

5.7 Motor Logics

The clock receiver arrangement utilizing the Texas Instruments, Inc. SN55107 clock receiver, as specified in the GFSC specification for an Advanced Very High Resolution Radiometer, is located on the motor logics printed circuit board. An output of the clock receiver is available on a connector pin for use in the interface logics.

The motor countdown logics convert the 0.9984 MHz clock receiver signal into 62.4 KHz for use in the switching regulators and 240 Hz 2Ø for use in the motor power supply.

The 0.9984 MHz input signal is first divided by 16 in a ripple counter to achieve the 62.4 KHz signal at pin 9 of A7. This signal is then buffered and is available for use in the switching regulators.

To obtain the 240 Hz 2Ø signal, the 62.4 KHz signal is divided in a series of counters. The first is a divide by thirteen counter which produces a 4.8 KHz signal at pin 9 of A4. This signal is then divided by 10 to obtain a 480 Hz signal at pin 9 of A1. The inverted and non-inverted forms of this signal are further divided by 2 in their respective J-K flip flops, and the 240 Hz 1Ø signal is present at pins 9 and 12 of B1. A reset circuit acts as a monostable and supplies a pulse to the clear

input of one of the J-K flip flops, B1 pin 2. The reset pulse insures the proper 90° phase relationship between the 20 240 Hz output.

A portion of the scan count logics is also included in the motor logics circuit. The time base for scan counting is the spacecraft 0.9984 MHz clock. A divide by 100 counter provides a 100 μ second (10 KHz) time base for the remainder of the counter and decoding.

The counter is designed to count continuously and be reset by the pick-up sync pulse. The reset logics for the entire scan count circuit are on this circuit.

The final circuit on this board is the sync pick-up circuit. There are two magnetic pick-ups in the motor housing which provide the inputs to the sync pick-up circuit.

The HA-2700 operational amplifiers act as level detectors and provide logic level pulses to the logic circuitry. The circuit is designed for redundant operation such that if either pick-up fails, a sync pick-up pulse will still be present at the output.

Drawing No. 8008045 is the schematic diagram of the motor logics (Figure 5-14). The motor logics timing diagram is shown in Figure 5-15.

5.8 Scan Count and Decode

The scan count and decode board provides the basic count-down of the scan period and the decoding of gating signals for the AVHRR electronics. The schematic diagram is given on Drawing 8008049 (Figure 5-16).

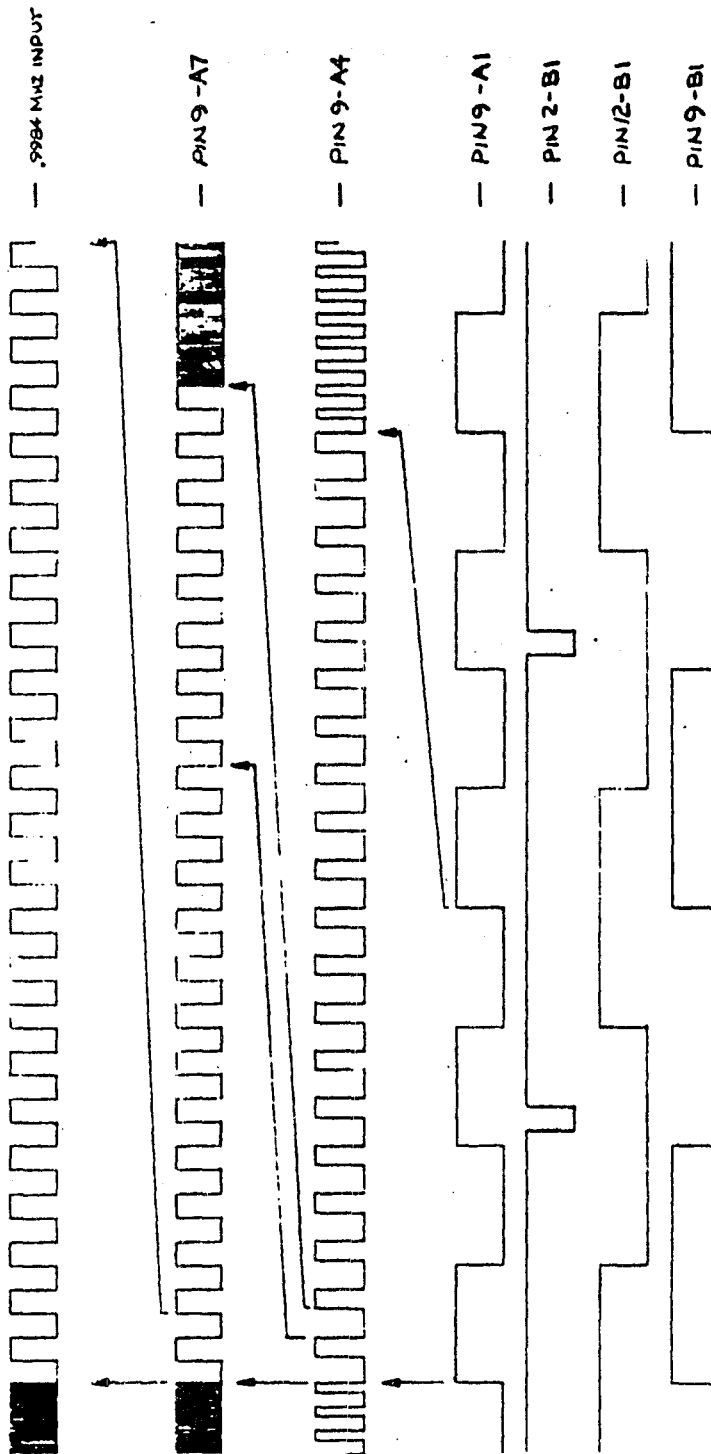
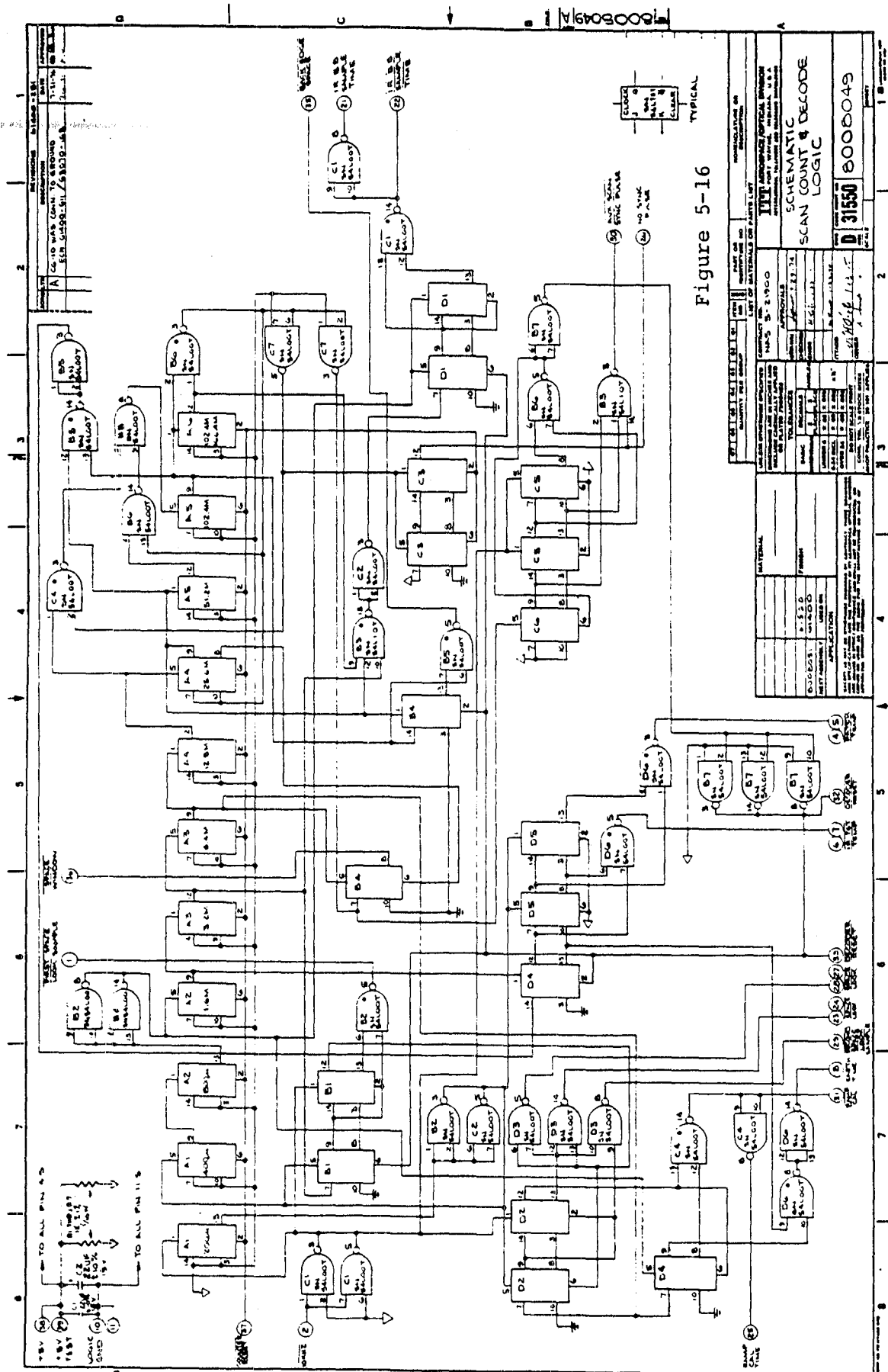


Figure 5-15 Motor Logic Circuit - Timing Diagram



A 10 KHz clock from the motor logics is the time base for the counter. The first six flip flops are a conventional binary ripple counter. The last four counting stages are a divide by 13 ripple counter. The counter is designed to repeat the scan period automatically but is normally reset by magnetic pick-up initiated reset pulse.

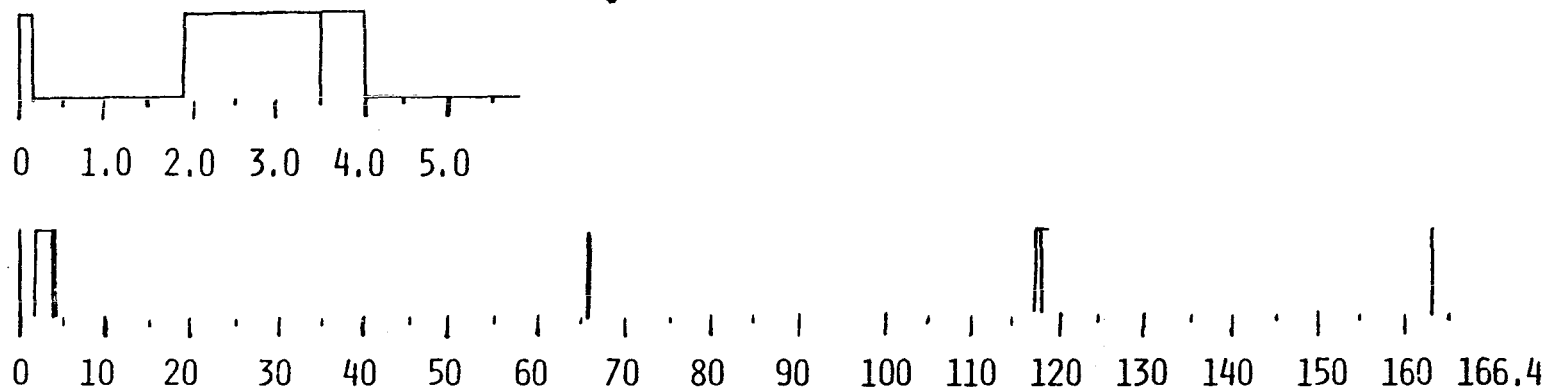
The method of decoding is setting flip-flops at the beginning and end of the desired time interval and decoding the set condition of the first and the reset condition of the second. The clock input is always the highest frequency of the decoded time, which arrangement when used with a ripple counter, provides unambiguous decoding.

The timing of the normal operation signals is shown in Figure 5-17. Timing for the voltage calibration signals is on Figure 5-18.

5.9 Output Data Control

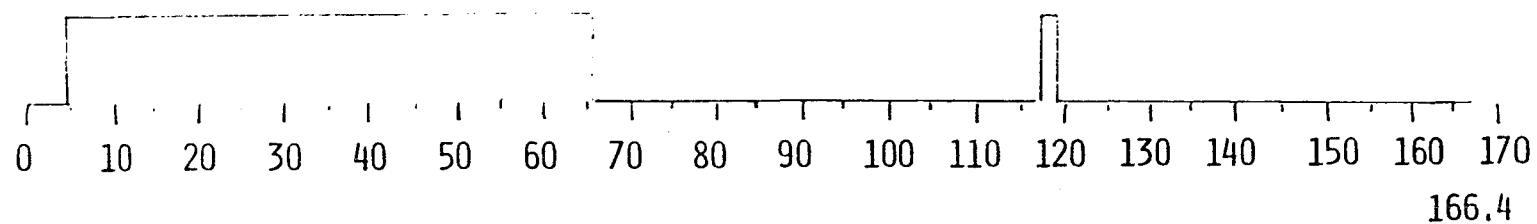
The logics for controlling the conversion of Analog to Digital Data and the transmission to the MIRP is shown on Schematic-Interface Logic No. 1 - 8009206 Figure 5-19 and Schematic Interface Logic No. 2 - 8009209 Figure 5-20. The timing for the output Data Control is shown in Figure 5-21.

By specification, the minimum time between samples from the MIRP can be 25 micro-seconds. With minimum timing, the A to D converter operates in the hold or convert mode for 16 microseconds and in the track or sample mode for 9 microseconds. For longer



0.0-0.1 SYNC PULSE
 1.9-3.5 AMPLIFIER SPACE REFERENCE SAMPLE
 3.5-4.0 RAMP CALIBRATION
 65.6-65.8 IR TARGET TEMPERATURE
 65.8-66.0 PATCH TEMPERATURE
 117.6-118.4 BLACK BODY TEMP - IR SAMPLE

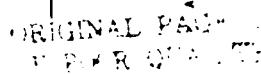
FIGURE 5-17 SCAN TIMING SIGNALS



4.0-65.6 SIMULATED EARTH SCENE

117.6-118.4 SIMULATED BACK SCAN TARGET

FIGURE 5-18 SCAN TIMING SIMULATED CALIBRATION



SPACECRAFT DATA PROCESSOR/AVHRR INTERFACE TIMING

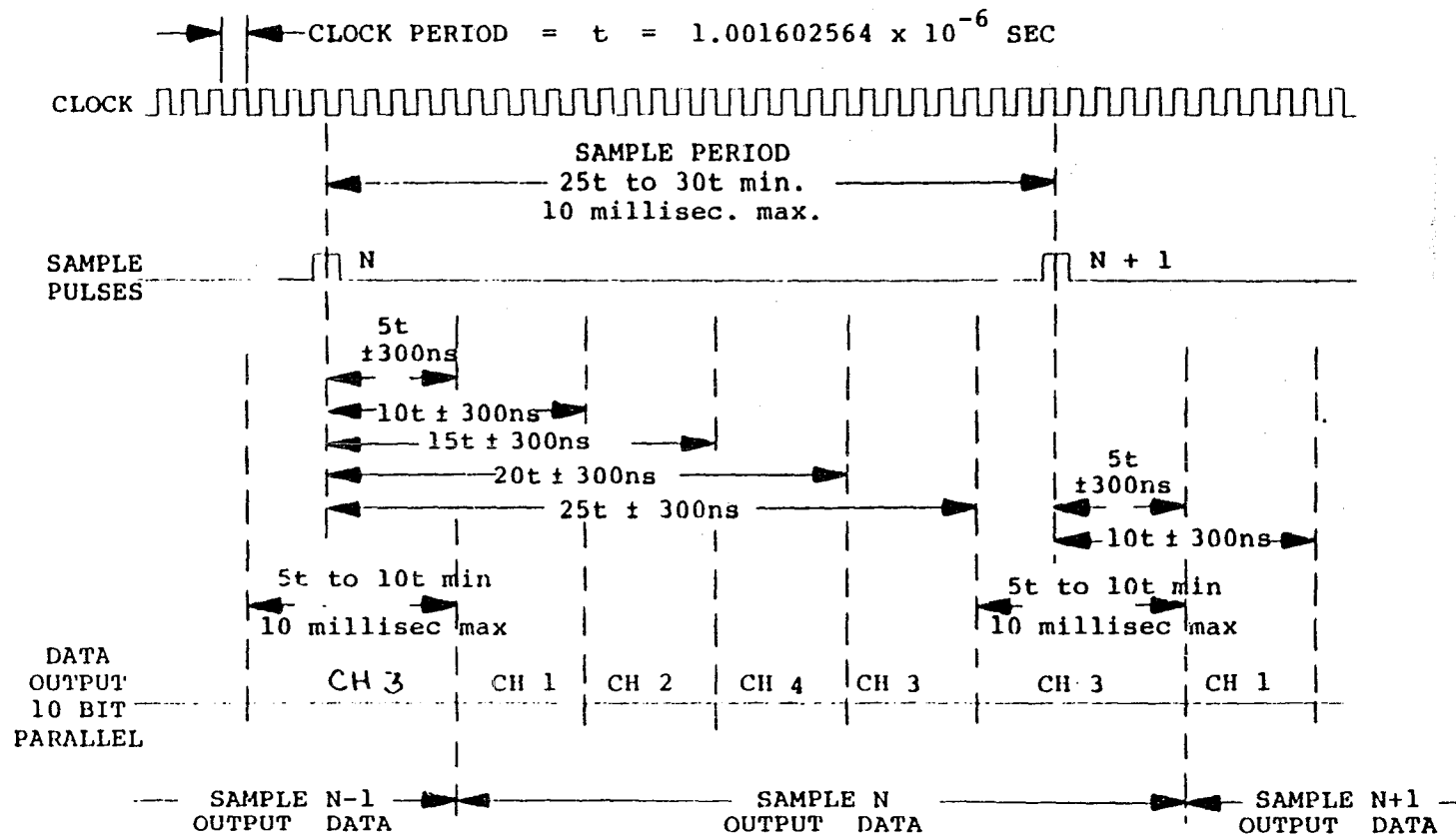


Figure 5-21

intervals between sample pulses, the track time is increased. The sample signal from the MIRP determines the transition from track to hold.

The A to D converter operates on a basic 3 microsecond conversion time. The time allowed for Channel 5 conversion is increased to 4 microseconds to minimize the data storage and gating circuits required.

The A to D converter provides for six input data channels. The target five channels correspond to the five channels of the specification. The sixth channel has multiplexed telemetry data and is switched in under logic control in place of channels 3, 4, and 5 of the appropriate time in the line scan.

Three microseconds (4 microseconds for channel 5) after a channel is selected a strobe signal is sent to the A to D which stores the digitized data in the A to D internal register. The data of this point is in Grey code. Within 0.5 microseconds the Grey to binary conversion is completed and valid binary data is present on the A to D output lines.

The data is later strobed into an intermediate storage register and in sequence to the output register whose outputs directly connect to the output drivers for the MIRP lines.

The following chart gives the timing data for the sequence in microseconds with respect to the MIRP select pulse.

	CH 1	CH 2	CH 4	CH 3	CH 5 **
Analog to Digital Conversion	0-3	3-6	6-9	9-12	12-16
Data in A to D internal register (Grey Code)	3-6	6-9	9-12	12-16	16-3*
A to D output (binary)	3.5-6	6.5-9	9.5-12	12.5-16	16.5-3*
Data in Intermediate register (Reg. 1)	4-7	7-10	10-15	15-20	20-4*
Data in output register (MIRP Signals)	5-10	10-15	15-20	20-25	25-5*

* Time of next conversion cycle.

** Channel 5 input is connected to the Output Data Amplifier of Channel 3.

5.10 Ramp Calibration Generator

The ramp calibration and simulated calibration functions have been combined to have the same digital to analog converter be the signal source for both and have the signal control and switching only a logic function. Drawing No. 8007963 sheets 1 and 2 is a schematic diagram of the ramp calibration generator (Figure 5-22).

The counter for the ramp calibration is a conventional 10-bit ripple counter. The outputs are gated to the D to A converter. The system is connected such that each successive scan will give a one-step voltage change in the direction of increasing radiance. This means that the signal will be increasing in voltage in channels 1 and 2 and be decreasing in voltage in channels 3 and 4.

Since ramp calibration signals of both polarities with respect to zero radiance are required, a digital offset (Binary Number 43) is maintained at all times other than ramp calibration time. During space look, the data amplifiers will re-zero on this offset allowing ramp calibration signals of both polarities from zero radiance. The following tables will illustrate this further.

Since the zero radiance voltages were specified at different intervals from the limits of the ramp calibration voltage (+0.25 volts and -0.1 volt) and +6.2 volts and +6.4 volts) the difference was split maintaining the 6.5 volt ramp calibration range giving a 0.275 volt excursion below minimum radiance. This gives a binary value of $1023/6.5 \text{ volts} \times 0.275 \text{ volt} = 43 \text{ bits}$.

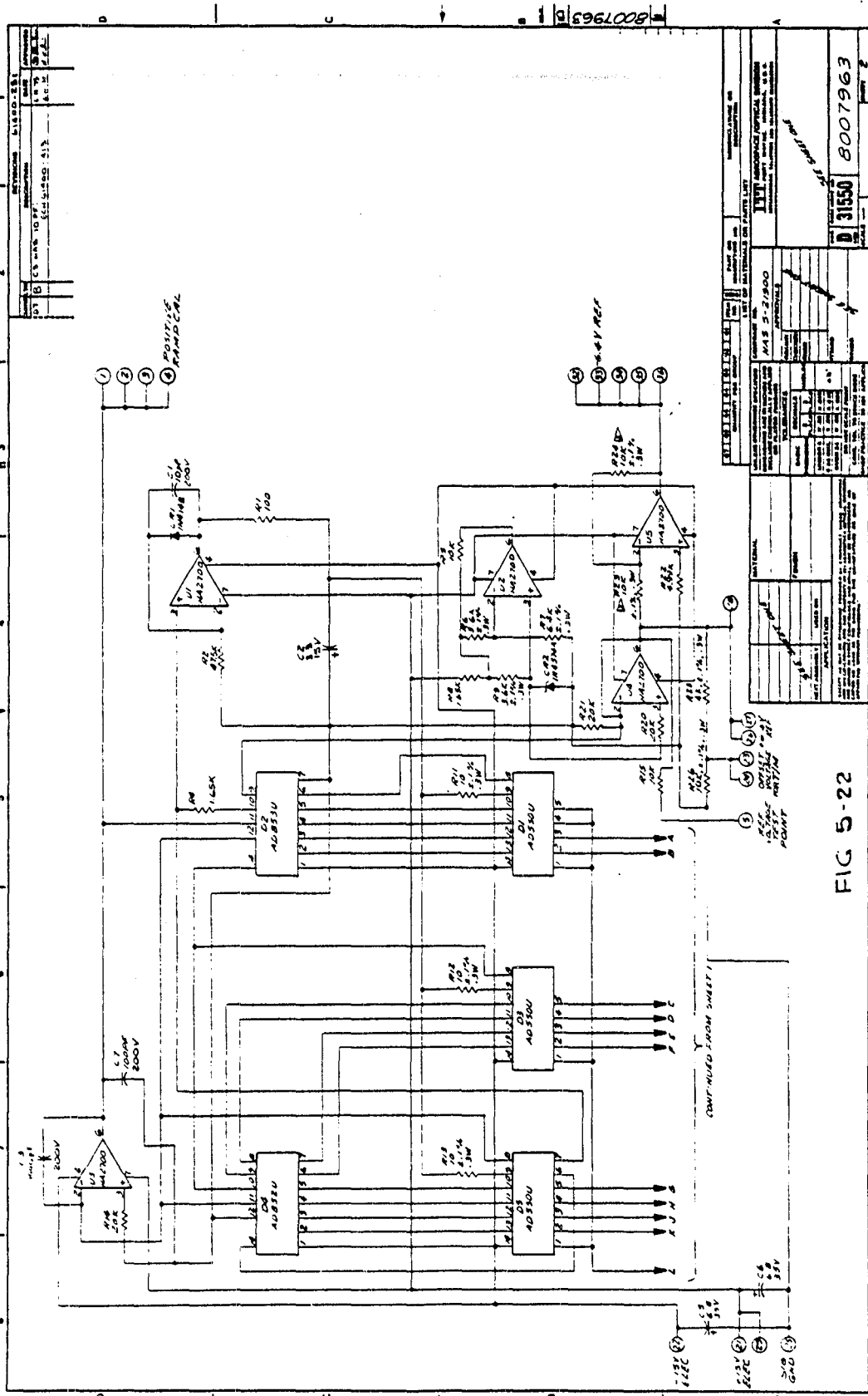


FIG 5-22

FIG 5-22 4-BIT DIGITAL-TO-ANALOG CONVERTER PARTS LIST PART NO. QTY. DESCRIPTION 1 1 AD530U 4-BIT DIGITAL-TO-ANALOG CONVERTER 2 1 100K 1% RES 3 1 100K 1% RES 4 1 100K 1% RES 5 1 100K 1% RES 6 1 100K 1% RES 7 1 100K 1% RES 8 1 100K 1% RES 9 1 100K 1% RES 10 1 100K 1% RES 11 1 100K 1% RES 12 1 100K 1% RES 13 1 100K 1% RES 14 1 100K 1% RES 15 1 100K 1% RES 16 1 100K 1% RES 17 1 100K 1% RES 18 1 100K 1% RES 19 1 100K 1% RES 20 1 100K 1% RES 21 1 100K 1% RES 22 1 100K 1% RES 23 1 100K 1% RES 24 1 100K 1% RES 25 1 100K 1% RES 26 1 100K 1% RES 27 1 100K 1% RES 28 1 100K 1% RES 29 1 100K 1% RES 30 1 100K 1% RES 31 1 100K 1% RES 32 1 100K 1% RES 33 1 100K 1% RES 34 1 100K 1% RES 35 1 100K 1% RES 36 1 100K 1% RES 37 1 100K 1% RES 38 1 100K 1% RES 39 1 100K 1% RES 40 1 100K 1% RES 41 1 100K 1% RES 42 1 100K 1% RES 43 1 100K 1% RES 44 1 100K 1% RES 45 1 100K 1% RES 46 1 100K 1% RES 47 1 100K 1% RES 48 1 100K 1% RES 49 1 100K 1% RES 50 1 100K 1% RES 51 1 100K 1% RES 52 1 100K 1% RES 53 1 100K 1% RES 54 1 100K 1% RES 55 1 100K 1% RES 56 1 100K 1% RES 57 1 100K 1% RES 58 1 100K 1% RES 59 1 100K 1% RES 60 1 100K 1% RES 61 1 100K 1% RES 62 1 100K 1% RES 63 1 100K 1% RES 64 1 100K 1% RES 65 1 100K 1% RES 66 1 100K 1% RES 67 1 100K 1% RES 68 1 100K 1% RES 69 1 100K 1% RES 70 1 100K 1% RES 71 1 100K 1% RES 72 1 100K 1% RES 73 1 100K 1% RES 74 1 100K 1% RES 75 1 100K 1% RES 76 1 100K 1% RES 77 1 100K 1% RES 78 1 100K 1% RES 79 1 100K 1% RES 80 1 100K 1% RES 81 1 100K 1% RES 82 1 100K 1% RES 83 1 100K 1% RES 84 1 100K 1% RES 85 1 100K 1% RES 86 1 100K 1% RES 87 1 100K 1% RES 88 1 100K 1% RES 89 1 100K 1% RES 90 1 100K 1% RES 91 1 100K 1% RES 92 1 100K 1% RES 93 1 100K 1% RES 94 1 100K 1% RES 95 1 100K 1% RES 96 1 100K 1% RES 97 1 100K 1% RES 98 1 100K 1% RES 99 1 100K 1% RES 100 1 100K 1% RES		FIG 5-22 4-BIT DIGITAL-TO-ANALOG CONVERTER PARTS LIST PART NO. QTY. DESCRIPTION 1 1 AD530U 4-BIT DIGITAL-TO-ANALOG CONVERTER 2 1 100K 1% RES 3 1 100K 1% RES 4 1 100K 1% RES 5 1 100K 1% RES 6 1 100K 1% RES 7 1 100K 1% RES 8 1 100K 1% RES 9 1 100K 1% RES 10 1 100K 1% RES 11 1 100K 1% RES 12 1 100K 1% RES 13 1 100K 1% RES 14 1 100K 1% RES 15 1 100K 1% RES 16 1 100K 1% RES 17 1 100K 1% RES 18 1 100K 1% RES 19 1 100K 1% RES 20 1 100K 1% RES 21 1 100K 1% RES 22 1 100K 1% RES 23 1 100K 1% RES 24 1 100K 1% RES 25 1 100K 1% RES 26 1 100K 1% RES 27 1 100K 1% RES 28 1 100K 1% RES 29 1 100K 1% RES 30 1 100K 1% RES 31 1 100K 1% RES 32 1 100K 1% RES 33 1 100K 1% RES 34 1 100K 1% RES 35 1 100K 1% RES 36 1 100K 1% RES 37 1 100K 1% RES 38 1 100K 1% RES 39 1 100K 1% RES 40 1 100K 1% RES 41 1 100K 1% RES 42 1 100K 1% RES 43 1 100K 1% RES 44 1 100K 1% RES 45 1 100K 1% RES 46 1 100K 1% RES 47 1 100K 1% RES 48 1 100K 1% RES 49 1 100K 1% RES 50 1 100K 1% RES 51 1 100K 1% RES 52 1 100K 1% RES 53 1 100K 1% RES 54 1 100K 1% RES 55 1 100K 1% RES 56 1 100K 1% RES 57 1 100K 1% RES 58 1 100K 1% RES 59 1 100K 1% RES 60 1 100K 1% RES 61 1 100K 1% RES 62 1 100K 1% RES 63 1 100K 1% RES 64 1 100K 1% RES 65 1 100K 1% RES 66 1 100K 1% RES 67 1 100K 1% RES 68 1 100K 1% RES 69 1 100K 1% RES 70 1 100K 1% RES 71 1 100K 1% RES 72 1 100K 1% RES 73 1 100K 1% RES 74 1 100K 1% RES 75 1 100K 1% RES 76 1 100K 1% RES 77 1 100K 1% RES 78 1 100K 1% RES 79 1 100K 1% RES 80 1 100K 1% RES 81 1 100K 1% RES 82 1 100K 1% RES 83 1 100K 1% RES 84 1 100K 1% RES 85 1 100K 1% RES 86 1 100K 1% RES 87 1 100K 1% RES 88 1 100K 1% RES 89 1 100K 1% RES 90 1 100K 1% RES 91 1 100K 1% RES 92 1 100K 1% RES 93 1 100K 1% RES 94 1 100K 1% RES 95 1 100K 1% RES 96 1 100K 1% RES 97 1 100K 1% RES 98 1 100K 1% RES 99 1 100K 1% RES 100 1 100K 1% RES
--	--	--

The earth scene during simulated calibration is derived from a divide-by-3 counter. The three states are decoded and gated through the two most significant bits giving signals of 1.626, 3.253, and 4.879 volts above minimum radiance.

A test connection has been added to allow three known values of ramp calibration signal to be sequentially gated out when calibrating. This signal must be matched to the amplifier gain which is a function of detector sensitivity.

The clock signal for both counters is derived from the scan timing logics.

The D/A Converter is a 10-bit current switching type converter. The output of the converter is a positive going 0 to 10.23 volt ramp consisting of 1023 steps. The output of the D/A converter is sent to a unity gain inverting amplifier located on the multiplexer board. These two outputs provide both polarity ramp signal for insertion into the data channels as required by circuit configuration.

The ramp calibration generator also provides ± 6.2 volt outputs for use as a stable reference voltage.

<u>VOLTAGE</u>	<u>CHANNELS 1 and 2</u>
+6.475	Channel Ramp Calibration Limit - Binary 1023
6.39375	A/D Converter Signal Limit
6.1	Maximum Scene Radiance
0.25	Zero Radiance - Binary 43
0	A/D Converter Signal Limit
-0.025	Channel Ramp calibration Limit - Binary 0

CHANNELS 3 and 4

+6.475	Channel Ramp Calibration Limit - Binary 0
6.39375	A/D Converter Signal Limit
6.2	Zero Radiance - Binary 43
0.3	Maximum Scene Radiance
0	A/D Converter Signal Limit
-0.025	Channel Ramp Calibration Limit - Binary 1023

5.11 Auxiliary Scan Timing

The auxiliary scan timing circuitry is added to provide continued operation of the AVHRR in the event of the loss of the pick-up signal which synchronizes the scan timing with the scan mirror position.

A block diagram of these circuits is given in Figure 5-23. The complete schematic is shown on Drawing 8008052 (Figure 5-24). The timing for auxiliary scan operation is shown in Figure 5-25. Timing signals are generated on the Scan Count and Decode Board.

The circuit operation is based on the fact that the minimum output signal on Channel 3 occurs when the radiometer views space. With the loss of the synchronizing pulse, the scan counter period is the same as the mirror rotational time but not in synchronism. Two samples of the output voltage are taken at time the scan counter timing indicates that the instrument is viewing space. From this point two different modes of operation ensue. If in the remainder of the scan a signal level lower than the average of the two samples is detected, the scan counter is reset. When the cold target

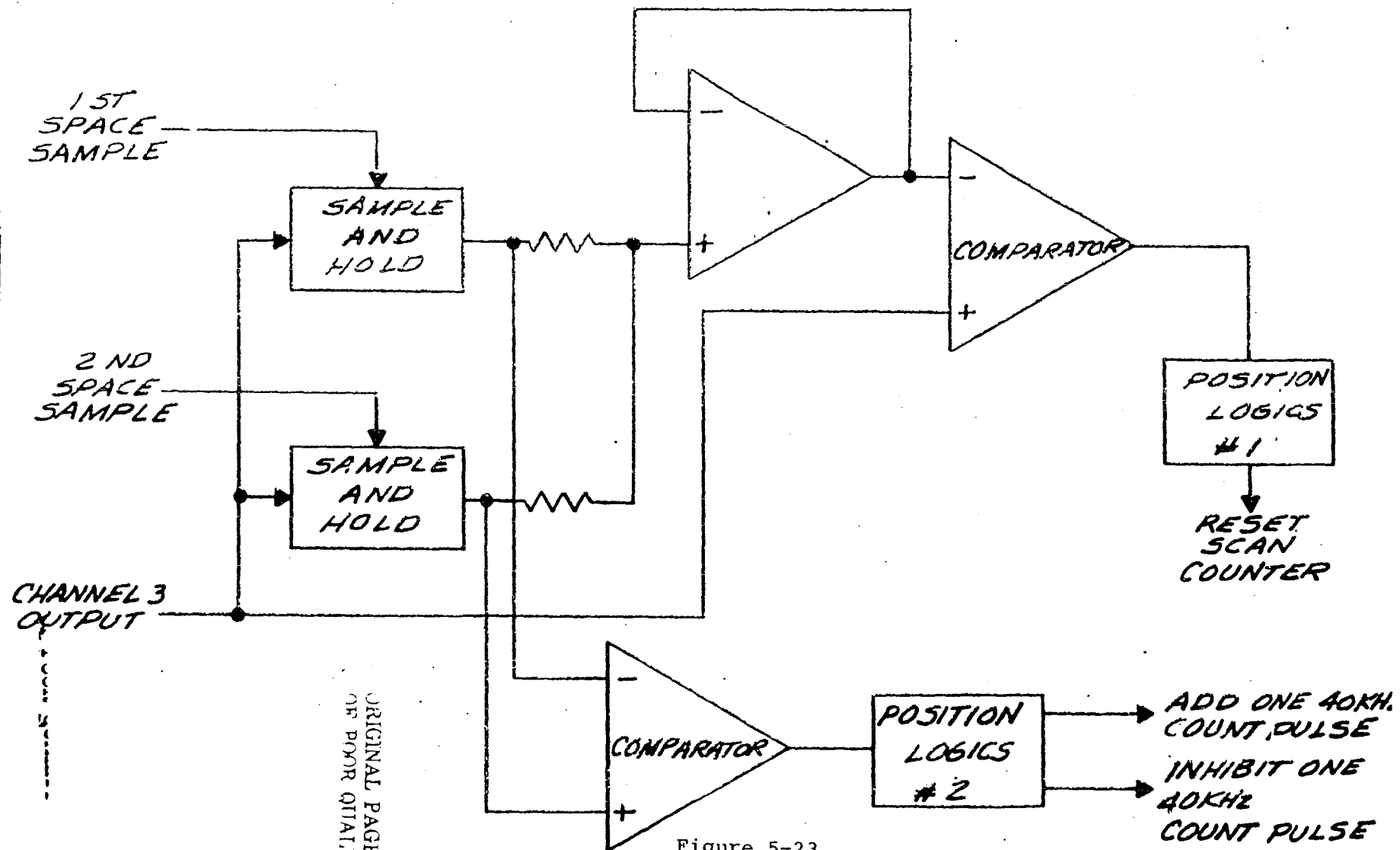
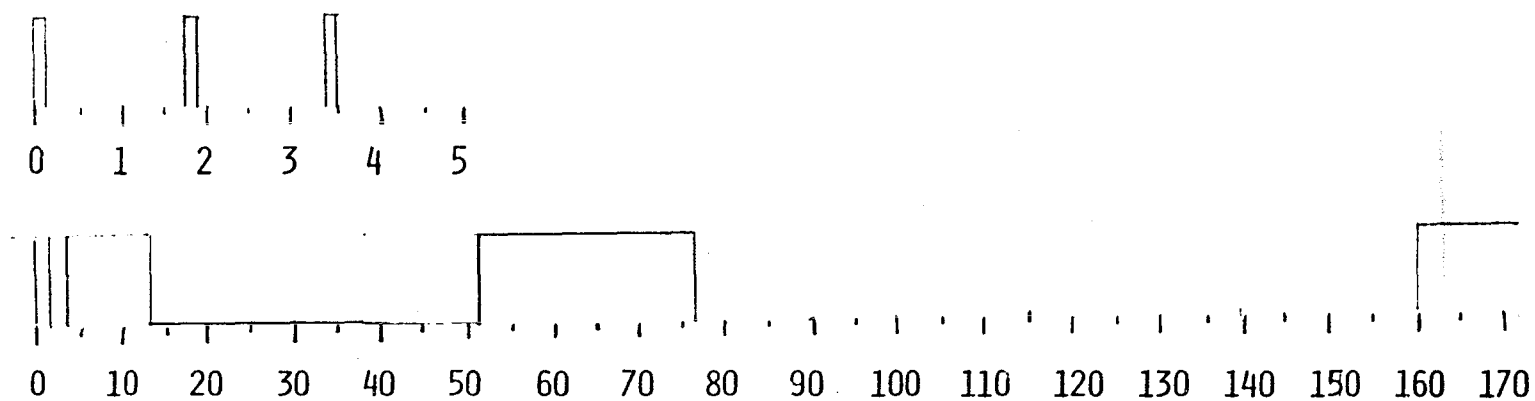


Figure 5-23

BLOCK DIAGRAM AUXILIARY SCAN TIMING

ORIGINAL PAGE IS
OF POOR QUALITY



0-0.1	SYNC PULSE
1.8-1.9	FIRST SPACE SAMPLE
3.4-3.5	SECOND SPACE SAMPLE
51.2-76.8	TRAILING EDGE SPACE WINDOW
160.0-170.0	SPACE WINDOW

FIGURE 5-25 AUXILIARY SCAN TIMING

which causes the reset is space, the reset places the counter within a few milliseconds of the correct point. This operation is performed only every 128th scan to allow the data amplifier to settle with the new reference. When the scan counter is near synchronism, a logic gate inhibits this circuit while the mirror is viewing space on the trailing edge of the earth view.

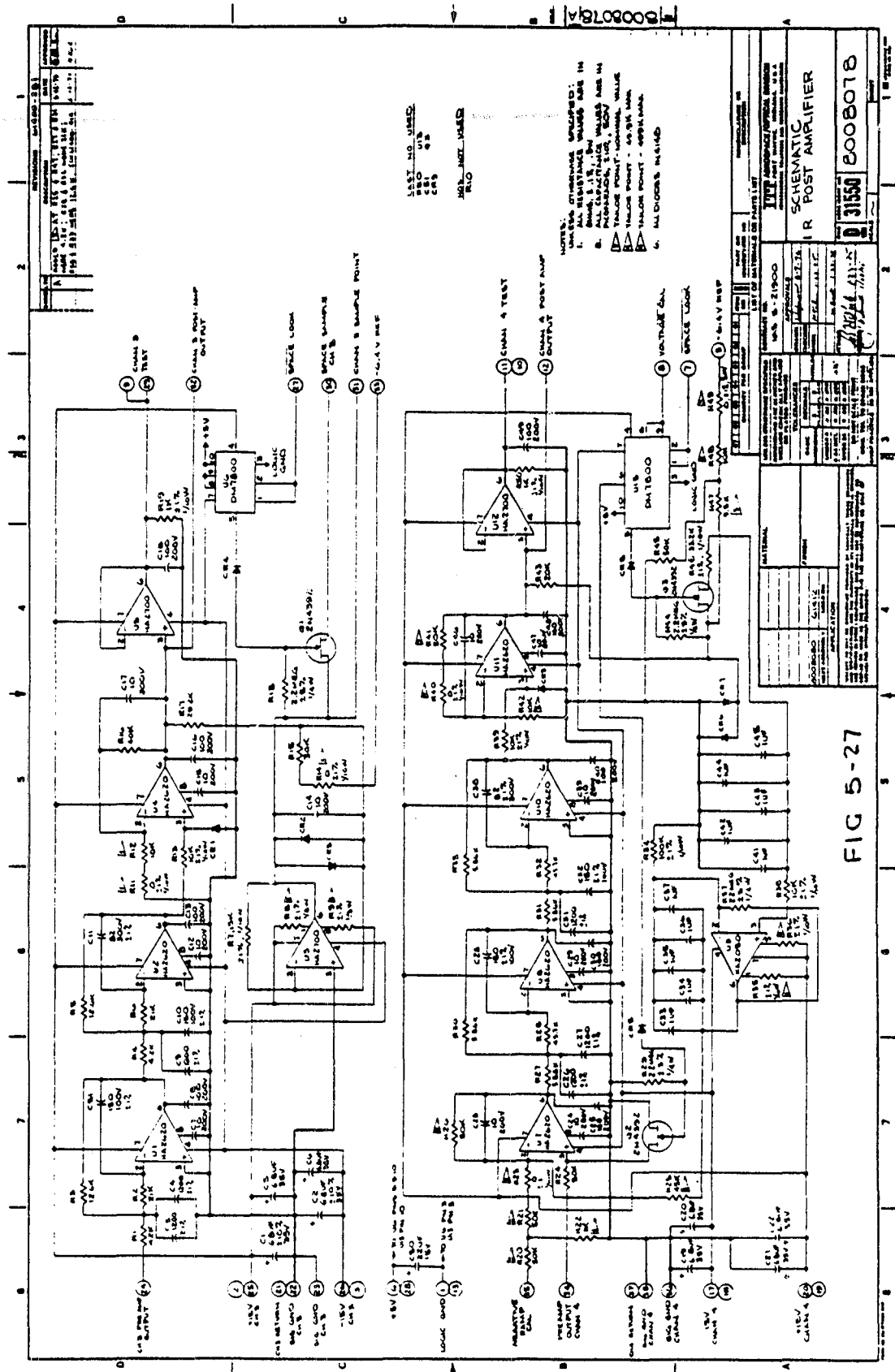
For finer positioning, the relative amplitudes of the two samples are compared. An up-down counter sums the net number of differences over sixteen scans. If a sufficient unbalance exists, the logic will cause a 40 KHz clock signal to be added or omitted, depending on the direction of unbalance. The counter limits are unbalanced in an attempt to cause the samples to go to the early portion of the space view as in the normal scan cycle.

5.12 Ch 3 Data Amplifier

The schematics depicting the Channel 3 amplifier chain are shown on Drawing 8008101 (Figure 5-26) and Drawing 8008078 (Figure 5-27).

The preamplifier has a positive and negative voltage regulator to provide additional regulation for the detector bias and to provide power supply isolation from the remaining electronics for these low level signals.

The input stage of the preamplifier is a differential pair consisting of transistors Q5 and Q7. Transistor Q4 provides a constant current source for Q5 and Q7. The detector signal is inserted at the base of Q5. Stage feed-back, zero-reference feedback, ramp calibration signals, and a DC offset signal are all summed at the base of Q7. This transistor circuit provides an open loop gain of approximately 2500. Amplifier U3 is included in the first stage to provide a single ended output for the signal.



Amplifier U4 is an additional stage of voltage gain.

Transistors Q3 and Q6 perform the function of shorting out the detector bias and the offset bias when operating in the Voltage Calibration mode. The removal of bias from the detector effectively eliminates the detector signal. The offset bias is simultaneously removed to allow the zeroing reference circuit to operate at close to normal operating conditions.

The first two post-amplifier stages comprise the pre-sampling filter. This filter is a four pole transitional Butterworth Thomas filter. The relative frequency response curve for the filter is shown in Figure 5-28. The two filter stages give a DC gain of approximately 9 to the chain. An additional stage provides additional gain and a relatively wide band output stage. A unity gain amplifier is used to provide a buffered output to the test connector.

The final amplifier output (inverted) is sampled through a FET and fed back to the preamplifier. This signal is stored in capacitors C14 through C18. This signal is fed back to the preamplifier input stage through amplifier U5 which is an FET input amplifier operating as a low pass amplifier. This amplifier is operated as a non-inverting amplifier providing feedback to the input during the sampling interval.

Sampling time constants are selected such that the amplifier output can be restored to zero during the 2 millisecond sampling time. The DC gain of the U5 amplifier stage allows correction

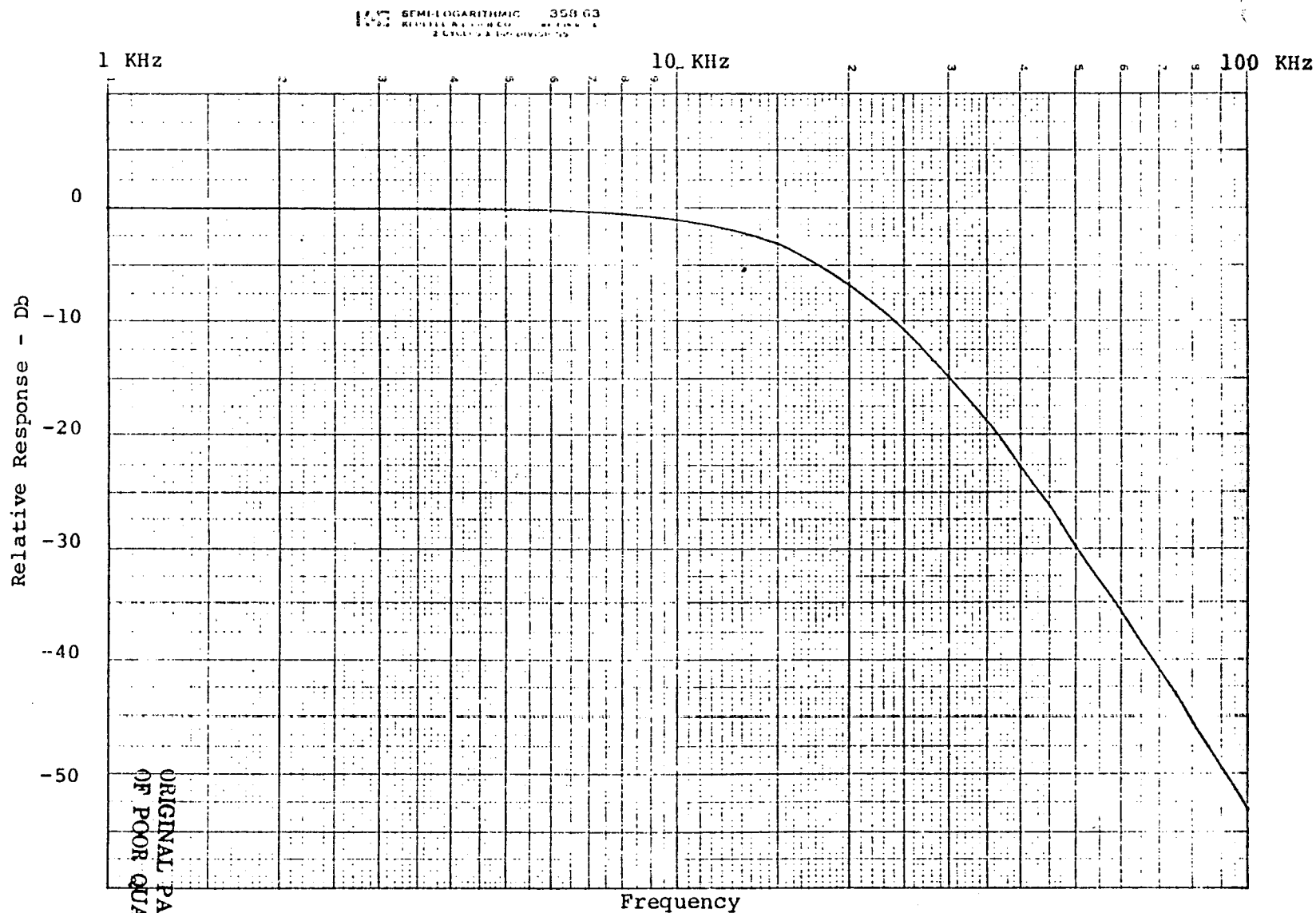


Figure 5-28 Four Pole Transitional Butterworth Thompson Filter Response

of DC offsets with very low DC shifts in the output signal.

A significant amount of tailoring is required in the Ch 3 amplifier to match the possible detector responsivity and bias currents. Provisions are made in several of the amplifier stages for a systematic adjustment by tailoring of gain with fixed resistors. The ramp calibration signal must then be tailored inversely to the overall amplifier gain.

Individual amplifier stages are designed for essentially flat frequency response (except for the filter stages) through the cut-off frequency. For board test the combined gain of the preamplifier and post amplifier will be set at approximately 50,000 which is more than any anticipated requirement. Any tailoring will then be a gain reduction which will not have an adverse affect on frequency response.

5.13 Channel 4 Amplifier

The schematic for the channel 4 preamplifier is shown on 8009217 (Figure 5-31). The channel 4 post amplifier is physically located with the channel 3 post amplifier (Figure 5-27).

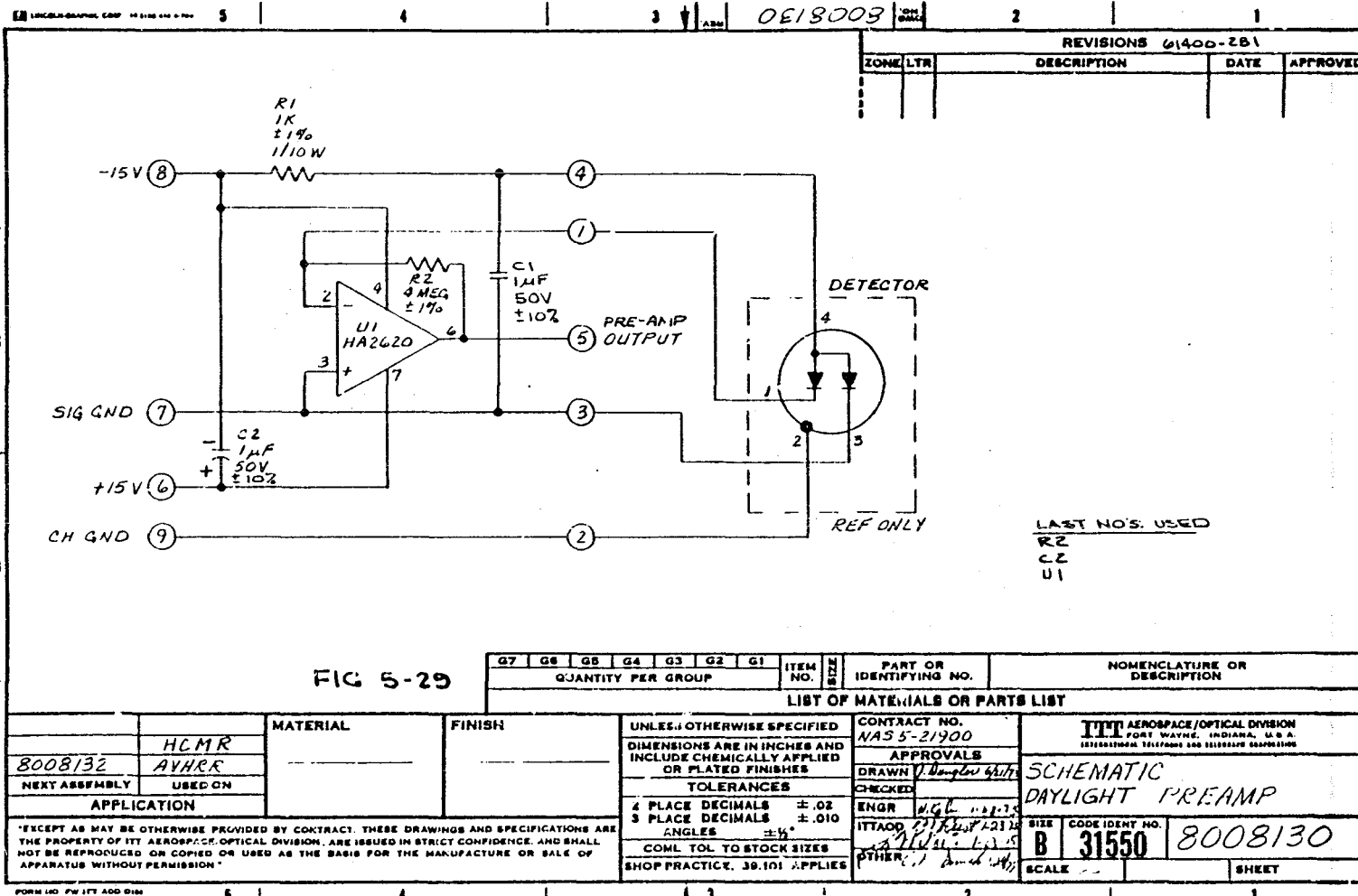
The channel 4 preamplifier is a current to voltage converter with a high (16 meg) feedback resistor for low noise operation. The detector is maintained with a low back bias for minimum detector noise output. This bias is tailored to match each detector

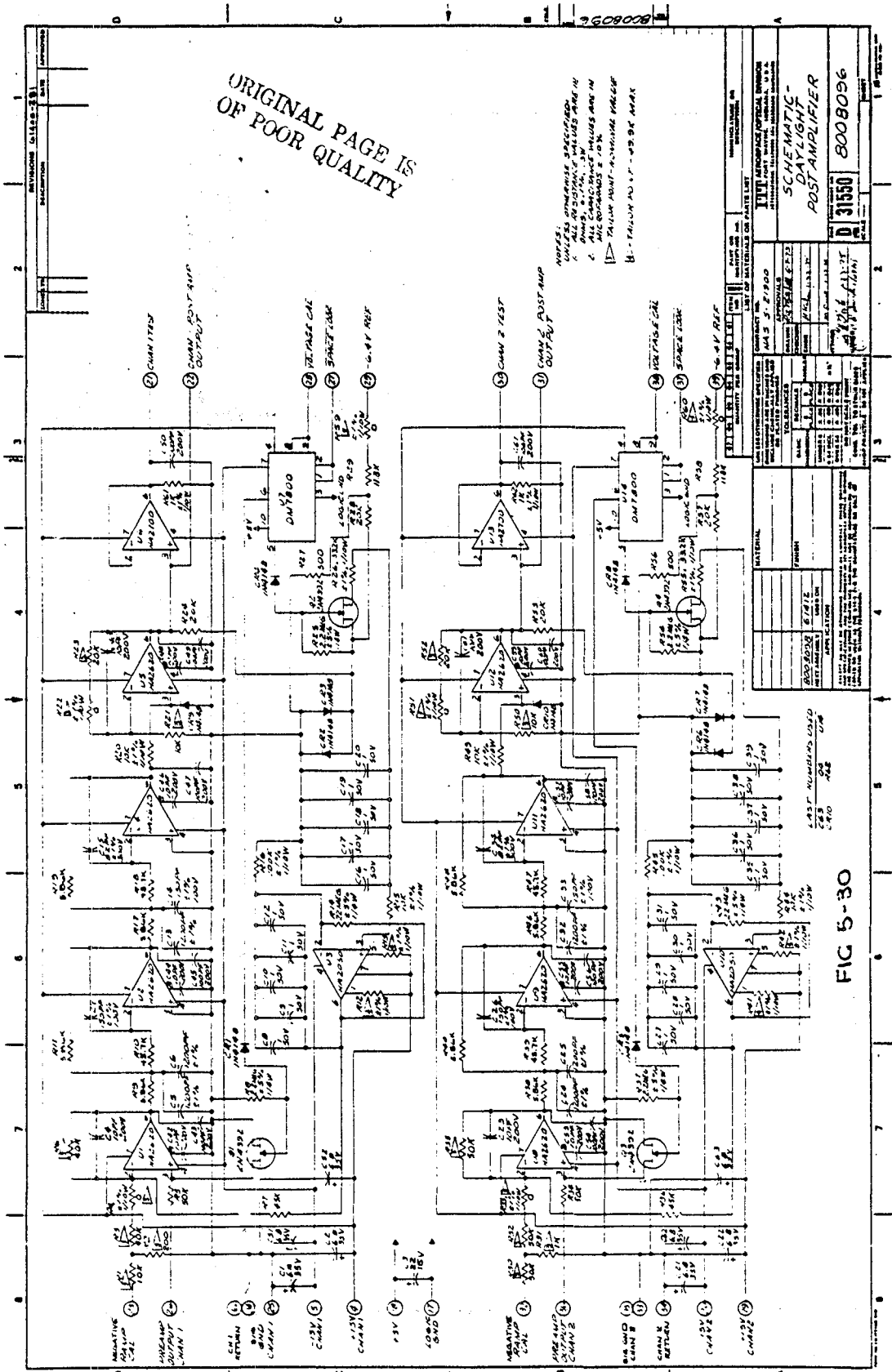
The Post Amplifier is identical to the Daylight Post Amplifier

5.14 Daylight Amplifiers

The schematics of the daylight amplifier system are shown in Drawing 8008130 (Figure 5-29) and Drawing 8008096 (Figure 5-30). The amplifiers for channel 1 and channel 2 are identical except for the tailoring required to match detector responsivity.

The preamplifiers are located in the optics module with the detectors directly connected to the preamplifier terminals.





The detectors are operated in biased mode as a current source. A 4 megohm feedback resistor is used to minimize noise current.

The post amplifiers for the daylight channels are essentially the same as the post amplifier for channel 3. The space sample for the zero reference is fed back to the input stage of the post amplifier. The ramp calibration signal is summed in at first post amplifier stage. A FET is used to short out the preamplifier signal during the Voltage calibration mode of operation.

5.15 Multiplexer Board

This printed circuit board contains the multiplexer for the 6th input channel of the analog-to-digital converter, the blackbody temp. IR TM circuits, and over-temperature monitor circuits for the patch and radiator.

The multiplexer consists of five FET switches feeding amplifier U3. The logic timing signals for control of the FET's are generated on Black Body Mux board. The four Black Body TM signals are sequenced in the same time position on a line scan basis. During the fifth line scan, none of the signals are gated providing a 0 volt marker in that time position. The low range patch temperature is the other multiplexed signal.

The blackbody temp - IR telemetry signals are two identical sample and hold circuits (amplifiers U12 and U13). The sample logic signal is generated on the Scan Count and Decode board and is to provide a sample of the two IR channel outputs at the time the scan mirror has a full view of the internal calibration target (internal blackbody).

The patch and radiator temperature TM voltages are fed to amplifiers U6 and U8 operating as comparators with a reference voltage. The amplifier outputs drive switching transistors in the patch and radiator heater circuits to remove power if the temperature exceeds the allowable figure (currently 40°C).

The schematic diagram for this board is shown in Figure 5-32.

5.16 Black Body Mux

A logic divide by five counter of the BB Temp (logic) signal with four of the counter states decoded provide the logic control signals for the time multiplexing of the four Black Body TM signals. The fifth undecoded state provides the marker scan.

Individual transistor Q2 and Q4 are used to drive each Earth Shield deploy solenoid. Feedback from the shield position switches remove transistor drive current through amplifier U6. The Earth Shield Disable removes all power from these circuits. An R-C delay in the base circuit limits the input current surge. See Figure 5-33.

5.17 Motor Power Supply

The motor power supply converts +22 volts DC (high power mode) or +18 volts DC (low power mode) into a two-phase 240 Hz square wave to drive the 80 pole scan mirror motor. The circuit is a conventional bridge switching inverter. Drawing No. 8007941 is the schematic diagram of the motor power supply (Figure 5-34).

The input signals from the Motor Logics circuit are AC coupled for ground isolation. The HA2620 operational amplifiers act as comparators and provide sufficient drive for the primary circuit to insure saturation of the inverter transistors.

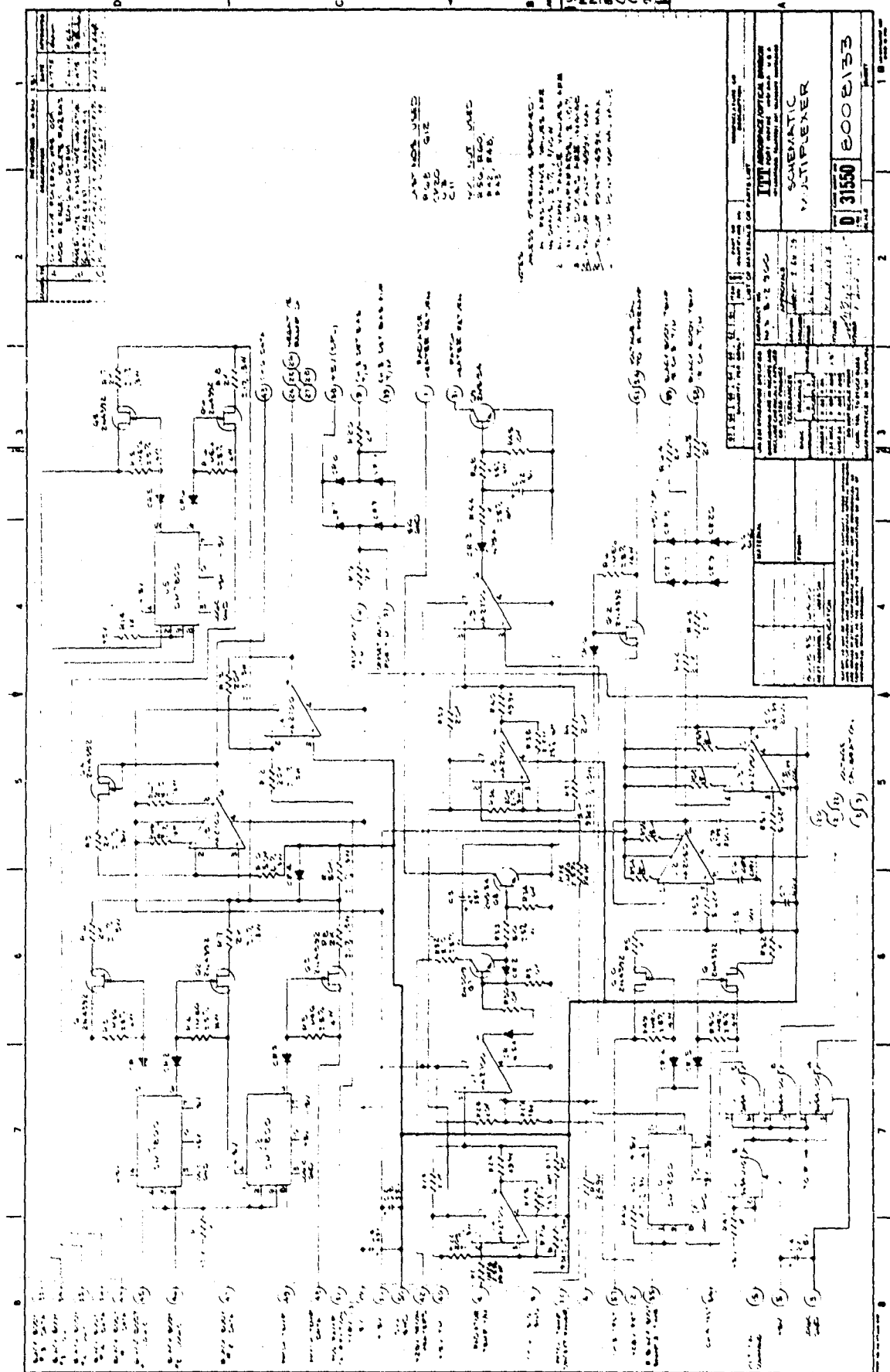
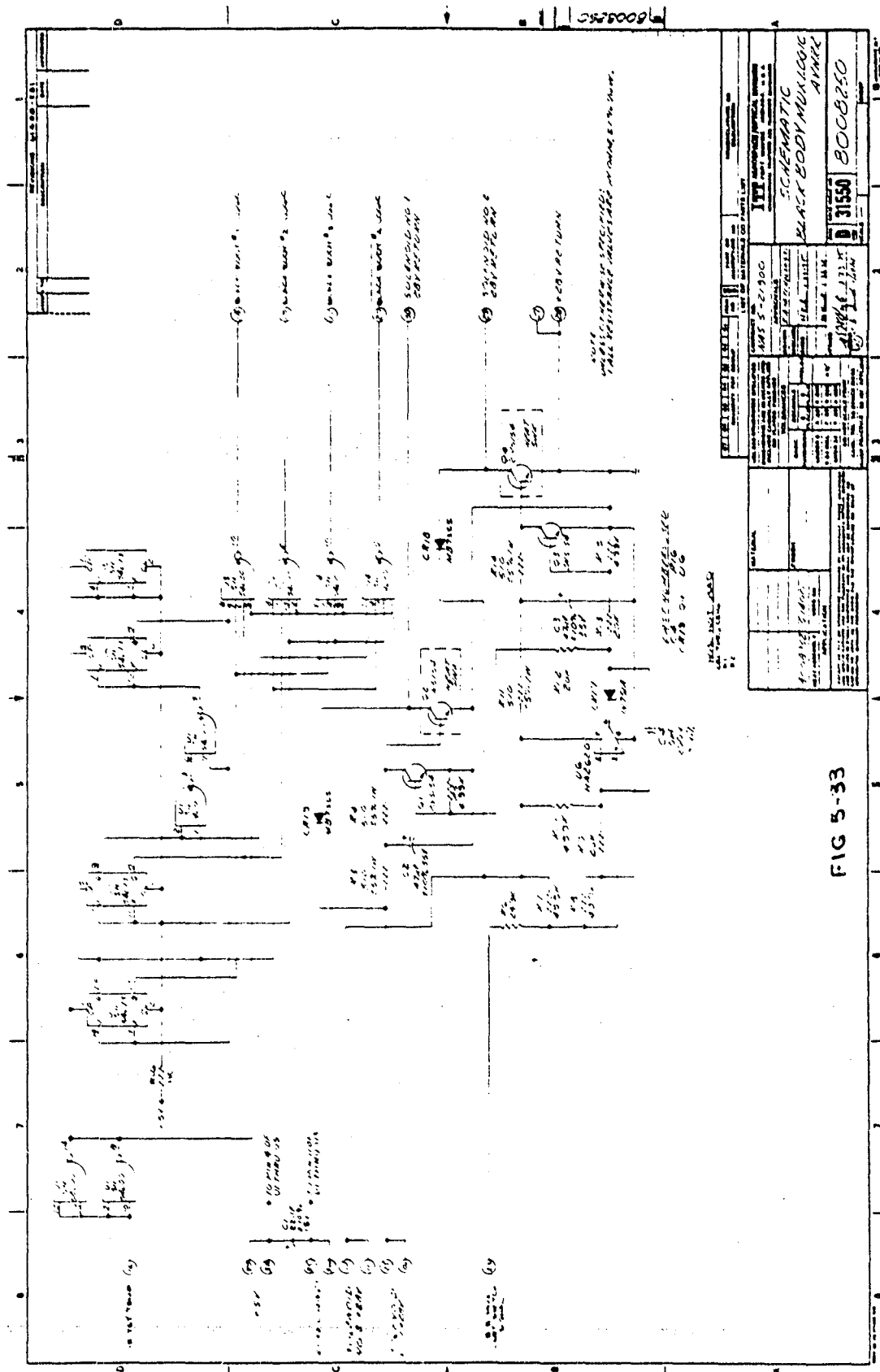


Figure: 5-22



5.18 Power Profile

Figure 5-35 depicts the power usage under the mode of operation indicated.

5.19 Interface Connectors

Table 5-1 lists the connections and type of connectors for the AVHRR Electrical Interface.

5.20 Electronics Drawings

Table 5-2 is a list of the drawings for the electronics printed circuit boards.

POWER PROFILE

FUNCTION	POWER	NORMAL OPERATION	TELEMETRY ONLY	MOTOR ON	COOLER HEATER	INSTRUMENT OFF
ANALOG TELEMETRY	1.89W	X	X	X	X	
A-D & ELECTRONICS **	12.91W	X				
SCAN MOTOR HIGH	4.48W	X		X		
SCAN MOTOR LOW	3.67W			X		
MOTOR LOGIC	1.3W	X	X	X	X	
CHANNEL 1	.84W	X				
CHANNEL 2	.84W	X				
CHANNEL 3	1.5W	X				
CHANNEL 4	1.16W	X				
COOLER HEATER	24.6W				X	
COOLER COVER DEPLOY	56.9W*					
STANDBY HEATER	22.8W***					X
		24.92W	3.19W	6.86W or 7.67W	27.79W	22.8W*

* Required only once for a period of approximately 1 sec.

** Measured PFM values. ETM total was 25.51W.

*** Supplied from TCE - not from +28V buss.

Table 5-1 Interface Connectors

<u>NO.</u>	<u>FUNCTION</u>	<u>GSFC STYLE</u>	<u>DESCRIPTION</u>
J1	Command	311P405-4P-C-12	37 Pin Male
J2	Digital TM	311P405-3S-C-12	25 Pin Female
J3	Power	311P405-3P-C-12	25 Pin Male
J4	Analog TM	311P405-4S-C-12	37 Pin Female
J5	Clock	311P405-1P-C-12	9 Pin Male
J6	Data Processor	311P405-2P-C-12	15 Pin Male
J7	Test	311P405-5S-C-12	50 Pin Female
J33	Pulse Load Heater	311P405-18-C-12	9 Pin Female

J1 COMMAND

<u>PIN NO.</u>	<u>FUNCTION</u>
1	Elec/Telemetry On
2	Elec/Telemetry Off
3	Motor/Telemetry On
4	Motor/Telemetry Off
5	Telemetry Not Locked On
6	Telemetry Locked On
7	Channel 1 Enable
8	Channel 1 Disable
9	Channel 2 Enable
10	Channel 2 Disable
11	Channel 3 Enable
12	Channel 3 Disable
13	Channel 4 Enable
14	Channel 4 Disable
15	Motor Low Power
16	Motor High Power
17	Patch Low
18	Patch High
19	
20	Patch Control Off
21	Patch Control On
22	Earth Shield Disable
23	Earth Shield Deploy
24	Cooler Heat Off
25	Cooler Heat On
26	Voltage Calibrate Off
27	Voltage Calibrate On

J1 COMMAND (Continued)

<u>PIN NO.</u>	<u>FUNCTION</u>
28	
29	
37	Chassis Ground

J2 DIGITAL TM

<u>PIN NO.</u>	<u>FUNCTION</u>
1	Earth Shield Status
2	Patch Control Status
3	Patch Mode Status
4	Motor Mode Status
5	Voltage Calibrate Status
6	Cooler Heat Status
7	Electronics/Telemetry Status
8	Motor/Telemetry Status
9	Telemetry Lock Status
10	Channel 1 Status
11	Channel 2 Status
12	Channel 3 Status
13	Channel 4 Status
14	
25	Chassis Ground

J3 POWER

<u>PIN NO.</u>	<u>FUNCTION</u>
1	+28V Buss
2	+28V Buss
3	+28V Buss (Motor)
4	+28V Buss (Motor)
5	Power Ground
6	Power Ground
7	AC 28V Return
8	AC 28V Return
9	+10V Buss
10	+10V Buss
11	+5V Buss
12	+5V Buss
13	Interface Power Ground
14	Interface Power Ground
15	Signal Ground
16	Signal Ground
17	Chassis Ground
18	Chassis Ground

J4 ANALOG TM

<u>PIN NO.</u>	<u>FUNCTION</u>
1	Radiator Temp. TM
2	Patch Power TM
3	Patch Temp TM Low Range
4	Patch Temp TM Ext Range
5	Black Body #1 TM
6	Black Body #2 TM
7	Black Body #3 TM
8	Black Body #4 TM
9	Motor Current TM
10	Elect. Current TM
11	Earth Shield Position TM
12	Electronics Temp. TM
13	Base Plate Temp. TM
14	A-D Conv. Temp. TM
15	Motor Hsq. Temp TM
16	Cooler Hsq. Temp. TM
17	Detector Bias Volt. Ch. 3 TM
18	
19	BB Temp. IR Ch. 3 TM
20	BB Temp. IR Ch. 4 TM
21	Offset Voltage TM
37	Chassis Ground

J5 CLOCK

<u>PIN NO.</u>	<u>FUNCTION</u>
1	Clock - Ref
2	Clock
3	Clock Shield
4	Chassis Ground

J6 DATA PROCESSOR

<u>PIN NO.</u>	<u>FUNCTION</u>
1	2^9 MIRP Data
2	2^8 MIRP Data
3	2^7 MIRP Data
4	2^6 MIRP Data
5	2^5 MIRP Data
6	2^4 MIRP Data
7	2^3 MIRP Data
8	2^2 MIRP Data
9	2^1 MIRP Data
10	2^0 MIRP Data
11	Chassis Ground
12	Sample Pulse From MIRP
13	Chassis Ground
14	Sync Pulse
15	Chassis Ground

J7 TEST

<u>PIN NO.</u>	<u>FUNCTION</u>
1	Test - Pick-up loss sim.
2	Ramp Cal. 3 level
3	Ch. 3 Test
4	Ch. 4 Test
5	Ch. 1 Test
6	Ch. 2 Test
7	REf. V Test Point
8	Pick-up #1 Test
9	Pick-up #2 Test
10	-15V Test
11	+15V Test
12	Clock Rcvr Test
13	Solenoid +28
14	Solenoid +28
15	+5V Test
17	Sync Pulse
50	Chassis Ground

J33 - PULSE LOAD HEATER

<u>PIN NO.</u>	<u>FUNCTION</u>
1	Pulse Load Heater
2	Pulse Load Heater Ret.
3	Temp. Control Sensor
4	Temp. Control Sensor
5	
6	
7	Chassis Ground
8	
9	

Table 5-2 AVHPR DRAWING NUMBERS

CIRCUIT NAME	SCHEMATIC	BOARD #	ASSEMBLY DRAWING	ASSEMBLY PROCEDURE	TEST PROCEDURE
POWER CONT. & SW. REG.	8007976	8007971	8007972	8008230	8008273
LOGICS REGULATORS	8007977	8007976	8007977	8008231	8008279
±15V REGULATORS	8007980	8007981	8007982	8008232	8008282
MOTOR SW. REG.	8007944	8007945	8007946	8008233	8008297
COMMAND RELAY #1	8008200	8008201	8008202	8008234	8008280
COMMAND RELAY #2	8008794	8008795	8008796	8008235	8008281
COMMAND RELAY #3	8009213	8008795	8008796	8009224	8009227
PATCH TEMP CONT. & T/M	8008120	8008121	8008122	8008236	8008290
T/M BOARD #2	8008127	8008128	8008129	8008237	8008291
MOTOR LOGICS	8008045	8008046	8008047	8008238	8008283
SCAN COUNT & DTC.	8008049	8008050	8008051	8008239	8008284
INTERFACE LOGICS #1	8009206	8009207	8009208	8008240	8008293
INTERFACE LOGICS #2	8009209	8009210	8009211	8009225	8009228
RAMP CAL. GEN.	8007963	8007964	8007965	8008241	8008285
AUX SCAN LOGICS	8008052	8008053	8008054	8008242	8008286
CH. 3 PRLAMP	8008101	8008102	8008103	8008243	8008294
CH. 4 PRLAMP	8009217	8009218	8009219	8009226	8009229
IR POST AMP	8008078	8008079	8008080	8008244	8008288
DAYLIGHT PREAMP	8008130	8008131	8008132	8008245	8008295
DAYLIGHT POST AMP	8008096	8008097	8008098	8008246	8008289
MULTIPLEXER	8008133	8008134	8008135	8008247	8008292
MOTOR POWER SUPPLY	8007941	8007942	8007943	8008248	8008296
BLACK BODY MIX	8008250	8008251	8008252	8008249	8008287

6.0 RADIANT COOLER

The radiant cooler has a simplicity of design (Figure 6.0-1) that reflects the advantageous orbit and the absence of spacecraft extensions in the anti-sun direction. It is a conservative design that employs proven hardware and techniques; there is ample cooling margin for both temperature control and possible thermal degradation. The specific requirements imposed on the detector cooler are as follows:

- a. The cooler shall be mounted on the anti-sun side of the space vehicle and shall look into a hemisphere (of cold space) except for the solid angle subtended by the earth. The cooler must be shaded from earth radiation.
- b. The nominal temperature of the infrared detectors shall be actively controlled at either 105K or 110K (selectable by command). At the beginning of orbital life, the uncontrolled temperature shall be 95K or less.
- c. During acquisition, the cooler field of view can sweep through the sun at a rate of 0.5 rpm for an undeterminate period. The cooler must operate with no degradation after this exposure.

We have assumed the earth shading requirement (a) applies to the patch or second stage of cooling and that the margin requirement (b) applies to the nominal orbit (450 n mi altitude and

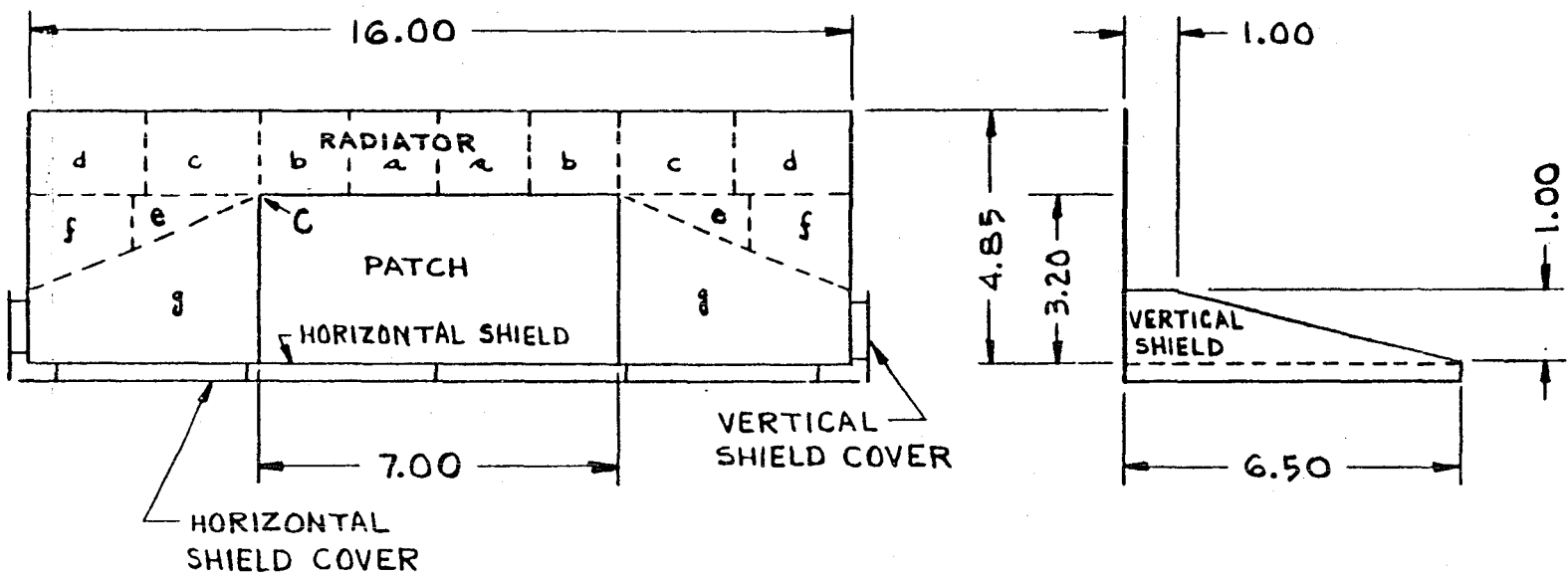


FIG. 6.0-1 BASIC DESIGN OF RADIANT COOLER (DIMENSIONS IN INCHES)

37.5° orbit normal to sun angle). The earth shield will be used as a protective cover during acquisition; exposure is limited to the shield cover, which reaches a maximum temperature of about 0°C during a continuous 0.5 rpm sweep through the sun (Section 6.5).

The design of the radiant cooler is described in detail in Sections 6.1 through 6.4. The performance is analyzed for the nominal condition and for variations in the orbital parameters. The anticontamination provisions to protect both thermal and optical surfaces are described in Section 6.6. Because of the relatively large amount of thermal loading through the optical port to the cooler, we have established detailed models that have been verified by thermal tests (Section 6.7).

The nominal in orbit characteristics of the cooler are summarized in Table 6.0-1 and 6.0-2.

6.1 Field of View

The hemisphere above the cooler patch is cold space except for the earth. As a result, any point on the patch can be shaded by a semicircular shield that matches the angle subtended by the earth and any vertical line by the semicircular shield for its top point. The smallest shield for the entire patch is then obtained by translating the latter shield along the horizontal dimension of the patch. We have modified this shield and increased the shading of the radiator by the use of small vertical sides. The maximum angle subtended by the earth is the solution to \sin

$\delta_m = R_m/R_m + h$, where R_m is the equatorial earth radius (3444.3 n mi) plus the tropical atmospheric height (9.1 n mi) and h is

Table 6.0-1 Nominal Characteristics of the Radiator

Temperature (a)	170.6 K	
Power radiated (a)	1.66 W	
Radiating area	55.2 in ²	
Conductive input (a)	0.195 W	11.7%
Insulation input (a)	0.592	35.6
Earth input	0.210	12.7
Covers input	0.388	23.4
Optical port input (a)	0.275	16.6
dT/dφ (b)	2.05 K (0.1 W) ⁻¹	

(a) For housing at 25°C

(b) Rate of change of temperature with input power at temperature shown.

Table 6.0-2 Nominal Characteristics of the Patch

Temperature (a)	105 K	
Power radiated	96.6 mW	
Radiating area	22.4 in ²	
Conductive input (b)	10.0 mW	10.4%
Insulation input (c)	15.4 mW	15.9
Joule heat input	2.3 mW	2.4
Optical port input	25.3 mW	26.2
Shield input	9.1 mW	9.4
Control power	34.5 mW	35.7
dT/dφ	0.31 K (mW) ⁻¹	

(a) Nominal control point.

(b) Including effect of support shields

(c) Radiative decoupling

the spacecraft altitude (450 n mi). The solution is $\beta_m = 62.20^\circ$. The actual shield completely covers 63.79° , which leaves a margin of 1.59° for spacecraft wobble (1°) and cooler alignment.

6.2 Shield

Figure 6.0-1 shows the radiant cooler shielded designed for use at an altitude of 450 n mi. The shield completely shades the patch (second stage of cooling) from the earth.

6.2.1 Cover Temperatures

Both the vertical and horizontal earth shields are insulated from external inputs by shield covers. The three optically polished shields are thermally and mechanically connected. However, the two vertical covers are not connected to the horizontal cover. The cover temperatures are listed in Table 6.2-1 for the range of sun angles (β_s) at the 450 n mi altitude (see memorandum of May 2, 1974).

The thermal balance equation that determines the temperature T_c of a cover is given by

$$\epsilon_c \sigma T_c^4 = F_{ce} (\epsilon_c W_e + \alpha_c W_r) + \alpha_c S_o < \sin i >$$

where ϵ_c = emissivity = 0.72 (silvered Teflon)

α_c = solar absorptivity = 0.08

F_{cs} = view factor from cover to earth; $\sin^2 \beta_e$ for a horizontal cover and $\frac{1}{\pi} (\beta_e \cos \beta_e)$ for a vertical cover, where β_e (62.17°) is the mean angle from nadir to the earth-tangent line.

Table 6.2-1 Shield Cover Temperatures

θ_s	Vertical	Horizontal
0°	167.8K	232.0K
27.83	187.4	241.9
37.5	190.1	238.6
67	195.6	238.7

Table 6.2-2 View Factors from Radiator to Earth

Element	Weight*	F_{ie}	
a	0.1046	0.011	832
b	0.1046	0.012	734
c	0.1345	0.013	825
d	0.1345	0.075	471
e	0.05575	0.002	673
f	0.12485	0.037	845
g	0.3412	0	
Radiator	1	0.019	454

*Relative area.

$\langle \sin i \rangle$ = orbital average of the solar incidence angle, taken to be zero when the cover is shaded from direct sunlight; $\frac{1}{\pi} \sin \beta_s (1 + \cos \Delta\mu_e)$ for a horizontal surface and $\frac{1}{2\pi} \sin \beta_s (1 + \cos \Delta\mu_e)$ for a vertical surface.

$\Delta\mu_e$ = $\arccos(\cos \beta_e / \sin \beta_s)$; zero when $\sin \beta_s \leq \cos \beta_e$, i.e., when the spacecraft is in direct sunlight throughout its orbit.

W_e = infrared exitance of earth = $2.1 \times 10^{-2} \text{ Wcm}^{-2}$

W_r = reflected solar exitance of earth = $1.68 \times 10^{-2} \sin \beta_s \text{ Wcm}^{-2}$

s_o = solar constant - 0.14 Wcm^{-2}

The equation for W_r is derived in Appendix I to Part I of the Final Report on Contract NAS5-10113 (Dec. 1967).

6.2.2 Shielding and View Factors

Figure 6.2-1 shows the projection of the shielded onto the scan earth disk as seen from an upper corner of the patch (i.e., from the most difficult point to shield). The shading from the earth is complete up to a disk angular radius of 63.79° .

The view factor F_{re} from the black radiator to the earth was determined by dividing the radiator into 14 elements, as shown in Figure 6.0-1. By symmetry, there are seven elements are shown in Figure 6.2-2. The view factors were calculated by means of the contour integral technique (R. V. Annable, Applied Optics, Jan. 1970 and July 1972). The results are given in Table 6.2-2.

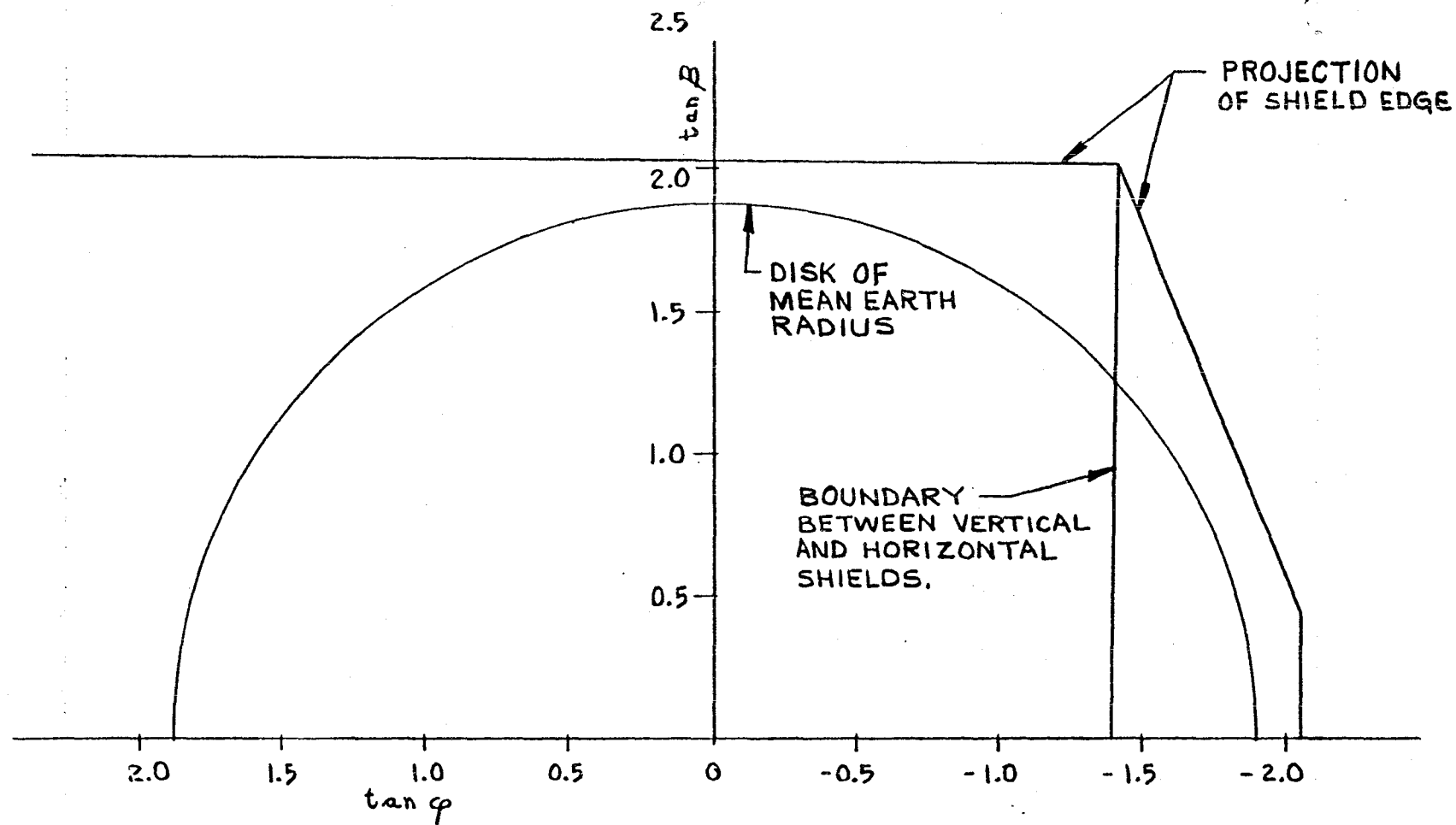


FIG. 6.2-1 PROJECTION OF SHIELD ONTO MEAN EARTH DISK AS SEEN FROM UPPER PATCH CORNER (POINT C IN FIGURE 6.0-1)

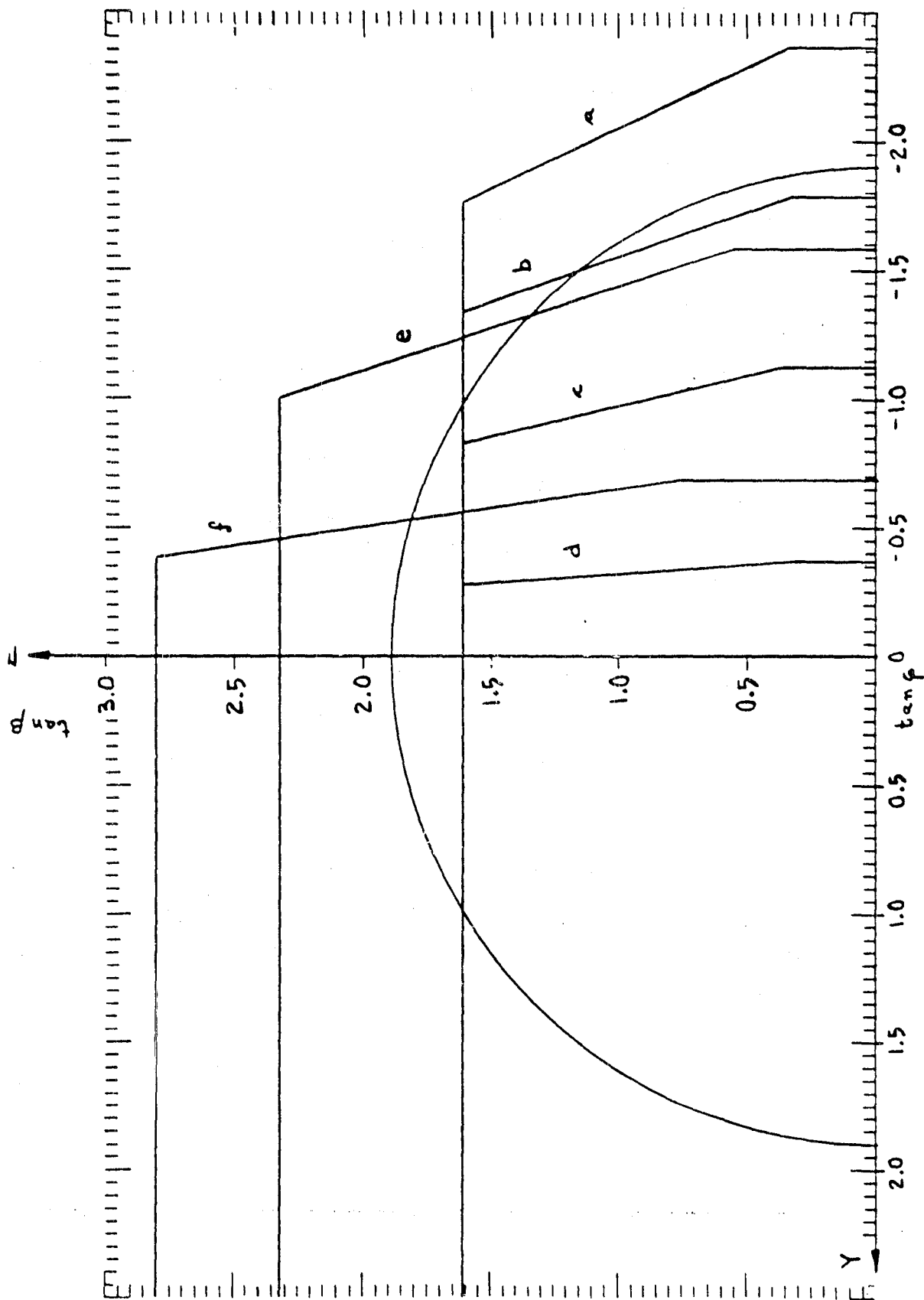


FIG. 6.2-2 PROJECTIONS OF SHIELD ON EARTH DISK AS SEEN FROM RADIATOR ELEMENTS.

The view factor F_{ps} from the patch to the shield was calculated in two parts. First, the view factor to the horizontal shielded was calculated using view factor algebra and the formula for two perpendicular rectangles with a common boundary (E. M. Sparrow and R. C. Cess, Radiation Heat Transfer, Brooks/Cole, 1966, Section 4-3). The result is

$$F_{ps1} = 0.37161$$

Secondly, the view factors to the vertical shields and their specular images in the horizontal were calculated from the center of the patch by the contour integral technique. As shown in Figure 6.2-3, each vertical shield and its complete specular image can be seen from the patch center. By symmetry, the view factors are the same to either vertical shield. The results are

$$F_{ps2} = 0.00359 \text{ to shield}$$

$$F_{ps2} = 0.00339 \text{ to shield image}$$

Finally we determine an effective view factor that can be used directly in the design equations. It is given by

$$F_{ps} = F_{ps1} + 2F_{ps2} + 2(1 - \epsilon_s) F_{ps2}^1,$$

where $(1 - \epsilon_s) = 0.965$ is the reflectivity of the horizontal shield.

The result is

$$F_{ps} = 0.3853$$

6.3 Radiator

The radiator and earth shield have a temperature T_r that is the solution to:

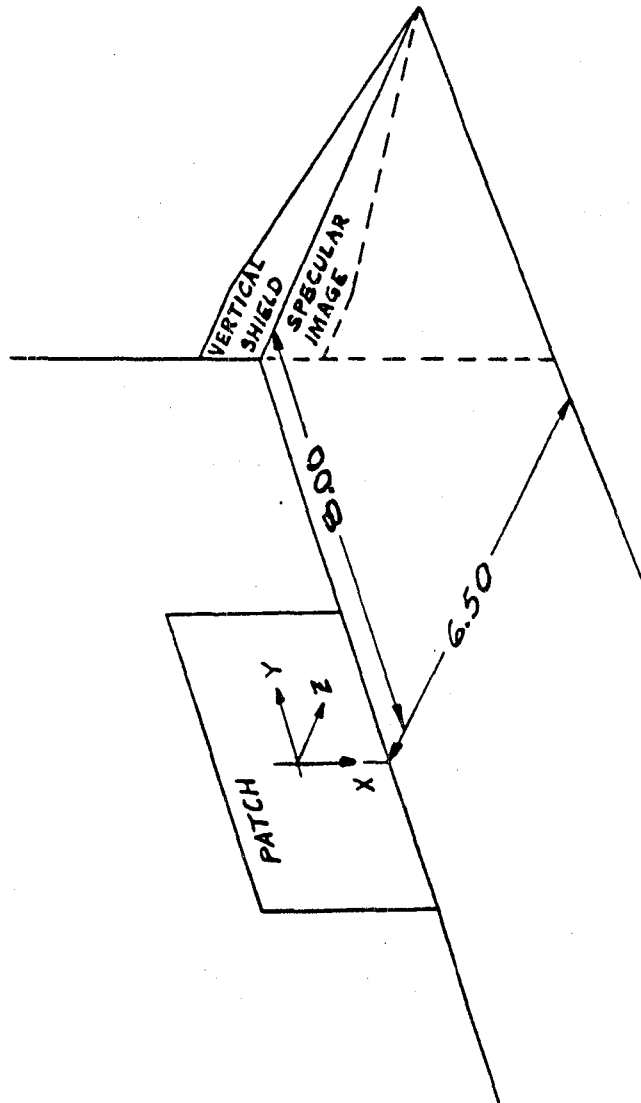


FIG. 6.2-3 GEOMETRY FOR CALCULATION OF VIEW FACTOR TO VERTICAL SHIELD AND ITS IMAGE.

$$\epsilon_r \sigma A_r T_r^4 = \phi_{er} + \phi_{cr} + \phi_i + \phi_k + \phi_o$$

where ϕ_{ab} = radiant power from a that is absorbed in b

e = earth (infrared and reflected sunlight)

r = black radiator, c - shield covers

ϕ_a = input from instrument through a

i = multilayer insulation; k = supports and wires;

o = optical port

$\phi_{er} = F_{re} (e_r W_e + \alpha_r W_r) A_r$

$\phi_{cr} = \frac{\sigma A_c}{A_c} (T_c^4 - T_r^4) + K_c (T_c - T_r)$, for each cover

F_{ab} = view factor from a to b; A_a = area of a

ϵ_a = emissivity of a; α = solar absorptivity of a

W_e = earth infrared exitance = $2.1 \times 10^{-2} \text{ Wcm}^{-2}$

W_r = earth reflected sunlight exitance

= $1.68 \times 10^{-2} \sin \beta_s \text{ Wcm}^{-2}$; β_s = orbit normal

to sun angle

A_c (horizontal) = 104 in^2 ; A_c (2 vertical) = 7.5 in^2

A_r = 55.2 in^2 ;

F_{re} = 0.01945 (Section 6.2)

$\epsilon_r = \alpha_r = 0.97$ (honeycomb cavity array covered with black paint)

$s_c = \frac{2}{\epsilon_c} - 1$; ϵ_c = emissivity of gold plating on facing surfaces of shield and cover = 0.035.

$$\begin{aligned}
K_c &= \text{thermal conductance of supports between shield} \\
&\quad \text{and cover} \\
&= 2.88 \times 10^{-3} \text{ WK}^{-1} \text{ (horizontal)}, \\
&= 1.44 \times 10^{-3} \text{ WK}^{-1} \text{ (2 vertical)} \\
\phi_i &= \frac{\sigma A_i}{S_i} (T_h^4 - T_r^4); A_i = 115 \text{ in}^2; S_i = 50 \\
T_h &= \text{instrument temperature} \\
\phi_k &= K_r (T_h - T_r); K_r = \text{thermal conductance between} \\
&\quad \text{h and r} = 1.14 \times 10^{-3} \text{ WK}^{-1} \\
\phi_o &= 0.257 (T_h = 20^\circ\text{C}) \quad 0.275\text{W} (25^\circ\text{C}), \quad 0.313 \text{ W} (35^\circ\text{C});
\end{aligned}$$

Because the thermal time constant of the radiator-shield is much greater than an orbital period, orbital averages are used for the earth inputs. The insulation factor of 50 is the minimum expected and was achieved on the ETM.

The thermal conductance K_r between the housing (main instrument) and the first stage of cooling consists of $1.35 \times 10^{-3} \text{ WK}^{-1}$ from the synthane support tubes and $0.18 \times 10^{-3} \text{ WK}^{-1}$ from the following electrical connections:

<u>Quantity</u>	<u>Diameter (inch)</u>	<u>Material</u>	
2	3.9×10^{-3}	Copper	} To radiator components
4	3.0×10^{-3}	Chromel	
2	5.0×10^{-3}	Chromel	
4	3.0×10^{-3}	Chromel	} To patch components
2	3.9×10^{-3}	Copper	
4	2.0×10^{-3}	Nickel	

All the electrical connections have a conductance length of 3.15 inches.

Table 6.3-1 shows the radiator temperature range of the 450 n mi altitude. The housing temperatures (T_h) are estimates based on the thermal analysis.

Table 6.3-1 Radiator Temperature Range

β_s	T_h	T_r
0°	20°C	165.6K
27.83	35	173.7
37.5*	25	170.6
67	20	170.1

* Nominal orbit (8:30 AM or 3:30 PM).

6.4 Patch

The thermal balance equation for the patch is

$$\sigma \epsilon_p A_p T_p^4 = \phi_s + \phi_k + \phi_i + \phi_j + \phi_o$$

where p = patch

s = earth shield (upper side)

k = thermal conductance including the influence of radiative inputs from the support shields

i = gold-to-gold radiative insulation

j = joule heat of detectors and temperature sensor

o = optical port

$$\phi_s = \sigma \epsilon_p \epsilon_s A_p F_{ps} T_r^4$$

$$\phi_k = M K_p (T_r - T_p); M = \text{dual mode multiplier}$$

$$\phi_i = \frac{\sigma A_i}{S_i} (T_r^4 - T_p^4); S_i = \frac{2}{\epsilon_i} - 1$$

$$\begin{aligned}
\phi_j &= 2.3 \times 10^{-3} \text{ W} \\
\phi_o &= 2.30 \times 10^{-2} \text{ W } (\beta_s = 0^\circ); 2.83 \times 10^{-2} \text{ W } (27.83^\circ); \\
&\quad 2.53 \times 10^{-2} \text{ W } (37.5^\circ); 2.41 \times 10^{-2} \text{ W } (67^\circ); \\
\epsilon_p &= 0.97 \text{ (black paint on honeycomb cavity array)} \\
\epsilon_s &= 0.035 \text{ (vacuum deposited aluminum)} \\
\epsilon_i &= 0.035 \text{ (gold plate)} \\
A_p &= 22.4 \text{ in}^2; A_i = 32.6 \text{ in}^2 \\
F_{ps} &= 0.3853 \text{ (Section 6.2)} \\
K_p &= 1.1875 \times 10^{-4} \text{ WK}^{-1}; M = 1.28
\end{aligned}$$

The thermal conductance K_p between the radiator and patch consists of the following connections:

Quantity	Diameter (inch)	Length (inch)	Material
4	3/16 x 5/32	2.70	G-10 synthane
4	0.002	2.70	nickel
4	0.003	2.70	chromel
2	0.005	2.70	chromel

The dual heat mode multiplier M was calculated using the approach described in the memorandum "Combined Radiative and Conductive Heat Transfer in the Patch Supports", from Contract 5-21651. A shield emissivity ϵ_s of 0.035 was used in the calculation; and the analysis was carried out for the case $T_s = T_r$ (i.e., the thermal gradient was evaluated at $x = \ell$).

The above equation does not include the input present during chamber testing as a result of reflection of the radiator power from the cold space target. Based on thermal tests and

their analyses, we estimate this input to be given by

$$7.5 \times 10^{-3} \frac{T_r^4}{164} W$$

for the 22.4 in² black radiating area.

The solutions to the patch thermal balance equation are listed in Table 6.4-1. In the nominal orbit, the temperature margin is 10.1K at the 105K control point. The corresponding control power is 35.7% of the total patch load. Or, stated another way, all other thermal inputs would have to increase by 55.5% in order to use up the margin.

6.5 Solar Exposure

If the cooler sweeps through the sun during acquisition, both the patch and radiator will be protected by the shield/cover. The exposure is therefore limited to the (horizontal) shield cover (which is in a vertical position during storage). The worst case is when the sun sweeps through a plane perpendicular to the plane of the shield cover. Even then, as shown by the following analysis, the shield cover has a worst case average temperature of only -0.5°C and a worst case maximum of -0.2°C. During this period, the cooler temperature will then be regulated at 40°C by the outgassing power circuit.

We may treat the shield cover as thermally isolated from the instrument. Its thermal balance equation is then

$$\sigma T^4 + \frac{\delta \rho_c}{\epsilon} \frac{dT}{dt} = \frac{\alpha}{\epsilon} H_s(t) + W_e + \frac{\alpha}{\epsilon} W_{rm}$$

Table 6.4-1 Patch Temperature Range

β_s	T_p (space)	T_p (chamber)
0°	92.8K	95.5K
27.83	96.7	99.6
37.5*	94.9	97.8
67	94.3	97.2

* Nominal orbit.

Table 6.4-2 Other Patch Parameters

$\Delta T_p / \Delta \Phi$	0.34K/mW @ 94.9K,	0.31K/mW @ 105K
Nominal margin	10.1K, space;	7.2K, chamber
Maximum margin	12.2K, space;	9.5K, chamber
Minimum margin	8.3K, space;	5.4K, chamber

where $\epsilon = 0.72$ is the emissivity of the cover and $\alpha = 0.08$ the solar absorptivity. The cover is treated as a plate of thickness δ , density ρ , and specific heat c . $H_s(t)$ is the solar irradiation as a function of time. For the sun in a plane perpendicular to the radiator, $H_s(t)$ is a train of cosine pulses given by

$$H_s(t) = \frac{2}{\pi} S_0 \left[1/2 + \operatorname{Re} \sum_{n=1}^{\infty} c_n \exp(j\omega_n t) \right]$$

where S_0 is the solar constant, Re is real part of, and

$$C_1 = \pi/4, \quad C_n = \frac{-1(-1)^{n/2}}{n^2 - 1}, \quad n = 2, 4, 6 \dots$$

$$\omega_n = \frac{2\pi n}{P}, \quad \frac{1}{P} = \text{frequency of rotation (0.5 rpm)}.$$

W_e is the infrared exitance of the earth (Section 6.2.1), and W_{rm} is the maximum reflected solar exitance. W_{rm} is given by (Appendix I to part I of the Final Report on Contract NAS 5-10113, Dec. 1967)

$$W_{rm} = \frac{\cos^2 \beta_e}{L - \sin \beta_e} \sin \beta_s S_0 A,$$

where $A = 0.4$ is the average solar reflection factor for the earth.

The worst case orbit is then $\beta_s = 67^\circ$, so that we have

$$W_{rm} = 4.86 \times 10^{-2} W_{cm}^{-2}$$

The steady state solution to the above differential equation is $\sigma T_o^4 = \frac{\alpha}{\pi \epsilon} S_0$ and yields the average radiator temperature of $T_o = 272.7K - 0.5^\circ C$. For small temperature changes about T_o we may now linearize the equation by means of $T = T_o + \theta T$

and extract the equation of the transient solution

$$4\sigma T_0^3 \Delta T + a \frac{d(\Delta T)}{dt} = \frac{2\alpha}{\pi\epsilon} S_0 \operatorname{Re} \sum C_n \exp(j\omega_n t)$$

where $a = \delta_{pc}/\epsilon$. The solution is

$$\Delta T(t) = \frac{\alpha S_0}{2\pi\sigma\epsilon T_0^3} \operatorname{Re} \sum \frac{C_n \exp(j\omega_n t)}{1 + j\omega_n \tau}$$

where $\tau = a/4\sigma\epsilon T_0^3$ is the thermal time constant. For a 0.03 inch aluminum plate ($\rho = 2.7 \text{ gms/cm}^3$, $c = 0.895 \text{ joules/gm}^\circ\text{C}$), we obtain $\tau = 10.34 \text{ mins}$. Taking the real part of the sum, we obtain

$$\Delta T(t) = \frac{S_0}{4\pi\sigma\epsilon T_0^3} \sum_{n=1}^{\infty} \frac{C_n}{1 + \omega_n^2 \tau^2} (\cos \omega_n t + \omega_n \tau \sin \omega_n t).$$

The maximum value of $\Delta T(t)$ occurs at $t = 0.19 P$ when $t = 0$ is the point of zero solar incidence angle. The resultant value is

$$\Delta T = 0.29^\circ\text{C}$$

The peak difference from average is reached about 55° of rotation after normal incidence and is very small compared with the average temperature. The maximum temperature, in fact, is only -0.2°C .

6.6 Anti-Contamination Provisions

The radiant cooler is designed to prevent optical or thermal contamination by either the cooler components themselves or by the instrument/spacecraft atmosphere. Specific provisions are (1) conditioning and de-contamination, (2) elimination of internal outgassing paths, and (3) positive protection of sensitive areas.

To outgas the cooler and prevent condensation of external contaminants from the instrument and spacecraft, the cooler will be heated to approximately 40°C for an extended period after acquisition. The same heaters will be used for any subsequent decontamination. The times required for a complete decontamination and for the cool down to operating temperatures are estimated in DIR No. 19. The cooler will be outgassed with the shield/cover closed and decontaminated with it open. In the open position, we require a power level of 14.0 watts on the radiator and 6.4 watts on the patch to achieve a 25°C temperature

Internal outgassing paths are eliminated by windows that seal the openings between the instrument and radiator and between the radiator and patch. The volumes within the cooler can outgas only by paths that lead directly to space.

To provide positive protection for sensitive areas, the window on the radiator is heated a nominal 8K above the radiator temperature and protected by a cold trap at the radiator temperature. The design and analysis of the window heater is covered in DIR. No. 15. The optical elements on the patch and the low emissivity rear areas of the patch are protected by a cold trap at the patch temperature.

6.7 Optical Port Loading

Three thermal tests were run on a feasibility model cooler and two tests run on the BBM. These tests were used to establish a mathematical model for the loading from the optical port opening onto the radiator and the patch. The opening is shown schematically in Figure 6.7-1. This is the configuration of the instrument final design.

6.7.1 Optical Loading on the Radiator

The optical loading on the radiator is

$$\phi_{or} = \epsilon_1 \sigma T_h^4 A_1 F_{12} (1 - P_2) + (1 - F_{12})$$

where A_1 equals πr_1^2 and P_2 is the fraction of room temperature radiation passed by the inner window. For an inner window of Irtran 2, P_2 is about 0.5 (corresponding to a cutoff wavelength of 14 μ m). The emissivity of the opening is 0.9 in the instrument, where an outer germanium window is added. Using the data given in Figures 6.7-1 and 6.7-2 plus Table 6.7-1 and 6.7-2, we obtain the calculated optical port loadings on the radiator in the final instrument design are then:

$$\phi_{or} (T_h = 20^\circ\text{C}) = 0.257\text{W}$$

$$\phi_{or} (T_h = 25^\circ\text{C}) = 0.275\text{W}$$

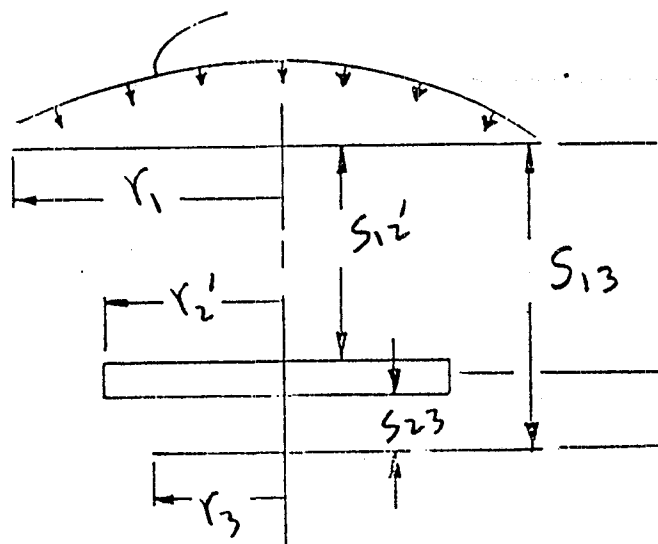
$$\phi_{or} (T_h = 35^\circ\text{C}) = 0.313\text{W}$$

6.7.2 Optical Loading on the Patch

The optical port loading on the patch consists of inputs from the instrument and the radiator. We will restrict the radiator input to that from the inner window itself; radiation at the radiator temperature (ie., the cold trap) is efficiently absorbed in the window. The input from the instrument to the patch is given by

$$\phi_{13} = \epsilon_1 \sigma T_h^4 P_2 \tau_2 F_{31} \gamma_3 A_3$$

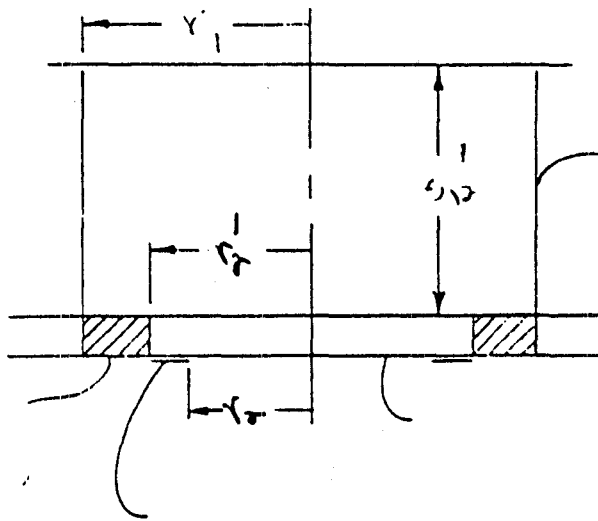
where τ_2 is the transmittance of the inner window for greybody radiation at the temperature T_h , γ_3 is the effective absorptivity of the patch opening.



	r_1	r_2'	r_3	s_{13}	s_{23}	s_{12}'
Instrument	0.630	0.570	0.415	0.855	0.07	0.685

Instrument Opening	Radiator Opening	Patch Opening
Germanium	Irtran 2	Optical elements & gold baffle

Figure 6.7-1 Characteristics of the Optical Opening to the Radiant Cooler (Dimensions in Inches)



r_1	r_2	r_2'	s_{12}'	F_{12}'
0.630	0.430	0.570	0.685	0.303

Figure 6.7-2 Optical Opening to the Radiator
in the Instrument (Dimensions in Inches)

Table 6.7-1 View Factors and Blockage Within the Optical Opening

$$F_{32} = 0.875$$

$$F_{31} = 0.319$$

$$F_{12} = 0.303$$

Table 6.7-2 Temperatures Within the Optical Opening
(Instrument Test)

Instrument	Radiator	Patch
20°C, 35°C	173.6K 181.7K	105K (b)
25°C, 20°C	178.6K 178.1K	(a)

(a) Heated Window

(b) Control Point

The effective absorptivity γ_3 is given by

$$\gamma_3 = \alpha_3 + (1 - \alpha_3) \rho_2 F_{33'} + (1 - \alpha_3)^2 \rho_2^2 (F_{33'})^2 \alpha_3 + \dots$$

$$\gamma_3 = \frac{\alpha_3}{1 - \rho_2 (1 - \alpha_3) F_{33'}}$$

where α_3 is the actual absorptivity of the patch opening, ρ_2 is the (specular) reflectance of the inner window, and $F_{33'}$ is the view factor from the patch opening to its own specular image in the inner surface of the window. The value of γ_3 was experimentally determined from; a theoretical model of α_3 is described in Section 6.7.3.

The input from the inner window attached to the radiator is given by

$$\phi_{23} = \sigma_{T_w}^4 \epsilon_2 F_{32} \gamma_3 A_3$$

The window temperature T_w is equal to the radiator temperature plus 8K. For an inner window of Irtran 2 and for greybody radiation in the range from 160K to 175K, the window emissivity ϵ_2 is approximately 0.6 and the window reflectance ρ_2 , approximately 0.2. Using the theoretical α_3 value of 0.675 (Section 6.7.3) and test values for ρ_2 (0.1), and $F_{33'}$ (0.743), the theoretical value of γ_3 is 0.692. The experimental γ_3 is 0.773 and is based upon test data from a feasibility model cooler.

Using the experimental value for γ_3 and the instrument parameters listed in Figures 6.7-1 and 6.7-2 and in Tables 6.7-1 and 6.7-2, we calculated ϕ_{op} for the final instrument. The results are given in Table 6.7-3.

Table 6.7-3 Calculated Patch Loading from Optical Port (Instrument)

β_s	T_h	ϕ_{op}
0°	20°C	0.0230 W
27.83	35	0.0283
37.5	25	0.0253
67	20	0.0241

6.7.3 Absorptivity of the Instrument Patch Opening (Theoretical Model)

To complete the consideration of optical port loading, we constructed a theoretical model for the absorptivity α_3 of the patch opening in the instrument cooler. A view of the patch opening as seen from the inner window is shown in Figure 6.7-3. The area b_1 occupied by the Channel 3 spectral filter and its specular image b_2 in the infrared dichroic are effectively black. Thus in area b_1 , some radiation is absorbed in the Channel 3 filter or transmitted by the filter and absorbed in the cavity below; the remainder is reflect to b_2 , where it is either absorbed or transmitted by the dichroic and absorbed below.

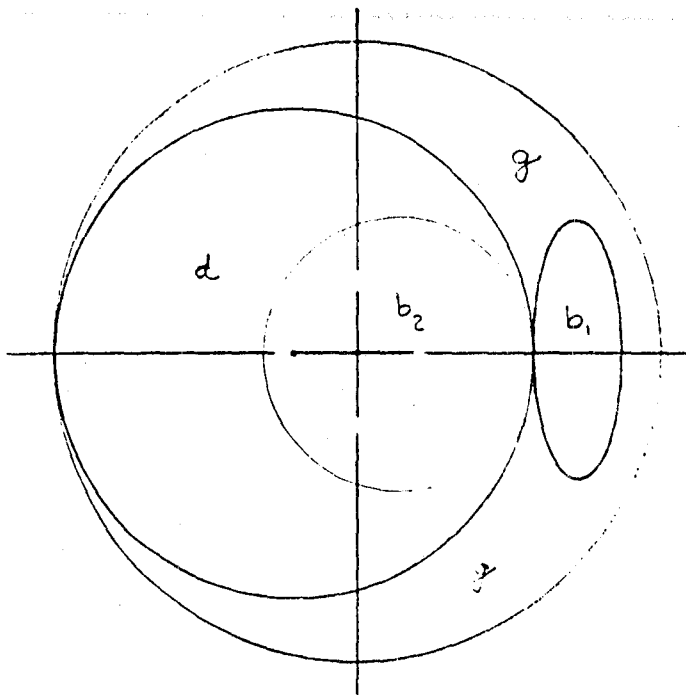
The effective absorptivity of the area d (dichroic minus area b_2) is igven by

$$\alpha_d' = \alpha_d + (1 - \alpha_d) \alpha_g'$$

where α_d = actual absortivity of area d = 0.4

α_g' = effective absorptivity of gold baffle g

This equation assumes that radiation not absorbed or transmitted by d (the fraction α_d) is specularly reflected to the gold baffle. The value given for α_d is an estimate for the infrared dichroic on a germanium substrate. Thus for radiation at the instrument temperature, only about 0.5 is transmitted through the inner Irtran window. For a dichroic with a separation wavelength of 9.0 μm , about 0.4 is transmitted and therefore absorbed. For radiation at the radiator temperature, about 0.2 of the total is reflected if the dichroic reflects over the band from 9 μm to 16 μm . If the dichroic has



- g = Gold Baffle
- b_1 = Opening For Channel 3
- b_2 = b_1 Reflected In Dichroic
- d = Dichroic Minus b_2

Figure 6.7-3 Top View of Optical Opening on Patch
(Note that the model applies to the
breadboard model used in Test 4.)

the properties of a germanium substrate beyond 16 μm , the remaining fraction of 0.8 has an absorptivity equal to approximately 0.47, the transmittance of the substrate. The value of α_d for radiator emission is then 0.8×0.47 or about 0.4.

In order to calculate the effective absorptivity α_g , of the gold baffle, we assumed that the gold is in the form of a diffuse gold plating. We then have

$$\alpha_g' = \alpha_g + (1 - \alpha_g) F_{gg} \alpha_g' + F_{gb1} + F_{gb2}$$

where α_g is the infrared absorptivity (0.035) of the gold plating and F_{ij} is the view factor from area i to area j . This equation can be solved for α_g' ; we then have

$$\alpha_g' = \frac{\alpha_g + (1 - \alpha_g) F_{cb1} + F_{gb2} + F_{gd} (\alpha_d + (1 - \alpha_d) F_{db1})}{1 - (1 - \alpha_g) F_{gg} + F_{gd} (1 - \alpha_d) F_{dg}}$$

The view factors F_{ij} were approximated by

$$F_{ij} = \frac{A_j}{\sum A_j}$$

This equation is strictly true only for a sphere. For the components in the patch opening of the instrument, we have

$$A_3 = 0.636 \text{ in}^2 \text{ (0.9 inch diameter opening)}$$

$$A_{b1} = 0.126 \text{ in}^2 \text{ (0.4 inch diameter)}$$

$$A_{b2} = a A_{b1} = 0.178 \text{ in}^2$$

$$A_d = \pi 0.7 \times 1 - A_{b2} = 2.021 \text{ in}^2$$

$$A_g = \frac{1}{2} \pi \cdot 0.45 \times 0.75 - A_{b1} = 0.404 \text{ in}^2$$

$$\Sigma A_i = 3.365 \text{ in}^2$$

$$F_{ij} = 0.12$$

$$F_{ib1} = 0.04$$

$$F_{ib2} = 0.05$$

$$F_{id} = 0.60$$

$$F_{io} = 0.19$$

We then have for the effective absorptivities

$$\alpha_g' = 0.435$$

$$\alpha_d = 0.66$$

Finally, the value of α_3 can be calculated as the area-weighted average

$$\alpha_3 = \frac{1}{A_3} A_g' \alpha_g' + A_{b1}' + A_{b2}' + A_d' \alpha_d'$$

where the primes on the areas denote projection into the opening A_3

$$A_g' = 0.210 \text{ in}^2$$

$$A_{b1}' = 0.041 \text{ in}^2$$

$$A_{b2}' = 0.126 \text{ in}^2$$

$$A_d' = 0.259 \text{ in}^2$$

For the above values of α_g' and α_d' , we then have

$$\alpha_3 = 0.675.$$

7.0 CALIBRATION

7.1 Thermal Channels Calibration

The infrared calibration signal to the AVHRR is the difference in signals from a calibration blackbody of known temperature and a blackbody of essentially zero exitance. The zero level source is provided by deep space during in-flight calibration and by a liquid nitrogen cooled black cavity during chamber calibration. Other calibration requirements are listed in Table 7.1-1. We have interpreted the temperature calibration accuracy of the chamber targets (B.b.) to mean the equivalent temperature accuracy determined by all error sources.

7.1.1 Calibration Accuracy

The absolute radiometric calibration of the instrument is to have an accuracy of $\pm 0.5K$ throughout the calibration range of each channel. Before we consider how this requirement can be met, let's define some terms. In particular, we can differentiate between precision (or sensitivity) and accuracy by means of the following:

Precision: A measurement is regarded as precise if the dispersion of values, i.e., the standard deviation σ , is small.

Accuracy: A measurement is regarded as accurate if the values cluster closely about the correct value.

By accuracy of an individual measurement or of an average of measurements is usually meant the maximum possible error (constant and/or random) that could influence the observed value. It is frequently thought of in terms of the number of significant figures to which a value can be regarded as correct.

TABLE 7.1-1 Requirements for Thermal Channels Calibration

A. Inflight Blackbody

- a. Measured with platinum resistance thermometers
Appropriately arrayed to adequately define the
temperature.
- b. Temperature sensor instrumentation accuracy of
 $\pm 0.1\text{K}$.
- c. To be compared with the chamber targets during
thermal vacuum calibrations.

B. Chamber (Standard) Blackbodies

- a. Greater emissivity, temperature stability, and
temperature sensor accuracy than inflight target.
- b. Absolute temperature measurement accurate to
 $\pm 0.5\text{K}$.

The precision is limited by the instrument noise, i.e., by the sensitivity. In order to measure the noise of the instrument and to reduce its effect on the absolute radiometric calibration, a set of n measurements will be made at each calibration point. The precision (or sensitivity) is then given by the best estimate of the standard deviation (see for example, D.C. Baird, Experimentation: An Introduction to Measurement Theory and Experiment Design, Prentice - Hall, 1962).

$$\sigma = \left[\sum (x - \bar{x})^2 / (n-1) \right]^{1/2},$$

where x is an individual measurement and \bar{x} the average of n measurements. On the other hand, the standard deviation of the average of n measurements is given by

$$\sigma_n = \sigma / n^{1/2}$$

The influence of the instrument noise and of all other random errors can therefore be reduced to the point where the accuracy of a calibration is determined by the systematic errors in the calibration target itself. This could be done during both the chamber (Section 7.1.2) and in-flight (Section 7.1.3) calibration. There are 10 calibration points (elemental dwell times) during each scan of a target, and so for a 1 minute period, we have $n = 3600$.

Before we consider the errors in the calibration targets, however, let's list all the components and procedures that can limit the accuracy of a calibration. We can identify two major

areas, within which there may be important subareas. They are as follows:

- A. Calibration target
 - a. Temperature: Measurement $\left\{ \begin{array}{l} \text{Sensor} \\ \text{Instrumentation} \end{array} \right.$
Gradients or uniformity
Control (chamber)
 - b. Non-blackness
- B. Electronics
 - a. Noise (NETD)
 - b. Signal processing: Digitization
Recording
Transmission (In-flight)
Ground Processing

We will limit ourselves to errors from sources A and B.a. We are therefore assuming that the experiment is so designed that the errors contributed by B.b. are negligible by comparison.

If the difference in surround between chamber targets can be made zero or very small, the non-blackness errors will be greatly reduced and the accuracy of the calibration limited only by the errors and uncertainties in the calibration target temperature. Accuracy estimates for the chamber calibration are given in Table 7.1-2 and for the in-flight calibration in Table 7.1-3.

We see that we have met our objective of 0.5K for the total channel calibration error throughout the temperature range of both channels.* In addition, the total in-flight error at 295K

* We have arbitrarily set the lower limit in Channel 4 at 250K, where the noise equivalent temperature difference is approximately 1K.

Table 7.1-2 Accuracy of Chamber Calibration

Temperature:

Measurement	Sensor	$\pm 0.05K$
	Instrumentation	± 0.05
	Control	± 0.05
Gradients' base (uniformity)		$\pm 0.10^*$
Honeycomb (1K)*		± 0.06
Wall	Diff from box ($\pm 1K$)*	± 0.0026
	Gradient within (5K)*	± 0.00045
Accuracy (max of errors + uncertainties)		0.32K

Non-blackness

Net from standard-cold space difference
(10K difference in surrounds):

Channel	T	$\delta^2 T$
3	185K	+0.018K
3	320	-0.046
4	250	+0.027
4	320	-0.016

Total accuracy (including noise for $n = 3600$)**

Channel	T	δT
3	185K	0.35K
3	320	0.37
4	250	0.37
4	320	0.34

* Actual value of gradient.

** Based on specified NETD of 0.12K at 300K.

Table 7.1-3 Accuracy of In-flight Calibration For T = 295K *

Temperature:

Measurement	Sensor	$\pm 0.05K$
	Instrumentation	± 0.10
Gradients	Base	± 0.08
	Honeycomb (1K)	± 0.08
		± 0.31

Non-blackness:

Channel	δT
3	-0.080
4	-0.029

Total accuracy (including noise for n = 3600)

Channel	δT
3	0.39K
4	0.34

* Exclusive of errors from scattered sunlight (Section 3.11)

has a comparable value when the calibration is made in the absence of direct sunlight (See Section 3.11). In the following sections, we consider in detail how we obtained the estimate listed in Tables 7.1-2 and 7.1-3.

7.1.2 Chamber Calibration Targets

Errors and uncertainties in the exitance (emitted Wcm^{-2}) of the calibration target arise from its temperature inaccuracies (Section 7.1.2.1) and its deviation from blackness (Section 7.1.2.2). Because a calibration signal is equal to the difference in signals from a calibration target and a cold space target, the inaccuracy from non-blackness is greatly reduced by making the two targets the same form and exposing them to the same surround.

7.1.2.1 Temperature Uncertainty

The accuracy of the calibration target temperature is limited by measurement errors, control stability, and gradients. The uncertainty in a temperature measurement relative to the international practical temperature scale (IPTS-68, which is essentially identical to the absolute thermodynamic temperature scale) is $\pm 0.10K$. About half of this is the calibration accuracy; the remainder is produced by the sensor, bridge, and power supply. The latter produce errors that are largely random in nature, as do the readout device and temperature controller. The readout device introduces an error that can be kept small, about $\pm 0.01K$ for an integrating digital voltmeter. The stability of the controller is about $\pm 0.05K$.

The base gradient or uniformity can be held to $\pm 0.10\text{K}$. We have included this variation as part of the calibration error. In fact, the base temperature will be measured with an array of calibrated platinum sensors. The average of this array should then provide a measurement whose gradient error is less than the actual gradient. The gradient through the honeycomb can be estimated from the measurements on a similar target (A. R. Karoli, J. R. Rickey, and R. E. Nelson, Appl. Opt. 6, 1183, 1967). The honeycomb gradient was 1.6K in a 290K target that had a view factor of about 0.5 to a warm surround at 25°C . If the target temperature were reduced to 210K , the gradient would increase to about 2.5K . However, the view factor to the warm surround is reduced to 0.2 in our design, so the gradient is about 1.0K .

Moreover, the corresponding increase in the radiance temperature is much less than the gradient because most of the normal emission comes from the base and walls near the base. When the instrument views the calibration target at normal incidence during a calibration, the nominal cavity emissivity of 0.999327 (Section 7.1.2.2) may be divided between the base honeycomb and the cavity walls. For the nominal paint emissivity of 0.92, the base has a normal emissivity of 0.996696. Therefore 0.002631 of the normal cavity emissivity arises in the cavity walls (and is seen by reflection in the base). The emissivity of the base may, in turn, be divided among emission from the base bottom, the flat top area of the honeycomb, and the walls

of the honeycomb. The fraction of flat area of 0.025, so that the emissivity from the top is 0.92×0.025 and from the bottom, 0.92×0.975 . The remainder of base emissivity, $0.996\ 696 - 0.92 = 0.076\ 696$ arises in the sides of the honeycomb. We will assume that the walls of the cavity emit at the bottom temperature of the base and that the base honeycomb sides have an exitance equal to the average of the basebottom and honeycomb flats. The effective exitance M_E of the target seen at normal incidence is then

$$0.999\ 327\ M_E = 0.061\ 348\ M_F + 0.937\ 979\ M_B,$$

where F denotes base flats and B base bottom. Now a calibration temperature will be the measured value of the base bottom B. In both Channels 3 and 4, we find that a honeycomb gradient $T_F - T_B = \pm 1B$ results in a calibration error $T_E - T_B = \pm 0.061K$ (see Table 7.1-6 in Section 7.1.2.2).

The temperature errors introduced by deviations in the cavity wall temperature were analyzed for Contract NAS5-21651 (HIRS for Nimbus F)*. This analysis shows that the wall temperature deviations (difference from the base and internal gradient) introduce a temperature uncertainty of only about $\pm 0.003K$. As a result, the total temperature uncertainty in the chamber target is approximately 0.32K.

7.1.2.2 Deviation from a Blackbody

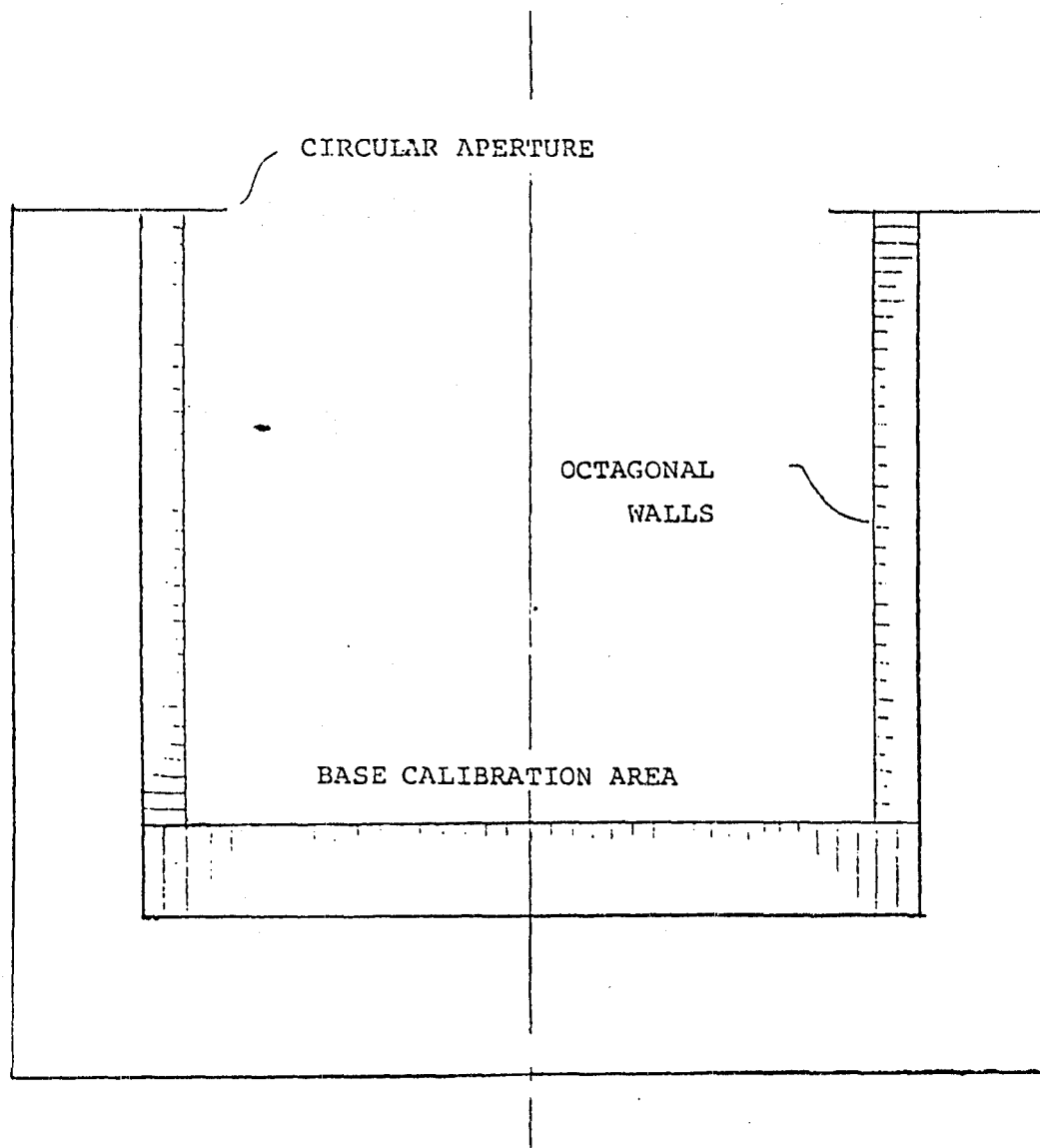
The uncertainties in the calibration of the instrument are expressed as absolute temperature errors in blackbody sources

*Memo from R. V. Annable "Deviations in the Wall Temperature of the Chamber Calibration Target", dated 6-28-72.

within the calibration range of each channel. The principles and practice of absolute radiometry are explored by R. E. Bedford and A. R. Karoli in Volume 14 of Advances in Geophysics (Precision Radiometry, ed. by A. J. Drummond, Academic Press, 1970). We have already covered the uncertainty in the temperature of the calibration target (Section 7.1.2.1). We now wish to consider the uncertainties produced by non-black calibration and cold space targets.

The real problem here is not the small decrease in target emission below that of a blackbody, but the reflection of the higher temperature surround. The calibration target consists of a honeycomb array with a length to width ratio of 4:1 (or its emissivity equivalent in another geometrical form) housed in a tube whose length is equal to the aperture diameter (Figure 7.1-1). The tube is covered on its inner wall with a honeycomb array whose length to width ratio is 2:1. In this way, we obtain a second, large cavity in addition to the array of small cavities. It is also equivalent to controlling a large fraction of the target surround. The tubular enclosure must not be thermally attached to the base calibration target; this would induce significant thermal gradients in the target. In addition, the cavity mouth and base must be sufficiently large that only the base is seen by the instrument during a calibration.

Because a calibration depends on the difference in signals from the calibration and cold space targets, the accuracy can be further increased by making both targets in the same form and exposing them, as nearly as possible, to the same surround. We have an estimate of the residual non-black error based on a



ORIGINAL PAGE IS
OF POOR QUALITY

Figure 7.1-1 Chamber Calibration Target

calibration target surround of 293K and a space target surround of 283K; it ranges from +0.018 to -0.046K in Channel 3 and from 0.027 to -0.016K in Channel 4.

The base of the calibration target is in the form of honeycomb cavity array in which the cavities have a length to width ratio of 4:1 (A.R. Karoli, J. R. Hickey, and R. E. Nelson, Appl. Opt. 6, 1183 (1967)). A single cavity may be approximated by a cylinder whose emissivity is given by (P. Campanaro and T. Ricolfi, J. Opt. Soc. Am. 57, 48 (1967).)

$$\epsilon_c = \epsilon + \left[\frac{\rho \alpha^2}{2} \left(1 + \frac{4}{\alpha^2} \right)^{\frac{1}{2}} - 1 \right] - \frac{\rho^2 \alpha^2}{2} \left[\frac{1 + \frac{2}{\alpha^2}}{\left(1 + \frac{4}{\alpha^2} \right)^{\frac{1}{2}}} - 1 \right]$$

where α = ratio of height to radius

ϵ = normal surface emissivity

ρ = hemispherical surface reflectivity

For high emissivity materials, the normal and hemispherical emissivity are nearly equal (m. Jakob, Heat Transfer, Vol. I, Wiley 1949, Sections 4.9 and 7.2) and ρ is nearly equal to $(1 - \epsilon)$.

The flat area of the array is about 2.5 percent of the total source area. The effective normal emissivity of the array is then

$$\epsilon_A = 0.975 \epsilon_c + 0.025 \epsilon$$

The formula of Companaro and Ricolfi for the normal emissivity of a cavity in the array can also be used to calculate the emissivity of the large cylinder (i.e., the complete target). The cavity array normal emissivity becomes the wall emissivity of the cylinder. To use the formula, we also need the hemispherical emissivity of the cavity array. This can be calculated from the limiting value formula of Treuenfels (J. Opt. Soc. Am. 53, 1162, 1963) or interpolated from the results of Sparrow and Cess (Radiation Heat Transfer, Brooks/Cole, 1966, pp. 164-165). However, when the cavity array normal emissivity and hemispherical reflectivity are used in the formula of Companaro and Ricolfi, we find that the normal emissivity of the cylinder exceeds unity even for an initial surface emissivity as low as 0.89.

To overcome this problem, we will use the formula developed by Bauer and Bischoff (Appl. Opt. 10, 2639, 1971). For a cylindrical cavity with a plane bottom perpendicular to the axis, they obtain a normal reflectivity of

$$\rho_c = \rho_o (1 - \rho_o)^{-1} [1 + (L/R)^2]^{-1}$$

where ρ_o is the normal reflectivity of the inner surface and L/R is the length to radius ratio (α in the formula of Companaro and Ricolfi). According to the nomenclature developed by Nicodemus, et. al. (Appl. Opt. 9, 1474, 1970), ρ_o is the directional-hemispherical reflectance for normally incident flux, that is, the fraction of normally incident flux that is reflected into a hemisphere. It is also equal to the hemispherical-directional

reflectance for normally incident flux, that is, the fraction of normally incident flux that is reflected into a hemisphere. It is also equal to the hemispherical-directional reflectance factor for normally reflected flux, that is, the fraction of hemispherically incident flux that is reflected in the normal direction.

Equation (1) is based on experimental measurements and holds for large value of α , the range of validity depending on the value of ρ_o . However, it yields a conservative result at all values of α , i.e., the calculated value of ρ_c is always greater than or equal to the experimental value. To begin with, we applied the equation to the cavity array in which 2.5 percent of the area is flat. The results are given in Table 7.1-4, where they are compared with those from the equation of Companaro and Ricolfi. We will assume the surface emissivity has a nominal value of 0.92.

The normal reflectivity ρ_N of the complete target can now be calculated from equation (1) by setting $\rho_o = 1 - \epsilon_A$. The space in the chamber limits the α value of the large cylinder to 2:1. The measurements of Bauer and Bischoff (op. cit.) show that the actual reflectivity will be less than that calculated from the formula because of the relatively low value of a . The results of the complete target are given in Table 7.1-5 at four values of the initial surface emissivity ϵ when the walls also have an L/R ratio of 8:1.

Table 7.1-4 Normal Emissivity of the Honeycomb Cavity Array

ϵ Surface	B&B	ϵ_A	C&R
0.89	0.99 6 396		0.99 5 451
0.91	0.99 6 266		0.99 6 304
0.92	0.99 6 696		0.99 6 726
0.93	0.99 7 121		0.99 7 145

Fraction of flat area = 0.025

L/R ratio of cavities = 8.

Table 7.1-5 Normal Reflectivity of In-Chamber Target With
4:1 Honeycomb Array on the Base and Walls

ϵ	ρ_N
0.89	0.000 925
0.91	0.000 750
0.92	0.000 663
0.93	0.000 577

If we neglect multiple reflections between the wall and base of the cavity, we can write the cavity emissivity as

$$\epsilon_N = \epsilon_b + a \epsilon_w,$$

where b = base, w - wall, and a is a constant. For 4:1 cavities on both the base and the wall, we have

$$a = \frac{\epsilon}{\epsilon_b} - 1 = 0.002\ 050$$

If the 4:1 honeycomb on the walls is replaced with 2:1, the wall emissivity is reduced to 0.993013. Using the same value of a, the normal cavity emissivity is then reduced to

$$\epsilon_N = 0.996\ 696 - 0.002650 \times 0.993013 = 0.999\ 327$$

Now the deviation of ϵ_N from unity produces an apparent change in the target radiance given by

$$\delta M = (1 - \epsilon_N) (M_s - M_t)$$

where M is the blackbody exitance and the subscripts s and t denote surround and target, respectively. If the change in exitance is small, the corresponding change in effective blackbody temperature is given by

$$\delta T = \frac{\delta M}{DM/dT}$$

The values of M are given in Table 7.1-6 for Channels 3 (4) at temperatures in the range from 185K (250K) to 321K. The values of δT at representative temperatures are then as follows:

Channel	T	δT
3	185K	0.229K
3	320	-0.0164
4	250	0.0903
4	320	0.0118

Again a calibration depends on the difference between the calibration and space targets, and we can further reduce the non-black errors by constructing the targets in the same geometry and placing them in surrounds as identical as possible. In order to estimate the residual error after taking the difference between targets, we will assume that the calibration target has a surround at 293K and the space target, a surround at 283K. The relative net error in terms of blackbody radiance is then

$$M_{\lambda} = \frac{3.7413 \times 10^4}{\lambda^5} - \frac{1.4388 \times 10^4}{\lambda T} - 1$$

$$\delta^2 M = \epsilon_N M_t + (1 - \epsilon_N) M_{s1} - (1 - \epsilon_N) M_{s2} - M_t$$

$$\delta^2 M = (1 - \epsilon_N) (M_{s1} - M_{s2} - M_t)$$

where s1 denotes the surround the calibration target and s2 the surround of the cold space target. The corresponding errors in blackbody temperature are given in Table 7.1-7 for the representative temperatures.

7.1.2.3 Surround Difference Measurement

In order to verify that the space clamp target and calibration target are exposed to the same surrounds, it was suggested early in the AVHRR program that the two targets be switched in the chamber. This would show if surround reflections were contributing any error to one or the other target. A simpler check can be done by simply comparing the channel 4 signals when it views each target. When the calibration target is run

Table 7.1-6 In-Band Radiant Exitance

	<u>T (K)</u>	<u>(Emitted W cm⁻²)</u>
Channel 3:	185	1.973×10^{-4}
	186	2.047×10^{-4}
	283	2.304×10^{-3}
	293	2.703×10^{-3}
	295	2.787×10^{-3}
	296	2.829×10^{-3}
	300	3.003×10^{-3}
	301	3.048×10^{-3}
	320	3.962×10^{-3}
	321	4.013×10^{-3}
Channel 4:	250	4.174×10^{-6}
	251	4.436×10^{-6}
	283	2.479×10^{-5}
	293	3.931×10^{-5}
	295	4.295×10^{-5}
	296	4.481×10^{-5}
	300	5.331×10^{-5}
	301	5.561×10^{-5}
	320	1.183×10^{-4}
	321	1.228×10^{-4}

Table 7.1-7 Net Non-Black Calibration Error

Channel	T	δ^2_T
3	185K	0.0184 K
3	320	-0.0464
4	250	0.0266
4	320	-0.0156

to 175K, its exitance is below the noise level of the AVHRR in Channel 4. If the output of Channel 4 is then, the same when viewing the cold space target, we can assume that the surrounds are not influencing the accuracy of the calibration in the thermal channels.

Table 7.1-8 shows the calibration data taken in channels 3 and 4 of the ETM on October 6, 1975. The baseplate temperature is $+30^{\circ}\text{C}$. The data shows that in channel 4, the output is identical when viewing the cold space target and the calibration target. As expected the channel 3 output shows some signal from the calibration target at 175K.

From this we conclude that there is no significant calibration error introduced into the thermal channels due to surround differences.

7.1.3 In-Flight Calibration Target

The in-flight calibration is provided by views of the internal blackbody at the housing temperature and of the zero level signal at deep space temperature.

7.1.3.1 Temperature Uncertainty

The temperature measurement error is $\pm 0.05\text{K}$ from the sensor calibration and $\pm 0.10\text{K}$ (specified value) from the instrumentations. Additional temperature uncertainties arise from the gradients within the internal target. The nominal gradient across the base of the target is $\pm 0.08\text{K}$, as determined by the thermal analysis of the instrument. The effective value of this gradient will again be reduced by using an array of

<u>CHANNEL 3 OUTPUT</u>			<u>CHANNEL 4 OUTPUT</u>	
<u>Cal. Target</u> <u>Tamp.</u>	<u>Cal. Target</u> <u>Signal</u>	<u>Space</u> <u>Signal</u>	<u>Cal. Target</u> <u>Signal</u>	<u>Space</u> <u>Signal</u>
K	mvolts	mvolts	mvolts	m volts
320	760.0	6187.5	931.2	6256.8
315	1112.8	6187.5	1879.0	6256.5
305	1769.3	6187.1	3357.1	6257.1
295	2349.6	6187.5	4325.6	6258.1
285	2878.4	6187.5	5035.	6257.1
275	3438.4	6188.1	5495.	6258.1
265	3893.4	6193.7	5822.8	6263.7
255	4284.3	6193.4	6007.1	6264.0
245	4636.2	6193.1	6123.4	6263.7
235	4960.3	6193.7	6189.3	6263.1
225	5225.0	6193.7	6230.0	6264.6
215	5450.6	6193.1	6247.5	6264.0
205	5641.2	6192.8	6254.0	6264.0
195				
185	5906.2	6193.4	6259.0	6263.1
175	5993.7	6193.7	6264.6	6264.6

TABLE 7.1-8

ETM AVHRR CALIBRATION RUN SHOWING

SURROUNDS EFFECT

calibrated platinum sensors to measure the base temperature. The worst case honeycomb gradient is 1.0K (DIR No. 18). Following an analysis similar to that given in Section 7.1.2.1, we find that the corresponding uncertainty in radiance temperature at normal incidence is 0.08K. The total temperature uncertainty of the internal inflight target is then 0.31K.

7.1.3.2 Deviation from a Blackbody

The internal target has a normal emissivity of 0.995 when coated with a black paint whose emissivity is 0.92. The deviation from a blackbody reduces the signal from the target itself but introduces an additional signal from the surround. To obtain the most accurate calibration of the internal target, we would have to compare its signal with that of the more accurate chamber target when the internal target is in the range of surrounds encountered in orbit. The worst case non-blackness errors is shown below to be about 0.08K in Channel 3 and -0.03K in Channel 4.

The internal calibration target is in the form of a honeycomb cavity array in which the length to width ratio is 4:1. Specifically, the basic material has a thickness of 0.001 inch and a cavity width (distance between flats) of 0.060 inch. Each cavity has two walls of its own (where the joined material has a double thickness) and four shared walls or a total of four. The ratio of flat to total target area is then

$$\frac{4 A_w}{A_c + 4 A_w}$$

where A_w is the top area of a wall and A_c the area of a cavity. If w is the distance between flats and t the thickness, we then have

$$A_w = \frac{t}{\sqrt{3}} (w - t)$$

$$A_c = \frac{2}{\sqrt{3}} (w - t)^2$$

when the cavity openings are in the form of hexagons. For the above dimensions, the ratio of flat to total surface area is 0.045, and the normal emissivity is given by

$$\epsilon_N = 0.045\epsilon + 0.955 \epsilon_c$$

where ϵ is the emissivity of the black paint and ϵ_c the normal emissivity of the cavity.

The value of ϵ_c can be calculated from the formula of Bauer and Bischoff (Section 7.1.2.2). The results are listed in Table 7.1-9; the paint emissivity is 0.92.

In the case of the in-flight target, the non-black temperature error is given by

$$\delta T = \frac{\delta M}{dM/dT}$$

where $dM/dT = 4.263 \times 10^{-5} \text{ Wcm}^{-2} \text{ K}^{-1}$ in Channel 3 and $1.859 \times 10^{-6} \text{ Wcm}^{-2} \text{ K}^{-1}$ in Channel 4 for a target at $T = 295\text{K}$. The apparent change in target radiance δM is given by

$$\delta M = (1 - \epsilon_N) F_{te} M_e - (1 - F_{ti}) M_t$$

Table 7.1-9 Normal Emissivities of the Internal
Inflight Calibration Target

ϵ	ϵ_c	ϵ_N
0.89	0.998 099	0.994 584
0.91	0.998 478	0.994 947
0.92	0.998 662	0.995 122
0.93	0.998 842	0.995 294

where F_{te} = view factor from target to earth = 0.21
 F_{ti} = view factor from target to instrument = 0.741
 M_e = infrared exitance of earth
 M_t = infrared exitance of the target and instrument

The view factors are taken from the thermal analysis of the instrument; they are the values when the instrument is viewing the internal target. As a worst case, we will assume the earth is at its minimum temperature of 185K.* Using the exitance values from Table 7.1-6 and the target emissivity of 0.995 122, we obtain

$$\delta T \text{ (Channel 3)} = -0.080K$$

$$\delta T \text{ (Channel 4)} = -0.029K$$

for the non-blackness errors in the inflight calibration at $T = 295K$.

7.1.3.3 Scattered Sunlight Error

Depending on its location on the spacecraft and the orbit normal to sun angle (β_s), the in-flight target may be exposed to direct sunlight during the nighttime portion of the orbit. The diffuse reflection of direct sunlight from the target can produce a significant error in the calibration of Channel 4; this subject is covered in Section 3.11.

* The corresponding exitance in Channel 4 is $1.944 \times 10^{-8} \text{ Wcm}^{-2}$.

8.0 THERMAL DESIGN

The thermal design of the AVHRR Instrument was described in Dir #38 on the pages which follow. The validity of the thermal design was established during Solar Simulation Tests performed at NASA/GSFC using the ETM.

The Thermal Interface Drawing for AVHRR is given in Figure 8-1 (page 8-19).



**AEROSPACE/OPTICAL
DIVISION**

3700 E. Pontiac Street
Fort Wayne, Ind. 46803
(219) 423-9636 - TWX 810-332-1413

To: R. H. Foote

From: J. D. Crawford, *JC*

Date: April 13, 1976

Subject: DIR #38 Final Thermal Model Analysis

CC: R. Annable, T. Diederich, C. Soest, J. Stark

Summary

The analysis of the AVHRR thermal model has been completed. This analysis has included orbit normal to sun angles of 0° , 28° , and 68° which correspond to the warmest, coolest, and extreme orbits. Worst case studies were made within each orbit with the warmest orbit being analyzed with maximum solar, earth IR and albedo inputs; surface finish maximum alpha and minimum ϵ ; and good attainable insulation blanket. The coolest orbit was the 68° orbit which was analyzed with minimum solar, earth IR and albedo inputs; surface finish minimum alpha and maximum ϵ and a not too good insulation blanket. Studies were made with the instrument electronics "on", "Off" and "off - with make-up heaters."

The radiating area of the baseplate, node 50, was trimmed to $.46 \text{ ft}^2$ resulting in an effective louver ϵ of $.44$ for the warmest nominal orbit. This same area resulted in an effective louver ϵ of between $.32$ and $.26$ for both the nominal 0° and 68° orbit. Worst case studies for the hot orbit indicated that the maximum louver ϵ would be $.45$; while the worst case study for the coldest orbit indicated that the louver effective ϵ would be $.16$.

Analysis of the worst case off instrument for heater size indicated that for the coldest orbit 22.8 watts were required to maintain an instrument baseplate temperature of 14.6°C .

Procedure

The thermal analysis for the TIROS-N AVHRR has been performed with the 100 node BAN program supported by view factor, projected area, flux calculations and summation programs. A preprocessor was also used to prepare the data formats for the view factor and projected area programs and also to be data for computer plots. A list of the nodal designations is included in Table I and Figures A and B show the relative node location.

The solar input and albedo inputs were calculated for 10° orbital steps throughout the 0° , 28° and 68° orbits. Those values were then summed and averaged to get the steady state orbital average value. The solar constant used was 429 B/h Ft^2 , the IR flux value was 75.15 B/hr Ft^2 and the albedo used was $.30$. Values for α and ϵ are listed in Table IIA and Table IIB and include the range of values expected for the listed materials and nodes. The values for the internal power are measured values and will not change 3-2 by any significant amount.

Conduction Couplings

All conductive couplings are calculated from dimensions taken from detail drawings. The value for the conductivity of the couplings is listed in Table III. Conductance through joints is used for all applicable joints and assumed to be a nominal 72 B/hr Ft².

Radiative Couplings

The radiative couplings were obtained from calculated and estimated view factors and calculated areas. Where the configuration was repetitive, a view factor calculation program was run to get the necessary factors; if a particular shape appeared only once, its value was estimated from a shape factor graph. Block F's were used in this simulation program. Since all of the internal emissivities were relatively high, a product was used rather than the effective emissivities.

Scan Mirror Modeling

The view factors for the scan mirror and cavity areas were obtained by calculating the view factors for ten mirror positions and averaging these values. Solar, albedo and Earth IR inputs to the scan cavity area were calculated with no mirror blockage and then 50% of the flux was assigned to the mirror (25% each to front and back) and 50% to the scan cavity area in question. While these assignments are rather arbitrary, they are better than assuming no mirror as in previous models.

Nominal Case Analysis

The AVHRR instrument was thermally designed to the nominal solar input and surface finish values of the 0, 28 and 68 degree orbits (orbit normal to sun angle). Active thermal control is maintained by using louvers to maintain a nominal IMP temperature of 15°C with an effective emissivity of between .26 and .45. This range of effective louver emissivity was obtained by using a silver teflon surface on the plus velocity electronics surface and trimming the base radiating area - node 50 - to .46 ft². All other exposed surfaces, except insulation surfaces, have black surfaces to minimize scattered light. The insulation surfaces consist of an aluminized Kapton outer layer with 10 layers of multilayer insulation.

Table IV is a listing of the nodal temperatures and emissivities for the nominal case orbits and a radiating area of 1.37 ft². In the 28° orbit the warmest instrument node temperature in the 15 volt regulator board which is 37°C and the remainder of the instrument temperatures range down to 7°C in the electronics baseplate area. The insulation blanket ranges from -99°C to 40°C. These temperatures are maintained with an effective emissivity through the louver of .44.

In the colder orbits (0° and 68°) the warmest electronic temperature is again the 15 volt regulator and the coolest temperature is 6°C in the electronic baseplate area. Two temperatures to note are the 57°C on the scan mirror when in the 0° orbit and the telescope temperature of 21°C when in the 68° orbit. The scan mirror scans through the sun each rotation and receives maximum solar illumination with no blockage. The temperature of the mirror will be reduced rapidly at about a 4° orbit angle due to S/C blockage. The telescope temperature changes very slowly the incidence angle and area change are offset by the increase in exposure time. Emissivity for the cold orbits is between .25 and .31.

Worst Case Analysis

The AVHRR instrument was modeled for the worst case hot and cold orbits using the radiation area established in the steady state run. Worst case is defined as the range of values that could be expected at launch - surfaces were not degraded by the space environment. The following list defines the worst case condition:

<u>Variable</u>	<u>Warmest</u>	<u>Coldest</u>
Emissivity	Minimum	Maximum
Solar Radiation	Maximum	Minimum
Absorbtivity	Maximum	Minimum
Earth IR	Maximum	Minimum
Albedo	Maximum	Minimum
Blanket Conductance	Best Expected	Worst Expected
Power	Nominal	Nominal

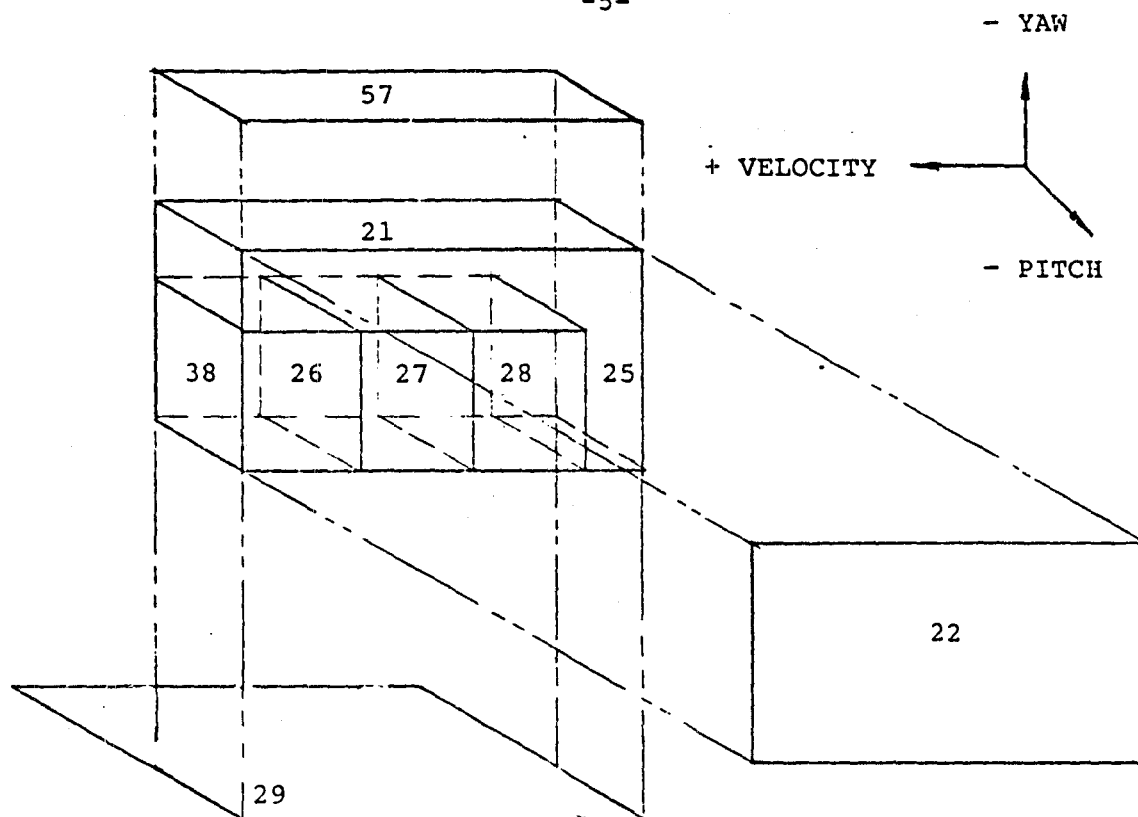
Simulations were run to determine if the worst case equivalent insulation conductance was the best or worst conductance. For the cold orbit the worst case is the worst expected blanket conductance, which leaks more heat to space, and the best expected blanket conductance in worst case for the warmest orbit, which leaks least heat to space. Table V lists the temperatures and emissivities for the worst case hot (28°) and cold (0° and 68°) orbits. The hot orbit ϵ is .05 below the maximum and the cold ϵ is .01 above the minimum.

Both the warmest and coldest nodes occur in the 0° degree orbit, the telescope receives no solar heating and the scan mirror is in the sun during the entire orbit with no S/C blackage. In the 68° degree orbit the scan mirror and scan cavity are the coldest nodes - running at 12°C .

Off Instrument Worst Case

When the instrument is turned off, make-up heaters must be turned on to maintain a baseplate temperature of 14°C. Table V. indicates the temperatures expected with 22.84 watts of heater power. Heaters rated at 15.8 and 7.0 watts are mounted on the baseplate and scan motor respectively. These heaters will maintain the scan mirror at 11°C and the telescope at 16°C.

-5-



23 CONNECTORS

24 HARNESS

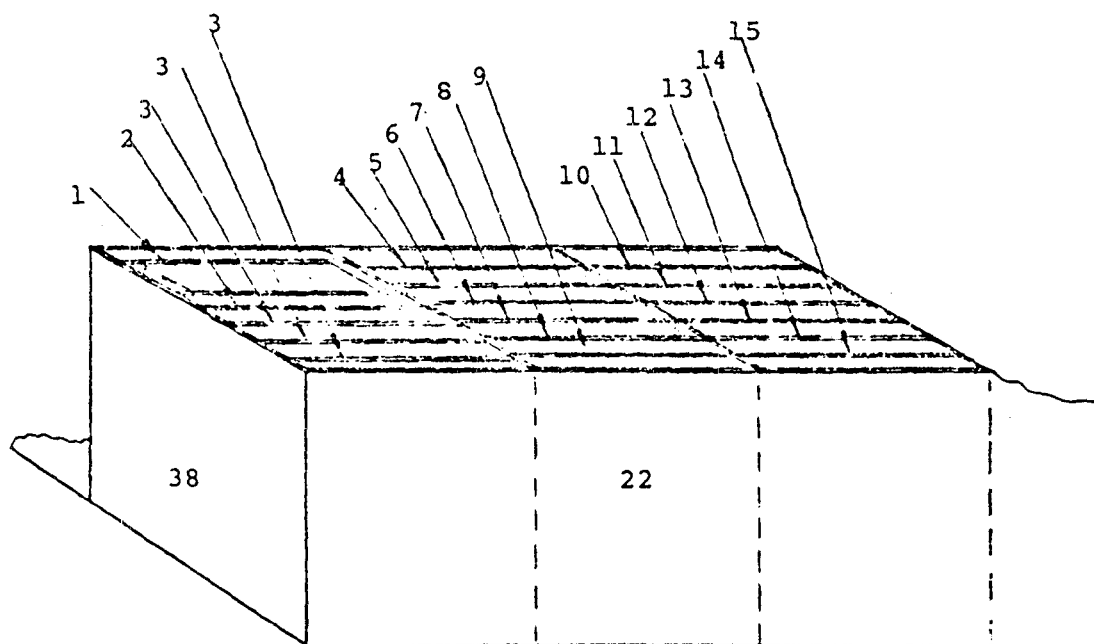


FIGURE A PICTORIAL NODE IDENTIFICATION - ELECTRONIC NODULE

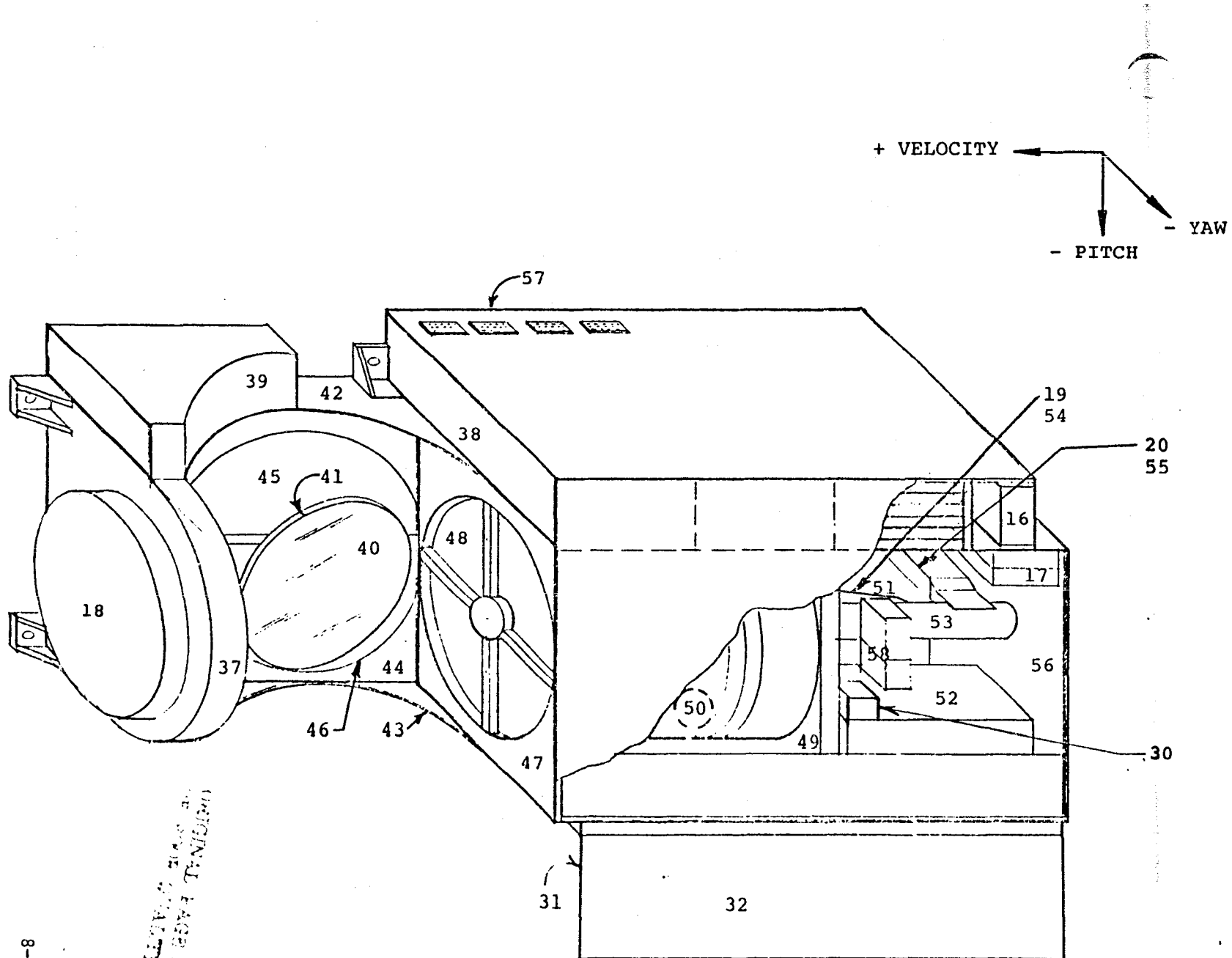


FIGURE B PICTORIAL NODE IDENTIFICATION - INSTRUMENT

<u>NODE NO.</u>	<u>NAME</u>	<u>MATERIAL</u>	<u>FINISH</u>
1	Power Converter	Nickel	None
2	+ -15V Regulator	P.C. Board	Solithane
3	Relay Bd 1 & 2 & 3	P.C. Board	Solithane
4	Patch Temp & TM	P.C. Board	Solithane
5	Telemetry #2	P.C. Board	Solithane
6	Aux Scan Logic	P.C. Board	Solithane
7	Scan Counter	P.C. Board	Solithane
8	Motor Logic	P.C. Board	Solithane
9	Black Body MUX	P.C. Board	Solithane
10	IR Post Amp	P.C. Board	Solithane
11	Daylight Post Amp	P.C. Board	Solithane
12	Ramp Calibration	P.C. Board	Solithane
13	Interface Logic #1	P.C. Board	Solithane
14	Interface Logic #2	P.C. Board	Solithane
15	Multiplexer	"	"
16	A/D Converter	P.C. Aluminum	Black Paint
17	Pre-Amplifier (vis)	Steel	Nickel
18	Scan Motor	Beryllium	Black Paint
19	Channel 1 Detector	Aluminum	Alodine
20	Channel 2 Detector	Aluminum	Alodine
21	Electronic Box, Anti-Sun	Magnesium	Dow 9
22	Electronic Box, Sun	Magnesium	Dow 9
23	Connector	Epoxy	Dow 9
24	Harness	Teflon	--
25	Electronic Box - Vel	Magnesium	Dow 9
26	Partition 1	Magnesium	Dow 9
27	Partition 2	Magnesium	Dow 9
28	Partition 3	Magnesium	Dow 9
29	Radiator 1	Magnesium	Dow 9
30	Pre-amplifier (IR)	Magnesium	Dow 9
31	Earth Shield, Specular	Aluminum	Specular
32	Earth Shield, Insul.	Mylar	Silver Teflon
33	Not Used		
34	Not Used		
35	Not Used		

TABLE 1 NODE IDENTIFICATION AND MATERIAL FOR THE AVHRR THERMAL MODEL

<u>NODE NO.</u>	<u>NAME</u>	<u>MATERIAL</u>	<u>FINISH</u>
36	Not Used		
37	Scan Motor Hsg	Aluminum	Alodine, Black Paint
38	Radiator, Electronics	Magnesium	Silver Teflon
39	Scan PS	Magnesium	Black Paint
40	Scan Mirror Front	Beryllium	Aluminum
41	Scan Mirror Rear	Beryllium	Gold
42	Cavity, Sun	Magnesium	Black Paint
43	Cavity, A-Sun	Aluminum	Black Paint
44	Base Cavity	Aluminum	Black Paint
45	Cal Target L	Aluminum	Black Paint
46	Cal Target S	Aluminum	Black Paint
47	Bulkhead, Tele	Aluminum	Black Paint
48	Telescope	Invar	Black Paint
49	Bulkhead, Center	Aluminum	Alodine
50	Base, Telescope	Aluminum	Alodine, Black Paint
51	Base, Optic	Aluminum	Alodine, Black Paint
52	Cooler Housing	Aluminum	Gold
53	Telescope Optics	Aluminum	Alodine
54	Channel 1 Relay	Aluminum	Alodine
55	Channel 2 Relay	Aluminum	Alodine
56	End, Optics	Magnesium	Dow 9
57	Cover, Electronics	Magnesium	Dow 9, Black Paint
58	L.W. Relay	Aluminum	Alodine
59	Insulation + Velocity	Mylar	None
60	Insulation Anti-Sun	Mylar	None
61	Insulation - Velocity	Mylar	None
62	Insulation, Sun	Mylar	None
63	Insulation, Nadir	Mylar	None
64	Spacecraft	--	--

TABLE 1 (Continued)

<u>T</u> <u>Surface</u>	Min $\frac{\alpha}{\text{Max}}$	Min $\frac{\epsilon}{\text{Max}}$
Silver Teflon (.005)	.06 - .12	.74 - .78
3 M Black Velvet	.94 - .98	.89 - .93
Black Honeycomb Target	.98	.99
Gold Plate	.32 - .36	.04 - .08
Aluminum Scan Mirror	.08 - .16	.04 - .05
Kapton-Aluminized (.003)	.43 - .47	.77 - .83

Table II A Values of Surface Finishes Used On
External Surfaces

<u>Surface</u>	<u>ε</u>
3 M Black Velvet	.91
Black Amodize	.85
Alodine	.85
Nickel Plating	.06
Deposited Aluminum	.05
Stainless Steel	.17
Teflon	.90
Solithane 113	.82

Table II B Value of Surface Finishes Used On
Internal Surfaces

<u>Material</u>	<u>Thermal Conductivity B/hr-in-F^o</u>
Aluminum	10.65
Stainless Steel	.572
Invar	.517
Synthane G-10	.015
Fused Silica	.067
Beryllium	7.04
Copper	18.92
Magnesium	7.48
Heat Conductive Epoxy	.074

Table III Thermal Conductivity Values For
Materials Used in the AVHRR Instrument

TABLE IV NODAL TEMPERATURES FOR AVHRR/1 INSTRUMENT ON,
15°C CONTROL POINT, NOMINAL SURFACE FINISHES

	<u>28°</u>	<u>68°</u>	<u>0°</u>
1	28.87	28.52	28.24
2	36.95	36.69	36.40
3	24.90	24.59	24.29
4	22.60	22.19	21.97
5	24.36	24.12	23.85
6	26.63	26.45	26.17
7	25.56	25.40	25.11
8	26.85	26.68	26.40
9	23.03	22.80	22.55
10	27.84	27.44	27.23
11	31.27	31.04	30.79
12	28.68	28.50	28.22
13	25.90	25.73	25.44
14	26.16	25.98	25.70
15	27.02	26.80	26.55
16	28.58	28.28	28.00
17	22.73	22.06	21.96
18	20.66	15.08	23.31
19	22.71	20.65	18.62
20	22.65	20.60	18.58
21	18.68	17.81	17.73
22	20.55	20.17	19.99
23	22.52	23.16	22.60
24	16.94	18.96	17.93
25	22.60	22.35	22.08
26	21.27	20.75	20.58
27	21.09	20.58	20.41
28	20.70	20.15	20.00
29	18.32	17.29	17.18
30	18.58	17.54	17.43
31	18.01	16.95	16.78
32	18.02	16.95	16.79
33	18.32	17.29	17.18
34	18.32	17.29	17.18
35	18.33	17.30	17.18
36	18.33	17.30	17.18
37	20.13	14.65	22.24
38	18.22	17.91	17.41
39	18.99	14.01	17.96
40	25.86	14.98	57.30
41	25.86	14.98	57.27
42	18.24	14.02	17.69
43	17.53	13.25	17.11
44	17.72	13.33	17.17
45	17.65	13.06	16.88
46	18.05	13.14	17.38
47	16.88	14.35	15.87
48	28.75	21.04	10.79
49	17.42	16.45	16.36
50	16.43	15.30	15.74
51	16.20	15.73	15.62
52	17.55	16.40	16.16
53	20.76	18.57	16.35
54	21.04	18.93	16.84
55	21.04	18.93	16.83
56	17.73	16.91	16.71
57	7.61	12.44	10.47
58	20.26	18.32	16.53
59	-13.38	-9.19	-66.86
60	-99.11	-93.95	-102.57
61	-54.06	-49.20	-60.05
62	-39.46	-21.43	-34.44
63	-58.92	-51.19	-88.07
64	-269.44	-269.44	-269.44

ε .44 .26 .32

LOWER RADIATING AREA 1.37 ft.²

TABLE V NODAL TEMPERATURES FOR AVHRR/1 INSTRUMENT ON 15°C CONTROL POINT,
WORST CASE HOT AND COLD AND INSTRUMENT OFF WITH HEATERS

HOT ORBIT
28°

COLD ORBIT
68°

COLD ORBIT OFF WITH HEATERS
68°

N	CENT.
1	28.6
2	36.7
3	24.6
4	22.3
5	24.0
6	26.3
7	25.2
8	26.5
9	22.7
10	27.6
11	31.0
12	28.3
13	25.5
14	25.8
15	26.7
16	28.1
17	22.6
18	22.2
19	22.8
20	22.8
21	18.5
22	20.3
23	22.0
24	16.1
25	22.1
26	21.0
27	20.8
28	20.5
29	17.9
30	16.8
31	17.7
32	17.7
33	17.9
34	17.9
35	17.9
36	17.9
37	21.6
38	18.0
39	20.1
40	29.8
41	29.8
42	19.1
43	18.4
44	18.6
45	18.5
46	18.9
47	17.2
48	30.3
49	17.3
50	16.5
51	16.1
52	17.4
53	20.9
54	21.2
55	21.2
56	17.6
57	6.1
58	20.3
59	3.2
60	-97.8
61	-50.2
62	48.1
63	-52.5
64	-269.4

N	CENT.
1	27.9
2	36.1
3	23.9
4	21.6
5	23.6
6	25.9
7	24.9
8	26.2
9	22.2
10	26.9
11	30.5
12	28.0
13	25.2
14	25.4
15	26.2
16	27.5
17	21.5
18	13.8
19	19.7
20	19.6
21	17.1
22	19.4
23	23.1
24	19.7
25	21.6
26	20.1
27	19.9
28	19.4
29	16.1
30	15.1
31	15.9
32	15.9
33	16.1
34	16.1
35	16.1
36	16.1
37	13.4
38	17.2
39	12.9
40	12.5
41	12.5
42	13.0
43	12.1
44	12.3
45	12.0
46	12.1
47	13.5
48	19.2
49	15.7
50	14.7
51	15.3
52	15.6
53	17.6
54	17.9
55	17.9
56	16.1
57	14.7
58	17.3
59	3.4
60	-91.5
61	-46.4
62	-11.2
63	-52.7
64	-269.4

N	CENT.
1	10.5
2	10.2
3	10.2
4	11.1
5	10.7
6	10.6
7	10.6
8	10.5
9	10.4
10	11.1
11	10.8
12	10.6
13	10.6
14	10.5
15	10.5
16	10.8
17	12.4
18	12.5
19	13.0
20	13.0
21	12.0
22	10.2
23	9.7
24	8.4
25	10.6
26	10.9
27	10.9
28	11.0
29	11.7
30	10.9
31	12.3
32	12.3
33	11.7
34	11.7
35	11.7
36	11.7
37	12.1
38	9.0
39	11.0
40	11.3
41	11.3
42	11.2
43	10.8
44	11.1
45	10.8
46	10.9
47	11.9
48	16.4
49	12.9
50	14.6
51	12.7
52	13.1
53	13.1
54	13.1
55	13.1
56	11.9
57	6.0
58	12.9
59	2.2
60	-91.6
61	-47.3
62	-12.3
63	-53.0
64	-269.4

$\epsilon = .45$

$\epsilon = .16$

$\epsilon = .15$

8-14



**AEROSPACE/OPTICAL
DIVISION**

**3700 E. Pontiac Street
Fort Wayne, Ind. 46803
(219) 423-9636 - TWX 810-332-1413**

To: R. H. Foote
From: J. D. Crawford *JC*
Subject: Revised Answers to MDR Question 15

Date: May 6, 1976
Revised: May 10, 1976

Attached are Tables 1 and 2 which list the solar and earth inputs for the external nodes. Table 3 lists the radiant outputs for the external nodes. These values have been updated to the thermal runs dated 4/7/76.

/am

Attachment

Node Number	Description	NOMINAL 0° ORBIT BTU/HR			NOMINAL 28° ORBIT BTU/HR			NOMINAL 68° ORBIT BTU/HR		
		ER	ERTH	ALB	ER	ERTH	ALB	ER	ERTH	ALB
37	Scan Motor Housing	.0	2.6	.2	3.6	2.6	.8	.1	2.6	1.3
38	Radiator Electronics	.0	2.9	.2	11.3	2.9	1.1	14.8	2.9	1.6
39	Scan Power Supply	.0	2.6	.3	3.5	2.6	1.1	.3	2.6	2.2
40	Scan Mirror Front	61.4	7.2	.5	10.7	7.2	1.9	.1	7.2	3.1
41	Scan Mirror Rear	61.4	7.2	.6	10.7	7.2	1.9	.1	7.2	3.1
42	Cavity, Sun	.0	.4	.1	.0	.4	.1	.0	.4	.2
43	Cavity Anti-Sun	.6	.0	.0	1.5	.0	.0	.2	.0	.0
44	Base Cavity	.0	.0	.0	.0	0.0	.0	.0	.0	.0
45	Cal Target, Large	.0	5.3	.4	3.6	5.3	1.5	.1	5.3	2.6
46	Cal Target, Small	.6	4.0	.3	8.9	4.0	.8	.0	4.0	1.2
47	Bulkhead, Telescope	.0	2.2	.2	3.1	2.2	.6	.0	2.2	1.1
48	Telescope	.0	5.9	.4	21.2	5.9	1.5	11.2	5.9	2.7
59	Insulation + Velocity	.0	8.8	.7	39.8	8.8	1.4	41.4	8.8	4.5
60	Insulation Anti-Sun	.0	7.9	.0	0.0	7.9	1.9	.1	7.9	5.1
61	Insulation - Velocity	.0	12.9	1.0	1.0	12.9	3.4	.9	12.9	6.5
62	Insulation, Sun	143.6	17.6	4.1	153.2	17.6	6.8	34.3	17.6	10.0
63	Insulation, Nadir		28.9	7.3	36.5	29.0	26.1	31.1	29.0	50.3

TABLE 1

SOLAR AND EARTH INPUTS FOR THE AVHRR/1 EXTERNAL NODES, NOMINAL SURFACES FINISHES

Node Number	Description	WORST CASE CC 68° ORBIT BTU/HR			WORST CASE HOT 28° ORBIT BTU/HR		
		ER	ERTH	ALB	ER	ERTH	ALB
37	Scan Motor Housing	.1	2.5	.9	3.8	2.7	1.0
38	Radiator Electronics	14.4	2.8	1.5	11.9	3.0	1.1
39	Scan Power Supply	.3	2.5	2.0	3.7	2.6	1.2
40	Scan Mirror Front	.1	7.0	2.5	11.3	7.4	2.2
41	Scan Mirror Rear	.1	7.0	2.5	11.3	7.4	2.2
42	Cavity, Sun	.0	.3	.1	.0	.4	.2
43	Cavity Anti-Sun	.2	.0	.0	1.6	.0	.0
44	Base Cavity	.0	.0	.0	.0	.0	.0
45	Cal Target, Large	.1	5.1	2.3	3.7	5.4	1.6
46	Cal Target, Small	.0	3.9	1.1	9.4	4.1	.8
47	Bulkhead, Telescope	.0	2.1	1.0	3.3	2.2	.6
48	Telescope	10.7	5.8	2.4	22.2	6.1	1.7
59	Insulation + Velocity	56.0	8.6	4.2	41.8	9.1	1.5
60	Insulation Anti-Sun	.1	7.7	4.8	.0	8.2	2.1
61	Insulation - Velocity	.9	12.5	6.1	1.1	13.3	3.6
62	Insulation, Sun	51.7	17.1	9.4	160.7	18.1	7.2
63	Insulation, Nadir	29.7	28.1	47.0	38.3	29.8	27.8

TABLE 2

SOLAR AND EARTH INPUTS FOR THE AVHRR/1 EXTERNAL NODES, HOT AND COLD CASES

Revised May 10, 1976

Node Number	Description	NOMINAL SUR. FINISHES			WORST CASE		OFF 22.8 WATT HEATERS WATTS
		QROUT 0° ORBIT WATTS	QROUT 28° ORBIT WATTS	QROUT 68° ORBIT WATTS	QROUT HOT WATTS	QROUT COLD WATTS	
37	Scan Motor Housing	4.3	4.1	3.8	4.1	3.8	3.7
38	Radiator Electronics	3.4	3.4	3.4	3.4	3.5	3.1
39	Scan Power Supply	1.8	1.9	1.7	1.8	1.7	1.7
40	Scan Mirror Front	.5	.3	.3	.3	.3	.3
41	Scan Mirror Rear	.9	.6	.5	.4	.6	.6
42	Cavity, Sun	.5	.5	.5	.5	.5	.5
43	Cavity Anti-Sun	.7	.7	.7	.7	.7	.7
44	Base Cavity	1.4	1.4	1.3	1.4	1.3	1.3
45	Cal Target, Large	4.2	4.2	3.9	4.3	3.9	3.8
46	Cal Target, Small	2.2	2.2	2.1	2.2	2.0	2.0
47	Bulkhead, Telescope	3.3	3.3	3.2	3.2	3.2	3.1
48	Telescope	3.7	4.7	4.2	4.6	4.2	4.0
44)	LOUVERS	14.3	19.8	11.7	20.0	7.4	6.5
50)							
51)							
ε	EFFECTIVE ε OF LOUVERS	.32	.44	.26	.45	.16	.15

TABLE 3

RADIANT OUTPUTS FOR THE AVHRR/1 EXTERNAL NODES, NOMINAL AND WORST CASES

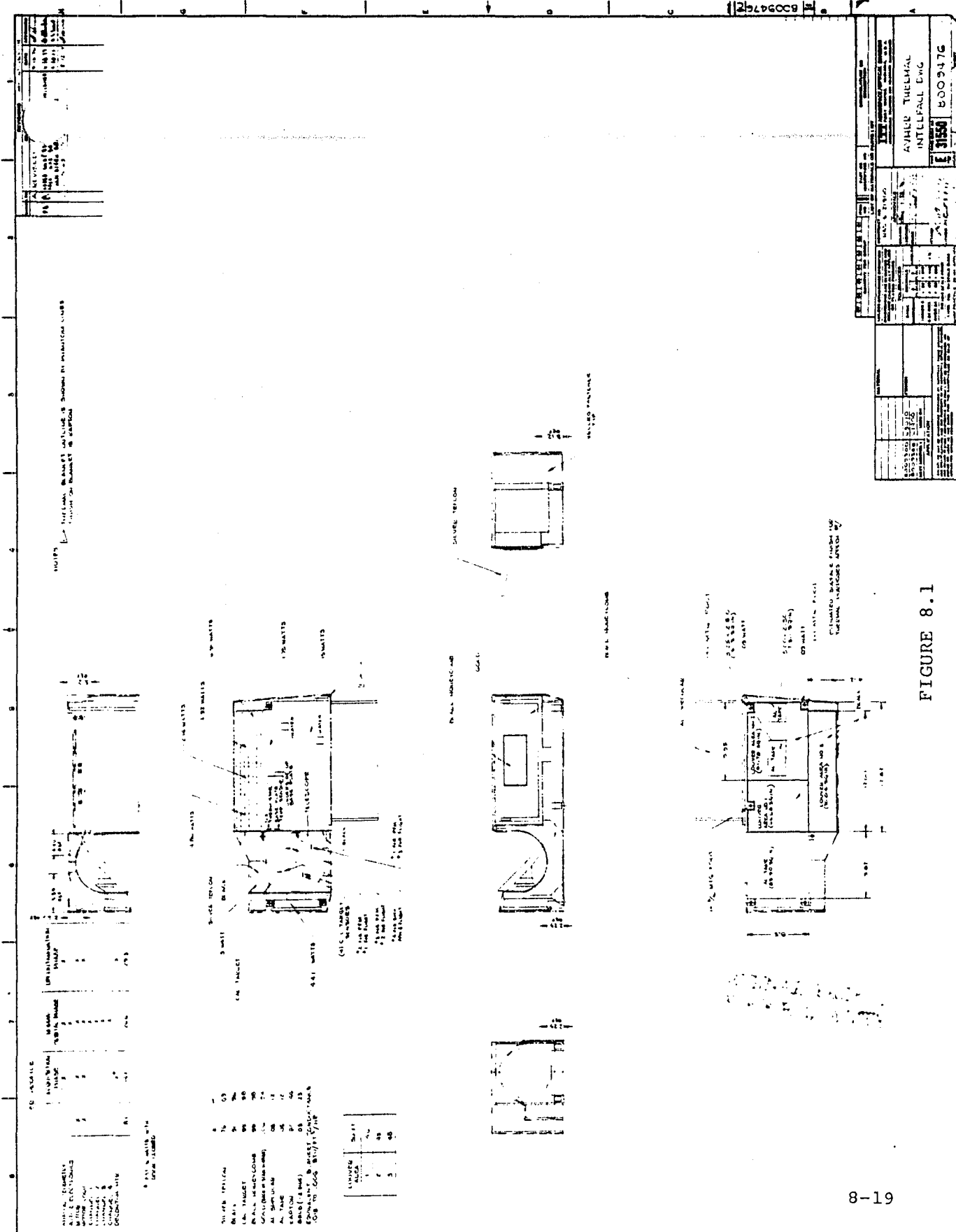


FIGURE 8.1

9.0 TEST AND CALIBRATION DATA

Summaries of the test results for Instruments SN101, SN102, SN103 and SN104 are given in the following pages.

For detailed test results and calibration data, refer to:

Alignment and Calibration Data Book, AVHRR/1-FM101

Alignment and Calibration Data Book, AVHRR/1-FM102

Alignment and Calibration Data Book, AVHRR/1-FM103

Alignment and Calibration Data Book, AVHRR/1-FM104

SUMMARY OF
TEST RESULTS
FOR SN101

FM101 AVHRR TEST RESULTS

<u>ITEM</u>	<u>SPEC LEVELS</u>	<u>MEASURED</u>
SIZE	MAX. 31" x 11" x 15"	EXCLUDING THERMAL BLANKET 29.94" x 9.75" x 14.062"
WEIGHT	60 LB. MAX	59.094 LB.
ACCELERATION	NO TEST ON FM	NA
POWER	27 WATTS	24.78 WATTS
VIBRATION	SEE SPEC. PARA. 4,4,4,3	PASSED 3RD VIBRATION PROBLEMS COVERED BY MFR'S
ACOUSTICS	NO TEST ON FM	NA
JITTER	± 17 μ SEC/98%	100% AT 15 ⁰ BASEPLATE

CENTER OF GRAVITY	DOOR OPEN	DOOR CLOSE
X	5.097	5.187
Y	15.26	15.26
Z	6.959	7.047

FM101 AVHRR TEST RESULTS

PARAMETER	SPECIFICATION	MEASURED
CHAN 1 & 2 SIGNAL STABILITY	± 100 MV OVER TEMP. RANGE 10°C TO 30°C	CHAN #1 = 77 CHAN #2 = 118
CHAN 1 & 2 SPECTRAL RESPONSE	SEE PARA. 3.4.2 OF SPEC	CHAN #1 ALL OKAY CHAN #2 OUT OF SPEC
THERMAL CHAN. NEAT	≤ 0.12 K @ 300K	CHAN 3 .05(B.P. 15°C) CHAN 4 .06(B.P. 15°C)
CHAN 3 & 4 SIGNAL STABILITY	± 100 mv OVER TEMP RANGE 10°C TO 30°C	CHAN 3 CH 4 113 mv 42 mv
CHAN 3 & 4 SPECTRAL RESPONSE	SEE PARA 3.4.2 OF SPEC.	CHAN 3 ALL OKAY CHAN 4 ALL OKAY
SCAN JITTER	98% WITHIN \pm 17 SEC (1/2 IFOV)	SCENE - 99% LINE - 98%
SCAN LINEARITY	LINE TO LINE: $\pm 1/2$ IFOV (98%) 20 MINUTES: ± 1 IFOV (98%)	< 1/2 IFOV < 1 IFOV

FM101 AVHRR TEST RESULTS

<u>PARAMETER</u>	<u>SPECIFICATION</u>	<u>MEASURED</u>
IFOV Size to 50% Points	1.3 ± 0.2 MILLIRADIANS	SCAN CROSS SCAN
		CH 1 1.32 CH 1 1.33
		CH 2 1.32 CH 2 1.29
		CH 3 1.13 CH 3 1.31
		CH 4 1.24 CH 4 1.30
CHANNEL REGISTRATION	ALL CENTERS WITHIN 0.10 MRAD	INITIALLY ≤ 0.08 MRAD
		AFTER VIB ≤ 0.08 MRAD
SYSTEM MTF	30% AT LIMITING FREQ	CH 1: 47% CH 3: 53%
		CH 2: 53% CH 4: 53%
S/N RATIO SOLAR CHANNELS	10.0 MVOLTS NOISE 3/1 @ .5% ALBEDO	CHAN 1: 1.98 MVOLTS
		CHAN 2: 2.90 MVOLTS

C-2

AVHRR TEST RESULTS

<u>PARAMETER</u>	<u>SPECIFICATION</u>	<u>MEASURED</u>	
		CH 1	CH 2
SIGNAL AMPLITUDE CH 1 & CH 2	CH 1 = $5.012 \pm .100$	5.051	5.671
	CH 2 = $5.674 \pm .100$		
	SPACE LOOK = $.25 \pm .05$.229	.236
SIGNAL AMPLITUDE CH 3 & CH 4	$320 \pm 1^{\circ}\text{K} = 0.3 \pm .1\text{V}$.767	.762
	SPACE LOOK = $6.2 \pm .05\text{V}$	6.207	6.203

ITEM	SPEC	MEASURED
COMMAND OPERATION		OPERATION AND DIGITAL TM LEVEL VERIFIED
ANALOG TM		INSTRUMENT STATUS MEASURED
TURN ON TRANSIENT (28V)		
ELECTRONICS	1.4A MAX. @ 20 MA/μSEC	690 MA - 2.8 MA/μSEC.
MOTOR	1.4A MAX. @ 20 MA/μSEC	680 MS - .33 MA/μSEC
COOLER HEAT	3.3A MAX. FOR 2 M.S.	2.4A FOR 500 μSEC
EARTH SHIELD	2.1A MAX. FOR 1 SEC	1.7 FOR .6 SEC
CONDUCTED RIPPLE (28V)		
MOTOR - LOW	9 MA P - P	7 MA P - P
MOTOR - HIGH	9 MA P - P	6 MA P - P
ELECT. & ALL CH'S)	20 Hz 3% (27 MA)	<20 Hz - 20 MA/>20 Hz - 2 MA
FULL INST.)	20 Hz 1% (9 MA)	<20 Hz - 20 MA/>20 Hz - 4 MA
SUSCEPTIBILITY	.25 VPP TO 1.5 KHZ .50 VP TO P TO 10 MHZ	WORST CASE .28V @ 1 KHZ
CONDUCTED RIPPLE(+10V)	1 MA MAX.	NONE - DISCERNIBLE
CONDUCTED RIPPLE (+5V)	1 MA MAX.	NONE - DISCERNIBLE

ITEM	SPEC	MEASURED
OVER-VOLTAGE	28V TO 39V	± 15 V REGULATED VOLTAGES VARY 3 MV - +5 V SUPPLY VARIES 46 MV.
AMPLIFIER ZEROING	CH 1 .250 ± 0.050 CH 2 .250 ± 0.050 CH 3 6.2 ± 0.50 CH 4 6.2 ± 0.50	228.18 MV 237.50 MV 6201.36 MV 6206.8 MV
AMPLIFIER LINEARITY	± 6.25 MV (±DATA CONV.)	CH 1 - 4.0 MV MEASURE WITH CH 2 - 2.5 MV RAMP CAL AND CH 3 - 6.3 MV DATA CONVERTER CH 4 - 12.0 MV
RAMP CAL RANGE	0.025 TO +6.475	CH 1 6502 SWING CH 2 6492 SWING CH 3 6552 SWING CH 4 6460 SWING

ITEM	SPEC	MEASURED				
AMPLIFIER DROOP	.39% OF FULL SCALE (25 MV)	CH 1	13 MV			
		CH 2	4 MV			
		CH 3	.5 MV			
		CH 4	1 MV			
VERIFICATION OF TM IN DATA STREAM	--		<u>TM</u>	<u>DATA</u>		
		BB1	2.388	2.391		
		BB2	2.413	2.413		
		BB3	2.392	2.393		
		BB4	2.415	2.422		
		PATCH				
		TEMP	3.369	3.372		
BB SAMPLE TM	--		<u>TM</u>	<u>DATA</u>		
		CH 3	2.494	2.490		
		CH 4	4.419	4.419		
VOLTAGE CAL VERIFICATION	3 EARTH SCENE LEVELS 1 B.B. LEVEL DETECTOR DISABLED		1	2	3	4
		CH 1	1.856	3.481	5.106	5.916
		CH 2	1.844	3.473	5.092	5.912
		CH 3	1.256	2.898	4.537	0.442
		CH 4	1.367	2.987	4.600	0.560
		VERIFIED DET. DIS.				

ITEM	SPEC	MEASURED
AUXILIARY SCAN	NONE	VERIFIED

CALIBRATION EQUATIONS

RADIATOR TEMP	$^{\circ}\text{K}$	=	34.97	+	143.8	
PATCH POWER	MW	=	$2V^2$			
PATCH TEMP LOW RANGE	$^{\circ}\text{K}$	=	5.14V	+	91.9	
PATCH TEMP EX RANGE	$^{\circ}\text{K}$	=	44.92V	+	94.7	
BB#1 TM	$^{\circ}\text{C}$	=	$.0349V^2$	+	8.204V	+ 3.499
BB#2 TM	$^{\circ}\text{C}$	=	$.0349V^2$	+	8.204V	+ 3.499
BB#3 TM	$^{\circ}\text{C}$	=	$.0349V^2$	+	8.204V	+ 3.499
BB#4 TM	$^{\circ}\text{C}$	=	$.0349V^2$	+	8.204V	+ 3.499
MOTOR CURRENT	MA	=	60V			
ELECTRONICS CURRENT	MA	=	191V			
EARTH SHIELD POSITION		=	($<2V$)	CL	(2-4)MID	$>\Delta$ OPEN
ELECTRONICS TEMP	$^{\circ}\text{C}$	=	-5.82V	+	39.9	
BASE PLATE TEMP	$^{\circ}\text{C}$	=	-7.75V	+	34.8	
A TO D TEMP	$^{\circ}\text{C}$	=	-8.33V	+	86.16	
MOTOR HOUSING TEMP	$^{\circ}\text{C}$	=	-7.75V	+	34.8	
COOLER HOUSING TEMP	$^{\circ}\text{C}$	=	-7.75V	+	34.8	
DETECTOR BIAS VOLTS		=	4.33V	-	21.33	
BB IR CH3	$^{\circ}\text{C}$	=	$58.15 - .1972V^3$	$14.51V - .1383V^2 + .01118V^4$		
BB IR CH4	$^{\circ}\text{C}$	=	$48.35 + 1.0396V^3 - .1141V^4$	$.4809V - 3.953V^2$		
OFFSET VOLTAGE	TM	=	1.33V			

SUMMARY OF
TEST RESULTS
FOR SN102

FM 102 TEST RESULTS

<u>ITEM</u>	<u>MEASURED</u>												
SIZE	x y z 9.72" x 30.19" x 14.12"												
WEIGHT - INSTRUMENT	58.95 lbs.												
THERMAL BLANKET	ADD 17 oz.												
POWER	25.00 WATTS												
VIBRATION	MR E03426, MR E03427, MR E03428												
JITTER	>98% 10-30° BASEPLATE												
CENTER OF GRAVITY	<table><tr><th></th><th>DOOR OPEN</th><th>DOOR CLOSED</th></tr><tr><td>x</td><td>4.643"</td><td>4.597"</td></tr><tr><td>y</td><td>12.980"</td><td>12.980"</td></tr><tr><td>z</td><td>1.360"</td><td>1.470"</td></tr></table>		DOOR OPEN	DOOR CLOSED	x	4.643"	4.597"	y	12.980"	12.980"	z	1.360"	1.470"
	DOOR OPEN	DOOR CLOSED											
x	4.643"	4.597"											
y	12.980"	12.980"											
z	1.360"	1.470"											
CH 1 & 2 SIGNAL STABILITY	10°C - 30°C BASEPLATE												
	CH 1 20 mv												
	CH 2 169 mv												
CH 1 & 2 SPECTRAL RESPONSE	SEE DATA												
THERMAL CHANNEL NEAT	CH 3 = .038 Degrees Kelvin @ 300K° CH 4 = .047 Degrees Kelvin @ 300K°												
CH 3 & 4 SIGNAL STABILITY	CH 3 (10°-20°C) 108 mv CH 4 (10°-20°C) 98 mv												
CH 3 & 4 SPECTRAL RESPONSE	SEE DATA												
SCAN LINE NONLINEARITY	12.5 usec												
I FOV	CH 1 1.36mr (S) 1.36mr (XS) 2 1.34 1.36 3 1.36 1.11 4 1.21 1.19												
4 CHANNEL REGISTRATION	0.032 Milliradian												

COOLER MARGIN

11.9K @ 15C Baseplate

	<u>SCAN</u>	<u>XSCAN</u>
SYSTEM MTF	CH 1 48.4%	45.5%
	2 47.5%	47.0%
	3 50.0%	46.0%
	4 57.1%	57.3%
SOLAR CH NOISE (10mv = 3:1 S/N @ 0.5% Albedo)	0.243 mv CH 1	0.483 mv CH 2
SIGNAL AMPLITUDE		
CH 1 & CH 2	CH 1 5.038V (81% Albedo)	0.250V
	CH 2 5.650V (91% Albedo)	0.267V
CH 3 & CH 4	CH 3 0.300V (320K)	6.207V
	CH 4 0.300V (320K)	6.210V
COMMAND OPERATION	INSTRUMENT RESPONSE AND DIGITAL TELEMETRY LEVELS VERIFIED.	
ANALOG TM	INSTRUMENT STATUS MEASURED, VOLTAGES CORRESPOND TO INSTRUMENT CONDITION.	
TURN ON TRANSIENTS	ELEC ON	5.7 ma/μsec
	MTR ON	0.37 ma/μsec
	COOLER HTR	2.75 amp/700μsec
	EARTH SHIELD	1.25A/10 ms
CONDUCTED RIPPLE (28v)	MTR (L)	3 ma P/P
	MTR (H)	5 ma P/P
	ELEC AND ALL CHs	11 ma
	FULL INSTR.	22 ma
SUSCEPTIBILITY (Input on buss at which Channel 4 shows excess noise.)	OK CH 4 has 9.7 mv Noise for >0.72V @ 15.3KHz	
CONDUCTED RIPPLE +10V	NONE DISCERNIBLE	
+ 5V	None DISCERNIBLE	
OVERVOLTAGE (Internal supply change for a 39V buss.)	<u>Voltage</u>	<u>Change</u>
	+15V	0 mv
	+ 5V	30 mv

AMPLIFIER ZEROING

CH 1	0.250V
2	0.267V
3	6.207V
4	6.211V

SYSTEM DATA CHANNEL LINEARITY Spec = ± 12.5 mv

CH 1	7 mv
2	4 mv
3	8 mv
4	4 mv

RAMP CAL RANGE

(3/4 - 1/4) Level Spec
= 3.25 ± 50 mv

	<u>1/4</u>	<u>1/2</u>	<u>3/4</u>	<u>(3/4 - 1/4)</u>
CH 1	1.595	3.219	4.839	3.244
2	1.619	3.244	4.870	3.251
3	1.630	3.254	4.863	3.233
4	1.609	3.241	4.858	3.259

AMPLIFIER DROOP

CH 1	2 mv	CH 3	0 mv
2	1 mv	4	3 mv

VERIFICATION OF TM IN DATA STREAM

	<u>TM</u>	<u>DATA</u>
BB 1	1.310	1.306
2	1.358	1.356
3	1.255	1.256
4	1.314	1.313

PATCH

2.647	2.649
-------	-------

BB SAMPLE

3	2.383	2.386
4	4.647	4.656

VOLTAGE CAL VERIFICATION

	<u>1/4</u>	<u>1/2</u>	<u>3/4</u>	<u>B.B.</u>
CH 1	1.862	3.487	5.112	5.920
2	1.887	3.518	5.143	5.956
3	1.368	2.982	4.606	0.556
4	1.332	2.962	4.587	0.525

(Internal BB Level $\xrightarrow{\uparrow}$)

AUX SCAN

VERIFIED

COHERENT NOISE

NONE OBSERVED

INSTRUMENT CALIBRATION

SEE DATA SHEETS

FM 102

CALIBRATION EQUATIONS

RADIATOR TEMP	$^{\circ}\text{K}$	=	34.97V	+	143.8
PATCH POWER	MW	=	$2V^2$		
PATCH TEMP LOW RANGE	$^{\circ}\text{K}$	=	5.16V	+	91.25
PATCH TEMP EX RANGE	$^{\circ}\text{K}$	=	$1.96V^2$	+	34.8V + 94.6
BB#1 TM	$^{\circ}\text{C}$	=	$.0349V^2$	+	8.204V + 3.499
BB#2 TM	$^{\circ}\text{C}$	=	$.0349V^2$	+	8.204V + 3.499
BB#3 TM	$^{\circ}\text{C}$	=	$.0349V^2$	+	8.204V + 3.499
BB#4 TM	$^{\circ}\text{C}$	=	$.0349V^2$	+	8.204V + 3.499
MOTOR CURRENT	mA	=	60V		
ELECTRONICS CURRENT	mA	=	191V		
EARTH SHIELD POSITION		=	(<2V) CL (2-4) MID >Δ OPEN		
ELECTRONICS TEMP	$^{\circ}\text{C}$	=	-5.82V	+	39.9
BASEPLATE TEMP	$^{\circ}\text{C}$	=	-7.75V	+	34.8
A TO D TEMP	$^{\circ}\text{C}$	=	-8.33V	+	86.16
MOTOR HOUSING TEMP	$^{\circ}\text{C}$	=	-7.75V	+	34.8
COOLER HOUSING TEMP	$^{\circ}\text{C}$	=	-7.75V	+	34.8
DETECTOR BIAS VOLTS		=	4.33V	-	21.33
BB IR CH 3	$^{\circ}\text{C}$	=	58.15 -	14.51V -	$.1383V^2$ -
			$.1972V^3$	+	$.01118V^4$
BB IR CH 4	$^{\circ}\text{C}$	=	48.35 +	$.4809V$ -	$3.953V^2$ +
			$1.0396V^3$	-	$.1141V^4$
REFERENCE (OFFSET) VOLTAGE		=	1.33V		

SUMMARY OF
TEST RESULTS
FOR SN103

FM 103 TEST RESULTS

<u>ITEM</u>	<u>MEASURED</u>														
SIZE	<u>x</u>	<u>y</u>	<u>z</u>												
	9.72" x	30.19" x	14.12"												
WEIGHT - INSTRUMENT	58.75 lbs.														
THERMAL BLANKET	ADD 17 oz.														
ACCELERATION	NA														
POWER	24.78 WATTS														
VIBRATION	OK; EXCEPT MR 3421														
ACOUSTICS	NA														
JITTER	100% \pm 17.2 μ sec														
CENTER OF GRAVITY	<table><tr><th></th><th>DOOR OPEN</th><th>DOOR CLOSED</th></tr><tr><td>x</td><td>4.637 "</td><td>4.549 "</td></tr><tr><td>y</td><td>12.921 "</td><td>12.921 "</td></tr><tr><td>z</td><td>1.303 "</td><td>1.387 "</td></tr></table>				DOOR OPEN	DOOR CLOSED	x	4.637 "	4.549 "	y	12.921 "	12.921 "	z	1.303 "	1.387 "
	DOOR OPEN	DOOR CLOSED													
x	4.637 "	4.549 "													
y	12.921 "	12.921 "													
z	1.303 "	1.387 "													
CH 1 & 2 SIGNAL STABILITY	10 $^{\circ}$ C - 30 $^{\circ}$ C		change												
	CH 1	171 mv													
	CH 2	314 mv													
CH 1 & 2 SPECTRAL RESPONSE	SEE DATA														
THERMAL CHANNEL NEAT	CH 3 = .06 Degrees Cent.														
	CH 4 = .04 Degrees Cent.														
CH 3 & 4 SIGNAL STABILITY	CH 3 (10 $^{\circ}$ -20 $^{\circ}$ C)	80 mv													
	CH 4 (10 $^{\circ}$ -20 $^{\circ}$ C)	100 mv													
CH 3 & 4 SPECTRAL RESPONSE	SEE DATA														
SCAN LINEARITY	20MIN	24 μ sec	98%												
IFOV	CH 1	1.31mr (S)	1.31 mr (XS)												
	2	1.25	1.25												
	3	1.32	1.22												
	4	1.24	1.25												
CHANNEL REGISTRATION	CH3/CH4	0.108 mr.													
	SEE MR 3421														

	<u>SCAN</u>	<u>XSCAN</u>
SYSTEM MTF	CH 1 49%	51%
	2 50%	50%
	3 46%	60%
	4 49%	51%
SOLAR CH NOISE	9.8 mv CH 1	7.3 mv CH 2
SIGNAL AMPLITUDE		
CH 1 & CH 2	[CH 1 4.481v	0.237v
	CH 2 5.644v	0.250v
CH 3 & CH 4	[CH 3 0.307v	6.158v
	CH 4 0.354v	6.206v
COMMAND OPERATION	INSTRUMENT RESPONSE AND DIGITAL TELEMETRY LEVELS VERIFIED.	
ANALOG TM	INSTRUMENT STATUS MEASURED, VOLTAGES CORRESPOND TO INSTRU- MENT CONDITION.	
TURN ON TRANSIENTS	ELEC ON	4.4 ma/ μ sec
	MTR ON	0.55 ma/ μ sec
	COOLER HTR	3.5 amp/600 μ sec
	EARTH SHIELD	2a/10 ms
CONDUCTED RIPPLE (28v)	MTR (L)	2 ma P/P
	MTR (H)	9 ma P/P
	ELEC AND ALL CHs	SEE DATA
	FULL INSTR.	SEE DATA

SUSCEPTIBILITY

OK CH 4 7.8 mv for
> 0.8v 10KHz

CONDUCTED RIPPLE +10v
+ 5v

NONE DISCERNIBLE
NONE DISCERNIBLE

OVER VOLTAGE

±15v 0 mv
+ 5v 40 mv

AMPLIFIER ZEROING

CH 1	0.232 v
2	0.245 v
3	6.210 v
4	6.200 v

AMPLIFIER LINEARITY

CH 1	2.4 mv
2	0.7 mv
3	5.6 mv
4	3.6 mv

RAMP CAL RANGE

	<u>1/4</u>	<u>1/2</u>	<u>3/4</u>
1	1.584v	3.224v	4.858v
2	1.596	3.329	4.859
3	1.609	3.227	4.865
4	1.583	3.218	4.851

AMPLIFIER DROOP

CH 1 0 CH 3 2 mv
2 0 4 2 mv

VERIFICATION OF TM IN DATA STREAM

	<u>TM</u>	<u>DATA</u>
BB 1	1.1260v	1.1234v
2	1.1160	1.1140
3	1.2410	1.2378
4	1.3060	1.3062
PATCH	2.788v	2.787v
BB SAMPLE	3 2.519v	2.519v
4	4.716	4.707

VOLTAGE CAL VERIFICATION

	1	2	3	4
CH 1	1.856	3.487	5.118	5.930
2	1.875	3.506	5.137	5.951
3	1.359	2.984	4.602	0.553
4	1.350	2.968	4.587	0.550
	(Internal BB _____↑)			

AUX SCAN

VERIFIED AFTER BOARD CHANGE
SEE MR 3399

COHERENT NOISE

NONE OBSERVED

INSTRUMENT CALIBRATION

SEE DATA SHEETS

FM 103
TM CALIBRATION EQUATIONS

RADIATOR TEMP	$^{\circ}\text{K}$	=	34.97V	+	143.8
PATCH POWER	MW	=	2V^2		
PATCH TEMP LOW RANGE	$^{\circ}\text{K}$	=	5.135V	+	93.5
PATCH TEMP EX RANGE	$^{\circ}\text{K}$	=	1.99 V^2	+	$34.68\text{V} + 96.6$
BB#1 TM	$^{\circ}\text{C}$	=	$.0349\text{V}^2$	+	$8.204\text{V} + 3.499$
BB#2 TM	$^{\circ}\text{C}$	=	$.0349\text{V}^2$	+	$8.204\text{V} + 3.499$
BB#3 TM	$^{\circ}\text{C}$	=	$.0349\text{V}^2$	+	$8.204\text{V} + 3.499$
BB#4 TM	$^{\circ}\text{C}$	=	$.0349\text{V}^2$	+	$8.204\text{V} + 3.499$
MOTOR CURRENT	MA	=	60V		
ELECTRONICS CURRENT	MA	=	191V		
EARTH SHIELD POSITION		=	$(<2\text{V}) \text{ CL } (2-4)\text{MID } >4 \text{ OPEN}$		
ELECTRONICS TEMP	$^{\circ}\text{C}$	=	-5.82V	+	39.9
BASE PLATE TEMP	$^{\circ}\text{C}$	=	-7.75V	+	34.8
A TO D TEMP	$^{\circ}\text{C}$	=	-8.33V	+	86.16
MOTOR HOUSING TEMP	$^{\circ}\text{C}$	=	-7.75V	+	34.8
COOLER HOUSING TEMP	$^{\circ}\text{C}$	=	-7.75V	+	34.8
DETECTOR BIAS VOLTS		=	4.33V	-	21.33
BB IR CH3	$^{\circ}\text{C}$	=	$58.15 - 14.51\text{V} - .1383\text{V}^2 -$ $.1972\text{V}^3 + .01118\text{V}^4$		
BB IR CH4	$^{\circ}\text{C}$	=	$48.35 + .4809\text{V} - 3.953\text{V}^2 +$ $1.0396\text{V}^3 - .1141\text{V}^4$		
REFERENCE (OFFSET) VOLTAGE		=	1.33V		

SUMMARY OF
TEST RESULTS
FOR SN104

FM104 TEST RESULTS

<u>ITEM</u>	<u>SPECIFICATION</u>				<u>MEASURED</u>		
<u>Size</u>	Max.	<u>X</u>	<u>Y</u>	<u>Z</u>	<u>X</u>	<u>Y</u>	<u>Z</u>
		11"	31"	15"	9.75"	30.31"	14.13"
<u>Weight</u>	Max.	60 lbs.			Instrument = 58.81 lbs. Thermal Blanket = 17 ozs.		
<u>Power</u>	Max.	27 watts			24.92 watts		
<u>Center of Gravity</u>	N/A				<u>Door Open</u>	<u>Door Closed</u>	
					X 4.67"	4.59"	
					Y 12.95"	12.95"	
					Z 1.51"	1.60"	

FM104 TEST RESULTS (cont'd)

<u>ITEM</u>	<u>SPECIFICATION</u>	<u>MEASURED</u>
<u>Spectral Response</u>	Para. 3.4.2	All 4 channels meet spectral response requirements.
<u>CH 1 & CH 2 Signal Stability</u>	+100 mV @ 100% albedo from 10° to 30° baseplate temperature	CH 1 = 60 mV CH 2 = 99 mV
<u>CH 3 & CH 4 Signal Stability</u>	CH 3 = +100 mV @ 320°K +1° from 10° to 21° baseplate CH 4 = +100 mV @ 320°K +1° from 10° to 30° baseplate	CH 3 = 173 mV (+91/-82) CH 4 = 8.3 mV measured 10-20° C 17 mV extrapolated 10-30° C
<u>Solar Channel Noise</u>	Min. 3:1 S/N @ .5% albedo	>10:1
<u>Thermal Channels NEAT</u>	0.12° kelvin @ 300°K scene	CH 3 = 0.039°K CH 4 = 0.076°K

FM104 TEST RESULTS (cont'd)

<u>ITEM</u>	<u>SPECIFICATION</u>	<u>MEASURED</u>		
<u>Vibration</u>	Spec. Para. 4.4.4.3	All prepost vibration measurements within specification. MR. E03442 generated MR. E03443 generated		
<u>Scan Plane Alignment</u>	Max. 0.5 milliradian Δ prepost vibration	<u>Pre-Vib</u>	<u>Post Vib</u>	<u>Δ</u>
		Nadir +0.76 90° +2.96	+0.66 +2.97	0.10 mr. 0.01 mr.
<u>Channel Registration</u>	All IFOV centers within 0.1 mr diameter circle	<u>Pre-Vib</u>	<u>Post Vib</u>	
		0.066 mr.	0.0698 mr.	
<u>IFOV Size</u>	1.31 + 0.2 milliradian at 50% point	<u>Scan</u>	<u>X-Scan</u>	
		CH 1: 1.39 x 1.42		
		CH 2: 1.36 x 1.37		
		CH 3: 1.22 x 1.31		
		CH 4: 1.17 x 1.18		
<u>System MTF</u>	Min. 30% at limiting frequency	<u>Scan</u>	<u>X-Scan</u>	
		CH 1 = 46% x 46%		
		CH 2 = 47% x 48%		
		CH 3 = 54% x 47%		
		CH 4 = 55% x 55%		

FM104 TEST RESULTS (cont'd)

<u>ITEM</u>	<u>SPECIFICATION</u>	<u>MEASURED</u>																									
<u>Cooler Margin</u>	No higher than 99.5°K at nominal orbit	93°K Based on 36mW control @ 105°K																									
<u>Signal Amplitude CH 1 & CH 2</u>	6.1 + .10V @ 100% albedo CH 1 12 bulbs = 81.4% = 5.012V CH 2 6 bulbs = 92.7% = 5.673V	CH 1 = 5.011V CH 2 = 5.718V																									
<u>Signal Amplitude CH 3 & CH 4</u>	0.300 + .10V @ 320 + 1°K	CH 3 = 0.435V @ 320°K CH 4 = 0.396V @ 320°K																									
<u>Amplifier Zeroing</u>	CH 1 & CH 2 0.250 + .05V CH 3 & CH 4 6.200 + .05V	CH 1 = 0.226V CH 2 = 0.250V CH 3 = 6.196V CH 4 = 6.196V																									
<u>Voltage Cal Levels</u>	3 earth scenes, 1 BB level	<table><tr><td></td><td><u>1</u></td><td><u>2</u></td><td><u>3</u></td><td><u>4</u></td></tr><tr><td>CH 1</td><td>1.844</td><td>3.463</td><td>5.088</td><td>5.894</td></tr><tr><td>CH 2</td><td>1.869</td><td>3.500</td><td>5.125</td><td>5.932</td></tr><tr><td>CH 3</td><td>1.300</td><td>2.929</td><td>4.562</td><td>0.495</td></tr><tr><td>CH 4</td><td>1.350</td><td>2.969</td><td>4.588</td><td>0.546</td></tr></table>		<u>1</u>	<u>2</u>	<u>3</u>	<u>4</u>	CH 1	1.844	3.463	5.088	5.894	CH 2	1.869	3.500	5.125	5.932	CH 3	1.300	2.929	4.562	0.495	CH 4	1.350	2.969	4.588	0.546
	<u>1</u>	<u>2</u>	<u>3</u>	<u>4</u>																							
CH 1	1.844	3.463	5.088	5.894																							
CH 2	1.869	3.500	5.125	5.932																							
CH 3	1.300	2.929	4.562	0.495																							
CH 4	1.350	2.969	4.588	0.546																							

FM104 TEST RESULTS (cont'd)

<u>ITEM</u>	<u>SPECIFICATION</u>	<u>MEASURED</u>			
<u>Ramp Cal Range</u>	Nominal - 0.025 to 6.475V (6.5V swing)		<u>1/4</u>	<u>1/2</u>	<u>3/4</u>
		CH 1	1.567	3.193	4.814
		CH 2	1.594	3.224	4.849
		CH 3	1.597	3.223	4.850
		CH 4	1.603	3.233	4.857
					3.247
					3.256
					3.253
					3.254
<u>Amplifier Linearity</u>	<u>+ 12.5mV max.</u>	CH 1 - 4mV			
		CH 2 - 6mV			
		CH 3 - 6mV			
		CH 4 - 4mV			
		Includes ramp source and data converter.			
<u>Verification of TM in Data Stream</u>	<u>+ 12.5mV Δ</u>		<u>TM</u>	<u>Data</u>	<u>Δ</u>
		BB1 =	3.555V	3.556V	1mV
		BB2 =	3.586V	3.588V	2mV
		BB3 =	3.525V	3.525V	0
		BB4 =	3.552V	3.554V	2mV
		Patch Temp.	2.507V	2.496V	11mV
<u>BB Sample TM</u>	<u>+ 12.5mV Δ</u>		<u>TM</u>	<u>Data</u>	<u>Δ</u>
		CH 3 =	2.787	2.784	3mV
		CH 4 =	5.051	5.051	0

FM104 TEST RESULTS (cont'd)

<u>ITEM</u>	<u>SPECIFICATION</u>	<u>MEASURED</u>
<u>Command Verification</u>	N/A	All command operations and digital T/M levels verified.
<u>Analog Telemetry</u>	N/A	All analog T/M points correspond to instrument status.
<u>Over Voltage</u>	Spec. Para. 3.2.2.3.1	Proper operation of instrument verified at bus-voltages from 26 to 39V.

FM104 TEST RESULTS (cont'd)

<u>ITEM</u>	<u>SPECIFICATION</u>	<u>MEASURED</u>		
<u>Turn On Transients</u>		<u>Max</u>	<u>Rate</u>	
Electronics	1.4A max @ 20mA/μsec	610mA	- 3mA/μsec	
Motor	1.4A max @ 20mA/μsec	570mA	- .38mA/μsec	
Cooler Heat	3.3A max 2ms duration	2.6A	- 900μsec	
Earth Shield	2.1A max 1 sec duration	1.75A	- .82 sec	
<u>Conducted Ripple</u>				
	<u><20Hz</u>	<u>>20Hz</u>	<u><20Hz</u>	<u>>20Hz</u>
Motor Low	27mA max	9mA max	<15mA	<5mA
Motor High			<15mA	<5mA
Elec. & All Channels			<20mA	<5mA
Full Instrument			<20mA	<5mA
+10V	2mA max		<1mA	
+5V	1mA max		<.5mA	
<u>Susceptibility</u>				
	0.25V p-p to 1.5kHz		Worst case =	
	0.50V p-p to 10MHz		800mV @ 11-15kHz	

FM104 TEST RESULTS (cont'd)

<u>ITEM</u>	<u>SPECIFICATION</u>	<u>MEASURED</u>
<u>Scanner Jitter</u>	98% within $\pm \frac{1}{2}$ IFOV for 20 min.	>98% for all baseplate temp.
<u>Scanner Long Term Drift</u>	$\leq \pm \frac{1}{2}$ IFOV for 20 min.	0
<u>Coherent Noise</u>	Spec. Para. 4.2.7.2	None Observed

FM 104

CALIBRATION EQUATIONS

RADIATOR TEMP	$^{\circ}\text{K}$	=	34.97V	+	143.8	
PATCH POWER	MW	=	2V^2			
PATCH TEMP LOW RANGE	$^{\circ}\text{K}$	=	$.033\text{V}^2$	+	4.98V	+ 91.9
PATCH TEMP EX RANGE	$^{\circ}\text{K}$	=	1.97V^2	+	34.87V	+ 94.6
BB#1 TM	$^{\circ}\text{C}$	=	$.0349\text{V}^2$	+	8.204V	+ 3.499
BB#2 TM	$^{\circ}\text{C}$	=	$.0349\text{V}^2$	+	8.204V	+ 3.499
BB#3 TM	$^{\circ}\text{C}$	=	$.0349\text{V}^2$	+	8.204V	+ 3.499
BB#4 TM	$^{\circ}\text{C}$	=	$.0349\text{V}^2$	+	8.304V	+ 3.499
MOTOR CURRENT	MA	=	60V			
ELECTRONICS CURRENT	MA	=	191V			
EARTH SHIELD POSITION		=	($<2\text{V}$)	CL	(2-4)MID	$>\Delta$ OPEN
ELECTRONICS TEMP	$^{\circ}\text{C}$	=	-5.82V	+	39.9	
BASEPLATE TEMP	$^{\circ}\text{C}$	=	-7.75V	+	34.8	
A TO D TEMP	$^{\circ}\text{C}$	=	-8.33V	+	86.16	
MOTOR HOUSING TEMP	$^{\circ}\text{C}$	=	-7.75V	+	34.8	
COOLER HOUSING TEMP	$^{\circ}\text{C}$	=	-7.75V	+	34.8	
DETECTOR BIAS VOLTS		=	4.33V	-	21.33	
BB IR CH 3	$^{\circ}\text{C}$	=	$58.15 - .1972\text{V}^3$	$14.51\text{V} - .01118\text{V}^4$	1383V^2	-
BB IR CH 4	$^{\circ}\text{C}$	=	$48.35 + 1.0396\text{V}^3$	$.4809\text{V} - .1141\text{V}^4$	3.953V^2	+
REFERENCE (OFFSET) VOLTAGE		=	1.33V			

10.0 LIST OF DESIGN INFORMATION REPORTS

Design Information Reports written on this program are listed below.

<u>DIR #</u>	<u>Subject</u>
1.	AVHRR Sensitivity - Harber/Koczor
2.	AVHRR Collimator - Diffraction Effects - R. Koczor
3.	Effects of Optical Surface Errors on Diffraction Limited MTF - R. Annable
4.	Approach to the Optical Alignment and Channel Registration of the AVHRR - R. Annable
5.	The Effect of Detectors on the Instrument Spectral Response, Part 1, Channels 3 & 4 - R. Koczor
6.	Theoretical Design to Meet the Polarization Requirements in Channels 1 and 2 - R. Annable
7.	Polarization Design and Analysis Based on OCLI Measured Data - R. Annable
8.	Using "Standard" Silicon Detectors for Channels 1 and 2 - R. Koczor
9.	Effect of Scan Mirror Power on Diffraction Limited MTF - R. Annable
10.	Visible In-Flight Calibration - R. Koczor
11.	Orientation of the Visible Calibration D.R.T. - R. Koczor
12.	Solar Channel Spectral Characteristics, Part 1 - R. Koczor
13.	Solar Channel Sensitivity - R. Koczor
14.	The Absence of Coma in an Afocal Pair of Confocal, Coaxial Parabolic Mirrors - R. Annable
15.	Heating of the Radiator Window for Contamination Protection - R. Annable
16.	AVHRR Test Collimator Design - R. Koczor
17.	The Effect of Collimator Aberrations on the Diffraction Limited MTF - R. Annable
18.	Worst Case Honeycomb Temperature Gradient in the In-Flight Thermal Calibration Target - R. Annable
19.	Cool Down and Decontamination Times for the Radiant Cooler - R. Annable
20.	Scanner Jitter, Linearity, and Alignment Tests - R. Koczor
21.	Optimization of IFOV Size and Shape, Pre-Sampling Filter, and Sample Rate - R. Foote
22.	Thermal Math Model Analysis - Crawford/Wright
23.	Thermal Math Model Analysis, OFF Instrument - Crawford/Wright
24.	Measurement of Low Emissivity - R. Koczor

DIR #Subject

25.	AVHRR Scan Motor Lubricant Evaluation and Selection - J. Stark
26.	AVHRR TM Calibration - N. Franklin
27.	MSM Vibration Test - J. Stark
28.	BBM Acceptance Test Results - Owens/Koczor
29.	Completion of Thermal Math Model - J. Crawford
30.	MSM Vibration #2 - J. Stark
31.	Effect of Loss of Radiant Cooler Temperature Regulation - R. Harber
32.	Worst Case Analysis - L. Roffelsen
33.	AVHRR MSM Vibration #3 - J. Stark
34.	Spectral Response Measurements on AVHRR ETM - R. Harber
35.	Pinning of Critical Parts - C. Soest
36.	Cooler Door Momentum - C. Soest
37.	Scattered Light Test Results of AVHRR BBM - R. Koczor
38.	Final Thermal Model Analysis - J. Crawford
40.	LTM Final Report - C. Soest
42.	AVHRR Data Amplifier Signal Droop - H. Kalina
43.	Channel 4 Coherent Noise in AVHRR PFM - R. Foote
44.	AVHRR Scanner Long Term Drift Measurement-Larry Howell

End of Document